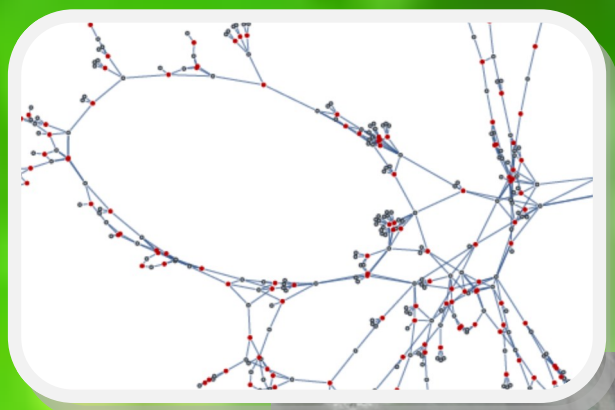


MODELLING FOR ENGINEERING AND HUMAN BEHAVIOUR 2014

Instituto Universitario de Matemática Multidisciplinar



L. JÓDAR, L. ACEDO, J. C. CORTÉS

AND J. R. TORREGROSA, EDITORS

INSTITUTO UNIVERSITARIO DE
MATEMÁTICA MULTIDISCIPLINAR

im²

Instituto de Matemática Multidisciplinar



GENERALITAT
VALENCIANA



UNIVERSITAT
POLITÈCNICA
DE VALÈNCIA

MODELLING FOR ENGINEERING, & HUMAN BEHAVIOUR 2014

Instituto Universitario de Matemática Multidisciplinar
Universitat Politècnica de València
Valencia 46022, SPAIN

Edited by
Lucas Jódar, Luis Acedo, Juan Carlos Cortés and Juan Ramón Torregrosa
Instituto Universitario de Matemática Multidisciplinar
Universitat Politècnica de València
I.S.B.N.: 978-84-606-5746-0

CONTENTS

1. **E. Lamprianidou, J. Villanueva-Oller, L. Acedo, J.-A. Moraño and R.-J. Villanueva**, Random Network Models of the Brain with High Connectivity Pag: 1-7
2. **F. Aznar, M. Pujol, R. Rizo and M.-J. Pujol**, Modelling Robust Swarm Deployment for Aerial Indoor Robots Using Virtual PheromonesPag: 8-11
3. **J. Benajes, R. Payri, J. Gimeno and P. Martí-Aldaraví**, Comparison of an Eulerian Spray Atomization model with DNS results. Adjustment of inter-facial surface density transport equation parameters Pag: 12-15
4. **E. Campbell, A. E. Ilaya-Ayza, J. Izquierdo and R. Pérez-García**, Self organizing maps and clustering techniques to sectorize water supply networks based on energy criteria Pag: 16-21
5. **M.-C. Casabán, J.-C. Cortés and L. Jódar**, Solving random heat problems in a semi-infinite bar with unhomogeneous boundary value conditions Pag: 22-28
6. **R. Cervelló-Royo, J.-C. Cortés, A. Sánchez-Sánchez, F.-J. Santonja and R.-J. Villanueva**, Country Risk Score forecasting for BRICS emerging markets by means of a diffusion model Pag: 29-33
7. **B. Chen-Charpentier and I. Diakite**, A Mathematical Model of Bone Remodeling with DelaysPag: 34-37
8. **R. Company, V. N. Egorova and L. Jódar**, Transforming American call option problem preserving qualitative properties of solution Pag: 38-42
9. **M.-C. Casabán, J.-C. Cortés, A. Navarro-Quiles, J.V. Romero, M.-D. Roselló and R.-J. Villanueva**, The use of Random Variable Transformations for solving nonlinear random differential equations Pag: 43-49
10. **M. Fakhrary, R. Company and L. Jódar**, A five-point stencil scheme for pricing American options under Bates model Pag: 50-54
11. **L. Bayón, P. Fortuny Ayuso, J. A. Otero, P. M. Suárez and C. Tasis**, Cyclic coordinate descent in a class of bang-singular-bang problems Pag: 55-58
12. **J. Galindo, H. Climent, A. Tiseira and L.M. García-Cuevas**, Effect of the numerical scheme resolution on quasi-2D simulation of an automotive radial turbine under highly pulsating flowPag: 59-63

13. **P.J. García Nieto, E. García-Gonzalo, J.R. Alonso Fernández and C. Díaz-Muñiz**, An hybrid PSO optimized SVM-based model for predicting a successful growth cycle of the *Spirulina platensis* from experimental data in open raceway ponds Pag: 64-69
14. **A. H. Encinas, J. Martín-Vaquero, A. Queiruga-Dios and V. Gayoso-Martínez**, Using high-order finite difference methods in nonlinear Klein–Gordon equations Pag: 70-74
15. **M. Osa, N. Guadalajara and R. Escartín**, Modelling improvement of pain and quality of life in osteoporosis patients treated with teriparatide Pag: 75-78
16. **J. Izquierdo, E. Campbell, I. Montalvo and R. Pérez-García**, Injecting problem-dependent knowledge to improve evolutionary optimization search ability Pag: 79-84
17. **B. Kleefeld and J. Martín-Vaquero**, SERK methods for solving nonlinear multi-dimensional parabolic PDEsPag: 85-89
18. **F. J. Mora, R. Rizo, M. Pujol, F. Aznar and Mireia Sempere**, A Formal Specification of Autonomous Agent Systems with Subsystems Inspired by Biology Pag: 90-95
19. **L. Acedo, F. Palmí, F. J. Santonja and R. J. Villanueva** , Building networks of sexual contacts from real statistical dataPag: 96-101
20. **C. Matonoha and Š. Papáček**, On the connection and equivalence of two methods for solving an ill-posed inverse problem based on FRAP dataPag: 102-105
21. **F. Pedroche and J. A. Verdoy**, Comparison of some measures of Competitive Balance in regular seasons of European Basketball leagues Pag: 106-110
22. **E. De la Poza, L. Jódar and M. Martínez**, Modeling the growth of electoral support to emergent parties in a crisis environment: The case of Valencian Community ..Pag: 111-116
23. **A. Pujol, A. Jimeno-Morenilla and J. L. Sánchez-Romero**, A hybrid SVM-LBP approach for face recognition Pag: 117-120
24. **G. Ribes and A. Peralt**, Modelling the co-creation between students and universities and its effects to loyalty and satisfaction Pag: 121-127
25. **P. Ruiz, J. Sastre, J. Ibáñez and E. Defez** , A new efficient algorithm for matrix exponential computation Pag: 128-133
26. **B. Sevilla-Villanueva, K. Gibert and M. Sànchez-Marrè**, The Role of Statistical Tests on Cluster Interpretation Pag: 134-137
27. **A.J. Torregrosa, A. Broatch, F.J. Arnau and M. Hernández**, Development of a non-linear quasi-3D model for engine gas-exchange modelling Pag: 138-141
28. **J. A. Guzmán, F. J. Moreno and I. D. Torres**, Formal Specification of a Planning Algorithm with Logic of Predicates Extended to Compositions of Learning Paths Pag: 142-146

29. **J. C. García-Díaz and O. Trull**, Multiple seasonal Holt–Winters models applied to Spanish short–term electricity demand forecasting: an alternative to the Red Eléctrica de España model Pag: 147-150
30. **J. Alegre-Sanahuja, J. C. Cortés, F.J. Santonja and R. J. Villanueva**, Analysis of mobile Apps lifecycle. Epidemiological modelling approach by random networks Pag: 151-160
31. **M. A. Castro, F. Rodríguez, J. Cabrera and J. A. Martín**, A compact difference scheme for second order dual-phase-lagging models of heat conduction Pag: 161-165
32. **F.J. Salvador, D. Jaramillo-Císcar, J. V. Romero and M. D. Roselló**, Simulation of atomization process in diesel sprays Pag: 166-173
33. **A. Vidal-Ferrándiz, S. González-Pintor, D. Ginestar, G. Verdú, C. Demazière and M. Asadzadeh**, Use of discontinuity factors in high-order finite element methods Pag: 174-177
34. **A. Vidal-Ferrándiz, R. Fayez, D. Ginestar and G. Verdú**, Moving meshes to solve the time-dependent neutron diffusion equation in hexagonal geometryPag: 178-181
35. **A. Cordero, A. Franques and J. R. Torregrosa**, Second-order implicit methods for estimating the solution of turbulence problemsPag: 182-186
36. **J. A. Conejero, C. Jordán and E. Sanabria-Codesal**, A computational graph-based algorithm for the management of a car-rental-servicePag: 187-190
37. **Á. A. Magreñán, J. M. Gutiérrez and L. Orcos** , Damped Newton’s method for solving problems associated to the Stewart-Gough platformPag: 191-194
38. **A. Fraile, J. A. Sicilia, E. Larrodé, Á. A. Magreñán and L. Orcos**, Decision model to optimize the location of logistics and transport facilities in urban environments Pag: 195-198
39. **J. A. Sicilia, C. Quemada, B. Royo and D. Escuín**, An optimization algorithm for solving the rich vehicle routing problem based on metaheuristics Pag: 199-203
40. **Á. A. Magreñán, A. Cordero, L. Orcos, C. Quemada, J. A. Sicilia and J. R. Torregrosa**, An innovative mathematical simulation tool of integrated frequency synthesizers in order to estimate the main figures of merit with high accurate Pag: 204-207
41. **L. Hilario, A. Falcó, N. Montés and M.C.Mora** , A matrix-based optimization algorithm for shape deformation using parametric curves Pag: 208-213
42. **D. Budzko, J.L. Hueso, E. Martínez and C. Teruel**, Dynamical Study while Searching Equilibrium Solutions in N -body Problem Pag: 214-217
43. **S. Gigola, L. Lebtahi and N. Thome**, On the inverse eigenvalue problem of Hermitian reflexive matrixPag: 218-222

Random Network Models of the Brain with High Connectivity

E. Lamprianidou^b, J. Villanueva-Oller[★], L. Acedo^b*, J.-A. Morano^b,
and R.-J. Villanueva^b

(^b) Instituto Universitario de Matemática Multidisciplinar,
Building 8G, Door C, Second Floor,
Universitat Politècnica de València, 46022 Valencia, Spain

([★]) Centro de Estudios Superiores Felipe II,
Aranjuez, Madrid, Spain

November 28, 2014

1 Introduction

One of the main challenges in the simulation of even reduced areas in the brain is the presence of a large number of neurons and a large number of connections among them. Even from a theoretical point of view the behaviour of dynamical models of complex networks with high connectivity is unknown, precisely because the cost of computation is still unaffordable and it will likely be in the near future. In this work we discuss the simulation of a cellular automata network model of the brain including one million nodes with a maximum average of three hundred connections per neuron. The computation power required for the massive calculation of networks with such level of complexity was achieved thanks to a distributed computing environment based upon the BOINC (Berkeley Open Infrastructure for Network Computing) platform. Moreover, in this work we consider the interplay among

*e-mail: luiacrod@imm.upv.es

excitatory neurons (which induce the excitation of their neighbours) and inhibitory neurons (which prevent resting neurons from firing and induce firing neurons to pass to the refractory state). It is known that inhibitory neurons constitute up to a third of the total neural population in any brain tissue and their role as modulators of the global brain activity is key in the prevention of aberrant firing patterns. In particular, neural network dysfunctions in the excitatory and inhibitory circuits have been proposed as a mechanism in Alzheimers disease. A failure in the inhibitory GABAergic circuits is also related to a wide variety of conditions ranging from Epilepsy to Huntingtons Disease. Our objective is to classify the normal (noisy but asymptotically constant patterns) and the abnormal (high oscillations with spindle-like behaviour) patterns of activity in the model brain and their stability and parameter ranges in order to determine the role of excitatory and inhibitory compensatory effects in healthy and diseased individuals.

2 The cellular automata network model

It is a basic fact of the architecture of the brain that it constitutes a network of some kind. This was already disclosed in the pioneering works of Ramón y Cajal [1]. Every single neuron is also a complex biophysical device capable of interacting with their neighbours by a wide range of electrochemical signals based upon 100 neurotransmitters [2, 3]. The most important ones are glutamate (in excitatory synapses) and γ -aminobutyric acid (in inhibitory synapses). So, from the point of view of mathematical modelling, we can consider that neurons classify in two main types: The excitatory ones, which induce the firing of their postsynaptic neighbours, and the inhibitory neurons which produce the opposite effect, i. e., they prevent other neurons from firing or turn firing neurons into the refractory state [4].

According to their state we have:

- Resting Neurons: They are in electrochemical equilibrium.
- Firing Neurons: Sending signals to other neurons along their synapses.
- Refractory Neurons: After the firing state the neurons become refractory so they cannot be excited again for a short period of time.

Both excitatory and inhibitory resting neurons can be activated but they behave differently in relation to their neighbours. The signal sent by an

excitatory neuron contribute to the excitation of a neighbour but if the signal is sent by an inhibitory neuron it can deactivate a neighbouring firing neuron or prevent a resting neuron to evolve to the firing state.

To build our model we have chosen a random network [7] with 10^6 nodes and a large average connectivity degree. As maximum we considered $k = 300$ because of computational limitations. In this network, thirty per cent of the nodes are labelled as inhibitory cellular automata networks, the rest being excitatory. This is supported by neurological evidence [5].

The evolution of the cellular automata [6] states in the random network is performed according to the following stochastic rules performed every single time step:

- We check every firing neuron in the network. For every firing neuron we generate a pseudorandom number, x and if $x \leq \nu$, the state is changed to refractory. Notice, that this implies that the transition is governed by a Poisson process with an average transition time $1/\nu$. Firing neurons can also become refractory by the action of an inhibitory firing neighbour. This happens with probability γ for each neighbour.
- We check the transitions from the refractory to the resting state. In this case, the transition probability is λ .
- For every resting neurons we take into account their firing neighbours. Excitatory firing neurons in their neighbourhood can excite the resting neurons with probability α and the inhibitory firing neurons may deactivate it (if the test resting neuron has been activated already by an excitatory firing neighbour) with probability γ .

The temporal evolution of this model is a very time-consuming task. So, we were forced to apply distributed computing techniques to simulate the brain network in the desired scale of one million nodes.

3 Distributed Computation of the Phase Diagram

In order to get a global picture of the different behaviour displayed by the random network cellular automata model we prepared a set of 155,000 parameter combinations with the restriction $\alpha = \gamma$. The identity of the excitatory and

inhibitory probabilities was chosen because of physiological plausibility and, also, because we found that the interesting oscillatory patterns were found with this condition. As commented before, to carry out all these simulations in a network with 10^6 nodes and an average connectivity degree $k = 300$ is beyond the capabilities of a single computer in which it would require years of computation time.

To achieve the objective of simulating all these tasks we resorted to the BOINC software. BOINC is an open source software used in many other projects as known as SETI@home [8, 9] or Climate Prediction [10]. The setting, preliminary results and details of such an implementation for epidemiological models and our brain model in particular was discussed in another publication [11].

Most of the behaviour were characterized by an asymptotic dynamical stable state for the number of resting, firing and refractory neurons of each type. However, for some sets of parameters in a very precise range we find oscillatory behaviour as shown in Fig. 1. To identify the tests corresponding to oscillatory behaviour we used an algorithm based upon the Discrete cosine transform, DCT, as described by X. Li et al. [12] and selected only those whose first coefficient of the transform was sufficiently large (at least 100,000). The DCT for the simulation in Fig. 1 is shown in Fig. 2. The results

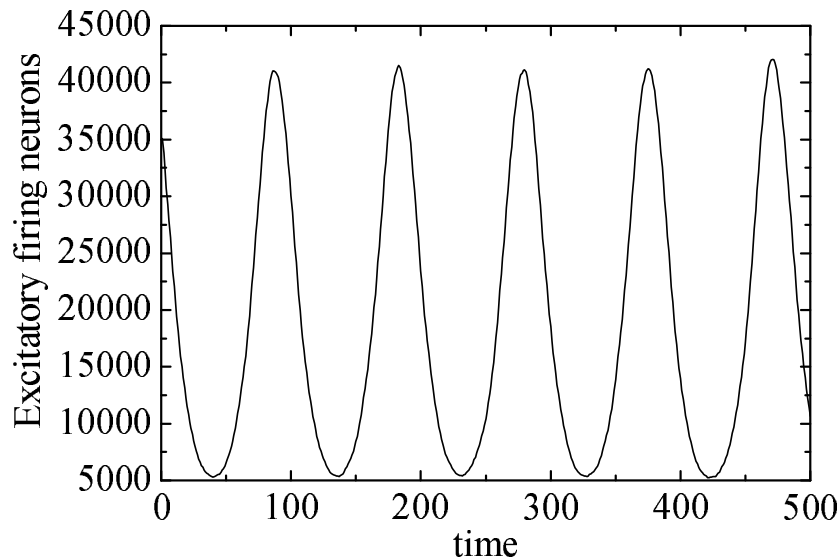


Figure 1: A typical test exhibiting periodic behaviour.

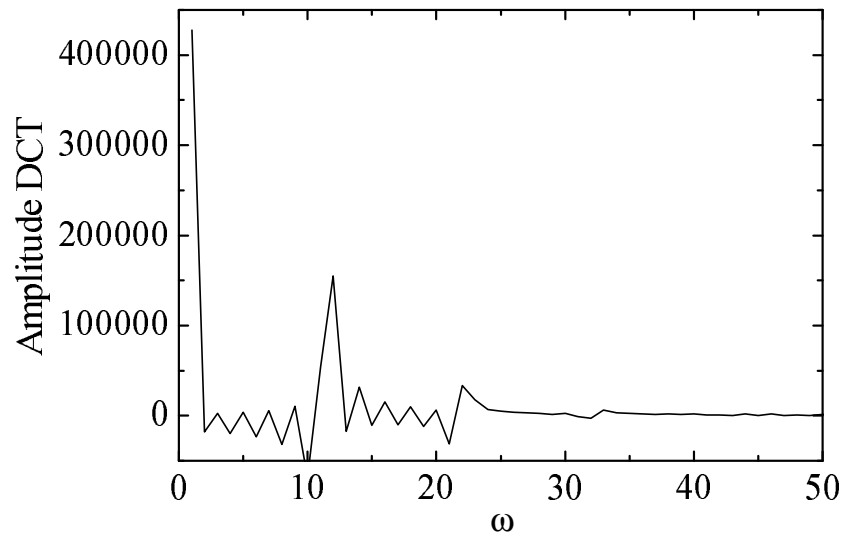


Figure 2: Discrete cosine transform of the test in Fig. (1).

displayed in Fig. (1) are reminiscent of the regular oscillations appearing in the EEG of epileptic patients during the so-called ictal phase [13].

4 Conclusions

In this work we have developed a large-scale cellular automata model [6] of the brain in which the synapses are modelled by the bonds in a random network [7]. The individual cellular automaton is either excitatory or inhibitory in their action upon other cellular automata in the network. This way we intend to capture the essential dynamical features of the real brain, i. e., neurons are organized in a neuron and there are two basic types of neurons: excitatory which can induce the firing of other neurons and inhibitory, which can trigger the transition of firing neurons to the refractory state or prevent the firing of a resting one being, simultaneously, connected to a firing excitatory neuron.

We have considered a network that, to the best of our knowledge, is more complex than any previous simulation attempt of this kind of models: a total of 10^6 cellular automata were considered with an average of $k = 300$ bonds with other nodes of the network. The simulations are so time consuming that a distributed computing solution based upon the BOINC software was developed to obtain the dynamical behaviour for 155,000 different tasks [11].

In the phase diagram of behaviour both asymptotically stable and oscillatory signals are found. The oscillatory behaviour occurs only in a very restricted parameter set and it could be assimilated into the ictal phase of epilepsy and other disorders. As this happens only for precise values of the excitatory probability and the transition rates from firing to refractory and to resting, our results could be relevant in the control of epileptic seizures [13].

References

- [1] S. Ramón y Cajal, Ramón y Cajal's Croonian Lecture: La fine structure des centres nerveux, *Proceedings of the Royal Society of London* 53 (1894) 444–468.
- [2] M. Abeles, *Corticonics: Neural circuits of the cerebral cortex*, Cambridge University Press, Cambridge, 1991.
- [3] E. R. Kandel, J. H. Schwartz, T. M. Jessel, *Principles of Neural Science*, Fourth Edition, McGraw-Hill, New York, 2000.
- [4] W. Gerstner, W. M. Kistler, *Spiking neuron models: Single neurons, populations and plasticity*, Cambridge University Press, 2002. Available online at: <http://icwww.epfl.ch/~gerstner/BUCH.html>
- [5] S. Lamb, J. J. Webster, *Language and reality: Selected writings of Sydney Lamb*, Bloomsbury Academic, London, 2006.
- [6] S. Wolfram, *A new kind of science*, Wolfram media Inc., 2002.
- [7] B. Bollobás, *Random Graphs*, 2 ed., Cambridge University Press, Cambridge, 2001.
- [8] E. Korpela, D. Werthimer, D. Anderson, J. Cobb, M. Leboisky, Seti@home-massively distributed computing for SETI, *Computing in Science & Engineering* 3 (1) (2001), pp. 78 – 83. doi:10.1109/5992.895191.
- [9] SETI@home [cited March 2nd, 2011]. <http://setiathome.berkeley.edu>

- [10] Climate prediction [cited March 2nd, 2011].
<http://climateprediction.net/>
- [11] J. Villanueva-Oller, L. Acedo, J. A. Morano and A. Sánchez-Sánchez, Epidemic Random Network Simulations in a Distributed Computing Environment, *Abstract and Applied Analysis*, Volume 2013, Article ID 462801, 2013.
- [12] X. Li, J. Wang, B. Huang, S. Lu, The DCT-based oscillation detection method for a single time series, *Journal of Process Control* 20 (2010) 609-617.
- [13] J. Engel Jr., *Seizures and Epilepsy*, F. A. Davis Company, Philadelphia, 1989.

Modelling Robust Swarm Deployment for Aerial Indoor Robots Using Virtual Pheromones

Fidel Aznar^{b*}, Mar Pujol^b, Ramón Rizo^b and Maria-Jose Pujol[†]

(*b*) Department of Computer Science and Artificial Intelligence

University of Alicante, San Vicent del Raspeig, Alicante (E-03080). Spain

(*†*) Department of Applied Mathematics

University of Alicante, San Vicent del Raspeig, Alicante (E-03080). Spain

November 28, 2014

1 Introduction

Deploying a robotic swarm in order to cover a certain area of space is a subject that is being actively researched. An important application of this task is to provide emergency support devices that will allow the creation of supporting networks to cover and extract information of dangerous or unreachable places. For example, in disasters such as earthquakes or floods can be very helpful to set up a communication network inside a building to extract information from its environment or to prepare a more complex mission. In this case, only a single point of entry must be sufficient to deploy the whole swarm and cover the environment. Therefore, robots must create a network reachable from the outside of the building, being always connected between them. For this task indoor drones stand out for their versatility, because of the environment accessibility is unknown due to possible alterations.

Multi-robot deployment has become a fundamental research topic in the field of multi-robot systems [3]. Although there are many applications related

*fidel@dccia.ua.es. This work has been supported by the Spanish Ministerio de Economía y Competitividad, project TIN2013-40982-R.

to multi-robot deployment, many of them rely on pre-established communication network or external localization service. This precludes its application to emergency tasks, where we are not able to assume the existence of communication networks or GPS.

2 UAV Deployment Behaviour

Initially, our behaviour will start with an agent in *beacon* (landing) state, which indicates the entry point to explore the environment. Then, an aircraft in *wander* (flying) state will be added at regular intervals. A part of this microscopic behaviour is inspired by the one presented in [1, 2], where swarm individuals could stay in two different states: in flight or landed. In UAVs system autonomy is a significant limitation. The *wander* individuals emit pheromones around them when moving with a certain radius and intensity. In the same way, in the transition between *wander* and *beacon* states, the vehicles will emit a pheromone footprint with larger radius and intensity than the previous one. This footprint is emitted only once, losing so its intensity over time, where the rate for decreasing per second is indicated by the parameter.

The navigation of the individuals who are in the state *wander* is established by a potential field function, determined by three components: the first component is obtained as a vector pointing to the area of lower intensity of pheromones in the range of the vehicle, so that the importance of a detected pheromone decreases within the square of the distance. The second component, determines the obstacle avoidance part. It is obtained by calculating a vector pointing to the area with fewer obstacles detected by the ultrasonic sensors. Finally, we will consider that the data perceived by sensors and sent to the actuators could contain inaccuracies, so a random component will be included in our selection process in order to make the next move taking into account the intrinsic uncertainty of robotic systems.

For the detailed analysis of the microscopic model it is essential to provide a mathematical model, able to analyze the global behaviour of the swarm in a given environment. The main reason for using a state-based behaviour is to allow the macroscopic model to be modelled as a recurrence equation taking into account the transitions between system states. Thereby, this macroscopic model can help us to predict the total number of individuals needed to cover an area of the environment, to adjust the radius of pheromone

emission for optimal covering or even to make an estimate of the energy required by the swarm to develop their task. The most important part to be analyzed in this behaviour is the transition between the two states of the system, *wander* and *beacon*. This is for example more valuable than getting the final distribution of individuals position, as this can be easily estimated by knowing the environment to be covered.

3 Experimentation

Although there are many parameters that can be studied, the radius of pheromones takes special importance for this behaviour. This is a distinguishing feature that determines not only the distance between swarm individuals, but as discussed below, the average speed to complete the covering process. For coverage analysis we have used c_a that represents the percentage of area covered by each individual at any time, ie, it is assumed that an individual has memory and can store the necessary environmental data to be transmitted while it is in *wander* state.

In figure 1 an example of the result of coverage of this behaviour is presented for different maps and pheromone radius. In figure 1a the radio is constant at 20m. As we can see, the behaviour is functional regardless of the nature of the environment. In figure 1b the same environment is used with different pheromones radius between 10,20 and 30m. As it can be observed the difference when altering this parameter is the density of agents required to complete the coverage.

4 Conclusions and Future Lines

A microscopic model for a swarm behavior has been discussed in this paper, able to deploy and cover an unknown area in a fully decentralized way. This behaviour is adapted to the UAVs characteristics, establishing a power saving state for the individuals, taking into account the inherent actuators and sensors errors and providing a low computing load behaviour to be implemented on systems with limited computing capabilities, as it is often the case with this kind of vehicles. Furthermore, this behaviour is able to create its own communication network for sending internal and external behavioural information and for obtaining environmental data to be analyzed.

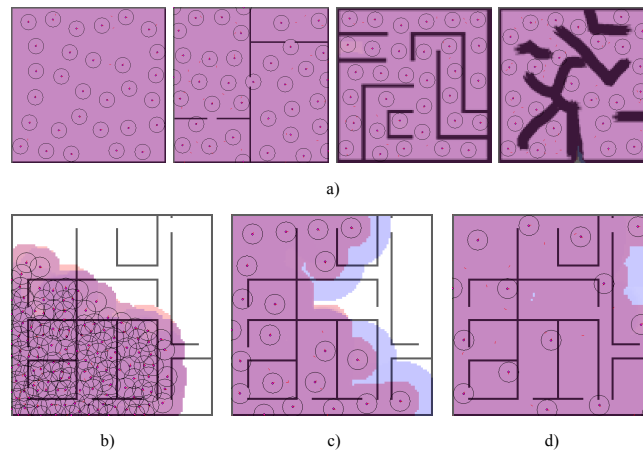


Figure 1: a) Environment covering results using the proposed microscopic behaviour with the default parameters and a pheromone radius of 20m. This behaviour terminates when $c_a \geq 95\%$. As previous figures red footprints represents the covered space (using c_a metric) and blue footprints defines the zones where the pheromones has been emitted. b) Status of the simulation at time, radius = (8144s,10m). c) (1700s,20m). d) (2000s,30m)

Currently, we are analyzing the energy required by the swarm by using our macroscopic model to determine the influence of the model parameters according to energy consumption.

References

- [1] T. Stirling, J. Roberts, J.-C. Zufferey, D. Floreano, Indoor navigation with a swarm of flying robots, in: Robotics and Automation (ICRA), 2012 IEEE International Conference on, IEEE, 4641–4647, 2012.
- [2] T. Stirling, S. Wischmann, D. Floreano, Energy-efficient indoor search by swarms of simulated flying robots without global information, *Swarm Intelligence* 4 (2) (2010) 117–143.
- [3] K. Suzuki, S. Makami, J. Akita, E.-I. Osawa, Development of cooperative small mowing robots, in: Computational Intelligence in Robotics and Automation, 2003. Proceedings. 2003 IEEE International Symposium on, vol. 3, IEEE, 1498–1502, 2003.

Comparison of an Eulerian Spray Atomization model with DNS results. Adjustment of inter-facial surface density transport equation parameters

J. Benajes^b, R. Payri^b, J. Gimeno^b, and P. Martí-Aldaraví^{b*}

(b) CMT - Motores Térmicos, Universitat Politècnica de València,
Edificio 6D, Camino de Vera s/n, 46022, Valencia, Spain.

January 12, 2015

1 Introduction

Computational Fluid Dynamics (CFD) models play a major role in the fuel injection and atomization area of research [1, 2] because they allow access to time- and length-scales which are not currently available for existing experimental techniques.

Traditionally, Discrete Droplet Models (DDM) have been successfully applied to simulate injection and combustion in internal combustion engines. Nonetheless they have important disadvantages such grid dependency. Then, an Eulerian description given by homogeneous flow models seems to be better approach; for example the Eulerian Spray Atomization (ESA) model [4, 5, 6]. Its main issue, which is the creation of droplets, was solve by Vallet et al. [3]. The mean size of liquid fragments is obtained with a new equation for the mean surface area of the gas-liquid interface per unit volume, Σ .

Nevertheless, Σ -transport equation includes several modeling constants which need to be fixed to accurately predict droplets size. One of the common

*e-mail: pedmar15@mot.upv.es

ways to give values to those constants, which is the objective of this work, is by comparison with Direct Numerical Simulations (DNS) such the ones performed by Ménard et al. [7, 8].

2 Methodology

The ESA model employed for this study has been described in detail in previous works [4, 5, 6]. In this and other homogeneous flow models applied to sprays, the Sauter Mean Diameter of droplets is computed through the liquid mass fraction and the gas-liquid inter-facial surface per unit volume. In the transport equation for this last magnitude Σ , there are three different source terms: one related to the mean velocity, another one to the turbulent velocity and the last one which tries to take into account coalescence of droplets.

In addition, a diffusivity coefficient for Σ has to be defined by establishing a value for the Schmidt number. Therefore, it is necessary to make precise modeling of four different terms, which include four different modeling constants: α_0 , α_1 , C and Sc_Σ . The physical meaning of each constant is given later.

The case of study is exactly the same (i.e. same boundary conditions) than the one employed by Ménard et al. [7]. Incompressible liquid is injected at 100 m/s into quiescent atmosphere of air compressed up to 25 kg/m³ of density. Mesh sensitivity studies were previously performed to obtain a solution independent of the mesh resolution.

A statistical study is carried to accomplish the objective of reducing the average error of Σ when ESA simulations are compared to DNS results. All four modeling constants are selected for the analysis, each of them with two levels, $\pm 25\%$ of the value given by Vallet et al. [3], but the Schmidt number which has three levels.

3 Results

After performing the statistical study, the constant that affects most the error in the prediction of Σ is the Schmidt number. The higher the diffusivity is, the more accurate the solution is. Thus, low values (lower than unity) are recommended.

The other three constants, though in a lesser grade, also affect the solution:

- α_0 scales the stretching of the liquid core due to the mean velocity. Higher values of this constant increases the production of inter-facial surface density. It turns out that this effect needs to be increased (higher values of α_0).
- α_1 scales the stretching of the liquid core due to the turbulent velocity. This factor needs to be reduced (lower values of α_1).
- C defines the equilibrium radius which at the same time determines the coalescence effect. It has been proved that the destruction of Σ (coalescence) needs to be increased (higher values of C).

An optimization has been also carried out. Recommended values are: $\alpha_0 = 1.25$, $\alpha_1 = 0.75$, $C = 3.125$ and $S_{c\Sigma} = 0.75$. Thus, the average error is reduced more than 25%, although there is room for further improvements.

4 Conclusions

A multilevel factorial statistical study has been performed over the four constants that appear in the inter-facial surface density transport equation of the ESA model. First order interaction between two factors were considered. Results have been compared to DNS results obtained from the literature.

The constant related to the diffusivity of inter-facial surface density, $S_{c\Sigma}$, is the most significant. Additionally, an optimum set of values within the range of variation ($\pm 25\%$) for the four constants has been obtained. Prediction in the distribution of Σ has been clearly improved, but the model still requires further work.

Tunning the present model does not lead to small errors when comparing with DNS results, so maybe it is recommended to change the model, as done by other authors, and then perform a new statistical study. Still, and over-prediction in spray width is expected due to the nature of the model.

References

- [1] R. Payri, B. Tormos, J. Gimeno and G. Bracho, *The potential of Large Eddy Simulation (LES) code for the modeling of flow in diesel injectors*, Mathematical and Computer Modelling, 52 (2010), pp. 1151–1160.
- [2] C. H. Lee and R. D. Reitz, *CFD simulations of diesel spray tip penetration with multiple injections and with engine compression ratios up to 100:1*, Fuel, 111 (2013), pp. 289–297.
- [3] A. Vallet, A. A. Burluka and R. Borghi, *Development of a Eulerian model for the “Atomization” of a liquid jet*, Atomization and Sprays, 11 (2001), 619–642.
- [4] J. M. Desantes, R. Payri, J. Gimeno and P. Martí-Aldaraví, *Simulation of the first millimeters of the Diesel spray by an Eulerian Spray Atomization model applied on ECN Spray A injector*, SAE Technical Paper 2014-01-1418 (2014).
- [5] R. Payri, S. Ruiz, J. Gimeno and P. Martí-Aldaraví, *Verification of a new CFD compressible segregated and multi-phase solver with different flux updates-equations sequences*, Applied Mathematical Modelling, Accepted on July, 12th, 2014. DOI: 10.1016/j.apm.2014.07.011.
- [6] F. J. Salvador, J. Gimeno, J. M. Pastor and P. Martí-Aldaraví, *Effect of turbulence model and inlet boundary condition on the Diesel spray behavior simulated by an Eulerian Spray Atomization (ESA) model*, International Journal of Multiphase Flow, 65 (2014), pp. 108–116.
- [7] T. Ménard, S. Tanguy and A. Berlemont, *Coupling level set/VOF/ghost fluid methods: Validation and application to 3D simulation of the primary break-up of a liquid jet*, International Journal of Multiphase Flow, 33 (2007), pp. 510–524.
- [8] R. Lebas, T. Ménard, P. A. Beau, A. Berlemont and F.-X. Demoulin, *Numerical simulation of primary break-up and atomization: DNS and modelling study*, International Journal of Multiphase Flow, 35 (2009), pp. 247–260.

Self organizing maps and clustering techniques to sectorize water supply networks based on energy criteria

E. CAMPBELL^b *, A.E. ILAYA-AYZA[†], J. IZQUIERDO[†],
and R. PÉREZ-GARCÍA[†]

(b, †) Fluing-Instituto de Matemática Multidisciplinar(IMM)- Universitat Politècnica de
València,
Camino de Vera SN, pc: 46015, Valencia, Spain.

November 30, 2014

1 Introduction

Water supply network (WSN)s segmentation or sectorization can be established as a technique oriented to enhance WSNs operative control. The technique implies the definition of areas (sectors or district metering areas) that can be partially isolated from the rest of the network. The isolation is carried out by installing new valves (closed valves) or cutting some pipes. Then, each of the resulting sectors is fed by a single (or few) entrance equipped with a flowmeter device so the inflow can be constantly monitored.

Since the 80's decade, when the first sectorization implementation at two British cities was reported [1], until now, the technique has become very popular, especially among Latin American and European water utilities.

Despite the benefits associated with the deployment of a sectorization layout, there are also some drawbacks that come along with these benefits. From the outset, the increasing of headloss due to pipe friction, which translates into pressure drop, can be mentioned as one of the most relevant. On

*encamgo1@upv.es

the other hand, a sectorization implementation requires the investment of economical resources, which in some context might be very limited. Finally, there is a risk of appearance of dead-end points where the water velocity is reduced drastically, allowing the development of microorganisms responsible for waterborne diseases.

From all above, it can be stated that a good sectorization layout has to balance a series of positive and negative aspects. The number of possible layouts may be considerably large, depending on the WSN extension and the looping configuration.

WSNs in the hydraulic simulation software EPANET are topologically built by nodes (connection between two or more pipes), and edges (pipes) which coincides with the topology of graphs. Such similarity allows the transformation of WSNs into graphs. When a WSN is transformed into a graph, the information contained in the pipes (*diameter, length, roughness, headloss, flow, etc.*) and nodes (*elevation, demand, geographical coordinates, emitters, etc.*) can be assigned to the links and the vertices of the graph, respectively. All this information can be seen as multidimensional vectors and thus, can be used for grouping purposes.

In this paper we propose the use of a combination of self organizing maps (SOM) and Hierarchical Clustering (HC) to take advantage of this multidimensionality in order to define sectors in real WSNs. In the next section, a brief description of SOM and HC is presented.

1.1 SOM, HC

SOMs are a type of neural network conceived to work by means of unsupervised training. The core idea behind them is to create a surface of unconnected nodes or neurons each one containing a random vector (*codebook*). The vectors of the data of study (input data or training vectors) are presented to the network several times and, at each step, they are compared to the *codebook* in the neurons. The neuron with the *codebook* closer to a given training vector is defined as the Best Matching Unit (BMU). The closeness between training vectors and *codebooks* is computed by means of the euclidean distance. Once a neuron is marked as BMU, its *codebook* is modified to be more similar to the entering vector. Then, the respective BMU influences the neighboring neurons according to a preset radio of influence (action). This makes that similar neurons end up together at the end of the training process, which is one of the features of the SOMs that makes

them very useful for classification and/or clustering purposes. One way to address the clustering problem over SOMs is through HC, which works based on the construction of clusters from a square dissimilarity matrix, following a scheme of hierarchy. It can be classified among the unsupervised machine learning methods and is broadly used in classification and pattern detection. The idea behind this method, is to build pairwise groups that successively merge with other groups until all the nodes of the graph are part of the same group (when a bottom-up strategy is followed), or groups, that successively subdivide themselves until all the clusters are formed by one single cluster or singleton (when a top-down strategy is followed). All the merges may be depicted through a dendrogram, which is a diagram in a X-Y plan, where the axis X contains all the observation or nodes, and the axis Y contains an altitude scale that establishes the value of each partition. One of the advantages of this technique in regard to other clustering techniques is the fact that it is not mandatory to initially set a number subdivision, and conversely, the subdivisions are based upon the topology of the data.

2 The Proposed Methodology

The methodology proposed in this work has three steps (see Figure 1): (1) in the first step the vectors of information or training vectors (*elevation, coordinates-x, coordinates-y*) storage in the nodes (n) of the WSN are represented in a 2-dimensional SOM. In the resulting SOM the nodes of the WSN that are more similar, are mapped either on the same neuron or on very close neurons. Then, (2) the neurons in the resulting map are clustered by means of HC and the outcome is represented in a dendrogram from where a partition that satisfies a size of sector restriction is selected. After this process, the WSN nodes of some sectors might appear unconnected to their main sector. In this case, the nodes are assigned as subsectors of the sector to where they are currently connected. If the diameter of the pipe that connects a sector to a subsector is large enough, the subsector can be considered as a new sector, otherwise, both of them are fused in one single sector. The pipes that connect nodes of different sectors are labeled as candidate pipes, which means that they can be selected as entrance of sector (with flowmeter) or as boundary valve. (3) Such definition is carried out through a multiobjective optimization process with Agent Swarm Optimization (ASO) [2]. The variable of decision is the state of the candidate pipes (open or closed), and

the objectives are: the minimization of the deviation of a resilience index (I_r) proposed by [3]; the minimization of the variation of headloss (h_L); the maximization of the variation of flow associated with leakages (real losses) (Q_L), and the minimization of the cost associated to the installation of the flowmeters (C_{fm}) and boundary valves (C_{cv}). It is important to note that the cost of a flowmeter is considerably higher than the cost of a boundary valve, therefore, the process tends to define more candidate pipes as boundary valves than flowmeters, which also allows water utilities to have more control over the leakages behavior at each sector.

$$\begin{aligned}
 &\text{Objective 1: } f(x) = \text{Min}(\Delta I_r) \\
 &\text{Objective 2: } f(x) = \text{Min}(\Delta h_L) \\
 &\text{Objective 3: } f(x) = \text{Max}(C_{\Delta Q_L}) \\
 &\text{Objective 4: } f(x) = \text{Min}(C_{cv} + C_{fm}) \\
 &\text{S.T } \forall n P \geq P_{min} \\
 &\text{Where P stands for nodal pressure}
 \end{aligned}$$



Figure 1: Flowchart of the process

3 Example of implementation

As example of implementation, a small section of the WSN of Managua City, Capital of Nicaragua, is sectorized using the methodology. Figure 2 shows the SOM obtained and its subdivision in three clusters.

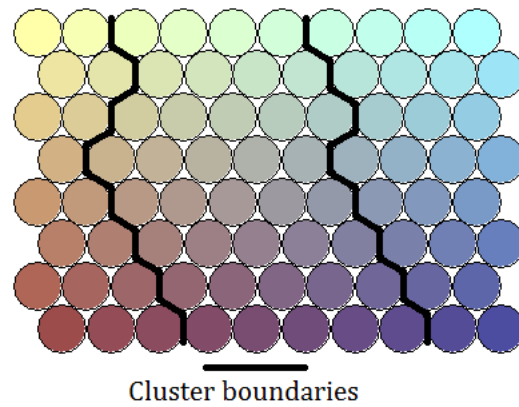


Figure 2: HC over the SOM of the example WSN

Figure 3 shows the final outcome obtained after implementing the methodology. It is important to note how some of the nodes of sector 3 appear in sector 1 and some nodes of sector 1 appear in sector 2, which is logical as the similarity between those nodes is very high. The diameter of the pipes that connect sectors 2 and 1 to their respective subsectors are very small, therefore, those subsectors are merged with the sectors to which they are currently connected.

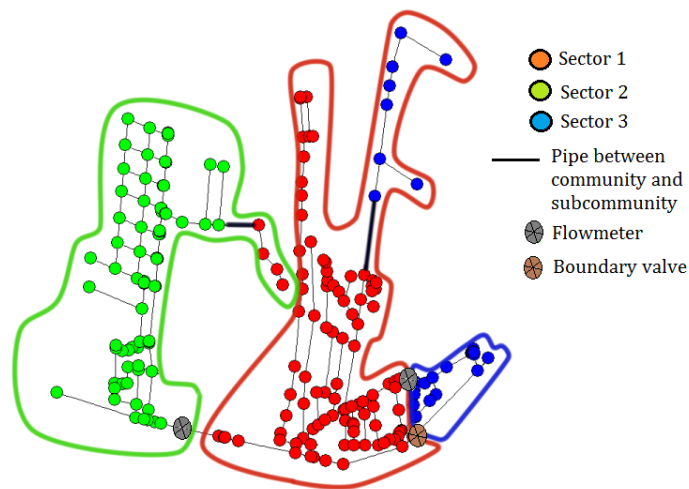


Figure 3: Sectorization layout obtained

4 Conclusion

This paper shows the applicability of clustering by means of a combination of SOMs and HC to identify sectors in WSNs. The methodology presented has as advantage the fact that the number of sectors, in which the network has to be subdivided, does not requires to be predefined. The use of optimization through ASO allows the identification of the entrances of each sector in a way that the negative impact (from an operative and economical perspective) associated to the deployment of the sectorization layout is minimized.

References

- [1] Malcom Farley. Are there alternatives to DMA? *Asian Water*, 26(10):12–18, 2010.
- [2] Idel Montalvo, Joaquín Izquierdo, Rafael Pérez-García, Manuel Herrera. Water distribution system computer-aided design by agent swarm optimization *Computer-Aided Civil and Infrastructure Engineering*, 29:433–448, 2014.
- [3] Ezio Todini. Looped water distribution networks design using a resilience index based heuristic approach *Urban Water*, 2(2):115–122, 2000.

Solving random heat problems in a semi-infinite bar with unhomogeneous boundary value conditions*

M.-C. Casabán[§], J.-C. Cortés[§] and L. Jódar[§]

(§) Instituto Universitario de Matemática Multidisciplinar,
Building 8G, access C, 2nd floor, Universitat Politècnica de València, Camino de Vera s/n,
46022 Valencia, Spain

macabar@imm.upv.es; jccortes@imm.upv.es; ljodar@imm.upv.es;

November 28, 2014

1 Introduction

The analysis of heat conduction involves modelling both temperature and heat flow. In practice, these quantities depend on a number of physical properties of the materials which often are not known from a deterministic point of view. Apart from uncertainties due to measurement errors needed to build physical models, the above comments motivate the consideration of random approaches to modelling heat conduction in heterogeneous medium. Hence, the consideration of uncertainty leads to a random scenario treated in this work by random differential equations. For these type of equations, the so-called L_p -calculus constitutes an adequate framework to solve them [1, 2]. We are mainly interested in L_2 and L_4 -calculus, which are usually referred to as mean square (m.s.) and mean four (m.f.) calculus. The m.s. approach, developed for both the ordinary and partial differential problems, has two desirable properties. First, the m.s. solution coincides with the one

*This work has been partially supported by the Spanish Ministerio de Economía y Competitividad grant MTM2013-41765-P.

obtained in the deterministic case, that is, when the random data become deterministic. Secondly, if $X_n(t)$ represents an approximation of the exact solution, $X(t)$, in the m.s. sense, then the expectation, $E[X_n(t)]$, and the variance, $\text{Var}[X_n(t)]$, will converge to the exact values, $E[X(t)]$ and $\text{Var}[X(t)]$, respectively, for each t , see Theorems 4.2.1 and 4.3.1. of [1].

This work deals with the construction of reliable solutions of the random heat model:

$$w_t(x, t) = L w_{xx}(x, t), \quad x > 0, \quad t > 0, \tag{1}$$

$$w_x(0, t) = g(t; B), \quad t > 0, \tag{2}$$

$$w(x, 0) = f(x; A), \quad x > 0, \tag{3}$$

by extending to the random scenario the Fourier cosine transform. Let us consider the positive 4-random variable (r.v.) L independent of r.v.'s A and B and such as its absolute statistical moments, $E[|L|^n]$, behave as $\mathcal{O}(H^n)$, i.e., there exist a non-negative integer n_0 and positive constants M and H such that

$$E[|L|^n] \leq MH^n, \quad \forall n \geq n_0, \tag{4}$$

and we assume that realizations of r.v. L have a positive lower bound $\ell_1 > 0$ such that

$$L(\omega) \geq \ell_1 > 0, \quad \forall \omega \in \Omega. \tag{5}$$

Furthermore, the moment generating function of r.v. $-L$, denoted by $\Phi_{-L}(t)$, verifies

$$\Phi_{-L}(t) = E[e^{-tL}] \quad \text{is locally bounded about } t = 0. \tag{6}$$

The 4-stochastic processes (s.p.'s) $g(t; B)$ and $f(x; A)$ are described as functions that depend on a single r.v. The same results are available, but with more complicated notation, by considering functions with a finite degree of randomness ([1, p.37]). We assume that $g(t; B)$ is a m.f. continuous s.p., and $f(x; A)$ is a m.f. absolutely integrable s.p. verifying

$$f(x; A) \text{ is a m.f. continuous s.p. and } \int_0^\infty (\|f(x; A)\|_4)^2 dx < +\infty. \tag{7}$$

2 Random Fourier Cosine Transform and its operational calculus

We define the *random Fourier cosine transform* of a 2-s.p. $\{u(x) : x > 0\}$ m.s. locally integrable in $[0, \infty[$, and m.s. absolutely integrable in $[0, \infty[$, i.e.

$\int_0^\infty \|u(x)\|_2 dx < +\infty$, as the 2-s.p.'s well-defined

$$\mathfrak{F}_c [u(x)] (\xi) = F_c(\xi) = \int_0^\infty u(x) \cos(\xi x) dx, \quad \xi > 0. \quad (8)$$

Following the ideas of the deterministic inverse Fourier cosine transform, see [3, chap.2], we define the *random inverse Fourier cosine transform* of a 2-s.p. $F_s(\xi)$ (and $F_c(\xi)$) m.s. locally and m.s. absolutely integrable by the formulae

$$\mathfrak{F}_c^{-1} [F_c(\xi)] (x) = \frac{2}{\pi} \int_0^\infty F_c(\xi) \cos(\xi x) d\xi, \quad x > 0. \quad (9)$$

Let $t > 0$ and assume that r.v. L has a positive lower bound satisfying condition (5). Then it is verified the following statements on the gaussian s.p. $q(x; L) = \frac{1}{\sqrt{\pi t L}} e^{-x^2/4tL}$:

$$\mathfrak{F}_c [q(x; L)] (\xi) = e^{-L t \xi^2}; \quad (10)$$

$$q(x; L) \text{ is m.f. continuous and } \int_0^\infty (\|q(x; L)\|_4)^2 dx < +\infty. \quad (11)$$

Using the *random Fourier exponential transform* and their convolution properties [4], we can obtain the convolution formula for the random Fourier Cosine:

$$\mathfrak{F}_c [m(x)] (\xi) \mathfrak{F}_c [n(x)] (\xi) = \sqrt{\frac{\pi}{2}} \mathfrak{F}_c [(m_p * n_p)(x)] (\xi), \quad \xi > 0, \quad (12)$$

where, it is easy to show (see [5, sec. 7.4] for the corresponding deterministic result) that

$$(m_p * n_p)(x) = \frac{1}{\sqrt{2\pi}} \int_0^\infty m(\kappa) \{n(x + \kappa) + n(|x - \kappa|)\} d\kappa, \quad x \geq 0, \quad (13)$$

for a $m(x)$ and $n(x)$ m.f. continuous s.p.'s defined on $[0, \infty[$ with $m_p(x), n_p(x)$ their even extension s.p.'s on the real line verifying $\int_0^\infty (\|m(x)\|_4)^2 dx < +\infty$ and $\int_0^\infty (\|n(x)\|_4)^2 dx < +\infty$, respectively.

3 Random heat problem with second kind boundary condition

Let us consider the auxiliary problem

$$u_t(x, t) = L u_{xx}(x, t), \quad x > 0, \quad t > 0, \tag{14}$$

$$u_x(0, t) = 0, \quad t > 0, \tag{15}$$

$$u(x, 0) = f(x; A), \quad x > 0, \tag{16}$$

and note that if $u(x, t)$ is a solution 2-s.p. of (14)–(16), and $v(x, t)$ is a solution 2-s.p. of the problem

$$v_t(x, t) = L v_{xx}(x, t), \quad x > 0, \quad t > 0, \tag{17}$$

$$v_x(0, t) = g(t; B), \quad t > 0, \tag{18}$$

$$v(x, 0) = 0, \quad x > 0, \tag{19}$$

then, by linearity: $w(x, t) = u(x, t) + v(x, t)$ is a solution 2-s.p. of problem (1)–(3). As problem (17)–(19) was solved in [6], we focus our attention on problem (14)–(16). Let us assume that problem (14)–(16) admits a solution 2-s.p. $u(x, t)$ m.s. locally and m.s. absolutely integrable, and let us denote $\mathfrak{F}_c[u(\cdot, t)](\xi) = \mathcal{U}(t)(\xi)$, $\xi > 0$, what means that $u(x, t)$ is regarded as a s.p. of the active variable x , for fixed $t > 0$. By applying the random Fourier cosine transform to the right-hand side of equation (14) and using the property $\mathfrak{F}_c[u''(x)](\xi) = -u'(0) - \xi^2 \mathfrak{F}_c[u(x)](\xi)$, $\xi > 0$ (see [6, Theorem 1]) together with condition (15), it follows that

$$\mathfrak{F}_c[u_{xx}(\cdot, t)](\xi) = -u_x(0, t) - \xi^2 \mathfrak{F}_c[u(\cdot, t)](\xi) = -\xi^2 \mathcal{U}(t)(\xi). \tag{20}$$

Applying the random Fourier cosine transform to the left-hand side of (14) and from Lemma 2 of [6], it follows that

$$\mathfrak{F}_c[u_t(\cdot, t)](\xi) = \frac{d}{dt} (\mathcal{U}(t)(\xi)). \tag{21}$$

Also from (16) one gets

$$\mathfrak{F}_c[u(\cdot, 0)](\xi) = \mathcal{U}(0)(\xi) = \mathfrak{F}_c[f(\cdot; A)](\xi) = F_c(\xi; A). \tag{22}$$

By linearity and (20)–(22) one gets the transformed random ordinary differential problem

$$\left. \begin{aligned} \frac{d}{dt}(\mathcal{U}(t)(\xi)) &= -L \xi^2 \mathcal{U}(t)(\xi), \quad t > 0, \\ \mathcal{U}(0)(\xi) &= F_c(\xi; A) \end{aligned} \right\}. \tag{23}$$

Assuming that r.v. L satisfies (6) and $F_c(\xi; A)$ is a 4-s.p., by Theorem 8 of [7] the solution 2-s.p. of problem (23) is given by

$$\mathcal{U}(t)(\xi) = F_c(\xi; A) e^{-t\xi^2 L}. \tag{24}$$

Taking into account the previous exposition in section 2 (see expressions (10)–(13)), it follows that a solution 2-s.p of problem (14)–(16) is given by

$$\begin{aligned} u(x, t) &= \mathfrak{F}_c^{-1} [\mathcal{U}(t)(\xi)](x) = \mathfrak{F}_c^{-1} [F_c(\xi; A) e^{-t\xi^2 L}](x) \\ &= \mathfrak{F}_c^{-1} [\mathfrak{F}_c[f(x; A)](\xi) \mathfrak{F}_c[q(x; L)](\xi)](x) \\ &= \mathfrak{F}_c^{-1} \left[\sqrt{\frac{\pi}{2}} \mathfrak{F}_c[(f * q)(x; A, L)](\xi) \right](x) \\ &= \sqrt{\frac{\pi}{2}} (f * q)(x; A, L) \frac{1}{2} \int_0^\infty f(\kappa; A) \{q(x + \kappa; L) + q(|x - \kappa|; L)\} d\kappa \\ &= \frac{1}{2\sqrt{\pi t L}} \int_0^\infty f(\kappa; A) \left(e^{-(x+\kappa)^2/4tL} + e^{-(x-\kappa)^2/4tL} \right) d\kappa. \end{aligned} \tag{25}$$

Finally, taking into account the solution 2-s.p. found in [6] for the subproblem (17)–(19) and by the linearity of solution $w(x, t)$, one gets a solution 2-s.p. for the problem (1)–(3) given by

$$\begin{aligned} w(x, t) &= \frac{1}{2\sqrt{\pi t L}} \int_0^\infty f(\kappa; A) \left(e^{-(x+\kappa)^2/4tL} + e^{-(x-\kappa)^2/4tL} \right) d\kappa \\ &\quad + 2\sqrt{\frac{L}{\pi}} \int_0^{\sqrt{t}} g(t - \nu^2; B) e^{-(x/2\nu\sqrt{L})^2} d\nu, \quad x > 0, \quad t > 0. \end{aligned} \tag{26}$$

Example 1 Consider the problem (1)–(3):

$$\begin{aligned} w_t(x, t) &= L w_{xx}(x, t), \quad x > 0, \quad t > 0, \\ w_x(0, t) &= tB, \quad t > 0, \\ w(x, 0) &= 50 e^{-x A}, \quad x > 0, \end{aligned}$$

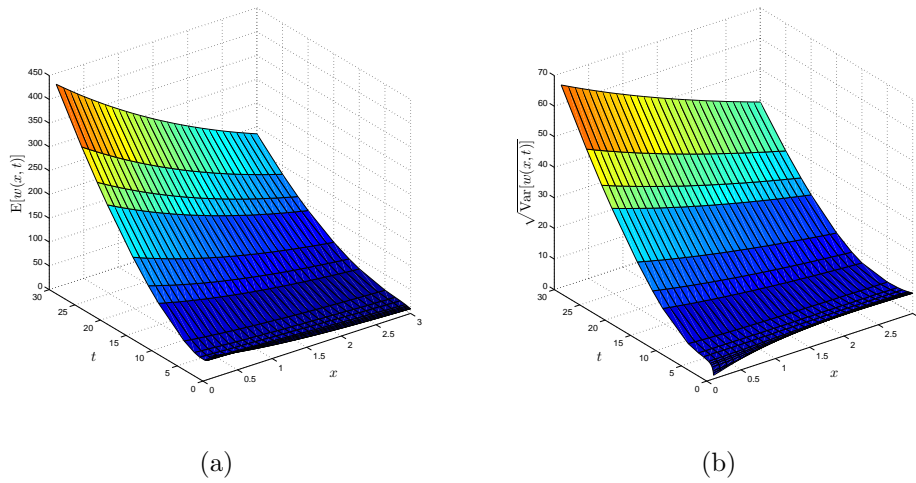


Figure 1: Three-dimensional approximations for the expectation $E[w(x, t)]$ (plot (a)), and, the standard deviation $\sqrt{\text{Var}[w(x, t)]}$ (plot (b)) on the spatial domain $x \in]0, 3]$ in the time interval $t \in [0, 30]$.

where the diffusion coefficient L follows a gamma distribution of parameters $\alpha = 2$ and $\beta = 1$ truncated on the interval $[0.5, 1]$, i.e., $L \sim \text{Trunc}[Ga(2, 1)]$; the spatial variation of the temperature at the left-end $x = 0$ is described by the s.p. $g(t; B) = t B$ where B is a gaussian r.v. of mean $\mu = 4$ and standard deviation $\sigma = 0.5$, i.e. $B \sim N(4; 0.5)$; the initial temperature is modelled by the s.p. $f(x; A) = 50 e^{-x A}$ being A a beta r.v. of parameters $\alpha = 3$ and $\beta = 2$, that is, $A \sim Be(3, 2)$. We assume that all r.v.'s, A , B and L are mutually independent.

Note that L is a positive \mathcal{L} -r.v. verifying conditions (4)–(5), and condition (6) since the moment generating function of r.v. $-L$:

$$\Phi_{-L}(t) = E[e^{-tL}] = \frac{2.87295 e^{-(1+t)}(-4 + 3e^{0.5(1+t)} - 2t + t e^{0.5(1+t)})}{(1+t)^2} \xrightarrow{t \rightarrow 0} 1,$$

is locally bounded about $t = 0$.

Since $E[B^4] = 3(0.5)^4 < \infty$ (see [1, p.26]), it verifies

$$\|g(t; B) - g(s; B)\|_4 = \|B\|_4 |t - s| \xrightarrow{t \rightarrow s} 0,$$

then the \mathcal{L} -s.p. $g(t; B)$ is m.f. continuous. Furthermore, the s.p. $f(x; A) = 50 e^{-x A}$ is m.f. absolutely integrable and verifies conditions given by (7).

Hence, all the hypotheses are satisfied and expression given by (26) is a solution 2-s.p. $w(x, t)$ of problem (1)–(3). Notice that the truncation of the intervals of integration for the computation of the expectation and variance in Figure 3 has been required.

References

- [1] T.T. Soong, Random Differential Equations in Science and Engineering. New York, Academic Press, 1973.
- [2] L. Villafuerte, C.A. Braumann, J.-C. Cortés and L. Jódar Random differential operational calculus: theory and applications *Comput. Math. Appl.*, 59:115–125, 2010.
- [3] A.J. Jerry, Integrals and Discrete Transformations with Applications and Error Analysis, *Pure and Applied Mathematics*, vol. 162, New York, Marcel Dekker, 1992.
- [4] M.-C. Casabán, R. Company, J.-C. Cortés and L. Jódar, Solving the random diffusion model in an infinite medium: A mean square approach, *Appl. Math. Model.* 38:5922–5933, 2014.
- [5] G.B. Folland, Fourier Analysis and Its Applications, Pacific Grove, Wadsworth & Brooks, 1992.
- [6] M.-C. Casabán, J.-C. Cortés, B. García-Mora and L. Jódar, Analytic-Numerical Solution of Random Boundary Value Heat Problems in a Semi-Infinite Bar, *Abstr. Appl. Anal.*, vol. 2013, Article ID 676372, 9 pages, 2013.
- [7] J.-C. Cortés, L. Jódar, M.-D. Roselló and L. Villafuerte, Solving initial and two-point boundary value linear random differential equations: A mean square approach, *Appl. Math. Comput.*, 219:2204–2211, 2012.

Country Risk Score forecasting for BRICS emerging markets by means of a diffusion model

R. Cervelló-Royo^b *, J.-C. Cortés[†], A. Sánchez-Sánchez[†],
F.-J. Santonja[‡] and R.-J. Villanueva[†].

(b) Department of Economics and Social Sciences, Universitat Politècnica de València, Spain

(†) Instituto Universitario de Matemática Multidisciplinar, Universitat Politècnica de València, Spain

(‡) Departamento de Estadística e Investigación Operativa, Universitat de València, Spain.

November 28, 2014

1 Introduction

Worldwide financial market instability has shaken confidence in global economies. This loss of confidence has a strong influence in the capital flows [1] and the investors' attitude towards some countries [2]. During last year, emerging market risk aversion has increased and investors have become more anxious over investment hotspots like the BRICS (Brazil, Russia, India, China and South Africa).

Brazil has turned to be considered most at risk from US tapering and political problems, China's slowdown has also exerted strong influence, Russia has also been affected by the rising tensions, etc. As a consequence, a lack of confidence has spread amongst some of those emerging markets leading to financial instability. In this respect, it would be interesting to use tools which allow to predict the trends and evolution of each country's confidence rating.

Country risk has become a topic of major concern for the international financial community over the last two decades. The importance of country

*e-mail: rocerro@esp.upv.es

ratings is underscored by the existence of several major country risk rating agencies [3]. In our study we use the CRS underscored by the Euromoney Agency [4], which evaluates the investment risk of countries across 15 criteria to determine the risks of default on a bond, losing direct investment or to global business relations, by surveying more than 400 international economists and other risk experts. CRS is calculated by assigning weights to these measures. CRS can represent a good indicator of the current situation of a country regarding measures of economic, political and financial risk in order to determine country risk ratings.

In this contribution, we present a diffusion model to study the dynamics of the CRS in five emerging markets (BRICS) which considers both the endogenous effect of each country policies and the contagion effect among them. Therefore, we consider that a crisis in one of the BRICS countries may focus investors attention on other BRICS countries with similar trends and general structural similarities and vulnerabilities [5].

Our objective is to predict the CRS trends over the next year, providing prediction tools for policy makers. Thus, with these tools, policy makers are able to design strategies, simulate different situations and analyze the effect of changes in order to improve the economic situation.

2 Modelling

This section is addressed to construct and justify the mathematical model used to describe the dynamics of the CRS of 5 BRICS countries which, according to previous exposition, provides a reliable economic indicator of the current situation of every country.

We propose a type-diffusion dynamic continuous mathematical model to study the evolution of the CRS of each BRICS country. Type-diffusion dynamic models have demonstrated to be powerful tools to study a wide range of applied problems in different areas including Economics and its related fields [6]. Although very complex models have been proposed based on this approach, all of them are mainly based on the following pattern:

$$\begin{aligned}
 x'_1(t) &= \alpha_1 x_1(t) + \beta_{14}(x_4(t) - x_1(t))x_1(t), \\
 x'_2(t) &= \alpha_2 x_2(t) + \beta_{21}(x_1(t) - x_2(t))x_2(t) + \beta_{24}(x_4(t) - x_2(t))x_2(t), \\
 x'_3(t) &= \alpha_3 x_3(t) + \beta_{34}(x_4(t) - x_3(t))x_3(t), \\
 x'_4(t) &= \alpha_4 x_4(t) + \beta_{41}(x_1(t) - x_4(t))x_4(t) \\
 &\quad + \beta_{42}(x_2(t) - x_4(t))x_4(t) + \beta_{43}(x_3(t) - x_4(t))x_4(t), \\
 x'_5(t) &= \alpha_5 x_5(t) + \beta_{54}(x_4(t) - x_5(t))x_5(t),
 \end{aligned}$$

where $x'_i(t)$ CRS of country i-th at the time instant t. As we shall see in detail later, our model considers:

- α measures the autonomous behaviour of each emerging country.
- β measures the diffusion behaviour; that is to say, the contagion between each pair of emerging countries.
- $x'_1(t)$ represents Brazil CRS. On Brazil, only China exerts influence.
- $x'_2(t)$ represents Russia CRS. On Russia; Brazil and China exert influence.
- $x'_3(t)$ represents India CRS. On India; only China exerts influence.
- $x'_4(t)$ represents China CRS. On China, Brazil, Russia and india exert influence.
- $x'_5(t)$ represents South Africa CRS. On South Africa, only China exerts influence.

The first one represents, through CRS, the autonomous economic behavior of each country and, the second one, the contagion effect for loss or gain of confidence both between and within clusters for each country. As we will see, in our case the resulting model based on 1 is non-linear.

3 Prediction

This section is divided into two parts. The first one, is devoted to model parameters estimation and CRS deterministic punctual forecasting over the next few months.

Parameter estimation

As we have previously pointed out, this subsection is firstly addressed to estimate the parameters of model. This task has been performed by fitting the model in the mean square sense to the available data. Computations have been carried out with Mathematica 8.0. The system of differential equations is numerically solved by taking as initial conditions the CRS data of January 9th, 2014 ($t = 0$) to April 28th, 2014 and the corresponding deterministic estimated parameters (Table 1 and Table 2).

Predictions

The obtained predictions after fitting the deterministic estimated parameters are represented in Figure 1. Red points represent data used in the adjustment, green points represent the data used for the validation and the blue line represents the model. The results showed that the Minimum difference corresponded to Russia on July 28th. The Maximum difference corresponded to China on June 23rd and the CRS average difference with respect to the predictions was 0.710775.

Country	CRS Initial condition by date							
	09/01/2014	27/01/2014	03/02/2014	10/02/2014	24/02/2014	03/03/2014	10/03/2014	
Brasil	59.33	58.89	58.89	58.78	58.78	58.77	58.77	
Russia	54.00	54.53	54.30	54.20	54.10	54.05	53.95	
India	51.00	50.74	50.70	50.65	50.60	50.59	50.58	
China	60.00	59.85	59.80	59.80	59.76	59.76	59.71	
South Africa	56.14	54.58	54.58	54.58	54.58	54.58	54.54	

Country	CRS Initial condition by date							
	17/03/2014	24/03/2014	31/03/2014	07/04/2014	14/04/2014	21/04/2014	28/04/2014	
Brasil	58.70	58.65	58.43	58.92	58.92	58.92	58.92	
Russia	53.91	53.80	53.64	50.48	50.48	50.48	50.48	
India	50.58	50.62	50.67	50.02	50.02	50.02	50.02	
China	59.71	59.68	59.64	61.37	61.37	61.37	61.37	
South Africa	54.54	54.54	54.54	53.84	53.84	53.84	53.84	

Table 1: Initial conditions the CRS data from January 9th, 2014 to April 28th, 2014.

Deterministic adjustment parameters		
Autonomous behavior parameters	Diffusion parameters	
α_1 : -0.199625	β_{14} : 0.141783	β_{42} : 0.004307
α_2 : -0.011665	β_{21} : 0.000012	β_{43} : 0.136496
α_3 : -1.062670	β_{24} : 1.941E-6	β_{54} : 0.189374
α_4 : 1.494890	β_{34} : 0.107705	
α_5 : -1.138860	β_{41} : 0.086754	

Table 2: Deterministic adjustment parameters.

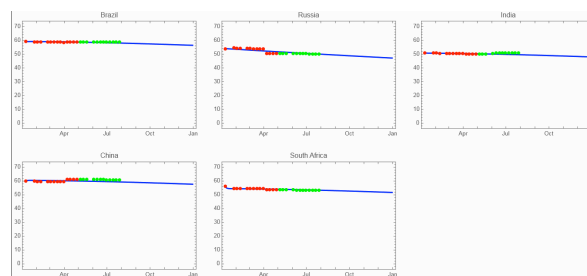


Figure 1: Scheme summarizing the techniques applied through this paper.

4 Conclusions

Worldwide financial crisis and changes in sovereign debts ratings have also affected emerging markets and their economies. Country Risk Score (CRS)

represents a measure of the level of confidence on each country and its economic health. The five BRICS countries have also invariably succumbed to increased risk this year, according to Euromoney's Country Risk Survey, in line with the global trend.

In this work, we present a diffusion model to study the dynamics of the Country Risk Score (CRS), for a total of 5 BRICS countries, which considers both the endogenous effect of each country politics and the contagion effect among them. Using data of CRS, we fit the model with the data estimating unknown autonomous behavior and transmission parameters.

The proposed dynamic diffusion model for the CRS of the 5 BRICS countries, depicts quite well the evolution of the CRS for most of them. As we can check in our results, over next month horizons a downward trend in the CRS dynamics should be noted for almost all BRICS countries in the next year.

Acknowledgments

This work has been partially supported by the Ministerio de Economía y Competitividad grant MTM2013-41765-P.

References

- [1] Fernández-Arias E, and Montiel PJ. The surge of capital inflows to developing countries: an analytical overview *World Bank Economic Review*, 10(1):51–77, 1996.
- [2] Dornbusch R, Park YC, and Claessens S. Contagion: understanding how it spreads *World Bank Research Observer*, 15(2):177–197, 2000.
- [3] Hoti S, and McAleer M. An empirical assessment of country risk rating and associated models *Journal of Economic Surveys*, 18(4):540–588, 2004.
- [4] Euromoney. <http://www.euromoney.com/poll/10683/PollsAndAwards/Country-Risk.html>. Accessed Oct, 18th 2014.
- [5] Ahluwalia P. Discriminating contagion: An alternative explanation of contagious currency crises in emerging markets *IMF Working Paper WP/00/14*, 2000.
- [6] Frambach RT. An integrated model of organizational adoption and diffusion of innovations *European Journal of Marketing*, 27(5):22–41, 1993.

A Mathematical Model of Bone Remodeling with Delays

B. M. Chen-Charpentier^b *; and I. Diakite[†]

(^b) Department of Mathematics, University of Texas at Arlington,
Arlington, TX 76019-0408,

([†]) Harvard Medical School, Harvard University,
Boston, MA 2115

November 28, 2014

1 Introduction

In vertebrates, the skeleton formed by bones provides support and protection to all other organs. Bone tissue is constantly being destroyed and reconstructed. Bone remodeling is a life-long process where mature bone tissue is removed from the skeleton (bone resorption) and new bone tissue is formed (ossification or new bone formation). This regeneration allows the bone to heal itself, for example in the case of fractures, and to adapt to stresses caused by normal activity that produce micro-damage.. The study of these processes is of great importance especially to be able to understand and cure bone diseases such as osteoporosis and myeloma [1]. There are two types of cells that are mainly in charge of the reconstruction, osteoclasts and osteoblasts [6]. An imbalance in the regulation of bone remodeling's two sub-processes results in many metabolic bone diseases, such as osteoporosis. The destruction and reconstruction of bone tissue is a periodic process that involves groups of cells working together in a basic multicellular unit (BMU). Spatial movement inside the BMU is small so models based on ordinary differential equations

*e-mail: bmchen@uta.edu

can be used. There are delays present due to the time it takes signals to be produce and transmitted and for cells to react to them. Bone remodeling is a very complicated process and not all mechanisms are known or completely understood.

It is known that there are two main groups of cells: osteoclasts and osteoblasts. Osteoclasts consist of precursor cells, active cells and dead cells. Osteoblasts consist of responding cells, active cells, differentiated cells (osteocytes and bone lining cells) and dead cells. There is a series of hormones and other signaling factors that control these processes including RANK, RANKL, OPG, vitamin D, calcitonin and estrogen, among others. For reviews of the factors involved see [7, 2, 3] and the references cited there.

There are several mathematical models of bone remodeling. They all involve simplifications. Some of these are those of Komarova et al., 2003, [4], Lemaire et al., 2004, [5] and Rattanakul et al., 2011, [8]. Lemaire et a. mention that they introduced a delay in their model but that the delay necessary to obtain a periodic solution was about two months, too large to be realistic. Several extensions of the model in [8] have included delays, for example, [9], but they involve four equations included the one for bone cells. Here we will work with Komarova’s model since it is the simplest involving only three equations and also has periodic solutions in the absence of delays for certain values of the parameters.

2 Mathematical model

Komarova et al.’s model involves only three types of cells explicitly, osteoclasts, osteoblasts and bone tissue. The model is

$$\frac{du_1}{dt} = \alpha_1 u_1^{\gamma_{11}} u_2^{\gamma_{21}} - \beta_1 u_1 \tag{1}$$

$$\frac{du_2}{dt} = \alpha_2 u_1^{\gamma_{12}} u_2^{\gamma_{22}} - \beta_2 u_2, \tag{2}$$

with u_1 and u_2 the density of osteoclasts and osteoblasts; α_1 and α_2 the differentiation rate of the osteoclast and osteoblast precursors; β_i the speed of the cell degradation process for $i = 1, 2$. The coefficients γ_{11} and γ_{22} describe the effectiveness of autocrine signaling, and γ_{21} and γ_{12} that of the paracrine signaling, which are regulated by the RANK, RANKL, OPG, TGF β and other factors. In particular, γ_{21} is the inhibition of osteoclast production due to osteoblasts, and γ_{12} is the osteoclast stimulation of osteoblast production.

All parameters are positive with the exception of γ_{21} .
 The equation for bone mass is

$$\frac{dz}{dt} = -k_1 \max\{u_1 - \bar{u}_1, 0\} + k_2 \max\{u_2 - \bar{u}_2, 0\}, \quad (3)$$

where z is total bone mass, $k_i, i = 1, 2$ are the normalized activities of bone resorption and formation, and \bar{u}_1 and \bar{u}_2 are the steady states for osteoclasts and osteoblasts, respectively.

In the bone reconstruction process there are several delays present since it takes time for the signals to travel, to be absorbed into the cells and for the cells to be affected. The largest delays are for the paracrine effects since they involve both osteoclasts and osteoblasts. We will consider a model with two delays, τ_1 and τ_2 , in the influence term of osteoclasts on osteoblasts and viceversa. More delays could be added but these two produce the desired behavior as explained later. By adding these two delays to system (1) and (2) we obtain the following system of delay differential equations (DDE's)

$$\frac{du_1(t)}{dt} = \alpha_1 u_1(t)^{\gamma_{11}} u_2(t - \tau_1)^{\gamma_{21}} - \beta_1 u_1(t) \quad (4)$$

$$\frac{du_2(t)}{dt} = \alpha_2 u_1(t - \tau_2)^{\gamma_{12}} u_2(t)^{\gamma_{22}} - \beta_2 u_2(t), \quad (5)$$

and same equation (3) for the bone mass.

In this paper we investigate numerically the existence of periodic solutions with delays. As mentioned above, Komarova's model has periodic for certain values of the parameters and we show that the delays, even very small ones, eliminate the periodic solutions. We also show that for values of the parameters for which there are no periodic solutions without delays, there are values of the delays that will produce periodic solutions. By starting with values of the parameters for which the original non-delay model has a stable focus, by increasing the delays it is possible to obtain periodic solutions. The values of the delays necessarily depend on the other parameters of the model. Numerical examples illustrate these points. These solutions are important because of their periodicity under the effects of biologically existing delays.

References

- [1] B.P. Ayati, C.M. Edwards, G.F. Webb and J.P. Wikswo, *A mathematical model of bone remodeling dynamics for normal bone cell populations and myeloma bone disease*, Biology Direct (2010), 5:28
- [2] J. C. Crockett, M. J. Rogers, F. P. Coxon, L. J. Hocking, M. H. Helfrich, Bone remodelling at a glance, Journal of Cell Science 124 (2011) 991-998
- [3] E. F. Eriksen, Cellular mechanisms of bone remodeling, Rev. Endocr. Metab. Disord. 11 (2010) 219-227
- [4] S.V. Komarova, R.J. Smith, S.J. Dixon, S.M. Sims, L.M. Wahl, *Mathematical model predicts a critical role for osteoclast autocrine regulation in the control of bone remodeling*, Bone 33(2), (2003) 206–2015.
- [5] V. Lemaire, F.L. Tobin, L.D. Greller, C.R. Cho, L.J. Suva, *Modeling the interactions between osteoblast and osteoclast activities in bone remodeling*, J. Theoretical Biology 229(3), (2004) 293–309.
- [6] T.J. Martin, K.W. Ng, *Mechanisms by which cells of the osteoblast lineage control osteoclast formation and activity*, J. Cell. Biochem. 56 (3), (1994) 357–366.
- [7] L. J. Raggatt, N. C. Partridge, Cellular and Molecular Mechanisms of Bone Remodeling, J. Biol. Chem. 285 (2010) 25103-25108
- [8] C. Rattanakul, Y. Lenbury, et al., *Modeling of bone formation and resorption mediated by parathyroid hormone: response to estrogen/PTH therapy*, Biosystems 70 (1), (2003) 55–72.
- [9] C. Rattanakul, S. Rattanamongkonkul, *Effect of calcitonin on bone formation and resorption: mathematical modeling approach*, Int. J. Mathl. Mod. Meth. Appl. Sci., 5 (8), (2011) 1363–1371.

Transforming American call option problem preserving qualitative properties of solution

R. Company*, V.N. Egorova†, and L. Jódar‡

(*) (†) (‡) Universitat Politècnica de València,
Camino de Vera s/n, 46022 Valencia, Spain

November 28, 2014

1 Introduction

In this chapter a finite difference scheme for the valuation of the price of American call options is proposed. American call option problem is shown as the following moving free boundary PDE, (see [3], for instance)

$$\frac{\partial C}{\partial \tau} = \frac{1}{2}\sigma^2 S^2 \frac{\partial^2 C}{\partial S^2} + (r-q)S \frac{\partial C}{\partial S} - rC, \quad 0 < S < B(\tau), \quad 0 < \tau \leq T, \quad (1)$$

together with the boundary and initial conditions

$$\frac{\partial C}{\partial S}(B(\tau), \tau) = 1, \quad C(B(\tau), \tau) = B(\tau) - E, \quad C(0, \tau) = 0, \quad (2)$$

$$C(S, 0) = \max(S - E, 0), \quad B(0) = \max\left\{\frac{r}{q}E, E\right\}. \quad (3)$$

where $\tau = T - t$ denotes the time to maturity T , S is the asset's price. $C(S, \tau)$ is the option price, $B(\tau)$ is the unknown early exercise boundary. The positive parameters appearing in (1) are the volatility σ , the risk free interest rate r , the continuous dividend yield q and the strike price E .

*e-mail: rcompany@imm.upv.es

†e-mail: egorova.vn@gmail.com

‡e-mail: ljodar@imm.upv.es

2 Front-Fixing method

Let us consider the dimensionless transformation (see [1], [4])

$$c(x, \tau) = \frac{C(S, \tau)}{E}, \quad S_f(\tau) = \frac{B(\tau)}{E}, \quad x = \ln \frac{B(\tau)}{S}. \quad (4)$$

Under transformation (4) the problem (1) - (3) can be rewritten in normalized form

$$\frac{\partial c}{\partial \tau} = \frac{1}{2} \sigma^2 \frac{\partial^2 c}{\partial x^2} - \left(r - q - \frac{\sigma^2}{2} + \frac{S'_f}{S_f} \right) \frac{\partial c}{\partial x} - rc, \quad x > 0, \quad 0 < \tau \leq T, \quad (5)$$

with new boundary and initial conditions

$$c(x, 0) = \max \left(\frac{r}{q} e^{-x} - 1, 0 \right), \quad S_f(0) = \max \left\{ 1, \frac{r}{q} \right\}. \quad (6)$$

$$\frac{\partial c}{\partial x}(0, \tau) = -S_f(\tau), \quad c(0, \tau) = S_f(\tau) - 1, \quad \lim_{x \rightarrow \infty} c(x, \tau) = 0, \quad (7)$$

Following the ideas of [4] and in order to solve the numerical difficulties derived from the discretization at the numerical boundary, we assume that (5) holds true at $x = 0$,

$$\frac{\sigma^2}{2} \frac{\partial^2 c}{\partial x^2}(0^+, \tau) - \left(q + \frac{\sigma^2}{2} \right) S_f(\tau) + r = 0. \quad (8)$$

The equation (5) is a non-linear differential equation on the domain $(0, \infty) \times (0, T]$. In order to solve numerically problem (5)-(7), one has to consider a bounded numerical domain. Let us introduce x_{\max} for large values of x in (7). Then the problem (5)-(7) can be studied on the fixed domain $[0, x_{\max}] \times (0, T]$.

3 Finite-difference method

In order to construct numerical solution the computational domain is covered by an uniform grid of $M + 2$ space points and N time levels with respective stepsizes h and k

$$h = \frac{x_{\max}}{M + 1}, \quad k = \frac{T}{N}, \quad (9)$$

$$x_j = hj, \quad j = 0, \dots, M + 1, \quad \tau^n = kn, \quad n = 0, \dots, N. \quad (10)$$

The approximate value of $c(x, \tau)$ at the point x_j and time τ^n is denoted by $c_j^n \approx c(x_j, \tau^n)$ and the approximate value of the free boundary is denoted by $S_f^n \approx S_f(\tau^n)$. Then a forward two-time level and centred in a space explicit scheme is constructed for internal spacial nodes as follows

$$\frac{c_j^{n+1} - c_j^n}{k} = \frac{1}{2} \sigma^2 \frac{c_{j-1}^n - 2c_j^n + c_{j+1}^n}{h^2} - \left(r - q - \frac{\sigma^2}{2} + \frac{S_f^{n+1} - S_f^n}{kS_f^n} \right) \frac{c_{j+1}^n - c_{j-1}^n}{2h} - r c_j^n. \quad (11)$$

The second order discretization of the boundary conditions (7) and (8) together with the scheme (11) for $j = 1$ allow to obtain the following explicit formula for the time evolution of the free boundary

$$S_f^{n+1} = d^n S_f^n = \frac{ac_0^n + bc_1^n + fc_2^n + \frac{c_2^n - c_0^n}{2h} - \alpha}{\frac{c_2^n - c_0^n}{2h} - \beta S_f^n} S_f^n, \quad n \geq 1. \quad (12)$$

4 Properties of the numerical solution

The next result shows that numerical scheme (11)-(12) preserves properties of the theoretical solution, (see [2]) as increasing in time free boundary and positivity and monotonicity of the option price.

Theorem 1. Let $\{c_j^n, S_f^n\}$ be the numerical solution of scheme (11) for a transformed American call option problem (5) and let d^n be defined by (12). Then under the following conditions

$$h < \frac{\sigma^2}{\left| r - q - \frac{\sigma^2}{2} \right|}, \quad k < \frac{h^2}{\sigma^2 + rh^2}, \quad \sigma^2 \neq 6q, \quad (13)$$

the numerical scheme (11) guarantees the following properties of the numerical solution:

1. $S_f^N \geq S_f^{N-1} \geq \dots \geq S_f^0 > 0$;
2. $c_0^n \geq c_1^n \geq \dots \geq c_{M+1}^n \geq 0$ for each fixed $n = 0, \dots, N$.
3. The scheme (11) is stable with respect to the norm $\|\cdot\|_\infty$;

Table 1: Comparison of the computational efficiency for the problem.

Asset Price	True Value	FDP	FDE	FF
40	0.002792	0.0025	0.0025	0.0028
80	3.041536	3.0414	3.0415	3.0414
120	24.564972	24.5654	24.5655	24.5644
	RMSE	6.4217-4	5.8822-4	3.5593-4
	CPU-time, sec	37.130	15.760	6.813

- The numerical solution computed by the scheme is consistent of order $O(h^2, k)$ with the equation (5) and boundary conditions (2), (8).

In order to compare computational efficiency, we consider the problem with the parameters:

$$r = 0.03, \quad q = 0.03, \quad \sigma = 0.4, \quad T = 0.5, \quad E = 100. \quad (14)$$

Since exact values are not known, the results of the binomial method with large steps (15000) are used for "True Value". FDP stands for the Crank-Nicolson finite-difference method with projected SOR iteration to impose the free boundary condition. FDE stands for the Crank-Nicolson finite difference method with elimination-back substitution. FF stands for the proposed explicit finite difference method combined with the front-fixing transformation with stepsizes $h = 10^{-3}$ and $k = 6.25 \cdot 10^{-6}$.

From the results presented in Table 1 we can conclude that the proposed method is competitive and effective, since it produces the similar error (RMSE) with smaller computational time (CPU).

5 Conclusion

A front-fixing method is applied to American call option with dividends pricing problem. An explicit finite difference scheme is constructed for numerical solution. Proposed method preserves very important qualitative properties of the solution such as positivity and monotonicity. The method is conditionally stable and consistent with the second order in space and the first order in time.

6 Acknowledgements

This work has been partially supported by the European Union in the FP7-PEOPLE-2012-ITN program under Grant Agreement Number 304617 (FP7 Marie Curie Action, Project Multi-ITN STRIKE-Novel Methods in Computational Finance) and the Ministerio de Economía y Competitividad Spanish grant MTM2013-41765-P.

References

- [1] Company, R., Egorova, V.N., Jódar, L.: Solving American Option Pricing Models by the Front Fixing Method: Numerical Analysis and Computing. *Abstract and Applied Analysis*, Vol. 2014, Article ID 146745, 9 pages, 2014. <http://dx.doi.org/10.1155/2014/146745>
- [2] Kim, I.J.: The Analytic Valuation of American Options. *The Review of Financial Studies*, 1990, Vol. 3, num. 4, p. 547-572.
- [3] Wilmott, P., Howison, S., Dewynne, J.: *The Mathematics of Financial Derivatives*. Cambridge University, Press, Cambridge, UK, 1995.
- [4] Wu, L., Kwok, Y.-K. A Front-Fixing method for the Valuation of American Option. *The Journal of Financial Engineering*, 1997, Vol. 6, N2, p. 83-97.

The use of Random Variable Transformations for solving nonlinear random differential equations

M.-C. Casabán^b, J.-C. Cortés^b *, A. Navarro-Quiles^b,
J.V. Romero^b, M.-D.Roselló^b and R.-J. Villanueva^b.

(^b) Instituto Universitario de Matemática Multidisciplinar,
Universitat Politècnica de València, Spain.

November 28, 2014

1 Introduction

In this paper we solve random homogeneous Riccati-type differential equations of the form

$$\left. \begin{aligned} \dot{X}(t) &= CX(t) + D(X(t))^2, & t \geq 0, \\ X(0) &= X_0, \end{aligned} \right\} \quad (1)$$

where all the input parameters X_0 , C and D are assumed to be absolutely continuous random variables (r.v.'s) defined on a common probability space, $(\Omega, \mathfrak{F}, \mathbb{P})$.

Equations of this type appear in Epidemiology to model the spread of an illness, or in Economy to describe the diffusion of new technologies, etc. Specifically, the so-called SI-type epidemiological model fits to pattern (1).

Solving random differential equations means to compute the solution stochastic process together with its main statistical functions, such as the mean and the variance. The computation of the first probability density

*e-mail: jccortes@imm.upv.es

function (1-p.d.f.) is a major challenge. It permits to have a full statistical description of the solution in every time instant t . In this work, we deal with the computation of the 1-p.d.f. of the solution $X(t)$ of problem (1).

Below, we state some results that will be useful to compute the 1-p.d.f. They come from the application of the Random Variable Transformation method (R.V.T.) in its general form, Theorem 4 [1].

Firstly, in the case that U is an absolutely continuous real r.v. defined on a probability space $(\Omega, \mathfrak{F}, \mathbb{P})$, with p.d.f. $f_U(u)$ and such that $U(\omega) \neq 0$ for all $\omega \in \Omega$, one can prove that the p.d.f. $f_V(v)$ of the inverse transformation $V = \frac{1}{U}$ is given by

$$f_V(v) = \frac{1}{v^2} f_U\left(\frac{1}{v}\right). \quad (2)$$

Second, if $\mathbf{U} = (U_1, U_2)$ is an absolutely continuous real random vector defined on a probability space $(\Omega, \mathfrak{F}, \mathbb{P})$, with joint p.d.f. $f_{\mathbf{U}}(u_1, u_2)$ such that $U_1(\omega) \neq 0$ for all $\omega \in \Omega$, one can demonstrate that the joint p.d.f. $f_{\mathbf{V}}(v_1, v_2)$ of the inverse-opposite transformation $\mathbf{V} = (V_1, V_2) = (\frac{1}{U_1}, -U_2)$ is given by

$$f_{\mathbf{V}}(v_1, v_2) = \frac{1}{(v_1)^2} f_{\mathbf{U}}\left(\frac{1}{v_1}, -v_2\right). \quad (3)$$

Finally, if $\mathbf{U} = (U_1, U_2, U_3)$ is an absolutely continuous real random vector defined on a probability space $(\Omega, \mathfrak{F}, \mathbb{P})$, with joint p.d.f. $f_{\mathbf{U}}(u_1, u_2, u_3)$, such that $U_1(\omega) \neq 0$ for all $\omega \in \Omega$, then it is easy to prove that the joint p.d.f. $f_{\mathbf{V}}(v_1, v_2, v_3)$ of the inverse-opposite-opposite transformation $\mathbf{V} = (V_1, V_2, V_3) = (1/U_1, -U_2, -U_3)$ is given by

$$f_{\mathbf{V}}(v_1, v_2, v_3) = \frac{1}{(v_1)^2} f_{\mathbf{U}}\left(\frac{1}{v_1}, -v_2, -v_3\right). \quad (4)$$

2 Solving the Homogeneous Riccati Differential Equation

To compute of the 1-p.d.f. of the solution s.p. of i.v.p. (1) in function of the p.d.f. of the input parameters X_0 , C and D , it is convenient to distinguish the cases collected in Table 1. As initial value problem (i.v.p.) (1) can be easily linearized, we will take advantage of the results obtained recently by some of the authors in [1] to conduct the analysis.

	I.V.P.(1)		
	CASE	random	deterministic
$\mathbb{P} [\{\omega \in \Omega : D(\omega) = 0\}] = 1$	I.1	X_0	c
	I.2	C	x_0
	I.3	(X_0, C)	
$\mathbb{P} [\{\omega \in \Omega : C(\omega) = 0\}] = 1$	II.1	X_0	d
	II.2	D	x_0
	II.3	(X_0, D)	
$\mathbb{P} [\{\omega \in \Omega : D(\omega) \neq 0 \neq C(\omega)\}] = 1$	III.1	X_0	(d, c)
	III.2	D	(x_0, c)
	III.3	C	(x_0, d)
	III.4	(X_0, D)	c
	III.5	(X_0, C)	d
	III.6	(D, C)	x_0
	III.7	(X_0, D, C)	

Table 1: List of different cases to solve the i.v.p. (1) from a probabilistic point of view.

With this aim, notice that making the change of variable

$$Z(t) = \frac{1}{X(t)},$$

using the following identification of the random inputs

$$Z_0 = \frac{1}{X_0}, \quad B = -D, \quad A = -C,$$

and taking $t_0 = 0$, the nonlinear i.v.p. (1) can be transformed into the linear i.v.p.

$$\left. \begin{aligned} \dot{Z}(t) &= AZ(t) + B, \quad t \geq t_0, \\ Z(t_0) &= Z_0. \end{aligned} \right\} \tag{5}$$

Now, we are ready to apply the results, obtained in [1] for the i.v.p. (5), to the Riccati differential equation (1). Notice that Cases I.1-I.3 corresponding to the situation where nonlinear coefficient $D = 0$ with probability one, can be omitted in our analysis since they correspond to the linear differential equation taking $B = 0$ with probability one.

For illustrative purposes, in the following we will deal with the cases listed in Table 2.

	I.V.P.(1)		
	CASE	random	deterministic
$\mathbb{P}[\{\omega \in \Omega : C(\omega) = 0\}] = 1$	II.1 II.3	X_0 (X_0, D)	d
$\mathbb{P}[\{\omega \in \Omega : D(\omega) \neq 0 \neq C(\omega)\}] = 1$	III.7	(X_0, D, C)	

Table 2: List of different cases analysed to solve the i.v.p. (1).

2.1 CASE II.1

Let us assume that X_0 is a r.v. with p.d.f. $f_{X_0}(x_0)$ and $d \in \mathbb{R} - \{0\}$. This situation corresponds to the following particular case of the linear i.v.p. (5)

$$\left. \begin{aligned} \dot{Z}(t) &= b, \\ Z(0) &= Z_0, \end{aligned} \right\} Z_0 = \frac{1}{X_0}, \quad b = -d. \tag{6}$$

Fixing $t \geq 0$ and applying formula (59) of [1], we get

$$f_Z(z) = f_{Z_0}(z - bt). \tag{7}$$

In order to express (7) in terms of the data, we take into account (6) and apply (2) to $U = X_0, V = Z_0$. This yields

$$f_Z(z) = f_{Z_0}(z + dt) = \frac{1}{(z + dt)^2} f_{X_0}\left(\frac{1}{z + dt}\right). \tag{8}$$

Considering the relationship between the solutions of i.v.p.'s (1) and (5), $X(t) = 1/Z(t)$, and applying (2) to $U = Z$ and $V = X$, with $Z = Z(t)$ and $X = X(t)$, for each $t \geq 0$, one gets

$$f_X(x) = \frac{1}{x^2} f_Z\left(\frac{1}{x}\right) = \frac{1}{x^2} \frac{1}{\left(\frac{1}{x} + dt\right)^2} f_{X_0}\left(\frac{1}{\frac{1}{x} + dt}\right).$$

Since $t \geq 0$ is arbitrary, this expression represents the 1-p.d.f. of the solution s.p. $X(t)$ of the i.v.p. (1)

$$f_1(x, t) = \frac{1}{(1 + dtx)^2} f_{X_0}\left(\frac{x}{1 + dtx}\right), \quad \forall t \geq 0. \tag{9}$$

2.2 CASE II.3

Now, we assume that both, the initial condition X_0 , and the nonlinear coefficient D , are r.v.'s with joint p.d.f. $f_{X_0,D}(x_0, d)$. This corresponds to the following particular case of the linear i.v.p. (5)

$$\left. \begin{aligned} \dot{Z}(t) &= B, \\ Z(0) &= Z_0, \end{aligned} \right\} \quad Z_0 = \frac{1}{X_0}, \quad B = -D. \tag{10}$$

Fixing $t \geq 0$ and applying formula (74) of [1], we get

$$f_Z(z) = \frac{1}{t} \int_{\mathcal{D}(Z_0)} f_{Z_0,B} \left(\xi, \frac{z - \xi}{t} \right) d\xi, \tag{11}$$

where $\mathcal{D}(Z_0)$ denotes the domain of r.v. $Z_0 = 1/X_0$. Now, we apply (3) to $U_1 = X_0$, $U_2 = D$, $V_1 = Z_0$ and $V_2 = B$ to express (11) in terms of the joint p.d.f. $f_{X_0,D}(x_0, d)$.

$$f_Z(z) = \frac{1}{t} \int_{\mathcal{D}(1/X_0)} \frac{1}{\xi^2} f_{X_0,D} \left(\frac{1}{\xi}, \frac{\xi - z}{t} \right) d\xi.$$

For each $t > 0$, considering $X = 1/Z$ and applying (2) one gets

$$f_X(x) = \frac{1}{x^2} f_Z \left(\frac{1}{x} \right) = \frac{1}{x^2 t} \int_{\mathcal{D}(1/X_0)} \frac{1}{\xi^2} f_{X_0,D} \left(\frac{1}{\xi}, \frac{x\xi - 1}{tx} \right) d\xi.$$

Since $t \geq 0$, in this case the 1-p.d.f. of the solution s.p. $X(t)$ of the i.v.p. (1) is given by

$$f_1(x, t) = \frac{1}{x^2 t} \int_{\mathcal{D}(1/X_0)} \frac{1}{\xi^2} f_{X_0,D} \left(\frac{1}{\xi}, \frac{x\xi - 1}{tx} \right) d\xi, \quad t > 0. \tag{12}$$

If $t = 0$, as $X(0) = X_0$ the 1-p.d.f. is just the marginal p.d.f. of the joint p.d.f. $f_{X_0,D}(x_0, d)$, hence

$$f_1(x, 0) = \int_{\mathcal{D}(D)} f_{X_0,D}(x_0, d) dd.$$

2.3 CASE III.7

In this last case, we assume that all the inputs (X_0, D, C) are r.v.'s whose joint p.d.f. is $f_{X_0, D, C}(x_0, d, c)$. This corresponds to the following particular case of linear i.v.p. (5)

$$\left. \begin{aligned} \dot{Z}(t) &= AZ(t) + B, \\ Z(0) &= Z_0, \end{aligned} \right\} Z_0 = \frac{1}{X_0}, \quad B = -D, \quad A = -C. \quad (13)$$

Fixing $t \geq 0$ and apply formula (157) of [1], we get

$$\begin{aligned} f_Z(z) &= \int_{\mathcal{D}(Z_3)} \int_{\mathcal{D}(Z_2)} f_{Z_0, B, A} \left(-\frac{(z - \xi - \eta)\eta}{\xi}, -\frac{\eta}{t} \ln \left(\frac{-\xi}{\eta} \right), \frac{1}{t} \ln \left(\frac{-\xi}{\eta} \right) \right) \\ &\times \frac{|\eta|}{\xi^2 t^2} \left| \ln \left(\frac{-\xi}{\eta} \right) \right| d\xi d\eta, \end{aligned}$$

where $Z_2 = B/Ae^{At}$ and $Z_3 = -B/A$.

Now, we will express $f_Z(z)$ as a function of (X_0, D, C) by applying (4) to $U_1 = X_0, U_2 = D, U_3 = C, V_1 = Z_0, V_2 = B$ and $V_3 = A$,

$$\begin{aligned} f_Z(z) &= \int_{\mathcal{D}(Z_3)} \int_{\mathcal{D}(Z_2)} f_{X_0, D, C} \left(-\frac{\xi}{(z - \xi - \eta)\eta}, \frac{\eta}{t} \ln \left(\frac{-\xi}{\eta} \right), -\frac{1}{t} \ln \left(\frac{-\xi}{\eta} \right) \right) \\ &\times \frac{|\eta|}{\eta^2 (z - \xi - \eta)^2 t^2} \left| \ln \left(\frac{-\xi}{\eta} \right) \right| d\xi d\eta. \end{aligned}$$

For each $t > 0$, considering $X = 1/Z$ and applying (2) one gets

$$\begin{aligned} f_X(x) &= \frac{1}{x^2} f_Z \left(\frac{1}{x} \right) \\ &= \int_{\mathcal{D}(Z_3)} \int_{\mathcal{D}(Z_2)} f_{X_0, D, C} \left(-\frac{x\xi}{(1 - x\xi - x\eta)\eta}, \frac{\eta}{t} \ln \left(\frac{-\xi}{\eta} \right), -\frac{1}{t} \ln \left(\frac{-\xi}{\eta} \right) \right) \\ &\times \frac{|\eta|}{\eta^2 (1 - x\xi - x\eta)^2 t^2} \left| \ln \left(\frac{-\xi}{\eta} \right) \right| d\xi d\eta. \end{aligned}$$

As $Z_2 = e^{At}B/A = D/(Ce^{Ct})$ and $Z_3 = -D/C$, the 1-p.d.f. of the solution s.p. $X(t)$ to the i.v.p. (1) is given by

$$\begin{aligned} f_1(x, t) &= \int_{\mathcal{D}(-\frac{D}{C})} \int_{\mathcal{D}(\frac{D}{Ce^{Ct}})} f_{X_0, D, C} \left(\frac{-x\xi}{(1 - x\xi - x\eta)\eta}, \frac{\eta}{t} \ln \left(\frac{-\xi}{\eta} \right), -\frac{1}{t} \ln \left(\frac{-\xi}{\eta} \right) \right) \\ &\times \frac{|\eta|}{\eta^2 (1 - x\xi - x\eta)^2 t^2} \left| \ln \left(\frac{-\xi}{\eta} \right) \right| d\xi d\eta. \end{aligned}$$

If $t = 0$, as $X(0) = X_0$, the 1-p.d.f. of $X(t)$ is the (D, C) -marginal p.d.f. of $f_{X_0, D, C}(x_0, d, c)$

$$f_1(x, 0) = \int_{\mathcal{D}(D)} \int_{\mathcal{D}(C)} f_{X_0, D, C}(x_0, d, c) dd dc.$$

Acknowledgements

This work has been partially supported by the Ministerio de Economía y Competitividad grants MTM2013-41765-P and TRA2012-36932.

References

- [1] Casabán M.C., Cortés J.C., Romero J.V. and Roselló M.D., Determining the first probability density function of linear random initial value problems by the random variable transformation (r.v.t.) technique: A comprehensive study, *Abstract and Applied Analysis*, ID248512: 1–25, 2014.
- [2] Casabán, M.C., Cortés, J.C., Romero, J.V. and Roselló, M.D., Probabilistic solution of random homogeneous linear second-order difference equations. *Applied Mathematics Letters*, 34: 27–32, 2014.
- [3] Casella, G. and Berger, R.L., Statistical Inference. *Brooks/Cole* New York, 2002.
- [4] Kegan, B. and West, R.W., Modeling the simple epidemic with deterministic differential equations and random initial conditions, *Mathematical Biosciences*. 195: 179–193, 2005.
- [5] Soong, T.T., Random Differential Equations in Science and Engineering. *Academic Press* New York, 1973.

A five-point stencil scheme for pricing American options under Bates model

M. Fakharany^b *; R. Company^b, and L. Jódar^b

(^b) Instituto de Matemática Multidisciplinar, Universitat Politècnica de València,
Camino de Vera s/n, 46022 Valencia, Spain.

November 28, 2014

1 Introduction

The Bates model is considered one of the versatile models that describes the behavior of the currency options. In Bates model both the stochastic volatility and jump-diffusion are incorporated leading to the following partial integro-differential equation (PIDE) for European option case [1]

$$L(U) = \frac{\partial U}{\partial \tau} - \frac{1}{2}\nu S^2 \frac{\partial^2 U}{\partial S^2} - \rho\sigma\nu S \frac{\partial^2 U}{\partial S \partial \nu} - \frac{1}{2}\nu\sigma^2 \frac{\partial^2 U}{\partial \nu^2} - (r - q - \lambda\xi)S \frac{\partial U}{\partial S} - \kappa(\theta - \nu) \frac{\partial U}{\partial \nu} + (r + \lambda)U - \lambda \int_0^\infty U(S\eta, \nu, \tau) f(\eta) d\eta = 0, \quad (1)$$

$$f(\eta) = \frac{1}{\sqrt{2\pi\hat{\sigma}\eta}} \exp\left[-\frac{(\ln \eta - \mu)^2}{2\hat{\sigma}^2}\right], \quad (2)$$

where $U(S, \nu, \tau)$ is the unknown option price depending on the underlying S , the variance ν and the time to maturity $\tau = T - t$. The parameter r is the risk free interest rate, q is the continuous dividend yield, η is the jump amplitude of the jump diffusion process, λ is the jump intensity, ξ is the expected relative jump size, μ is the mean of the jump and $\hat{\sigma}$ is the standard

*fakharany@aucegypt.edu

deviation. Beside that the parameter κ is the mean reversion rate, θ is the long-run variance, σ is the volatility of the variance ν and ρ is the Wiener correlation parameter. The problem is subjected to the initial condition given by the payoff function $g_1(S, \nu)$ for call options

$$U(S, \nu, 0) = g_1(S, \nu) = \max\{S - E, 0\}. \tag{3}$$

The set of equations that describes the American option under Bates model is called the linear complementarity problem (LCP) such that

$$L(U) \geq 0, \quad U \geq g_1, \quad L(U)(U - g_1) = 0, \tag{4}$$

associated with the following boundary conditions

$$U(0, \nu, \tau) = g_1(0, \nu), \quad \lim_{S \rightarrow \infty} U(S, \nu, \tau) = \lim_{S \rightarrow \infty} g_1(S, \nu), \quad \lim_{\nu \rightarrow \infty} \frac{\partial U}{\partial \nu}(S, \nu, \tau) = 0. \tag{5}$$

2 The modified LCP

The presence of the mixed derivative in (1) causes several technical numerical problems; the discretization of this term yields negative coefficients which lead to oscillation in the numerical solution. Also these terms delay the convergence of the solution and inaccurate values [2]. In order to tackle this problem, authors in [3] used seven-point stencil scheme with restrictions on the coefficients.

Here in this work, the mixed derivative has been removed using the canonical transformation for second order linear PDE, see [5]. With the following change of variables

$$x = \sigma \tilde{\rho} \ln S, \quad y = mx - \nu, \quad W(x, y, \tau) = e^{(r+\lambda)\tau} U(S, \nu, \tau), \tag{6}$$

where $\tilde{\rho} = \sqrt{1 - \rho^2}$, the transformed operator for $L(U)$ is given by

$$\mathcal{L}(W) = \frac{\partial W}{\partial \tau} - \frac{\tilde{\rho}^2 \nu \sigma^2}{2} \left(\frac{\partial^2 W}{\partial x^2} + \frac{\partial^2 W}{\partial y^2} \right) - \hat{\delta} \frac{\partial W}{\partial x} - \tilde{\delta} \frac{\partial W}{\partial y} - I(W), \tag{7}$$

with

$$I(W) = \lambda \int_0^\infty W(x + \sigma \tilde{\rho} \ln \eta, \quad y + \rho \sigma \ln \eta, \tau) f(\eta) d\eta, \tag{8}$$

where

$$\hat{\delta} = \sigma\tilde{\rho}(\hat{\xi} - \frac{\nu}{2}), \tilde{\delta} = \sigma\rho(\hat{\xi} - \frac{\nu}{2}) - \kappa(\theta - \nu) \text{ and } \hat{\xi} = r - q - \lambda\xi. \quad (9)$$

Next, we change the variables of the integral part for matching its discretization with the differential part. Using $\phi = x + \sigma\tilde{\rho} \ln \eta$ into (8), we have

$$I(W) = \frac{\lambda}{\sqrt{2\pi\hat{\sigma}\tilde{\rho}\sigma}} \int_{-\infty}^{\infty} W(\phi, y + m(\phi - x), \tau) \exp \left[\frac{-1}{\hat{\sigma}^2} \left(\frac{\phi - x}{\sigma\tilde{\rho}} - \mu \right)^2 \right] d\phi. \quad (10)$$

Based on the transformation (6), the LCP (4) has the following form

$$\mathcal{L}(W) = \frac{\partial V}{\partial \tau} - D(W) - I(W) \geq 0, \quad V \geq g_2, \quad \mathcal{L}(W)(W - g_2) = 0, \quad (11)$$

where,

$$D \equiv \frac{\tilde{\rho}^2 \nu \sigma^2}{2} \left(\frac{\partial^2}{\partial x^2} + \frac{\partial^2}{\partial y^2} \right) + \hat{\delta} \frac{\partial}{\partial x} + \tilde{\delta} \frac{\partial}{\partial y}, \quad (12)$$

and

$$g_2(x, y) = W(x, y, 0) = \max\{e^{\frac{x}{\sigma\tilde{\rho}}} - E, 0\}.$$

The transformed boundary conditions are

$$\lim_{x \rightarrow \pm\infty} W(x, y, \tau) = \lim_{x \rightarrow \pm\infty} g_2(x, y), \quad \frac{\partial W}{\partial y} = 0, \quad mx - y \rightarrow \infty. \quad (13)$$

In light of (6), the rectangular boundary domain in $S - \nu$ plane $[S_1, S_2] \times [\nu_1, \nu_2]$, is converted into a rhomboid.

3 The numerical scheme

By using uniform mesh points (x_i, y_j) such that $x_i = a + ih, 0 \leq i \leq N_x$ and $y_j = y_0 + j|m|h, i \leq j \leq N_x + i$ where $h = (b - a)/N_x, a = \sigma\tilde{\rho} \ln S_1, b = \sigma\tilde{\rho} \ln S_2, y_0 = ma - \nu_2$ and $N_y = (\nu_2 - \nu_1)/|m|h$, the rhomboid computational domain is discretized. The first and second spatial derivatives of the operator D are approximated by the central finite difference, obtaining

$$D(W_{i,j}) \approx \check{B}(i, j)W_{i-1,j} + \check{C}(i, j)W_{i,j-1} - B(i, j)W_{i,j} + \hat{B}(i, j)W_{i+1,j} + \hat{C}(i, j)W_{i,j+1}, \quad (14)$$

where

$$\begin{aligned} \check{B}(i, j) &= \left(\frac{\check{\rho}^2 \sigma^2 \nu_{i,j}}{2h^2} - \frac{\check{\delta}_{i,j}}{2h} \right), \quad B(i, j) = \frac{\sigma^2 \nu_{i,j}}{m^2 h^2}, \quad \hat{B}(i, j) = \left(\frac{\check{\rho}^2 \sigma^2 \nu_{i,j}}{2h^2} + \frac{\check{\delta}_{i,j}}{2h} \right) \\ \check{C}(i, j) &= \left(\frac{\check{\rho}^2 \sigma^2 \nu_{i,j}}{2m^2 h^2} - \frac{\check{\delta}_{i,j}}{2|m|h} \right), \quad \hat{C}(i, j) = \left(\frac{\check{\rho}^2 \sigma^2 \nu_{i,j}}{2m^2 h^2} + \frac{\check{\delta}_{i,j}}{2|m|h} \right). \end{aligned} \quad (15)$$

Note that based on the transformation (6), we have a five-point stencil scheme for the operator D consequently, the computational cost will be minimized. Beside that there is no restriction on the coefficients.

The integral part is approximated using four-point open type formula which gives a high accuracy approximation, see[4]. Hence we have the following semi-discrete LCP

$$\frac{\partial \mathbf{W}}{\partial \tau} + A\mathbf{W} \geq 0, \quad \mathbf{W} \geq \mathbf{g}_2, \quad \left(\frac{\partial \mathbf{W}}{\partial \tau} + A\mathbf{W} \right)^T (\mathbf{W} - \mathbf{g}_2) = 0, \quad (16)$$

where A is a matrix of size $(N_x + 1)(N_y + 1) \times (N_x + 1)(N_y + 1)$ involving the differential and integral parts.

Finally, the time variable τ is discretized using the Rannacher scheme, such that the first four time levels are implemented using the implicit Euler while the rest of the time levels are obtained using Crank-Nicolson. The time variable is discretized in this manner to avoid the oscillation of the solution, see [3].

$$\tau^n = \begin{cases} \left(\frac{n}{2N_\tau} \right)^2 T, & n = 0, 1, 2, 3, \\ \left(\frac{n-2}{N_\tau-2} \right)^2 T, & n = 4, 5, \dots, N_\tau. \end{cases} \quad (17)$$

The time step size is given by $k_n = \tau^{n+1} - \tau^n$, $n = 0, 1, \dots, N_\tau - 1$. Hence we obtain the following sequence of LCPs

$$\begin{aligned} &LCP \left(I + k_n A, \mathbf{W}^{(n+1)}, \mathbf{W}^{(n)}, \mathbf{g}_2 \right), \quad n = 0, 1, 2, 3. \\ &LCP \left(I + \frac{1}{2} k_n A, \mathbf{W}^{(n+1)}, \left(I - \frac{1}{2} k_n A \right) \mathbf{W}^{(n)}, \mathbf{g}_2 \right), \quad n = 4, 5, \dots, N_\tau. \end{aligned} \quad (18)$$

The following example investigates the error for Bates model with negative correlation, the option prices are obtained using the **PSOR** method with the relaxation parameter $\omega = 1.5$.

Example Consider an American call option under Bates model with the following parameters $T = 0.5$, $E = 50$, $r = 0.06$, $q = 0.05$, $\theta = 0.05$, $\kappa = 2$,

$\sigma = 0.25$, $\hat{\sigma} = 0.7$, $\mu = -0.5$, $\lambda = 0.1$ and $\rho = -0.5$, the computational domain for $x \in [-1.5, 1.5]$ and $[\nu_1, \nu_2] = [0.1, 1]$. Table 1 shows the variation of the root mean square relative error (RMSRE) of the option value at $S = \{80, 90, 100, 110, 120\}$ for several values of domain discretizations (N_x, N_y, N_τ) . The reference values for the prices U are given in [3].

PSOR (N_x, N_y, N_τ)	RMSRE	CPU (sec)
(20, 10, 10)	0.2037	0.015
(60, 30, 25)	0.0871	0.217
(100, 50, 50)	0.0103	3.285
(130, 65, 75)	0.0078	15.458
(160, 80, 75)	0.0026	40.839

Acknowledgements

This work has been partially supported by the European Union in the FP7-PEOPLE-2012-ITN program under Grant Agreement Number 304617 (FP7 Marie Curie Action, Project Multi-ITN STRIKE-Novel Methods in Computational Finance) and the Ministerio de Economía y Competitividad Spanish grant MTM2013-41765-P.

References

- [1] D. S. Bates. Jumps and stochastic volatility: Exchange rate processes implicit Deutsche mark options, *Review Financial Studies*, vol. 9: 69—107, 1996.
- [2] R. Zvan, P. A. Forsyth, and K. R. Vetzal. Negative coefficients in two-factor option pricing models, *Journal of Computational Finance*, vol. 7: 37—73, 2003.
- [3] S. Salmi, J. Toivanen and L. Von Sydow. Iterative methods for pricing American options under the bates model, *Procedia Computer Science*, vol. 18: 1136—1144, 2013.
- [4] P. J. Davis, P. Rabinowitz, *Methods of Numerical Integration*, Second Edition, Academic Press, New York, USA, 1984.
- [5] P. R. Garabedian, *Partial Differential Equations*, AMS Chelsea Pubs. Co., 1998.

Cyclic coordinate descent in a class of bang-singular-bang problems

L. Bayón*, P. Fortuny Ayuso, J. A. Otero, P. M. Suárez, C. Tasis

Univ. of Oviedo. Department of Mathematics, E.P.I. Campus of Viesques,

Gijón, 33203, Spain.

November 28, 2014

1 Introduction

A continuous production process on a time interval, $[0, T]$, whose output has variable price $p(t)$ and whose production function is linear with respect to the consumption rate over time of the inputs, of limited availability, is posed as the maximization of a functional:

$$\int_0^T p(t)(f_1(t)z_1'(t) + \dots + f_n(t)z_n'(t))dt \quad (1)$$

with $z_i \in \{\widehat{C}^1[0, T] \mid z_i(0) = 0, z_i(T) = b_i\}$, with technical constraints for the consumption rate over time: $m_i \leq \dot{z}_i(t) \leq M_i, \forall i = 1, \dots, n$.

We abstract from this situation to tackle a general problem which studies a production process whose efficiency of production with respect to each input depends on time, on the stock of the various inputs, and on the consumption rate of other inputs. The main limitation will be the linearity of the functional with respect to consumption rates and stocks, which will imply that it is a bang-singular-bang optimal control problem. We propose an efficient method for finding the bang-singular-bang solution using a cyclic coordinate descent strategy combined with a suitable adaptation of the shooting method

*e-mail: bayon@uniovi.es

([2], and [1]). The corresponding boundary value problem derived from Pontryagin's Maximum Principle is solved without any initial guess regarding the structure of the solution.

The coordinate descent gives a convergent iterative method because of our assumptions, which are more general ([5]) than the usual ones ([3], [4]).

2 Statement of the variational problem

We consider the problem of maximizing the multidimensional functional

$$J(\mathbf{z}) = \int_0^T L(t, \mathbf{z}(t), \dot{\mathbf{z}}(t)) dt$$

with the integrand being

$$L(t, \mathbf{z}(t), \dot{\mathbf{z}}(t)) = \mathbf{z}^t A(t) \mathbf{z} + \mathbf{z}^t B(t) \dot{\mathbf{z}} + \dot{\mathbf{z}}^t C(t) \dot{\mathbf{z}} + \mathbf{s}(t)^t \cdot \dot{\mathbf{z}} + \mathbf{z}^t P \dot{\mathbf{z}} + \mathbf{r}(t)^t \cdot \mathbf{z}$$

on a suitable product $\mathbb{D} = \prod \mathbb{D}_i$ for

$$\mathbb{D}_i = \left\{ z_i \in \widehat{C}^1[0, T] \mid z_i(0) = 0, z_i(T) = b_i \text{ and } m_i \leq \dot{z}_i(t) \leq M_i \right\}$$

and where $A(t)$, $B(t)$, $C(t)$, $P(t)$, $r(t)$ and $s(t)$ are suitable matrices of continuous functions (not totally general).

3 Dimension one: the shooting method

The general case iterates over the one-dimensional one. To solve the latter, assume that all the components of \mathbf{z} and $\dot{\mathbf{z}}$ are fixed but the i -th one. Let $\mathbf{q} = (q_1, \dots, q_m) \in \mathbb{D}$ and write $L_{\mathbf{q}}^i(t, z_i, \dot{z}_i)$ as

$$L_{\mathbf{q}}^i := L(t, q_1(t), \dots, q_{i-1}(t), z_i, q_{i+1}(t), \dots, q_m(t), \dot{q}_1(t), \dots, \dot{z}_i, \dots, \dot{q}_m(t)).$$

We wish to solve the problem of maximizing the functional $J_{\mathbf{q}}^i : \mathbb{D}_i \rightarrow \mathbb{R}$

$$J_{\mathbf{q}}^i(z_i) := J(q_1, \dots, q_{i-1}, z_i, q_{i+1}, \dots, q_m) = \int_0^T L_{\mathbf{q}}^i(t, z_i(t), \dot{z}_i(t)) dt \quad (1)$$

on \mathbb{D}_i where one can write, for suitable functions:

$$L_{\mathbf{q}}^i(t, z_i, \dot{z}_i) = F_{\mathbf{q}}^i(t) + G_{\mathbf{q}}^i(t) z_i(t) + (H_{\mathbf{q}}^i(t) + P_{\mathbf{q}}^i(z_i)) \dot{z}_i(t).$$

Definition 1 The i -th efficiency function associated to $\mathbf{q} \in \mathbb{D}$ is:

$$\mathbb{Y}_{\mathbf{q}}^i(t) := \int_0^t G_{\mathbf{q}}^i(s)ds - H_{\mathbf{q}}^i(t)$$

Solutions of the optimization problem are characterized by

Theorem 1 Given $\mathbf{q} \in \mathbb{D}$, its i -th component $q_i(t)$ solves the optimization problem (1) for $J_{\mathbf{q}}^i$ if and only if there exists $k_i \in \mathbb{R}$ satisfying:

$$\mathbb{Y}_{\mathbf{q}}^i(t) \text{ is } \begin{cases} \leq k_i & \text{if } \dot{q}_i(t) = m_i \\ = k_i & \text{if } m_i < \dot{q}_i(t) < M_i \\ \geq k_i & \text{if } \dot{q}_i(t) = M_i \end{cases}$$

Hence, the one-dimensional problem is reduced to finding the i -th critical efficiency level. We prove that this can be done using an adaptation of the shooting method because the efficiency level is the zero of a continuous function, so that Bolzano’s Theorem applies.

4 General case: cyclic coordinate descent

The result for the general m -dimensional case is

Theorem 2 An admissible element $\mathbf{q} = (q_1, \dots, q_m) \in \mathbb{D}$, is a solution of problem (1), if and only if there exist $\{k_i\}_{i=1}^m \subset \mathbb{R}$ satisfying:

$$\mathbb{Y}_{\mathbf{q}}^i(t) \text{ is } \begin{cases} \leq k_i & \text{if } \dot{q}_i(t) = m_i \\ = k_i & \text{if } m_i < \dot{q}_i(t) < M_i \\ \geq k_i & \text{if } \dot{q}_i(t) = M_i \end{cases}$$

This theorem allows us to solve for each coordinate and then iterate (thus doing a “coordinate descent”). The compactness of the sets on which we work guarantees convergence.

5 Conclusions

We first solve, using techniques similar to the shooting method, the one-dimensional optimal control problem with a Lagrangian of the form:

$$L(t, z, \dot{z}) = F(t) + G(t)z(t) + (H(t) + P(z)) \dot{z}(t)$$

The shooting method in combination with Pontryagin's maximum principle and the theory of singular control provides the theoretical basis that has enabled us to construct an algorithm for solving the problem approximately and, in some cases, even analytically, despite the possible apparition of singular arcs of infinite order.

After tackling that one-dimensional problem, we show how we can also solve multidimensional problems whose Lagrangian is of the form (for specific types of matrices A, B, C and P):

$$L(t, \mathbf{z}(t), \dot{\mathbf{z}}(t)) = \mathbf{z}^t A(t) \mathbf{z} + \mathbf{z}^t B(t) \dot{\mathbf{z}} + \dot{\mathbf{z}}^t C(t) \dot{\mathbf{z}} + \mathbf{s}(t)^t \cdot \dot{\mathbf{z}} + \mathbf{z}^t P \dot{\mathbf{z}} + \mathbf{r}(t)^t \cdot \mathbf{z}$$

using the cyclical coordinate descent method.

References

- [1] M.S.Aronna, J.F. Bonnans and P. Martinon, *A Shooting Algorithm for Optimal Control Problems with Singular Arcs*, J. Optim. Theory Appl. 158 (2013), 419-459.
- [2] H. Maurer, *Numerical solution of singular control problems using multiple shooting techniques*, J. Optim. Theory Appl. 18(2) (1976), 235-257.
- [3] P. Tseng and D. Bertsekas, *Relaxation methods for problems with strictly convex costs and linear constraints*, Math. Oper. Res. 16(3) (1991), 462-481.
- [4] P. Tseng, *Convergence of a block coordinate descent method for nondifferentiable minimization*, J. Optim. Theory Appl. 109(3) (2001), 475-494.
- [5] L. Bayon, J.M. Grau, M.M. Ruiz and P.M. Suarez, *An application of the algorithm of the cyclic coordinate descent in multidimensional optimization problems with constrained speed*, Numerical Algorithms, 52(2) (2009), 129-149.

Effect of the numerical scheme resolution on quasi-2D simulation of an automotive radial turbine under highly pulsating flow

J. Galindo^b, H. Climent^b, A. Tiseira^b, and L.M. García-Cuevas^b *

(^b) CMT-Motores Térmicos, Universitat Politècnica de València, Valencia 46022, Spain.

November 28, 2014

1 Introduction

Automotive turbocharger turbines usually work under pulsating flow because of the sequential nature of engine breathing. However, existing turbine models are typically based on quasi-steady assumptions. In a previous work [?], a model where the volute is calculated in a quasi-2D scheme is presented. The objective of this work is to quantify and analyse the effect of the numerical resolution scheme used in the volute model. The conditions imposed upstream are isentropic pressure pulsations with different amplitude and frequency. The volute is computed using a finite volume approach considering the tangential and radial velocity components. The stator and rotor are assumed to be quasi-steady. In this work, different integration and spatial reconstruction schemes are explored. The spatial reconstruction is based on the MUSCL method with different slope limiters fulfilling the TVD criterion. The model results are assessed against 3D U-RANS calculations. The results show that, under low frequency pressure pulses, all the schemes lead to similar solutions. But, for high frequency pulsation the results can be very different depending upon the selected scheme. This may have an impact in noise emission predictions.

*e-mail: luiga12@mot.upv.es

2 Model description

The turbine models consists of the following parts:

- Fully one-dimensional elements for the turbine inlet and outlet, simulated with a finite-volume approach.
- A quasi-two-dimensional element for the volute, also simulated with a finite-volume approach, where source terms are added at each cell for the radial flow and the outlet is also connected to the inlet.
- Entropy-generating total enthalpy-conserving elements for the stator, coupled with a two-dimensional boundary elements model to get its outlet flow angle.
- An entropy-generating total-rothalpy element for the rotor.

The finite-volume elements are simulated using a density-based MUSCL approach to get second order total variation diminishing behaviour. 8 slope extrapolation limiters and four inter-cell fluxes models have been implemented and tested in this work, with varying degrees of aggressiveness, numerical diffusion and computational complexity. Also, three different classical explicit time-integration schemes have been used: first order Euler scheme, second order Heun's method and four-steps, fourth order Runge-Kutta method. The implementation exploits SIMD capabilities of common processors to produce the fastest results and, thus, the differences in simulation time are not only due to numerical complexity of the underlying algorithms, but also due to SIMD exploitability. The model is described in detail in [?].

3 Benchmark results

Figure 1 shows a comparison with experimental results of a totally one-dimensional model of the volute and a quasi-bidimensional volute with two different selections of schemes. The quasi-bidimensional volute produces better results, but there are also small differences between the two scheme sets.

Figure 2 shows the results of different combinations of schemes for two cases of which CFD results are available. Both cases use the same very high amplitude pressure pulse as a boundary conditions, but one of them is at low

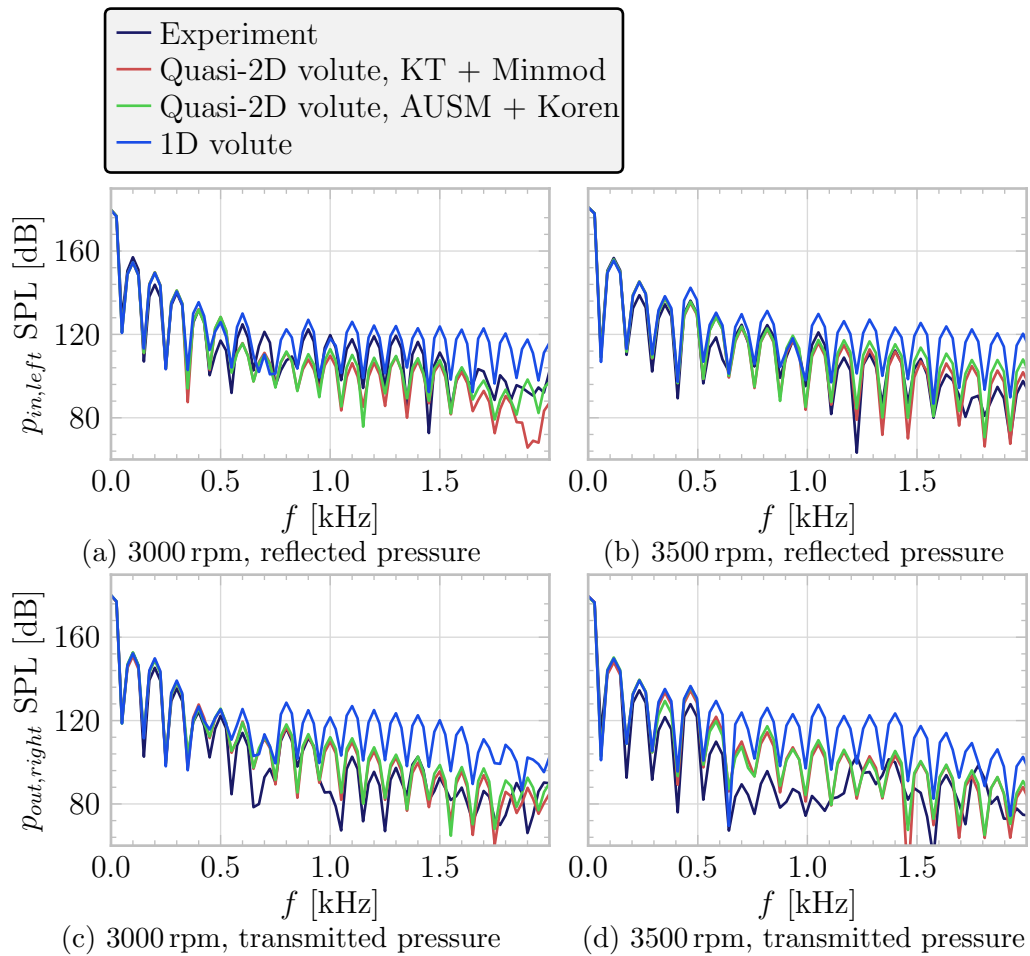


Figure 1: Model results using experimental data

frequency (130 Hz) and the other one is at a higher frequency (750 Hz). The graphics show the relative computational speed and the mass flow rate and power output amplitude errors. There are very little differences in error for the low frequency case, whereas the differences are more clear at high frequencies. Pareto optimality is achieved for a combination of the Kurganov and Tadmor central scheme or the Harten-Lax-Van Leer approximate Riemann solver coupled with the Minmod limiter, which also produces the fastest simulations. A second order time integration scheme appears to be enough to get good results, so higher and more time consuming schemes can be discarded.

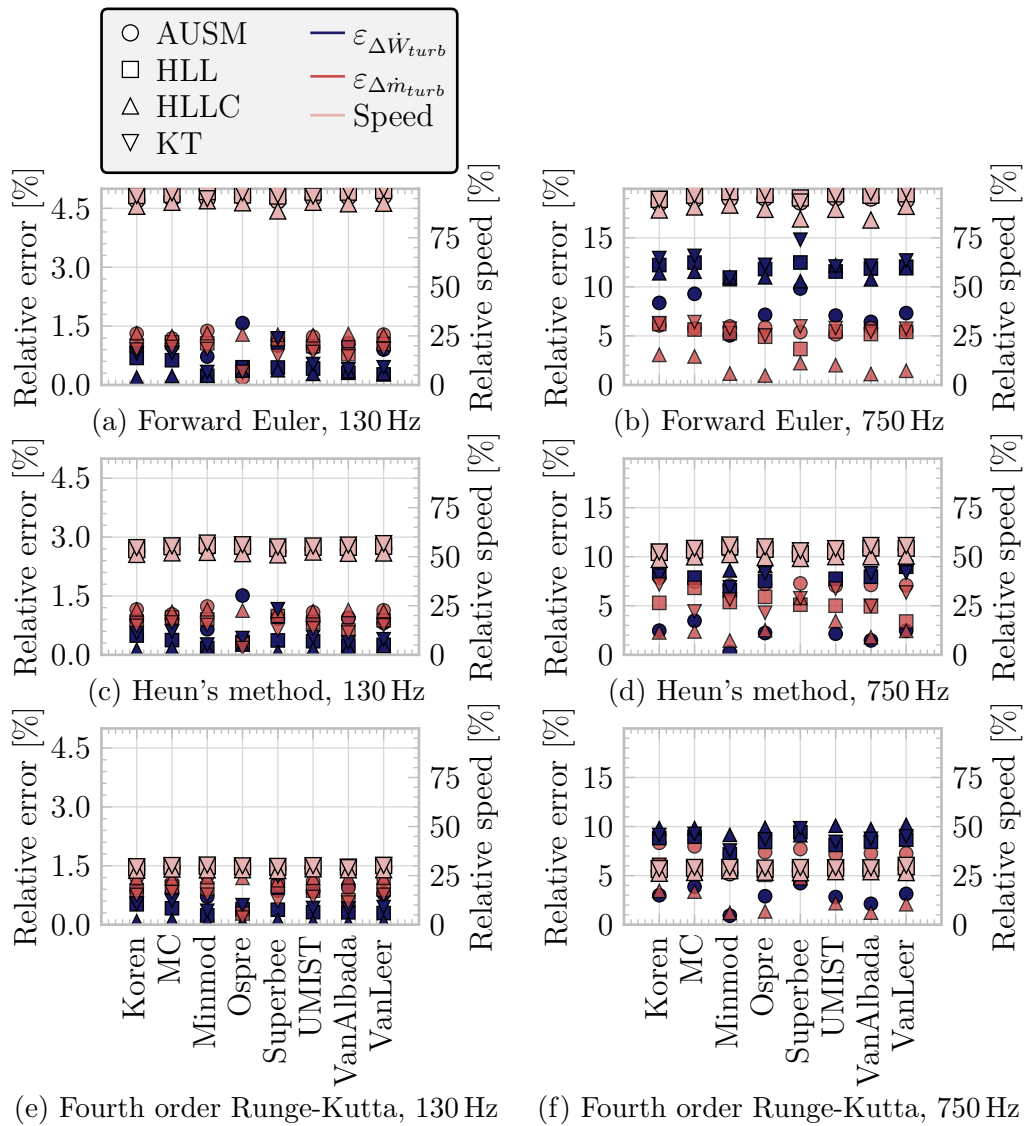


Figure 2: Solver test results

4 Conclusions

This work presents a study of the influence of several numerical schemes used in the quasi-bidimensional simulation of an automotive radial turbine, using several excitation frequencies for the boundary conditions. The model results

are compared with that of U-RANS simulations. The authors have found the following:

- The numerical error due to the discrete time integration is negligible for low frequencies due to the stiffness of the system and the usage of explicit time-integrators. At high frequencies, however, a second-order scheme is needed to produce the most accurate results. No appreciable improvements in the accuracy were found for a fourth order scheme: for a typical spatial mesh size of around 1 cm, the CFL condition renders the time-step low enough and the error is not bounded by the discrete time integration.
- The different inter-cell fluxes approximations and slope limiter functions have different degrees of numerical diffusion and computational cost, so an optimum selection can be performed:
 - At low frequencies, the differences between the different methods are negligible.
 - At high frequencies, Pareto optimality in model error is obtained using the Kurganov and Tadmor central scheme or the Harten-Lax-Van Leer approximate Riemann solver coupled with the Minmod limiter. This also produces the fastest results, with a computational speed-up of around 10 %.
- The optimum selection of schemes appears to give a couple of dB of extra accuracy against a bad selection for high frequencies.
- The authors expected higher computational cost differences between the schemes. The differences in vectorisation and SIMD usage and data locality between the different methods seemed to damp the expected variations in simulation speed. Future processors are expected to give different results, as new instruction sets and larger caches are added.

References

- [1] José Galindo Lucas, Andrés Tiseira Izaguirre, Pablo Fajardo, and Luis Miguel García-Cuevas. Development and validation of a radial variable geometry turbine model for transient pulsating flow applications. *Energy Conversion and Management*, 85(0):190 – 203, 2014.

An hybrid PSO optimized SVM–based model for predicting a successful growth cycle of the *Spirulina platensis* from experimental data in open raceway ponds

P.J. García Nieto^b * , E. García-Gonzalo^b,
J.R. Alonso Fernández[†], and C. Díaz-Muñiz[†]

(^b) Department of Mathematics, University of Oviedo,

Faculty of Sciences, C/ Calvo Sotelo s/n, 33007 Oviedo, Spain

([†]) Cantabrian Basin Authority, Spanish Ministry of Agriculture, Food and Environment,
Plaza de España 2, 33071 Oviedo, Spain.

November 28, 2014

Abstract

In this research work, a practical new hybrid model to predict the successful growth cycle of *Spirulina platensis* was proposed. The model was based on particle swarm optimization (PSO) in combination with support vector machines (SVM). This optimization mechanism involved kernel parameter setting in the SVM training procedure, which significantly influences the regression accuracy. PSO–SVM–based models were successfully used here to predict the *Chlorophyll a* (Chl-a) concentration (output variable) as a function of the following input variables: pH, optical density, oxygen concentration, nitrate concentration, phosphate concentration, salinity, water temperature and irradiance. Regression with three different kernels (linear, quadratic and RBF) was performed and determination coefficients of 0.94, 0.97, and 0.99, respectively, were obtained. Finally, conclusions of this study are exposed.

*e-mail: lato@orion.ciencias.uniovi.es (P.J. García Nieto)

1 Introduction

For the past two decades, research interests in different fields have been focus on *Spirulina platensis* as a consequence of its commercial importance as a source of protein, vitamins, essential amino acids, and fatty acids [1]. In this sense, to estimate the biomass production an often used parameter is Chl-a concentration. In this paper, Chl-a concentration was predicted from the other parameters [2] by applying support vector machines (SVMs) in combination with the Particle Swarm Optimization (PSO) technique [3]. In order to carry out the optimization mechanism corresponding to the kernel optimal hyperparameters setting in the SVM training, the particle swarm optimization (PSO) technique was used here with success. The PSO technique is a population-based search algorithm fundamented on the simulation of the bird flocking.

2 Materials and methods

2.1 Experimental dataset

In this study, *S. platensis* was cultivated in three open-channel shallow artificial ponds called raceway ponds and supplied by the American Type Culture Collection (ATCC). The total number of data processed was about 2340 values. Several variables were studied in detail in order to find the most beneficial values for a successful growth cycle of this alga. The eight input variables used in this innovative research work were [1, 2]: water temperature ($^{\circ}\text{C}$); irradiance (W/m^2); optical density (also called absorbance); pH values of the aqueous solution; nutrients (nitrates and phosphates) (mM); dissolved oxygen (DO) concentration (ppm); and salinity (ppt).

2.2 Support vector machine method (SVM)

Support vector machines (SVMs) are a set of related supervised learning methods used for classification and regression [4, 5]. The SVMs were originally developed for classification, and were later generalized to solve regression problems. This last method is called *support vector regression* (SVR). To sum up, if we use a SVM to solve a regression problem for data that is not linearly separable, then we need to first choose a kernel and relevant parameters that can be expected to map

the nonlinearly separable data into a feature space where it is linearly separable.

2.3 The Particle Swarm Optimization (PSO) algorithm

The algorithm Particle Swarm Optimization (PSO) is an evolutionary optimization algorithm [6], where a population of particles or proposed solutions evolves with each iteration, moving towards the optimal solution of the problem. PSO optimizes a problem by having a population of candidate solutions, here dubbed particles, and moving these particles around in the search-space according to simple mathematical formulae over the particle's position and velocity. Each particle's movement is influenced by its local best known position but, is also guided toward the best known positions in the search-space, which are updated as better positions are found by other *particles*. This is expected to move the swarm toward the best solutions.

2.4 The goodness-of-fit

A coefficient of determination value of 1.0 indicates that the regression curve fits the data perfectly. Furthermore, it is well known that the SVM techniques are strongly dependent on the SVM hyperparameters: the regularization factor C ; the hyperparameter that defines the ϵ -insensitive tube (allowable error); and σ that represents the kernel parameter if a radial basis function (RBF) is chosen. In this research work, the Particle Swarm Optimization (PSO) technique was applied. Therefore, a hybrid PSO-SVM-based model was applied to predict the *Chlorophyll a* (output variable) from the other eight remaining variables indicated above with success. In this way, 10-fold cross-validation was used. The regression modeling has been performed with SVR- ϵ using the LIBSVM library [7]. The searching in the parameter space has been made taking into account that the SVM algorithm changes its results significantly when its parameters increase or decrease a power of 10. We have worked with powers of ten and the searched parameters have been the exponents using the following 3-dimensional search space: $[-2, 2] \times [-4, 0] \times [-1, 3]$. The bounds (initial ranges) of the space of solutions used in PSO technique are shown in Table 1. The number of particles used has been 20. The

Table 1: Initial ranges of the three hyperparameters of the PSO–SVM–based models fitted in this study.

SVR hyperparameters	Lower limit	Upper limit
C	10^{-2}	10^2
ϵ	10^{-4}	10^0
σ	10^{-1}	10^3

stopping criterion is no improvement in the R^2 after ten iterations, together with maximum number of 500 iterations.

3 Analysis of results and discussion

Table 2 shows the optimal hyperparameters of the fitted SVM–based models found with the particle swarm optimization (PSO) technique.

Table 2: Optimal hyperparameters of the three fitted SVM models found with the PSO technique.

Kernel	Values of optimal hyperparameters
Linear	Regularization factor $C = 1.35$, $\epsilon = 0.064$
Quadratic	Regularization factor $C = 0.18$, $\epsilon = 0.022$, $\sigma = 55.95$, $a = 1.93$
RBF	Regularization factor $C = 50.05$, $\epsilon = 0.0042$, $\sigma = 2.20$

Table 3 shows the determination and correlation coefficients for all the PSO–SVM–based models for each of the three kernels analyzed here: linear, quadratic and RBF kernels, respectively.

Table 3: Coefficients of determination (R^2) and correlation coefficients for three hybrid PSO–SVM–based models fitted in this study

Kernel	Coefficients of determination (R^2)/correlation coefficients (r)
Linear	0.94/0.97
Quadratic	0.97/0.98
RBF	0.99/0.99

Finally, this work was able to predict a successful growth cycle of the *S. platensis* from *Chlorophyll a* values (output variable) as a function of the remaining input variables (irradiance, temperature, pH

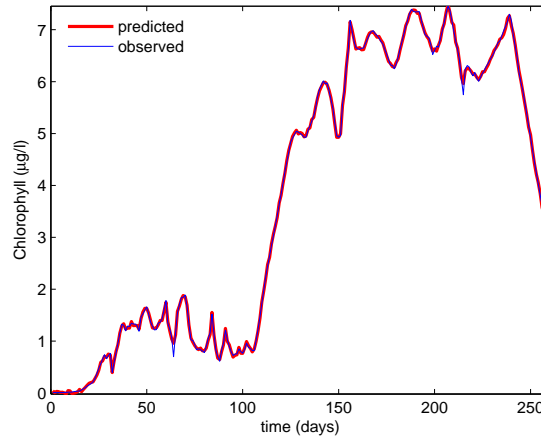


Figure 1: Comparison between the *Chlorophyll a* (measured in $\mu\text{g/l}$) observed and predicted by the hybrid PSO–RBF–SVM–based model in the prediction of a successful growth cycle of the *Spirulina platensis* (R^2).

values, dissolved oxygen, density, salinity, nitrate and phosphate concentrations) in agreement with the real experimental values of *Chlorophyll a* observed with a huge accurateness (see Fig. 1). Obviously, these results coincide again with the outcome criterion of goodness-of-fit (R^2) so that the SVM model with a radial basis kernel function (RBF–kernel) has been the best fitting.

4 Conclusions

The main findings in this research work can be summarized as follows:

- A hybrid PSO–RBF–SVM-based model in which PSO technique was used to optimize the hyperparameters corresponding to the best SVM model for the chlorophyll from irradiance, temperature, pH, oxygen, nitrate, phosphate, density and salinity values was achieved.
- Finally, a coefficient of determination of 0.99 was obtained when this hybrid PSO–SVM–based model was applied to experimental dataset for the RBF kernel considered (see Fig. 1).

Acknowledgements

This study was possible thanks to the collaboration between the Cantabrian Basin Authority (Ministry of Agriculture, Food and Environment of the Government of Spain) and University of Oviedo (Spain).

References

- [1] C.S. Reynolds, Ecology of Phytoplankton. New York, Cambridge University Press, 2006.
- [2] D.J. Barnes, and D. Chu, Introduction to Modeling for Biosciences. New York, Springer, 2010.
- [3] A. Selakov, D. Cvijetinović, L. Milović, and S. Mellon. Hybrid PSO–SVM method for short-term load forecasting during periods with significant temperature variations in city of Burbank *Applied Soft Computing*, 16:80–88, 2014.
- [4] I. Steinwart and, A. Christmann, Support Vector Machines. New York, Springer, 2008.
- [5] P.J. García Nieto, J. Martínez Torres, M. Araújo Fernández, and C. Ordóñez Galán. Support vector machines and neural networks used to evaluate paper manufactured using Eucalyptus globulus *Applied Mathematical Modelling*, 36(12):6137–6145, 2012.
- [6] R.C. Eberhart, Y. Shi, and J. Kennedy, Swarm Intelligence. San Francisco, Morgan Kaufmann, 2001.
- [7] C.–C. Chang, and C.–J. Lin. LIBSVM: a library for support vector machines *ACM Transactions on Intelligent Systems and Technology*, 2(3):1–27, 2011.

Using high-order finite difference methods in nonlinear Klein–Gordon equations

A. H. Encinas[†], J. Martín-Vaquero[†],
A. Queiruga-Dios[†], and V. Gayoso-Martínez^{b*}

([†]) E.T.S.I.I. Béjar, Universidad de Salamanca, Spain

(^b) Institute of Physical and Information Technologies (ITEFI),
Spanish National Research Council (CSIC), Madrid, Spain

November 28, 2014

1 Introduction

The nonlinear Klein–Gordon equation (nlKGE)

$$u_{tt} - u_{xx} + h_1(u) = h_2(x, t); \quad 0 \leq x \leq l, \quad 0 \leq t \leq t_e, \quad (1)$$

where $u = u(x, t)$ represents the wave displacement at position x and time t , and $h_1(u)$ is the nonlinear force, arises in the study of theoretical physics [1]. With a proper interpretation, the nlKGE describes the quantum amplitude for finding a point particle in various places and it also describes the relativistic wave function.

Several theoretical studies of the nlKGE have been developed. Many papers have focused on the existence and uniqueness of the smooth and weak solutions of these equations or studying their conservation laws. Those solutions are of interest in nuclear physics, condensed matter physics, high-energy physics, quantum field theory and many more (e.g., see [2, 3]).

Even though the numerical solutions to the nlKGE have received considerable attention in the literature (e.g., see [3, 4]), most of the methods

*e-mail: {ascen,jesmarva,queirugadios}@usal.es, victor.gayoso@iec.csic.es

developed so far are low-order in time or space, and some of them present limitations when they are extended to solve a large class of nKGEs.

In order to overcome the aforementioned limitations, in the present contribution we have developed and used fourth- and sixth-order methods for some of the best known nKGEs: the Form-I, the Form-II, and the Form-III equations. The proposed numerical methods are stable, either explicit or implicit, and easy to program.

2 Numerical methods to solve nKGEs

Consider the following one-dimensional nonlinear Klein–Gordon equations:

$$u_{tt} - u_{xx} - u + u^m = \psi(t, x), \tag{2}$$

$$u_{tt} - u_{xx} + au - bu^r + cu^{2r-1} = \psi(t, x), \tag{3}$$

$$u_{tt} - u_{xx} + au - bu^{1-r} + cu^{r+1} = \psi(t, x), \tag{4}$$

with initial conditions:

$$u(x, 0) = f(x), \quad 0 \leq x \leq l, \tag{5}$$

$$u_t(x, 0) = \bar{f}(x), \quad 0 \leq x \leq l, \tag{6}$$

and Dirichlet boundary conditions:

$$u(0, t) = g_1(t), \quad 0 \leq t \leq t_e, \tag{7}$$

$$u(l, t) = g_2(t), \quad 0 \leq t \leq t_e. \tag{8}$$

It is well known that the scheme $u_i^{n+1} = u_{i-1}^n + u_{i+1}^n - u_i^{n-1}$ works exactly for the equation $u_{tt} - u_{xx} = 0$ when $h = k$. Using this fact and cancelling the first terms of the local truncation error, a family of high order methods was derived in [5] for the non-homogeneous hyperbolic equation $u_{tt} - u_{xx} = q(x, t)$. We have used a similar idea to construct high-order finite difference methods for the three equations given above (2), (3), and (4).

If we consider that **those** equations can be written as

$$u_{tt} - u_{xx} = q(t, x, u), \tag{9}$$

with

$$q(t, x, u) = \psi(t, x) - \chi(t, x, u), \tag{10}$$

where $\chi(t, x, u)$ are the **last** terms in equations (2), (3), and (4), fourth-order methods can be obtained approximating the second derivatives in

$$u_i^{j+1} = u_{i-1}^j + u_{i+1}^j - u_i^{j-1} + k^2 \left(q_i^j + \frac{k^2((q_{xx})_i^j + (q_{tt})_i^j)}{12} \right). \quad (11)$$

The von Neumann stability analysis is not rigorously justified for non-linear equations, but it is often justified approximately, assuming that the solution $u(x, t)$ (and its numerical counterpart) does not vary too fast, **which** happens with most of these nonlinear Klein–Gordon equations.

The stability for the fourth-order implicit methods can be demonstrated as in [6] for the Phi-four equation (Form-I with $m = 3$). **In order to do that**, it is necessary to obtain the amplification factors and the roots of these polynomials **and check that** none of these expressions reach values over 1 (considered its absolute value).

Obviously, it is possible to obtain higher-order **methods in** a similar way. For example, we could use

$$u_i^{n+1} = u_{i-1}^n + u_{i+1}^n - u_i^{n-1} + k^2 \left(q_i^n + \frac{k^2((q_{xx})_i^n + (q_{tt})_i^n)}{12} + \frac{k^4((q_{xxx})_i^n + (q_{ttt})_i^n + (q_{ttt})_i^n)}{360} \right),$$

approximating $(q_{xx})_i^n + (q_{tt})_i^n$ with a fourth-order accurate formula, and the term $(q_{xxx})_i^n + (q_{ttt})_i^n + (q_{ttt})_i^n$ with a second-order method.

However, in this case, it is necessary to study the stability in a very different way, because it is difficult to obtain analytically the roots of polynomials with degree over 5. In addition to that, it is much more difficult to study when any of these expressions reach values over 1. Therefore, it is necessary to follow a similar procedure as in Theorems 2.2.1 and 2.2.3, and Corollary 2.2.2 in [7].

3 Numerical example

In this numerical example we have considered the Phi-four problem **given by** Equation (2) **for** $m = 3$ with the traditional initial and boundary conditions (5)-(8), such that the solution is

$$u(x, t) = \frac{\sqrt{2}}{\cosh \frac{x-2t}{\sqrt{3}}}. \quad (12)$$

The numerical errors when using this method (for different values of $h = \frac{1}{8}, \frac{1}{16}, \frac{1}{32}, \frac{1}{64}$ and $\frac{1}{128}$) are given at $t = 1$, $x = 0.25, 0.50$ and 0.75 in Table 1.

Table 1: Errors for the fourth-order method.

h	$x = 0.25$	$x = 0.5$	$x = 0.75$
$\frac{1}{8}$	8.489×10^{-7}	2.481×10^{-6}	2.018×10^{-6}
$\frac{1}{16}$	3.383×10^{-8}	1.097×10^{-7}	7.968×10^{-8}
$\frac{1}{32}$	1.711×10^{-9}	5.703×10^{-9}	3.661×10^{-9}
$\frac{1}{64}$	9.730×10^{-11}	3.244×10^{-10}	1.897×10^{-10}
$\frac{1}{128}$	5.657×10^{-12}	1.913×10^{-12}	1.052×10^{-11}

Our method converges at the expected rate, i.e. r_i is close to 4, when $r_i = \log_{c_i} err_i/err_1$, and err_i is the error obtained with h_i and $c_i = h_i/h_1$.

References

- [1] Ryan Sassaman and Anjan Biswas. Soliton perturbation theory for phi-four model and nonlinear Klein-Gordon equations. *Communications in Nonlinear Science and Numerical Simulation*, 14(8):3239 – 3249, 2009.
- [2] N. Ercolani, M. G. Forest, and D. W. McLaughlin. Geometry of the modulational instability III. homoclinic orbits for the periodic sine-Gordon equation. *Physica D*, 43(2-3):349 – 384, 1990.
- [3] J. Rashidinia, M. Ghasemi, and R. Jalilian. Numerical solution of the nonlinear Klein-Gordon equation. *Journal of Computational and Applied Mathematics*, 233(8):1866 – 1878, 2010.
- [4] Berna Bülbül and Mehmet Sezer. A new approach to numerical solution of nonlinear Klein-Gordon equation. *Mathematical Problems in Engineering*, 2013:1 – 7, 2013. Article ID 869749.
- [5] J. Martín-Vaquero and B.A. Wade. On efficient numerical methods for an initial-boundary value problem with nonlocal boundary conditions. *Applied Mathematical Modelling*, 36(8):3411 – 3418, 2012.

- [6] A. H. Encinas, J. Martín-Vaquero, A. Queiruga-Dios, and V. Gayoso-Martínez. Efficient high-order finite difference methods for nonlinear Klein-Gordon equations I. Variants of the Phi-four model and the Form-I of the nonlinear Klein-Gordon equation. *Nonlinear Analysis: Modelling and Control*, 2014. In Press.
- [7] J. C. Strikwerda. *Finite difference schemes and partial differential equations*. 2nd. ed., SIAM, Philadelphia, 2004.

Modelling improvement of pain and quality of life in osteoporosis patients treated with teriparatide

M. Osca*, N. Guadalajara† and R. Escartín*

(*)Hospital Obispo Polanco, Teruel, Spain

(†)Centro de Ingeniería Económica, Universitat Politècnica de València, Spain

1. Introduction

The Osteoporosis is a generalised metabolic disease characterised by loss of bone quantity and quality. In clinical terms, the disease remains silent until a bone fracture occurs, considered to be the most significant consequence of osteoporosis, which has been associated with increased risk of post-treatment fracture, higher direct health care costs, increased morbidity and mortality risk, worse quality of life and increased pain. Approximately 3 million people in Spain suffer this disease, of whom 2.5 million are women. Its incidence is expected to increase as society ages.

Health services managers work to prevent disease regardless of it being primary (new cases appearing), secondary (controlling the evolution of existing cases) or tertiary (reducing incapacities resulting from the disease). This is why pharmacological and non-pharmacological measures are adopted.

Different drugs are available to treat osteoporosis in post-menopausal women, which include teriparatide (TPTD). Since it was approved for the first time in the USA in 2002 and in the European Union in 2003 to treat osteoporosis in men and women, TPTD has been used as an alternative to currently available traditional therapies to treat this disease.

The aim of the present study was to model improvement in health-related quality of life and pain, and to lower the risk of fractures in patients with severe osteoporosis treated with subcutaneous TPTD.

2 Methodology

This is an observational prospective study that was conducted with 77 patients treated in the Pain Unit of the Obispo Polanco Hospital of Teruel (Spain). Teruel has a population of 36,000 inhabitants and the highest ageing index (%>65 years) in Spain. The inclusion criteria were patients diagnosed with severe prefracture osteoporosis between April 2006 and February 2014, and who were on TPTD treatment for 18 or 24 months. The exclusion criteria were treated patients but this drug prescription was incorrect, those who did not end treatment, and the ones whose died during follow-up. The study finally included 49 patients.

Pain and quality of life can be assessed using different scales. In our study, we used Visual Analogue Scale (VAS) to assess pain. This scale consists in a 10 cm horizontal line ranging from 0=no back pain to 10=worst possible back pain. We classified values

0-3 as slight pain, 3-6 as moderate pain and 7-10 as severe pain, and the scale values were recorded for the phases before and after being on TPTD treatment.

Different questionnaires that measure health-related quality of life exist. We employed EuroQOL- 5Dimension (EQ-5D), which has been widely used in studies into TPTD (Rajzbaum et al, 2014; Parthan et al, 2014) [1, 2], because it quickly and easily obtains data, and has also been used to assign health resources.

With EQ-5D, patients assessed their health status firstly according to levels of severity with dimensions (descriptive system) and then with a more general assessment VAS. It uses five health dimensions (mobility, self-care, usual activities, pain/discomfort, and anxiety/depression), which are all scored on a 3-point scale representing three degrees of severity (no problems, some problems, or extreme problems). Then levels of severity were coded. The UK scoring algorithm was used, whose coefficients were adapted to calculate the tariff (ST) in Spain (Badia et al, 1997) [3], which allowed comparisons between different countries to be made. The ST represents the calculated health status, whose values range between 1 (best imaginable health state) and 0 (death), although some negative values exist which are classified as being worse than death (Herdman, 2001) [4].

The mathematical models to express patient improvement were developed by firstly using the multiple linear regression analysis and ordinary least squares. The dependent and explanatory variables used in the analysis were:

Dependent variables:

- IVAS: Improvement in pain according to VAS, defined as the difference between the pre- and the post-treatment VAS so that the variable takes positive values when pain improves.
- IST: Improved ST, defined as the difference between the pre- and post-treatment ST, which takes positive values when health status improves.

Explanatory variables:

- Quantitative: Pre-treatment VAS, post-treatment VAS, pre-treatment ST, post-treatment ST, treatment duration, improved pain and health status.
- Dummy: pre-treatment fracture, post-treatment fracture, fracture type: vertebral, femur and radius.

Logistic regression models were used to estimate the likelihoods of health improving and of having a fracture after being on TPTD.

Three binary variables based on IVAS were used: $IVAS > 2$, $IVAS > 3$ and $IVAS > 4$. The $IVAS > 2$ points took a value of 1 if the patient's VAS improved by more than 2 points, and 0 otherwise. The other two variables ($IVAS > 3$ and $IVAS > 4$) were defined in the same way. A binary variable corresponding to fracture incidence during the post-treatment period was also used, which took a value of 1 if a fracture occurred during this period, and 0 otherwise. Here the explanatory variables used were the same ones as in the linear regression model.

3. Results

Better clinically improved bone pain was observed in most patients (82%) after receiving treatment. The mean initial VAS score was 5.42 (SD (standard deviation) = 1.696) and changed to 3.47 (SD=1.549) after treatment. Likewise, the mean initial ST

value was 0.358 (SD=0.271), which became 0.583 later (SD=0.348). In addition, quality of life improved in 61% of the patients, which coincides with other studies (Rajzbaum et al, 2014) [1].

The only explanatory variables for pain recovery to appear in the models were pre-treatment VAS (VASPRE) and pre-treatment ST (TSPRE). The other variables used (post-treatment VAS, post-treatment ST, treatment duration, fractures, etc.) were not significant in the analysis.

Although the explanatory power in the improved VAS model was not very strong (adjusted R^2 of 0.243), the explanatory variable coefficient (TSPRVE) was positive; that is, the higher the pre-treatment VAS (more pain), the better pain recover was; for each initial VAS point, pain either improved or reduced in 0.428.

In the ST based model, with weaker explanatory power (0.145), the opposite occurred: the TSPRE coefficient was negative. However, as the ST score was lower in patients with a poor health status, the model indicated that the ST in these patients was greater than in those patients whose initial health status was better. This indicates that treatment in both models was more effective in patients whose initial health status was worse.

Three logistic regression models were obtained with an improved VAS score, which improved by 2, 3 and 4 points, respectively. In the three models, VASPRE was the only explanatory variable used. The other variables were not significant.

4. Conclusions

Numerous studies into the influence of TPTD on bone remodelling and lowering the risk of fracture have been conducted. Many report a positive effect of TPTD, although others conclude quite the opposite. Studies into the effect of TPTD on reducing pain and improving quality of life are scarce, more recent and have been carried out in eight European countries. Nonetheless, no previous studies conducted on this subject in Spain have been found.

Although the present study conducted in Spain is quite incipient and has a small study sample, it confirms that TPTD reduces pain and improves the quality of life of osteoporosis patients. One major novel aspect that our study offers, unlike other studies, is that patients' initial health status is an important factor for improving VAS and ST. Patients with a poorer initial health status improve better.

References

1. G. Rajzbaum, F. Grados, D. Evans, S. Liu-Leage, H. Petto and B. Augendre-Ferrante. Treatment persistence and changes in fracture risk, back pain, and quality of life amongst patients treated with teriparatide in routine clinical care in France: Results from the European Forsteo Observational Study. *Joint Bone Spine*, 81:69–75, 2014.
2. A. Parthan, M. Kruse, I. Agodoa, S. Silverman and E. Orwoll. Denosumab: A cost-effective alternative for older men with osteoporosis from a Swedish payer perspective. *Bone*, 59:105–113, 2014.
3. X. Badia and X. Carné. La evaluación de la calidad de vida en el contexto de

ensayo clínico. *Med Clin*, 110:550-556, 1998.

4. M. Herdman, X. Badia and S. Berra. EuroQol-5D: a simple alternative for measuring health-related quality of life in primary care. *Atención Primaria*, 28(6): 425-430, 2001.

Injecting problem-dependent knowledge to improve evolutionary optimization search ability

Joaquín Izquierdo^b *, Enrique Campbell^b, Idel Montalvo[†],
and Rafael Pérez-García^b

(^b) Fluing-Instituto de Matemática Multidisciplinar(IMM)- Universitat Politècnica de València (Spain),

{jizquier, encamgo1, rperez}@upv.es

[†] 3SConsult GmbH, Albtalstrasse 13, 76137 Karlsruhe, Germany

montalvo@3sconsult.de

November 28, 2014

1 Introduction

The flexibility introduced by evolutionary algorithms (EAs) has allowed the use of virtually arbitrary objective functions and constraints in optimization, even when evaluations require, as for real-world problems, running complex mathematical and/or procedural simulations of the systems under analysis. The literature is very extensive in all the fields of engineering and science, and more specifically in the water industry, and, in particular, urban hydraulics, authors' field of expertise, regarding design, calibration, energy saving, etc. See, among many other references in the water industry [1, 2, 3, 4].

Even so, EAs are not a panacea. The heuristics behind a certain EA endows its elements with specific capabilities for efficiently solving some kinds of problems, while being clearly inefficient with problems of a different nature.

*jizquier@upv.es:

Also, EAs strongly rely on parameters. Fine-tuning those parameters is, in many cases, cumbersome and can be avoided by using adaptive and self-adaptive parameters. In agent swarm optimization (ASO) [3, 5, 6, 7], we have introduced an evolutionary hybridized platform of self-adaptive algorithms (EHPSA), which copes with these drawbacks.

However, above all, traditionally, the solution search process has been totally oblivious of the specific problem being solved, and optimization processes have been applied no matter the size, the complexity and the domain of the problem. Here, we justify that far-reaching benefits will be obtained from influencing more directly the way the search is performed, since algorithms adapting their behaviors to the problems will have more chances to succeed. A way to achieve this is by combining EAs knowledge based on the problem domain. Specifically, this paper proposes using Kohonen self-organizing feature maps (SOMs) [8] on sets of solutions evaluated after batches of generations of a run of an EA (or a suit of them) in order to extract knowledge to be used by the coming generations. This approach is applied to a very important optimization problem in Hydraulics, namely, the optimum design of water distribution networks (WDNs).

2 The rationale behind the proposal

In evolutionary optimization, many of the solutions evaluated during the search process are “forgotten” after one generation, and combined experience of several generations is typically not well exploited. Data mining (DM) techniques can enable deeper insight into the many “good” solutions that have just been simply glimpsed and have been rapidly disregarded because they were dominated by better solutions during an ephemeral moment in the evolution process. Our claim is that, by exploring a database obtained by suitably recording certain of those disregarded solutions, DM techniques can help better understand and describe how a system could react or behave after the introduction of changes. Our proposal is to use DM for dynamically and automatically generating knowledge that can be used to improve the efficiency of solution search processes.

The typical operation of an EHPSA aided by knowledge extraction we propose is the following. When initializing the EHPSA only random solutions are available. As a result, there is no possibility of knowledge extraction and the EHPSA, using its own search mechanisms (and perhaps some clear

expert rules), must work during a number of iterations to produce and collect new solution candidates. During these iterations, a database (DB) must have been created. The EHPSA will then stop the search, and the knowledge extraction algorithm will be launched to work on the DB. Hopefully, a number of pieces of knowledge will be obtained that will be used to guide the EHPSA during a new batch of iterations. Then a new DB of candidate solutions will be available. Again the knowledge extraction algorithm will produce probably new knowledge that, in its turn, will be used during the subsequent process of iteration. Assuming that injecting this knowledge will accelerate the convergence of the EHPSA, and taking into account that the EHPSA is controlled by a certain termination condition, it is expected that only a limited number of knowledge extraction processes will be eventually performed. When to stop the EHPSA to launch a knowledge extraction process is a matter that will need further insight and the target should be towards automatic execution.

Various DM techniques to handle large volumes of data, to scan the available information and track down understandable and useful knowledge have been devised. In this paper we explore Kohonen SOMs [8]. We use the implementation of SOMs in R, through the function *xyf*, [9].

3 Application to the Hanoi WDN

The Hanoi water distribution problem is a very well-known benchmarking problem in the WDN design field and has been attacked many times in the literature before. To gauge the effectiveness of our proposal, we consider this same problem. The network consists of one fixed head node, 34 pipes and 31 demand nodes subject to one load condition given by their associated demand. One has to find the diameters for the 34 pipes, such that the total cost of this network is minimal, and the pressure at each consumption node is at least 30 m. The complete setting can be found in [10].

According to the objective and the constraints adopted in this study, which coincide with the benchmark problem requirements, the optimization problem may be stated as

$$\text{Minimize } F(D) = \sum_{i=1}^{34} c(D_i)l_i + \sum_{j=2}^{32} \alpha H(p_{min} - p_j) \cdot (p_{min} - p_j),$$

s.t. the hydraulic conditions (see [11], for example).

The first summation corresponds to the cost of the pipes, and the second to the penalty for lack of pressure condition satisfaction. The cost $c(\cdot)$ is a nonlinear function depending on a discrete set of six commercially available diameters; D_i and l_i are diameter and length of pipe i . The factor α that multiplies with the pressure difference $\Delta p_i = p_{min} - p_i$ represents a fixed value, which becomes effective (by using the Heaviside function H) whenever the minimal pressure requirement, p_{min} , is not met by pressure p_j at node j . The variables in the problem are the diameters pertaining to the new pipes of the network or those of the rehabilitated pipelines. One therefore deals with determining the values that minimize the total cost of the pipelines while complying with the minimal pressure requirement of the network. This simple variant for the design of a WDN forms an NP-complete problem.

3.1 Application of the proposed synergy between EH-PSA and SOMs

One run of ASO with a population of 100 individuals was launched for 150 generations. This generated a database with 15000 registers. Thirty five columns constituted the fields of the database, which correspond to values for the diameter for each of the 34 pipes in the network, plus the objective value, corresponding to the cost of the network summed with the penalty incurred for not satisfying the minimum pressure value of 30m. The six diameters were coded 0, 1, . . . , 5, and the cost was discretized into excellent (first 3% cost-percentile), good (3 to 5%), poor (5 to 15%) and bad (the rest) solutions.

Then, a network with a hexagonal topology of 5×8 neurons (Figure 1) was trained based on this DB, and using the xyf -function, the pipe diameters being the independent variables and the qualitative cost the dependent variable.

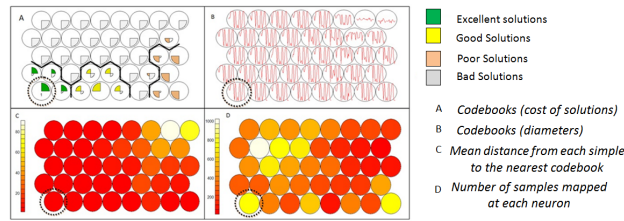


Figure 1: SOM after 150 iterations

The codebook of the neuron that gathers most of the current good solutions is obtained. It corresponds to the bottom leftmost neuron. The codebook of this neuron is given by the values in the shaded squares in Figure 2. Then, the codebook corresponding to this neuron is used to extract straightforward rules regarding the pipes analyzed. In any case, a small amount of randomness must be considered instead of taking the codebook values as hard rules to apply. After implementing these rules, the EHPSA continues with the iteration. In the specific run we are describing convergence for the EHPSA+SOM occurred at iteration 223. The optimum was then obtained. It corresponds to a network with a cost of 6.545325 million dollars and pipe diameters as noted in Figure 2 (non-shaded squares).

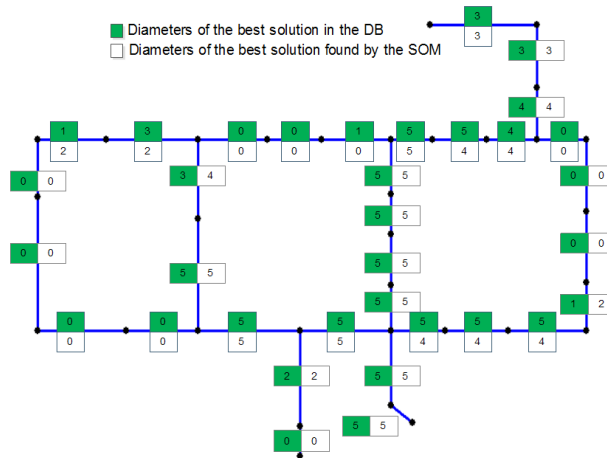


Figure 2: Hanoi network with codebook for the SOM and the optimal solution

References

- [1] I. Montalvo, J. Izquierdo, R. Pérez, M.M. Tung. Particle swarm optimization applied to the design of water supply systems *Computers & Mathematics with Applications*, 56(3):769–776, 2008.
- [2] J. Izquierdo, I. Montalvo, R. Pérez, M. Tung. Optimization in water systems: a PSO approach, in: Proc. Business and Industry Symposium (BIS), Ottawa, Canada, 2008.
- [3] I. Montalvo, Diseño óptimo de sistemas de distribución de agua mediante Agent Swarm Optimization, Ph.D. thesis, Universitat Politècnica de València, Valencia, Spain, 2011.
- [4] I. Montalvo, J. Izquierdo, M. Herrera, R. Pérez-García. Water supply system computer-aided design by agent swarm optimization *Computer-Aided Civil and Infrastructure Engineering*, 29(6):433–448, 2014.
- [5] I. Montalvo, J. Izquierdo, S. Schwarze, R. Pérez-García. Multi-objective particle swarm optimization applied to water distribution systems design: an approach with human interaction *Mathematical and Computer Modelling*, 52:1219–1227, 2010.
- [6] I. Montalvo, J. Izquierdo, R. Pérez-García, M. Herrera. Improved performance of PSO with self-adaptive parameters for computing the optimal design of water supply systems *Engineering Applications of Artificial Intelligence*, 23(5):727–735, 2010.
- [7] I. Montalvo, J. Izquierdo, R. Pérez, P.L. Igelsias. A diversity-enriched variant of discrete PSO applied to the design of water distribution networks *Optimization and Engineering*, 40(7):655–668, 2008.
- [8] T. Kohonen, Self-Organizing Maps. Berlin, Springer-Verlag, 2001.
- [9] R. Wehrens, L.M.C. Buydens. Self- and super-organizing maps in R: The kohonen Package *Journal of Statistical Software*, 21(5):1–19, 2007.
- [10] Z.Y. Wu, A.R. Simpson. Competent genetic-evolutionary optimization of water distribution systems *Journal of Computing in Civil Engineering*, 15(2):89–101, 2001.
- [11] J. Izquierdo, I. Montalvo, R. Pérez-García, A. Matías. On the complexities of the design of water distribution networks *Mathematical Problems in Engineering*, 2012:1–25, 2012.

SERK methods for solving nonlinear multi-dimensional parabolic PDEs

B. Kleefeld^b and J. Martín-Vaquero^{†*}

(b) Brandenburgische Technische Universität Cottbus, Institut für Mathematik,
D-03044 Cottbus, Germany,

(†) ETS Ingenieros industriales, Universidad de Salamanca,
E37700, Bejar, Spain.

November 28, 2014

1 Introduction

The class of problems of interest for stabilized explicit Runge-Kutta methods are problems for which the eigenvalues of the Jacobian matrix are known to lie in a long narrow strip along the negative real axis. This situation typically arises when discretizing parabolic equations or hyperbolic-parabolic equations such as advection-diffusion-reaction equations (with dominating diffusion or reaction). Stabilized Explicit Runge-Kutta (SERK) methods can easily be applied to large problem classes, have low memory demand and are especially suited for discretizations using the method of lines (MOL) of two and three dimensional parabolic PDEs. Usually second-order finite differences have been considered for these spatial discretizations. In this work, we would like to show the behavior of these algorithms when other procedures with faster convergence are employed.

Additionally we want to study what happens when any of the functions are not smooth. In these cases, the mechanisms to choose the length step of the algorithm are very sensitive. Hence, we propose different procedures to

*e-mail: jesmarva@usal.es

choose, both, the length step in time and later the number of stages, and we compare the numerical results.

2 SERK methods

For the construction of this kind of algorithms two problems need to be solved: i) Finding stability functions with extended stability domains along the negative real axis; ii) Finding explicit Runge-Kutta methods with those polynomials as stability functions.

We derived SERK2v2 in [7], by first obtaining polynomials with large stability regions using a modified Remes' type algorithm (see [8]) to calculate polynomials $R_s^2(z)$ of degree 10 up to 250 with damping $\eta = 0.975$ (the length of the stability region along the real axis decreases proportionally to this parameter but on the other hand the stability region is wider). Two-stages second-order Runge-Kutta methods are stable in the real axis only in the interval $[-2, 0]$ and other classical and more sophisticated algorithms have similar regions, however SERK methods studied in [7, 9] are stable in $[-0.8s^2, 0]$.

One advantage of stabilized explicit Runge-Kutta methods is that variable-step length produces almost no additional cost (only one extra evaluation of the function in the whole interval of integration) and thus the error can be controlled.

In this paper we would like to compare two ways to control the step size, and to study how we should choose the time step after a rejection.

i) Control formula 1: A step size strategy with memory that we previously used in [7, 9]:

$$h_{n+1} = \varrho h_n \frac{1}{\|est_{n+1}\|_2^{1/2}} \frac{h_n}{h_{n-1}} \left(\frac{\|est_n\|_2}{\|est_{n+1}\|_2} \right)^{1/2} \quad (1)$$

$\|est_n\|_2$ being a measure of the error after the step that we calculate like $\|est_n\|_2 = \sqrt{\frac{1}{n} \sum_{i=1}^n \left(\frac{err_i}{tol} \right)^2}$, where err_i denotes the i th component of the vector $y_1 - \tilde{y}_1$, where $\tilde{y}_1 = y_0 + hf(y_1)$. This strategy was first considered by H.A. Watts [10] and K. Gustafsson [5] and other well-known stabilized explicit Runge-Kutta methods such as ROCK2 or ROCK4 (see [1, 2]).

ii) Control formula 2: In this paper, we also propose another strategy

with memory

$$h_{n+1} = \varrho h_n \|est_{n+1}\|_2^{-\alpha} \|est_n\|_2^\beta. \quad (2)$$

We chose $\alpha = 0.35$, $\beta = 0.2$ as suggested in [4] and, in this case, $\tilde{y}_1 = y_0 + h(\gamma_1 f(y_0) + \gamma_2 f(y_1))$, with $\gamma_1 = 0.6$, $\gamma_2 = 0.4$.

Since we do not want any rejected steps, with both control formulae, we also limit the increase or decrease of the time step, i.e. $0.1 \leq \frac{h_{n+1}}{h_n} \leq 10$.

Non-smooth functions: In some cases, the PDEs have non-smooth data, or in other cases one (or more) of the functions even has jumps. This discontinuity typically produces a significant growth in the number of rejected steps. To avoid this, we propose that $\frac{h_{n+i+1}}{h_{n+i}} \leq 1$ for the two steps following the rejection ($i = 0, 1$) and $\frac{h_{n+i+1}}{h_{n+i}} \leq 2.5$ for the three steps after that ($i = 2, 3, 4$), unless the interval where there could be jumps has passed. Afterward we allow $\frac{h_{n+i+1}}{h_{n+i}} \leq 10$ again.

3 Numerical experiments

In a first example we consider the non-homogeneous parabolic problem [7] $u_t = du_{xx} + f(x, t)$ for $0 \leq x \leq 1$, $0 \leq t \leq 10.3$. The boundary and initial conditions as well as the specification of the possibly discontinuous heat source f are identical to [7]. We have smooth initial data but a mismatch at the boundaries.

Comparing the results of control formula 1 and 2, and controlling the increase of the step size after a rejection we can check that the error in both cases is comparable but the number of rejections and also the number of overall steps is smaller using control formula 2 which also seems to be faster.

If we do not control the increase of the step length after a rejection the error between the two methods is comparable whereas the number of rejections is clearly smaller using control formula 2. Comparing the methods - once using the step size control and once without step size control after a rejection - we see that in most cases the number of rejections reduces quite a bit using the step size control. In this numerical example ROCK2 and RKC are very efficient schemes, although - for both methods - the error is not below the specified tolerance.

The second example is the two-dimensional Brusselator reaction-diffusion problem (see [3] for the specification of the problem) subject to initial and boundary conditions such that $u(x, y, t) = e^{-(x+y+0.5t)}$, $v(x, y, t) = e^{x+y+0.5t}$.

We integrate this problem for $0 \leq x \leq 1$, $0 \leq y \leq 1$, $0 \leq t \leq t_{end} = 2$, taking $A = 1$, $B = 0$, $\alpha = 0.25$ and using $N = 100$ spacial nodes.

Using centered second order differences the error stagnates about $8d - 6$ for tolerances lower than $1d - 5$. Here we want to show how using higher-order finite differences can produce more efficient solutions with a smaller computational cost. Hence we will approximate second-order derivatives in space with fourth-order approximations

$$D_{xx}V_i = \frac{-V_{i+2} + 16V_{i+1} - 30V_i + 16V_{i-1} - V_{i-2}}{(12\Delta x)^2}, \quad i = 2, \dots, N - 2,$$

$$D_{xx}V_1 = \frac{10V_0 - 15V_1 - 4V_2 + 14V_3 - 6V_4 + V_5}{(12\Delta x)^2},$$

(and similarly for $i = N - 1$). When we choose these finite differences, the matrices have only real and negative eigenvalues. The largest eigenvalue (in absolute value) for second-order approximations is approximately $4N^2$, while for the fourth-order differences it is only $\frac{4}{3}$ times larger (approximately). Therefore, we can use a smaller number of nodes with fourth-order finite differences, and, although SERK schemes are only second-order in time, the errors can become smaller and CPU times too (since the number of equations is smaller and also the spectral radius is shorter).

Using fourth order approximations and only $N = 50$ spacial nodes yields smaller errors for small tolerance (about $5d - 9$ for a specified tolerance of $1d - 7$) while the CPU time reduces drastically. The number of overall steps stays about the same while the number of function evaluations reduces. Here we want to compare our results to the EETD-LOD method described in [3]. The EETD-LOD algorithm is a very efficient method based on exponential time differencing schemes, which has very good stability properties. It is second-order in time, and only second-order in space. The error is comparable to the error we obtain with the second order approximations in space and also has some kind of limitation, but the method is way slower than our method. For more numerical examples and details on the presented ones, we refer to [6].

References

- [1] Assyr Abdulle. Fourth order Chebyshev methods with recurrence relation. *SIAM J. Sci. Comput.*, 23(6):2041–2054, June 2001.

- [2] Assyr Abdulle and Alexei A. Medovikov. Second order Chebyshev methods based on orthogonal polynomials. *Numerische Mathematik*, 90(1):1–18, 2001.
- [3] H.P. Bhatt and A.Q.M. Khaliq. The locally extrapolated exponential time differencing lod scheme for multidimensional reaction-diffusion systems. *Journal of Computational and Applied Mathematics (submitted)*.
- [4] Kjell Gustafsson. Control theoretic techniques for stepsize selection in explicit Runge-Kutta methods. *ACM Trans. Math. Softw.*, 17(4):533–554, December 1991.
- [5] Kjell Gustafsson. Control-theoretic techniques for stepsize selection in implicit Runge-Kutta methods. *ACM Trans. Math. Softw.*, 20(4):496–517, December 1994.
- [6] B. Kleefeld and J. Martín-Vaquero. Solving partial differential equations with Stabilized Explicit Runge-Kutta methods efficiently. *Journal of Computational and Applied Mathematics (submitted)*.
- [7] B. Kleefeld and J. Martín-Vaquero. Serk2v2: A new second-order stabilized explicit Runge-Kutta method for stiff problems. *Numerical Methods for Partial Differential Equations*, 29(1):170–185, 2013.
- [8] J. Martín-Vaquero and B. Janssen. Second-order stabilized explicit Runge-Kutta methods for stiff problems. *Computer Physics Communications*, 180(10):1802 – 1810, 2009.
- [9] J. Martín-Vaquero, A.Q.M. Khaliq, and B. Kleefeld. Stabilized explicit Runge-Kutta methods for multi-asset American options. *Computers & Mathematics with Applications*, 67(6):1293 – 1308, 2014.
- [10] H. A. Watts. Step size control in ordinary differential equation solvers. *Trans. Soc. Compututer Simulation*, 1:15 – 25, 1984.

A Formal Specification of Autonomous Agent Systems with Subsystems Inspired by Biology

Francisco J. Mora ^{*}, Ramón Rizo, Mar Pujol,
Fidel Aznar, and Mireia Sempere

Department of Computer Science and Artificial Intelligence
University of Alicante, San Vicent del Raspeig, Alicante (E-03080). Spain

November 28, 2014

1 Introduction

In the last decade there has been a rapid growth in research of multiagent systems. Most studies have focused using semiformal diagrams or mathematically formalizing the behaviour of agents. We can find examples of this in the graphical modeling language AUML (Agent Unified Modeling Language), that is being standardized by Foundation for Intelligent Physical Agents (FIPA), and in standard languages for agent communications FIPA ACL (Agent Communication Language) and KQML (Knowledge Query and Manipulation Language). In this paper we propose a mathematical formal specification of multiagent systems based in the Z specification [1], emphasizing in the structure and defining the agents as a set of biological subsystems (nervous, reflex, sensory, reproductive, etc.). This formal specification based on biology, will help us to understand the structure and how the system works under high and low level.

^{*}e-mail: mora@ua.es

2 Agent Frameworks

Currently the research community agree on the need for standards to develop multiagent system applications, such as KQML or FIPA. However, these standards are not sufficient to allow a wide range of programmers can develop your own application using a multiagent system. To solve this problem, in recent years, have developed platforms that facilitate the design and implementation of multiagent systems. Although the use of a platform accelerates the development of the application, the learning and use of these platforms is not trivial, and requires considerable extra. We have made a study of several agent frameworks: JACK[2], MADKit[3], ZEUS[4] and JADE[5].

The Frameworks agents focus on creating the environment and the communication between agents, giving poor support in the internal construction of the agent. With these frameworks have been able to simulate systems and their behaviours, but when we implement real systems, it is difficult achieve several requirements as facilities to build the agent and the execution performance.

3 Micro Agents Model

Our research group works mainly in teleoperation systems where robots have sensors, cameras and motion actuators. The initial idea was to facilitate the construction of agents and to facilitate the communication between different system components. To do this, we came to deploy agent components as agents (from the point of logical seen micro-agents), each sensor, camera, actuator, etc. would be an agent. This allowed a fast implementation, easy integration and distribution platform. Current multiagent models and frameworks allow this design and implementation, especially those that allow teams and groups, like JACK and MADkit. In figure 1, we can see our teleoperation system class diagram based on JADE (all components are agents). On the one hand, the basic agents who provide JADE are in yellow: The parent class agent, and remote monitoring, management system and directory facilitator agents. Furthermore typical agents designed to model the

behaviour and the tasks planning. For the behaviour we define three agents, one for user commands, another to follow the established route and another for maintaining the basic security. To complete the scheme, we incorporate radar sensors, video capture and actuators agents.

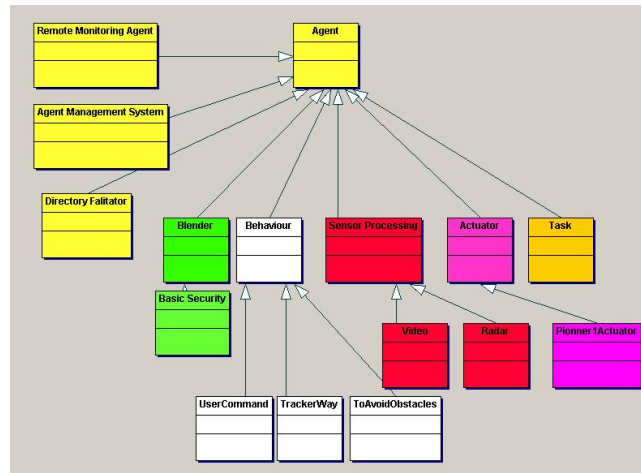


Figure 1: Micro Agents Jade design.

This model allowed us to accomplish our goal, but several problems were detected. On the one hand, the system was difficult to understand (the number of agents grew rapidly), modeling was ambiguous, and encapsulation was very poor. From the viewpoint of implementation is needed a higher communication speed between sensors and actuators and the rest of the system. Another problem was the lack of power processing and memory that we had in some parts of the system to run Java programs.

4 Organ Agents Model

The idea is create a model of multiagent systems with 2 levels, where agents are composed of other subsystems. The model must satisfy the following requirements: It must accommodate the concepts and models of agents, and it must be easily understandable, extensible that guarantees the reuse of components. We immediately asked the following question. Why not use subsystems inspired by biology? Its easy to understand, it has been tested

and optimized throughout evolution and it let us work 2 fully clear and distinct levels with different features. We could do biocompatible components to facilitate construction of the agent through reuse. There are different subsystems in biological organisms: Perception system, nervous system, locomotor system, speech and gesture systems, reasoning system (reflex, subconscious and conscious systems), reproduction system, immune system, etc. The subsystems of perception, locomotor and reasoning are used in classical multiagent system. The reproductive system is still very interesting for creating software agents, having a phase of courtship pheromones through a phase of dome for the exchange of genetic information. In the figure 2, we can see the Turing machine representation in our model inspired by biology. The perception subsystem is responsible for input the data. The control subsystem is composed by the brain (reflex, reasoning and learning organs). Locomotor and voice systems do the actions (output).

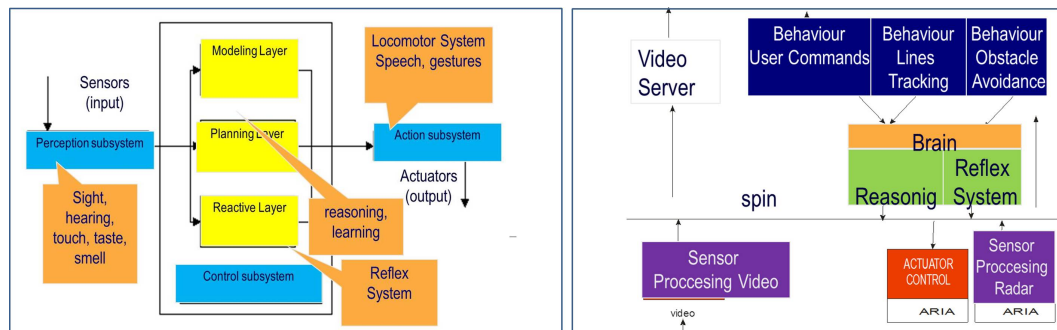


Figure 2: Turing machine representation. Figure 2b: Teleoperation organ agent model.

In the figure 2b, we can see our basic teleoperation system modeled with biological subsystems. We use the perception system and locomotor system as interface with agents, users, and other components or systems (Corba, Dcom, RMI, etc.). The inputs are received by the sensory system (in purple color). The brain runs algorithms to achieve different goals (obstacles avoid, track the road, etc.). The brain sends the information to the actuators (in red colour): engine control, information panel, speakers. The main communication between components takes place through the spine cord. The agent would communicate with other agents through the organs of perception and communication systems. Internal and external communications have different characteristics and are modeled differently (2 levels: organs and agents).

5 Organ Agents Mathematical formalization

The language Z is accessible to researchers from variety of different backgrounds and allows us to provide a consistent unified formal account of an abstract agent system. Precisely and unambiguously provide meanings for the common concepts. Allows formally define system modeling and system behavior. Well-structured to provide a foundation for subsequent development of increasingly more refined concepts. We have extended the model of Michael Luck and Mark d’Inverno [1] with the term organ agent. An organ is a set of objects and an agent is a set of organs.

The main components of the model are environment, objects, organs, agents and autonomous agents. They act in an environment in the schemas ObjectAction, OrganAction, AgentAction and AutonomousAgentAction respectively. For organs, agents and autonomous agents, we detail how they perceive in a given environment in OrganPerception, AgentPerception and AutonomousAgentPerception and we define their state in ObjectState, OrganState, AgentState and AutonomousAgentState.

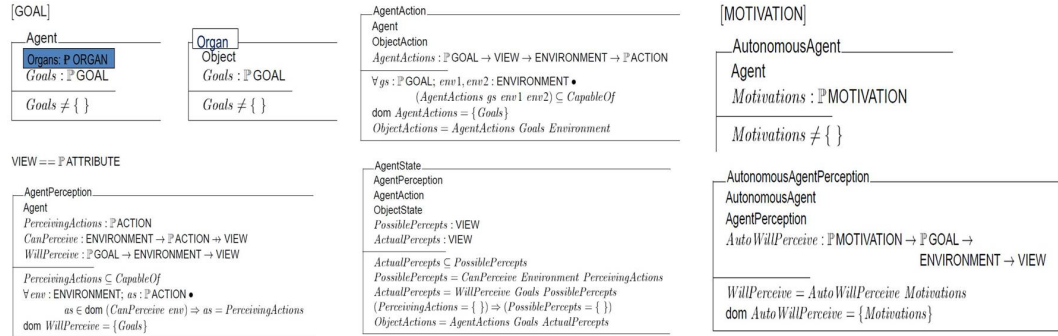


Figure 3: Definition of Organ, Agent, AgentAction and AgentState, Motivation, AutonomousAgent and AutonomousAgentPerception in Z language.

A goal is a state of affairs to be achieved in the environment. In order to ground the chain of goal adoption, to bring out the notion of autonomy, we use the motivation. A motivation is any desire or preference that can lead to the generation and adoption of goals and which affects the outcome of the reasoning or behavioural task intended to satisfy those goals.

6 Conclusions

We have achieved to model a multiagent system in 2 levels. (the agent level and the organ level). This allows us a different implementation for each level, each with different characteristics and performance. Thanks to this model, a rapid implementation is possible by reusing components. Also the use of third-party components and systems integration are enhanced. We model the system with a mathematical language, the Z language, which allows us to formalize the model, either the environment, agents, organs and behavior. And all in a model easily understandable, extensible that guarantees to reuse of components.

References

- [1] Luck, Michael, dInverno Mark. Structuring a Z Specification to Provide a Formal Framework for Autonomous Agent Systems. *ZUM '95: The Z Formal Specification Notation. Lecture Notes in Computer Science*, Volume(967):46–62, 1995.
- [2] Agent Oriented Software Pty. Ltd. JACK Intelligent Agents. <http://www.agentsoftware.com/>, 2003.
- [3] MADKIT. Multi-Agent Development KIT. <http://www.madkit.org>, 2002.
- [4] Collins and Ndumu. The Zeus Agent Building Toolkit. *ZEUS Technical Manual ZEUS Technical Manual*, 1999.
- [5] TILAB. JADE. Java Agent Development Framework. <http://www.sharon.cselt.it/projects/jade/>, 2002.

Acknowledgement

This work has been supported by the Spanish Ministerio de Economía y Competitividad project TIN2013-40982-R.

Building networks of sexual contacts from real statistical data

Luis Acedo[†], Francisco Palmi[‡] * ;
Francisco José Santonja[‡], Rafael Jacinto Villanueva[†]

(b) Departamento de Estadística y Investigación Operativa,
Universitat de València,

(†) Instituto de Matemática Multidisciplinar,
Universitat Politècnica de València,

November 28, 2014

1 Introduction

“Our world is full connected”. That expression could be the best one to explain the increasing interest based on the use of networks in the last years. One example is the paper by Milgram et al. [1], where it is presented the six grades theory, which suggest that two persons are connected by six links at most.

The born of the network-based analysis is often placed in 1735 when Euler presented the solution of the Königsberg bridge problem. Euler proved that it was impossible to walk the seven bridges of that city in such a way as to traverse each only once.

Since then, the network theory begins to be used in a lot of fields like the theory of the Electrical Circuits or the study of the molecular structure in Chemistry. As the computer science and the fields of operation research grew, networks were introduced in more interesting problems like allocation

*e-mail: palmi@alumni.uv.es

and transportation and during that time, psicologists began to develop the use of networks to study the interactions within social groups.

Nowadays, two important factors contribute to the growth of network theory: (i) an increasing tendency towards a systems-level perspective in the sciences and (ii) an accompanying facility for high-throughput data collection, storage, and management. [1]

2 Networks

The image given by a network shows perfectly the behaviour of a group of elements and the connections between them. For that reason, the term “network” has been used in a lot of different fields and in a lot of different ways, starting with the basic definition of network, set of connected nodes, and ending with the mathematical definition of network, which is the same as graph.

In order to identify the nature of the statistical foundation emerging in the analysis of network data, it is useful to have some initial sense of the contexts in which networks appears, the questions being asked, and the measurements being taken. One way to classify the networks is by the context where they appear. In this way, the networks are divided into four groups: technological networks, social networks, information networks and biological networks. These divisions are followed by Kolaczyk in [1] and by Newman in [2]

2.1 Technological networks

Probably, the most familiar networks to us are those with technological features. Technological networks are structures built artificially in order to obtain a more comfortable live and for research. Examples include transportation networks (e.g. networks of airlines routes or networks of roads or rails), communication networks (e.g. the Internet or the telephone networks) and energy networks (e.g. networks for deliver gas or electrical circuits). Maybe the basic example of the technological networks is the electric power grid, but nowadays, there is substantial interest in measuring and studying the network Internet is made up of.

2.2 Social Networks

Social networks have one of the longest histories of systematic study dating back to a least the 1930's. Social networks are usually built by a group or a set of groups of people and their links. The type of interactions considered in this area are constrained by the nature of the studied phenomenon. Some examples of that networks are the friendship networks, the job's relationships or the cooperation in order to accomplish a common objective, etc.

Traditional social networks studies often suffer of inaccuracy, subjectivity and small samples. Because of these problems many researchers have turned to other methods for proving social networks as collaboration networks. These networks are formed by the affiliations of a set of people in which participants collaborate in groups. A common example is the collaboration network of film actors.

2.3 Information Networks

The third network category is what we will call information or knowledge networks. The classic example of that type of networks is the citations between academic papers. In these networks, the nodes represents the researchers and the edges represent the co-authorships on papers. Another example is the World Wide Web, in which nodes are the Web pages and edges represent the referencing of one page by another (hyperlinks).

2.4 Biological Networks

A great part of the biologic systems are represented by networks. One group of examples are the Intra-cellular networks. Inside these groups exist the inter-cellular networks of neurons. On the other hand, networks describing interactions among complex organisms include ecological networks, such as those describing predator-prey relationships, and epidemiological networks describing the spread of diseases in the population.

3 Sexual networks

Nowadays, Sexual Transmission Diseases (STD) are an important health concern. Biomedical and behavioral interventions have been used to control the

spread of STDs with varying effectiveness. The reasons for successes and failures of these interventions are often not well understood [3]. Models of STD transmission dynamics have helped to elucidate the importance of “core” and “bridge” groups for the spread and the persistence of these pathogens within communities and have been used to develop specify policy guidance about necessary levels of coverage and appropriate targeting of treatment of vaccination to control the disease.

Schmid et al. [4] think that there are four major magnitudes appearing in all of the sexual behavior surveys and this is especially relevant for the performance of sexual networks in terms of disease transmission: (i) the cumulative distribution of lifetime number of partners, (ii) the distribution of partnership duration, (iii) the distribution of gap lengths between partnerships and (iv) the distribution of the number of recent partners.

The vaccine strategy against the Human Papilloma Virus (HPV) followed by the public health system in the Community of Valencia is based on [5]. In that work, Elbasha et al. study the transmission of the HPV using a system of Ordinary Differential Equations and describe a decay in the incidence of the HPV in 20 years. However, in other work performed by Fairley et al. [6], the authors report a rapid decay in the incidence a couple of years after the implementation of the vaccination program.

Our motivation is to improve Elbasha’s model using networks instead of ordinary differential equations and data of the population of the Community of Valencia to make the model more realistic and more closer to that population. Therefore, our objective is to build a random network that simulate the lifetime sexual contacts between the individuals of the Community of Valencia. In order to build that network, we use two sets of data: (i) Data about Lifetime Sexual Partners (LSP) per age and per gender that we found in the National Institute of Statistics and (ii) the demography of the Community of Valencia in 2012.

Before starting to build the network, we assume the following: (i) The network we are going to build will be static, (ii) people who are aged between 14-65 years are the only ones who have partners and (iii) links can only exist between people of the opposite gender. Of course, people without LSP will not appear in the network and the total sum of the LSP of all the males must be the same that total sum of the LSP of all the females.

We build the networks in two steps. At first, we have to assign to each node with its gender, its age and its number of lifetime sexual partners. To do this, we determine randomly the gender of the node, the group of age,

the exact age and finally, the number of LSP depending of the age of the group assigned. Then, we have to create the links between the nodes. It is well known that *people often join with people with similar habits*. In order to accomplish that principle we use the following weight function:

$$\pi(x, y) = \begin{cases} |x - y| & x, y \leq 4 \\ 0 & x, y > 4 \\ 100 & \text{otherwise} \end{cases}$$

Finally, to assign edges we use a metaheuristic assignment technique that combine greedy [8] and GRASP [7] algorithms with the above weight function. The main idea of that assignment is the following: when the labeling process finishes, we will have two lists with the number of LSP of each male and each female. The list of the females is ordered in descending order. Now begins the algorithm. For each female, we take all the males and check if the male still has free partner's sites. If the male has, then we calculate the weight of the current edge using the above function and add the pair to a list. Then, we order the list in descending order. In this step, if n_f is the number of LSP of the female,

- we take the first n_f weights and consequently, the first n_f males from the list (greedy), or
- we take randomly n_f weights, that is, n_f random males from the list (GRASP.)

Finally, we save the edges that we build and update the list of the males.

4 Conclusions

There are two main conclusions: (i) We have presented an algorithm to build likely networks using Valencian real data. (ii) We are going to use this algorithm to study the transmission dynamics of the HPV and other STD in Valencia in a more realistic way.

References

- [1] Eric D. Kolaczyk, Statistical Analysis of Network Data. Boston, Springer, 2009.

- [2] Newman, Mark E.J. The structure and function of complex networks. *SIAM review*, Volume(45):167–256,2003.
- [3] Robinson, K., Cohen, T. y Colijn, C. The dynamics of sexual contact networks: Effects on disease spread and control. *Theoretical population biology*, Volume81(2), 89-96, 2012.
- [4] Schmid, B. V. y Kretzschmar, M. Determinants of sexual network structure and their impact on cumulative network measures. *PLoS computational biology*, Volume8(4), 100-2470, 2012.
- [5] Elbasha, E. H., Dasbach, E. J. y Insinga, R. P. A multi-type hpv transmission model. *Bulletin of mathematical biology*, Volume(70(8)), 2126-2176, 2008.
- [6] Fairley G, Hocking J, Chen M, Donovan, Bradshaw C. Rapid decline in warts after national quadri- valent VPH vaccine program. *The 25th International Papillomavirus Conference*; 2009 May 8-14; Malmo, Sweden.
- [7] Mart, R., Resende, M. G. y Ribeiro, C. C. Multi-start methods for combinatorial optimization. *European Journal of Operational Research*, Volume(226(1)), 1-8, 2013.
- [8] Festa, P. y Resende, M. Grasp: Basic components and enhancements. *Telecommunication Systems*, Volume(46(3)), 253-271, 2011.

On the connection and equivalence of two methods for solving an ill-posed inverse problem based on FRAP data

C. Matonoha^b *, Š. Papáček[†]

(^b) Institute of Computer Science, Academy of Sciences of the Czech Republic,

Pod Vodárenskou věží 2, 182 07 Prague 8, Czech Republic,

([†]) University of South Bohemia in České Budějovice,

FFPW, CENAKVA, Institute of Complex Systems, Zámek 136, 373 33 Nové Hradky, Czech Republic.

November 28, 2014

1 Introduction

We deal with the inverse problem of model parameters identification using the spatio-temporal images acquired by the so-called FRAP (Fluorescence Recovery After Photobleaching) method [1]. In our previous work [2], we presented the problem formulation taking into account that the diffusion coefficient D is space independent (isotropic), but it can vary in time. The key idea behind the two coupled formulations of the inverse problem, i.e. a single parameter identification on one hand and the identification of the sequence $\{D_j\}$, where j is the index of time level, on the other hand, resides in fact that both the biological reality and the numerical process are under control. In particular, the time dependent diffusion coefficient can discover either an irregularity in the measurement process or a new dynamic phenomenon. Moreover, the experimental protocol consisted of the fluorescent signal time-sequence (on rectangular 2D domain) naturally induces M separated problem formulations between $(j - 1)^{th}$ and j^{th} time level.

*e-mail: matonoha@cs.cas.cz

2 Inverse problem formulation

Disregarding the possibility of the fluorescent particles to react, and assuming (i) local homogeneity, i.e. the concentration profile of fluorescent particles is smooth, (ii) isotropy, i.e. the diffusion coefficient D is space-invariant, and (iii) the possibility of one-dimensional simplification, we get the following Fick diffusion equation that represents the governing equation describing the unbleached particle concentration $y(x, \tau, p)$ ¹

$$\frac{\partial y}{\partial \tau} - p \frac{\partial^2 y}{\partial x^2} = 0 \quad (1)$$

on $[0, 1] \times [0, 1]$ with the initial and Dirichlet boundary conditions

$$y(x, \tau_0) = f(x), \quad x \in [0, 1], \quad (2)$$

$$y(0, \tau) = g_0(\tau), \quad y(1, \tau) = g_1(\tau), \quad \tau \in [0, 1], \quad (3)$$

as a function of dimensionless spatial coordinate $x := \frac{r}{L}$, time $\tau := \frac{t}{T}$, and re-scaled diffusion coefficient $p := D \frac{T}{L^2}$. Space and time coordinates are r and t , their characteristic quantities (in physical units) are L and T (e.g. the time interval between initial and last measurements), respectively.

Based on FRAP experiments, we have a 2D dataset in form of a table with $(N + 1)$ rows corresponding to the number of spatial points where the values are measured, and $(m + M + 1)$ columns with m pre-bleach and $M + 1$ post-bleach experimental values forming 1D profiles $y_{exp}(x_i, \tau_j)$, $i = 0 \dots N$, $j = -m \dots M$, where $x_0 = 0$ and $x_N = 1$.

We construct an objective function $Y(p)$ representing the disparity between the experimental and simulated time-varying concentration profiles, and then within a suitable method we look for such a value $p \in \mathcal{R}^M$ minimizing Y . Taking separately temporal (sub-index j) and spatial (sub-index i) data points, we get:

$$Y(p) = \sum_{j=1}^M Y_j(p_j) = \sum_{j=1}^M \sum_{i=0}^N [y_{exp}(x_i, \tau_j) - y_{sim}(x_i, \tau_j, p_j)]^2, \quad (4)$$

where p_j is the dimensionless diffusion coefficient in the j^{th} time interval $[\tau_{j-1}, \tau_j]$, and $y_{sim}(x_i, \tau_j, p_j)$ are the simulated values resulting from the solution of problem (1)–(3). The initial and boundary conditions are $y_{exp}(x_i, \tau_0)_{i=0}^N$, cf. (2), and $y_{exp}(0, \tau_j)$, $y_{exp}(1, \tau_j)$, $j = 1 \dots M$, cf. (3).

¹The linear relation between the concentration y and the measured level of fluorescence is assumed, indeed.

Our problem is ill-posed in the sense that the solution, i.e. the diffusion coefficients p_1, \dots, p_M , do not depend continuously on the initial experimental data. This led us to the necessity of using some stabilizing procedure. Usually, one has to use *a priori* information in order to solve the problem in a stable manner. Such *a priori* information as smoothness of the solution $p \in \mathcal{R}^M$ is expressed in form of the following (Tikhonov) regularized cost function to be minimized:

$$F(p, p_{reg}, \alpha) = \sum_{j=1}^M [Y_j(p_j) + \alpha (p_j - p_{reg})^2] \rightarrow \min_{p_{reg}, p > 0} \quad (5)$$

where $\alpha \geq 0$ is a regularization parameter and $p_{reg} \in \mathcal{R}$ is an expected value.

3 Tikhonov regularization vs. least squares with a quadratic constraint

Tikhonov regularization [3] is based on solving problem (5) for a given α which is denoted as $p^*(\alpha)$. It follows that $p_{reg}^*(\alpha)$ is the average value of $p_1^*(\alpha), \dots, p_M^*(\alpha)$. Now the question is how to choose a “right” (in some sense optimal) parameter α^* . Hansen proposed in [4] the so-called *L-curve criterion* consisting in finding the point of maximal curvature on the L-curve. However, in most cases this point is hard to determine. Fortunately, other equivalent approaches can be used. We follow the ideas of Hansen [4].

The first alternative approach to Hansen’s L-curve criterion consists in prescribing the value of $\|p^* - p_{reg}^*\|^2$ in advance. As the norm $\|p^*(\alpha) - p_{reg}^*(\alpha)\|^2$ diminishes for $\alpha \rightarrow \infty$, assume that we have prescribed the variance in the solution with some value ξ . According to Hansen, we can solve the following equivalent optimization problem with a quadratic constraint

$$p^*(\xi) = \arg \min_{p \in \mathcal{R}^M} Y(p), \quad \text{st.} \quad \|p - p_{reg}\|^2 \leq \xi, \quad p \geq 0, \quad (6)$$

where p_{reg} is the average value of p_1, \dots, p_M .

Suppose that we either know or can estimate the noise in input data. If we denote $y_{exp}^\delta(x_i, \tau_j)$ as real noisy data and $y_{exp}(x_i, \tau_j)$ as ideal data that would be measured without the noise, then

$$\sum_{j=1}^M \sum_{i=0}^N [y_{exp}^\delta(x_i, \tau_j) - y_{exp}(x_i, \tau_j)]^2 \leq \delta$$

where δ specifies the noise level (for the normally distributed non-correlated additive noise with the variance σ_0^2 , we have $\delta \approx M N \sigma_0^2$). This leads to another possibility to solve the optimization problem (5). As Hansen claims, the following optimization problem is again equivalent to the previous ones

$$p^*(\delta) = \arg \min_{p \in \mathcal{R}^M} \|p - p_{\text{reg}}\|^2, \quad \text{st.} \quad Y(p) \leq \delta, \quad p \geq 0. \quad (7)$$

In our most recent work [5], we provide the rigorous proof of the equivalence of problem (5) with the least squares with quadratic constraint formulation, i.e. with both (6) and (7). From a practical point of view, we prefer the constrained residuum based approach (7). The reason is following: while the Tikhonov regularization method (5) does not use the information about the noise level in data, approach (7) naturally takes into account the noise level and corresponds to Morozov's discrepancy principle as well, cf. [6].

References

- [1] R. Kaňa, O. Prášil, and C. W. Moullineaux. Immobility of phycobilins in the thylakoid lumen of a cryptophyte suggests that protein diffusion in the lumen is very restricted, *FEBS letters*, Volume (583):670–674, 2009.
- [2] Š. Papáček, R. Kaňa, and C. Matonoha. Estimation of diffusivity of phycobilisomes on thylakoid membrane based on spatio-temporal FRAP images, *Math. Comput. Modelling*, Volume 57(7-8):1907–1912, 2013.
- [3] A. N. Tikhonov, and V. Y. Arsenin, Solutions of ill-posed problems. V. H. Winston & Sons, Washington, D.C., John Wiley & Sons, New York-Toronto, Ont.-London, 1977.
- [4] P. C. Hansen, Rank-deficient and discrete ill-posed problems. SIAM, Philadelphia, 1998.
- [5] C. Matonoha, and Š. Papáček. On the connection and equivalence of two methods for solving an ill-posed inverse problem based on FRAP data, Manuscript submitted to *Journal of Computational and Applied Mathematics*, 2014.
- [6] V. A. Morozov. On the solution of functional equations by the method of regularization, *Soviet Math. Dokl.*, 7:414–417, 1966.

Comparison of some measures of Competitive Balance in regular seasons of European Basketball leagues

Francisco Pedroche* and José Antonio Verdoy

Institut de Matemàtica Multidisciplinària, Universitat Politècnica de València.

Camí de vera s/n 46022, València, Espanya

November 28, 2014

1 Introduction

There are different measures to assess the competitiveness of a sport league [5], [4], usually called *Competitive Balance* measures. In this talk we review some CB measures applied to basketball regular seasons. We focus on three points. On the first, we present different approaches to define the concept of competitiveness. On the second, we apply some CB measures to compare rankings corresponding to successive matchdays. On the third, we apply some of these CB measures to compare the final rankings from each league.

2 Measures

We use four CB measures: Standard deviation, HICB, Churn and NS. The standard deviation of wins is the most used measure in the sport literature, see e.g. [1], [3], [6]. It can be defined as follows: $\sigma = \sqrt{\frac{1}{n} \sum_{i=1}^n (w_i - 0.5)^2}$, where n is the number of teams and w_i is the ratio of wins of team i . Notice that low values of σ means low inequality among teams and therefore high

*e-mail: pedroche@imm.upv.es

CB. To compare seasons of different leagues we will use a normalization of σ given by: $\text{NAMSI} = \sqrt{\frac{\sum_{i=1}^n (w_i - \frac{1}{2})^2}{\sum_{i=1}^n (w_{i,max} - \frac{1}{2})^2}}$. The coefficient $w_{i,max}$ is the winning ratio of team i in a situation considered as having minimum competitiveness: team 1 wins all the matches, team 2 wins all except two matches (home and away), ... and team n loses all the matches.

The CB measure called HICB is defined as: $\text{HICB} = 100 n \sum_{i=1}^n s_i^2$, where s_i is the ratio of points scored by team i .

The measure called *Churn* is based on comparing two rankings (for example, two rankings at successive matchdays). Let $r(i)$ be the position of team i in ranking r . Then the *Churn* is defined as $C_t = \frac{1}{n} \sum_{i=1}^n |r(i) - r'(i)|$. To normalize this measure the most common procedure is to divide by the maximum churn, C_{max} , which is achieved when there is an inversion from r to r' (that is, the first team goes to the last position, the second goes to the penultimate position, etc). The resulting normalized churn is called *adjusted Churn*.

Finally, NS measure of CB is based on counting the crossings (permutations) produced when passing from one ranking to another one. To normalize this measure one can divide by the maximum number of crossings produced when there is an inversion from one ranking to the other. This measure is called NS since it stands for Normalized Strength; it can be associated to an analogous quantity borrowed from Complex Networks [2].

3 Data

We have considered four seasons (2010-2011 to 2013-2014) of four major European basketball leagues. The rankings can be obtained from the official sites of the analyzed basketball leagues [7], [8], [9] and [10]. We remark that there are differences on the number of teams among the considered leagues. This is a reason to use CB measures that take into account normalization factors.

4 Results

In this section we highlight some of the results obtained by applying the aforementioned CB measures to the above data. The results obtained by using HICB are very similar to those obtained by using σ . Thus, we omit results concerning HICB. In Figure 1 we show the evolution of σ (on the left) and the cumulative *adjusted Churn* for the Spanish ACB League. These plots have been done by computing the corresponding CB measure from matchday to matchday. From both plots we observe that there has been a decrease of competitiveness from season 2011-2012 to season 2013-2014.

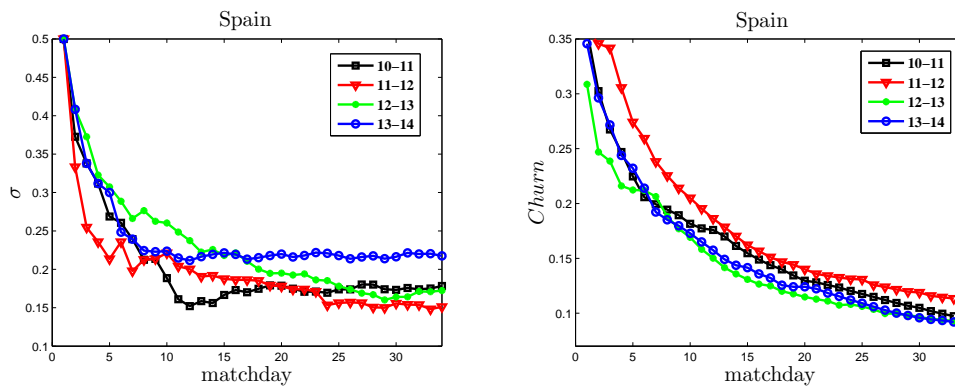


Figure 1: Evolution of σ (left) and cumulative *adjusted Churn* along four seasons of Spanish basketball league.

In Figure 2 we show two plots based on the final rankings of the four analyzed seasons and for the four surveyed leagues. On the left side of this figure we see that the values of NANSI for the Spanish league have been increasing since season 2011-2012. This means that the CB has been decreasing since then, in accordance with the results obtained above. In season 2013-2014 the most competitive league was the Italian league, followed by the Greece league and the Turkish one. By contrast, looking at the right side of Figure 2 we observe that in season 2013-2014 the most competitive league, according to cumulative NS, was the Greece league, followed by the Italian league and the Turkish one. Notice that different CB measures can show different trends about competitiveness.

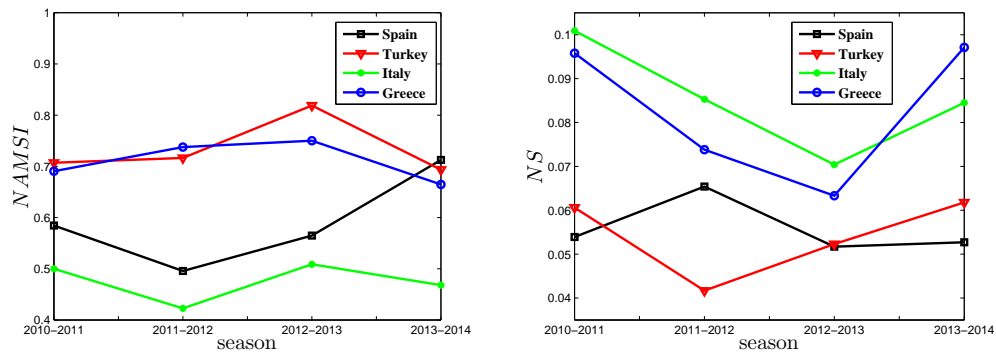


Figure 2: Values of NAMSI (left) and cumulative NS at the end of each season for the analyzed leagues.

5 Conclusions

We have shown different CB measures applied to four seasons of four European basketball leagues. The main conclusions about the competitiveness are the following: According to NAMSI, Italian and Spanish Leagues were the most competitive on seasons 2010-2011, 2011-2012 and 2012-2013. In season 2013-2014 the most competitive league was the Italian league, according to NAMSI. Regarding NS (which is based on the number of crossings produced from matchday to matchday) the most competitive league in season 2013-2014 was the Greece League followed by the leagues from Italy, Turkey and Spain. According to NS all the studied leagues have increased their competitiveness from season 2012-2013 to season 2013-2014, except the Spanish league that has maintained nearly at a constant level.

References

- [1] F. Addesa, *Competitive Balance in the Italian Basketball Championship*, *Rivista di diritto ed economia dello sport*, Vol. 7, Fasc. 1, 107-125, 2011
- [2] R. Criado, E. García, F. Pedroche, and M. Romance, *A new method for comparing rankings through complex networks: Model and analysis of competitiveness of major European soccer leagues*, *Chaos: An Interdisciplinary Journal of Nonlinear Science* . 23, 043114, 2013

- [3] S. Dobson, and J. Goddard, *The economics of football (2n ed.)*, Cambridge Univ. Press. (2011).
- [4] L. Groot, *Economics, uncertainty and European football : trends in competitive balance*. Edward Elgar cop. Northampton, USA. (2008)
- [5] M. Kringstad, *Competitive Balance in Complex Professional Sports Leagues*, Doctoral Thesis, The University of Leeds Leeds University Business School, 2008.
- [6] M. M. Perline, and G. C. Stoldt, *Competitive Balance in Men's and Women's Basketball: The Cast of the Missouri Valley Conference*, The Sport Journal, Vol. 10, No. 4, Fall 2007.
- [7] Liga Endesa (Spanish basketball league) <http://www.acb.com>
- [8] Esake League (Greek basketball league) <http://www.esake.gr/>
- [9] Lega (Italian basketball league) <http://www.legabasket.it/>
- [10] Beko (Turkish basketball league) <http://www.tbl.org.tr/beko>

Modeling the growth of electoral support to emergent parties in a crisis environment: The case of Valencian Community.

E. De la Poza^{1a*}, L. Jódar^{2b} and Marta Martínez^{1c}.

¹Facultad de Administración y Dirección de Empresas. Edificio 7J.

²Instituto Universitario de Matemática Multidisciplinar. Edificio 8G.

^{1,2}Camino de Vera s/n. 46022, Valencia (Spain).

e-mail address: ^aelpopla@esp.upv.es ; ^bljodar@imm.upv.es ;
^cm.martinez2890@gmail.com

Abstract

Lack of recovery of unemployment, more taxes, deterioration of the welfare system, high level of corruption and public debt, and lack of confidence in the Government's labour are driving a large proportion of the electoral register to support new emergent political parties. In this paper we construct a mathematical model to quantify this electoral change in the Valencian Community. By using a population model and splitting electoral options into five main categories, we modelled the dynamic transits among electoral choices by quantifying the expected electoral support scenario in the Valencian Community for the next local elections.

Keywords: mathematical population model, electoral analysis, socio-economic factors, robustness analysis.

1. Introduction

Lack of solutions for economic problems in all Europe combined with a high level of corruption, maintenance of privileges for politicians, and the cartelization of the main political parties in some countries like Spain [1].

Current Spanish law of political parties [2] obstructs the emergence of any kind of new political alternative given the high threshold of political support to achieve a seat in Parliament.

It is difficult to model human behaviour due to emotional, or even unpredictable irrational, human behaviour [3,4,5,6,7]. In this paper we propose a population mathematical model to quantify electoral behaviour in the next local elections in the Valencian Community taking into account the economic, sociological, psychological and demographic factors.

This paper is organised as follows: Section 2 deals with the model construction; Section 3 offers the results. Section 4 addresses the conclusions.

2. Model construction and justification

The study period of electoral behaviour began in June 2011 and ended in April 2015. This time interval has been divided into quarterly year periods, where $n=0$ represents the situation in June 2011 and period “ n ” means the number of quarters that have elapsed since June 2011.

Firstly the electoral register of the Valencian Community is split into five subpopulations:

$P(n)$: Expected voters of Conservative Popular Party (PP) in quarter n .

$S(n)$: Expected Voters of the Socialist Party (PSOE) in quarter n .

$E(n)$: Expected Voters of Extremist Parties with Parliament representation in quarter n .

Extremist parties are those that are:

- Separatists and/or
- Breakers of the capitalist system and/or
- Racists

$A(n)$: Expected Abstentions and blank voters in quarter n .

$U(n)$: Expected Voters of Emergent Political Parties (UPyD; Ciutatans, Compromís, and Podemos), those who have never had representation in the Valencian Parliament, or were irrelevant in quarter n .

Next we studied the dynamic subpopulation transits for the period since the last local elections in the Valencian Community and the expected schedule for the next ones (approx March 2015).

2.1 Coefficients modelling

The study population is variable given the income of new voters ($B_i(n-72)$, $0 \leq i \leq 4$), the amount of emigrants (M) and those voters (D) who have left the system, assumed constant due to the few changes in these demographic factors during the study period.

The transit between subpopulations is modelled through five coefficients:

- $\alpha_1(n)$: The economic factor
- $\alpha_2(n)$: Trust in the Government’s labour indicator
- $\alpha_3(n) = \alpha_3$: The poverty indicator
- $\alpha_4(n)$: Trust in the main opposition party
- $\alpha_5(n) = \alpha_5$: The hope coefficient

The initial subpopulations at the beginning of the study period (June 2011) were the electoral results of the previous Valencian elections [8].

Subpopulations change dynamically over time as they follow the influence of economic, sociological and demographic drivers, and this behaviour can be drawn according to the following block diagram (Figure 1):

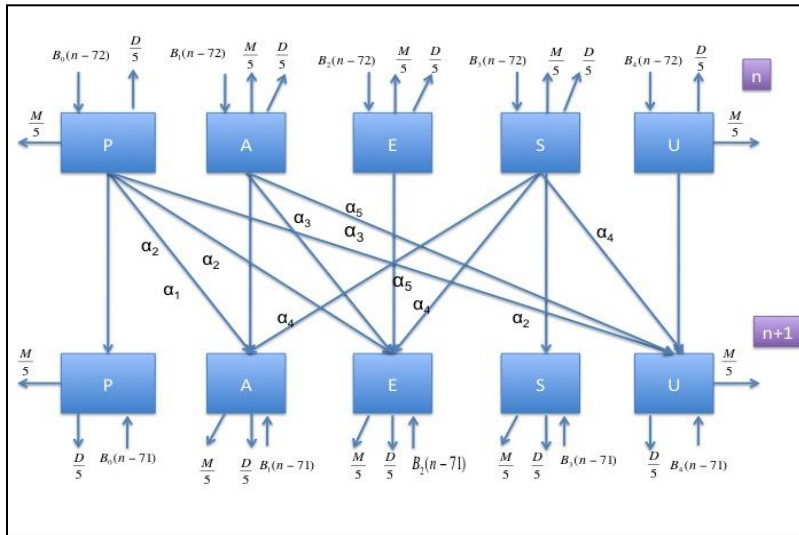


Figure 1: Dynamic electoral transits

The amount of new voters for each subpopulation is given by:

$\alpha_b(\alpha_b(n-72))$, is the birth rate of the Valencian population in quarter (n-72), [22]. $T(n-72)$ represents the Valencian population in the quarter, n-72; r_i is the proportion of new voters of each subpopulation obtained from the questionnaire to citizens becoming 18, passed in January 2012 N=400 (university students, community college students, employees).

P	9
S	8.60
AB	30.70
EX	20.90
U	30.80

Table 1. First time voters trend (as a %).

The exit of the model is due to the number of Valencian emigrations (64,000 people per year) [9], $M=16,051$. Also, the biological death measured with the death rate ($\alpha_d(n)$) in quarter n, [9], $D/5=13,596$. Then:

$$\alpha_d(n) * \frac{T(n)}{5} = \frac{D(n)}{5} = \frac{D}{5} \tag{2}$$

$\alpha_1(n)$ measures the variation between the unemployment rate of the Spanish population in the Valencian Community from June 2011 and for estimated quarter "n".

$$\alpha_1(n) = 0.01 * [\beta_1(n) - \beta_1(0)]; n \geq 1 \tag{3}$$

$$\alpha_1(0) = 0.01 * [\beta_1(0) - \beta_1(March2011)] = 0.01 * [19.97 - 0.21] = -0.0103 \tag{4}$$

where $\beta_1(0)$ is the unemployment rate in June 2011 and $\beta_1(March 2011)$ denotes the unemployment rate in the previous quarter (March 2011). From September 2014 to the end of the period, unemployment is assume to low by 0.25% per quarter.

$\alpha_2(n)$ measures the quarter-based change in the citizenship’s opinion about the Government’s labour.

$$\alpha_2(n) = [GLI(0) - GLI(n)] * 0.11005139, n \geq 1 \tag{5}$$

$$\alpha_2(0) = [GLI(March2011) - GLI(0)] * 0.11005139 \tag{6}$$

where $GLI(0)$ is the GLI measured in June 2011, while GLI (March 2011) is the GLI in the previous quarter (March 2011). The GLI indicator values for the period covering September 2014-March 2015 were forecasted following last year’s trend.

The poverty indicator $\alpha_3(n) = \alpha_3 = 0.005$ is the coefficient that estimates the radicalisation of votes. We assume that those people who did not vote in the last local elections due to their standard of living worsening and loss of confidence in the two main political parties will transit to the extremist subpopulation (E), but they will also transit to emergent political offers (U) to seek democratic political choices (Podemos and Compromís).

$\alpha_4(n)$ expressed the trust in the main opposition party

$$\alpha_4(n) = C * [\beta_2(n) - \beta_2(n - 1)], \tag{7}$$

where $\beta_2(n)$ is the political trust indicator value in quarter n obtained from [10], and C is a sociological constant adjusted by matching the electoral data of the last three Spanish General elections. After matching the data, we obtained $C = 0.00299$ [11].

From the time this study began (June 2011) to June 2014, the available data allowed us to compute coefficient α_4 . We assume that coefficient $\beta_2(n)$ will lower by 0.2 per quarter from June 2014 until March 2015.

The hope coefficient $\alpha_5(n) = \alpha_5 = 0.0508666$ measures the proportion of employed people aged 30-65 years who did not vote in the last elections and who move to emergent parties

$$\alpha_5(n) = \alpha_5 = \frac{1}{12} * 0.8 * 0.763 \tag{8}$$

where 0.8 is the proportion of people in the Valencian Community who is employed during the age interval [30,65]; 0.763 is the proportion of Valencian citizens during the age interval [30, 65]; 12 is the number of quarters in this study period.

The system of difference equations described as follows:

$$S(n + 1) = (1 + \alpha_4(n))S(n) + B_3(n - 72) - \frac{1}{5}(D + M) \tag{9}$$

$$P(n + 1) = (1 - \alpha_1(n) - \alpha_2(n))P(n) + B_0(n - 72) - \frac{1}{5}(D + M) \tag{10}$$

$$E(n + 1) = E(n) + B_2(n - 72) - \frac{3}{10}\alpha_4(n)S(n) + \frac{1}{2}\alpha_3A(n) + \frac{1}{10}\alpha_2(n)P(n) - \frac{1}{5}(D + M) \tag{12}$$

$$U(n + 1) = U(n) + \frac{6}{10}\alpha_2(n)P(n) - \frac{3}{10}\alpha_4(n)S(n) + \frac{1}{2}\alpha_3A(n) + \alpha_5A(n) + B_4(n - 72) - \frac{1}{5}(D + M) \tag{13}$$

$$\begin{aligned}
 A(n+1) &= (1 - \alpha_3 - \alpha_5)A(n) - \frac{4}{10}\alpha_4(n)S(n) + \frac{3}{10}\alpha_2(n)P(n) + \alpha_1(n)P(n) + B_1(n-72) - \frac{1}{5}(D+M) \\
 &= (1 - \alpha_3 - \alpha_5)A(n) - \frac{4}{10}\alpha_4(n)S(n) + (\frac{3}{10}\alpha_2(n) + \alpha_1(n))P(n) + B_1(n-72) - \frac{1}{5}(D+M)
 \end{aligned}
 \tag{11}$$

3. Results

The difference system can be explicitly solved by giving the following values in March 2015 corresponding to n=16.

Quarter	P	A	E	S	U
Jun -11	1,211,112	1,118,769	144,703	687141	237072
Sep -11	1,219,845	1,035,017	146,170	681572	295,556
Dec -11	1,187,939	995,964	150,571	671120	356,030
Mar -12	1,160,746	956,668	153,693	653134	410,890
Jun -12	1,109,973	945,296	154,994	632381	459,697
Sep -12	1,050,310	942,377	158,009	609494	511,734
Dec -12	980,226	948,406	163,647	588181	569,349
Mar -13	908,905	956,420	170,000	565345	627,855
Jun -13	836,932	964,538	177,042	543895	688,013
Sep -13	765,621	971,427	183,624	525038	747,765
Dec -13	707,953	964,576	190,682	505735	808,502
Mar-14	660,523	947,865	197,280	486672	868,115
Jun -14	615,860	929,500	202,953	467866	925,224
Sep -14	580,242	903,498	208,615	449330	981,282
Dec -14	547,711	875,973	214,057	431081	1,035,741
Mar-15	517,968	847,309	219,270	413130	1,088,517

Table 2. Subpopulations forecast (absolute values).

The results expressing the electoral register as a percentage compared with the electoral results from last elections (June 2011).

	P	A	E	S	U
June 2011	35.63%	32.92%	4.26%	20.22%	6.98%
March 2015	16.78%	27.45%	7.10%	13.39%	35.27%

Table 3. Forecasted electoral results compared with the last election ones.

4. Conclusions

The proposed model shows the end of the two-party system in the Valencian Community. The next government will be a coalition comprised of at least three parties, most likely a left wing coalition of PSOE (S) and several emergent parties (Compromís, Podemos) and/or extremist left wing parties (IU).

The model can be applied to any other geographical area if it bears in mind the (economic, sociological, demographic) factors and data of the electoral register.

References

- [1] A. Nieto, *El desgobierno de España*, (In Spanish) Ariel, Barcelona, 2012.
- [2] La Ley Orgánica 6/2002, de 27 de junio, de Partidos Políticos, (In Spanish).
- [3] L. Jódar, E. de la Poza, J.C. Cortés, L. Acedo, Preface: The challenge of modelling aggregated human behaviour, *Math Comput Model* 57, (2013) 1617-1618.
- [4] N. N. Taleb, *The black swan: The impact of the Highly Improbable*, Random House Publishing Group, New York, 2007.
- [5] R. M. Raafat, N. Chater, and C. Frith, Herding in humans, *Trends Cogn Sci*, vol. 13, no. 10, (2009) 420-428.
- [6] R. Girard, *Mimesis and Theory: Essays on Literature and Criticism, 1953-2005*, Stanford University Press, 2008.
- [7] N. A. Christakis and J. H. Fowler, *Connected: The Surprising Power of Our Social Networks and How They Shape Our Lives*, Back Bay Books, Little Brown and Company, USA, 2009.
- [8] Portal Argos, Banco de datos municipal www.argos.gva.es, (In Spanish).
- [9] Spanish Institute of Statistics www.ine.es
- [10] Center for Sociological research (CIS) available at <http://www.cis.es/cis/opencms/EN/>.
- [11] E. De la Poza, L. Jódar, and A. Pricop, Mathematical Modeling of the Propagation of Democratic Support of Extreme Ideologies in Spain: Causes, Effects, and Recommendations for Its Stop, *Abstr Appl Anal*, vol. 2013, Article ID 729814, 8 pages, 2013. doi:10.1155/2013/729814.

A hybrid SVM-LBP approach for face recognition

Francisco A. Pujol^b *; Antonio Jimeno-Morenilla^b,
and José L. Sánchez-Romero^b

(^b) Dpto. Tecnología Informática y Computación,
Universidad de Alicante, Alicante (Spain)

November 28, 2014

1 Introduction

Face recognition approaches are often classified depending on the method used to obtain the facial features. Thus, holistic methods use the whole face region as the raw input. They include well-known techniques, such as Principal Components Analysis (PCA) [1]. On the other hand, local or feature-based methods extract certain features, such as eyes, nose and mouth; their locations and local statistics are the input to the recognition stage. Some of most used algorithms in this area are Elastic Bunch Graph Matching (EBGM) [2] and Local Binary Patterns (LBP) [3].

Local Binary Patterns are considered one of the texture descriptors with better recognition results. They use a statistical feature extraction by binarizing of the neighborhood of every image pixel with a local threshold determined by the central pixel. However, one of its main drawbacks comes from the length of the resulting feature vectors.

In this work, we will first propose a mathematical model based on PCA for the reduction of the feature vector by using only the most important (i.e., the principal) LBPs. Thus, the resulting feature vectors database reduces its

* e-mail:fpujol@dtic.ua.es

dimensionality almost 80% compared to the original LBP approach. Then, for the classification stage, a Support Vector Machine (SVM) will be trained to decide whether the LBPs previously calculated belong or not to a certain person [4]. Finally, an extensive set of experiments have been performed with a public face database. From these experiments, our hybrid SVM-LBP approach achieves almost 95% of correct recognitions in average and, consequently, these results show the effectiveness of our proposed method.

2 Development of a hybrid LBP-SVM face recognition system

Local Binary Patterns (LBP) are a robust descriptor of microstructures in images. This operator labels the pixels of an image and thresholds each neighborhood of 3×3 pixels by using the central pixel value. Thus, the gray value of each pixel g_p in the neighborhood is compared to the gray value g_c of the central pixel. If g_p is greater than g_c , then it is assigned '1', and '0' if not. The LBP label for the central pixel (x, y) of each region in the image, considering a neighborhood of P pixels, is obtained as:

$$LBP_P(x, y) = \sum_{p=0}^{P-1} s(g_p - g_c)2^p \quad , \text{ where } s(x) = \begin{cases} 1, & x \geq 0 \\ 0, & x < 0 \end{cases} \quad (1)$$

The histograms of the LBP codes are calculated over each block and then concatenated into a single histogram representing the face image. Next, our main interest is to reduce the dimensionality of the feature vector. Assuming that the number of regions which an image is divided into is constant, reducing the vector must come from the number of LBPs considered to form this feature vector. In this work, Principal Component Analysis (PCA) will be used to reduce the dimensions of the feature vectors.

Our approach involves two phases: in the first one, the system is trained. Thus, the following steps are followed:

1. Select a training set of n images.
2. Pre-process images: detect faces and normalize sizes.
3. Create the n LBP histograms for the training set.

4. Apply PCA to compute the r principal LBP histograms.

Then, the second step implies the validation of our approach for recognition. In this case, the steps to be followed are:

1. A new input image enters the system and it is pre-processed as in the training process.
2. The LBP histogram M is calculated and projected into the subspace created by PCA to obtain M_ψ .
3. The resulting projected histogram M_ψ is classified, i.e., the face in the input image is recognized.

In order to classify the resulting histograms, in this work we propose the use of Support Vector Machines (SVM). As our approach has to identify a certain number of users q , a multi-class SVM will be used.

3 Results

Table 1 shows the results on the recognition rate when the number of LBP eigenvectors, r , is modified; thus, images are normalized to a size of 60×90 pixels and a Radial Basis Function kernel was chosen for the SVM classifier.

Table 1: Selection of the number of Principal LBPs.

Number of LBP eigenvectors r	Recognition rate (%)
8	75.1
12	88.4
14	94.5
20	94.7
30	94.7

From these results, it becomes clear that from $r = 14$ eigenvectors, the recognition rate remains almost constant, even when $r = 30$. Therefore, $r = 14$ is the number of eigenvectors selected for our approach. Since there were 69 LBP feature vectors in the original training database (which had 23 persons and 3 images per person, i. e., 3 LBP histograms per person),

the use of PCA results in a reduction of 79.71% in the dimensionality of the training database, with a recognition rate of 94.5%.

Let us now compare our system with some other existing algorithms for face recognition. The results are shown in Table 2. From this comparison, it is shown that the better results were given by our algorithm, approximately 1% better than the original LBP approach (94.5% vs. 93.6%)

Table 2: Comparison between methods.

Algorithm	Recognition rate (%)
PCA	67.1
SVM	72.0
EBGM	83.8
Original LBP	93.6
Our method	94.5

To sum up, our method had the higher recognition rates for the database considered and reduced almost 80% the dimension of the feature vectors database. Consequently, we believe that our hybrid LBP proposal can be used as an alternative of the original LBP method for face recognition.

References

- [1] Gumus E., Kilic N., Sertbas A., and Ucan O.N. Evaluation of face recognition techniques using PCA, wavelets and SVM *Expert Syst. Appl.*, 37(9):6404–6408, 2010.
- [2] Chakraborty M., Chanda K., and Mazumdar D. A novel statistical model to evaluate the performance of EBGM based face recognition. In *Perception and Machine Intelligence* (pp. 288–297). Springer Berlin Heidelberg, 2012.
- [3] Ahonen T., Hadid A., and Pietikäinen, M. Face recognition with local binary patterns. In *Computer vision-ECCV 2004* (pp. 469–481). Springer Berlin Heidelberg, 2004.
- [4] Kim S.K., Park Y.J., Toh K.A., and Lee S. SVM-based feature extraction for face recognition *Pattern Recognition*, 43(8): 2871–2881, 2010.

Modelling the co-creation between students and universities and its effects to loyalty and satisfaction

Gabriela Ribes Giner^b * , Agustín Peralt[†]

(b) Polytechnic University of Valencia,

Department of management. Faculty of Business Administration and Management

(†) European University of Valencia,

Department of Business Management. Faculty of Business Administration and Management

November 28, 2014

1 Abstract

This article's goal is to investigate to what extent co-creation (the student works together with the University in order to add value to the educational service) contributes to key marketing outcomes of loyalty and satisfaction , From a conceptual research model with some hypothesized relations based on an in-depth literature review, a structural equation model (SEM) is used to analyze those hypothesized relationships between co-creation and its relation with the level of satisfaction and trust for the students with their universities. The results are useful for the decision-making related to the marketing policies for the Educational Institutions.

Keywords:Co-creation, SEM satisfaction, loyalty, universities.

*gabrigi@omp.upv.es:

2 Introduction

Competition among universities is getting tougher and tougher which has caused them to create more student-focused marketing strategies. More and more universities need to understand and respond to the necessities and expectations of the service they are going to receive. With this focus on the student the idea of co-creation has appeared as an advantage for companies or institutions as regards the competition. (Hemsley et Al, 2006; Mansfield and Warwick 2006; Maringe, 2010)

In spite of co-creations contribution to enhancing the perception that students have of the university, it has been found that the universities are not really taking full advantage of the potential that co-creation provides. Universities should be changing their strategy from just giving education to students to actually co-creating it with their participation and support. In spite of the importance of co-creation to universities, there has been scarce research on its effects. (Mathis, 2013; Carvalho and Oliveira, 2010)

Co-creation has been defined in a variety of ways. For instance, it as how companies interact with customers in order to provide a better added value in the service, or it is composed of different ways of communicating and interacting with the receivers while the added value is being created. (Lusch and Vargo, 2006; Gustafson et Al 2012)

In education it has been pointed out that the only way to enhance satisfaction among students is to become familiar with their needs and afford them with quality value. Several authors highlight the relationship between co-creation and satisfaction. The positive relationship between student satisfaction and loyalty has been discovered in several studies. Loyalty is a key issue in co-creation and it has been defined in many ways. One definition defines loyalty as the creation and maintenance of long-term relationships with the consumer, especially when it comes to repeat purchases. In this research, through a literature review, we want to consider possible relationships between co-creation and marketing outputs in order to suggest a model to be later validated that responds to the issues raised by Rajah et al (2008)

3 Proposed Model

3.1 Co-creation and satisfaction

In reviewing the literature, several authors stress the positive and direct relationship between co-creation and satisfaction (Shaw et al, 2011, Lee, 2012; Grisseman and Stokurger-Sauer 2012; Dong, Evans and Zou, 2010).

3.2 Satisfaction and loyalty

Several studies stress the positive relationship between satisfaction and loyalty of the student (Mavondo et al, 2004, Marzo-Navarro, 2013, Bowden and D'Alessandro 2011; Helgesen and Nettet 2007, ThuraueHennig et al 2001).

3.3 Co-creation and loyalty

This relationship between loyalty and repeat purchases intention as shown on this definition is the result of many studies that prove it (Liang and Yan 2011; Chinomona and Sandala , 2013).

So therefore the proposed model is in Figure 1.

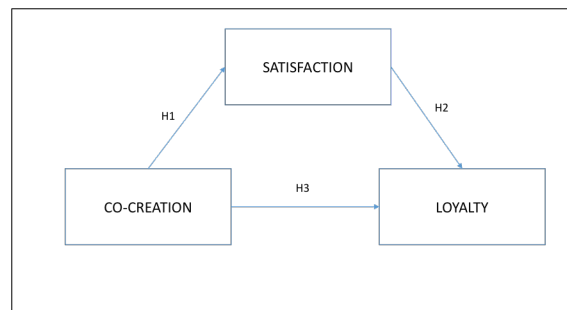


Figure 1: Proposed model for Co-creation and its relationship with Satisfaction and Loyalty

Methodology used is SEM (Structural Equation Modelling), also called "covariance structure analysis" is a confirmatory technique used mainly to check if a certain theoretical model is valid. SEM estimates a series of multiple regression equations, although interrelated by specifying a structural model.

3.4 Results

To confirm the dimensionality of the measurement scales, prior to testing the In order to confirm the suitability of a measurement model, it is critical to check that data (quality of the fit) and convergent and divergent validity are properly fitted. Convergent validity checks that the constructs are well explained by means of their observable variables while divergent validity checks that the observable variables of a construct (latent variable) correlate better with other observable variables of the construct itself than with other constructs observables variables. For convergent validity it must be checked that factor loadings (regression coefficients) of the observable variables in each construct are significantly different from zero and greater than 0.5. Furthermore, it must be verified that that Composite Reliability (CR) is greater than 0.7 and that average variance extracted (AVE) the degree that a latent is explained by its observed variables is greater than 0.5. All t values are significant at 99

To complete the verification of the divergent validity (verifies that each latent variable represents a separate dimension) these 2 conditions are must be met ((Fornell and Larcker, 1981) MSV (Maximum Shared Variance) ; AVE (Average Variance Extracted) ASV (Average Shared Variance) ; AVE (Average Variance Extracted)

We also found that confidence intervals calculated from shared variance, indicating the correlation between the latent factors, do not contain value 1, which means that the scales have divergent validity

Once the CFA is validated, the SEM must be analysed in order to test the suggested hypotheses on a theoretical level.

Like the CFA model, it is essential that the SEM model meets minimum fit quality.

As shown in the table 6, the proposed structural model provided a good fit since virtually all quality indices are within the acceptance thresholds to consider the model as valid (except GFI, although it is very close) (Hair, J. et al (2010)).

Therefore, by way of summary, the main conclusions of the model are presented:

- Co-creation influences deeply and in a positive way on student Satisfaction (H1, regression coefficient 0.85).

- Satisfaction influences moderately and in a positive way on student Loyalty (H2, regression coefficient 0.34).
- Co-creation influences moderately and in a positive way on student Loyalty (H3, regression coefficient 0.41).
- Satisfaction partially acts as mediator in the relationship between Co-Creation and Loyalty.

References

- [1] Carvalho SW, de Oliveira Mota M. The role of trust in creating value and student loyalty in relational exchanges between higher education institutions and their students. *Journal of Marketing for Higher Education* 2010;20(1):145-165.
- [2] Chinomona R, Sandada M. Service Quality Level as the Determinant of Consumer Emotional Loyalty and Fantasy in South Africa's Pick and Pay Chain Stores. *Mediterranean Journal of Social Sciences* 2013;4(3):579.
- [3] Dong B, Evans KR, Zou S. The effects of customer participation in co-created service recovery. *Journal of the Academy of Marketing Science* 2008;36(1):123-137.
- [4] Fornell C, Larcker DF. Evaluating structural equation models with unobservable variables and measurement error. *J Market Res* 1981:39-50.
- [5] Grisseman US, Stokburger-Sauer NE. Customer co-creation of travel services: The role of company support and customer satisfaction with the co-creation performance. *Tourism Management* 2012;33(6):1483-1492.
- [6] Gustafsson A, Kristensson P, Witell L. Customer co-creation in service innovation: a matter of communication? *Journal of Service Management* 2012;23(3):311-327.
- [7] Hair J, Black W, Babin B, Anderson R. *Multivariate data analysis*. 7th ed2010. 2010.

- [8] Helgesen . Marketing for higher education: A relationship marketing approach. *Journal of Marketing for Higher Education* 2008;18(1):50-78.
- [9] Hemsley-Brown J, Oplatka I. Universities in a competitive global marketplace: A systematic review of the literature on higher education marketing. *International Journal of Public Sector Management* 2006;19(4):316-338.
- [10] Lee SM, Olson DL, Trimi S. Co-innovation: convergenomics, collaboration, and co-creation for organizational values. *Management Decision* 2012;50(5):817-831.
- [11] Liang C, Wang W. Integrative research into the financial services industry in Taiwan: Relationship bonding tactics, relationship quality and behavioural loyalty. *Journal of Financial Services Marketing* 2005;10(1):65-83.
- [12] Lusch RF, Vargo SL. SERVICE-DOMINANT LOGIC AS A FOUNDATION FOR A GENERAL THEORY. The service-dominant logic of marketing: Dialog, debate, and directions 2006:406.
- [13] Mansfield PM, Warwick J. Gender differences in students' and parents' evaluative criteria when selecting a college. *Journal of Marketing for Higher Education* 2006;15(2):47-80.
- [14] Maringe F. The meanings of globalization and internationalization in HE: Findings from a world survey. *Globalization and internationalization in higher education: Theoretical, strategic and management perspectives* 2010:17-34.
- [15] Marzo-Navarro M, Pedraja-Iglesias M, Rivera-Torres MP. Measuring customer satisfaction in summer courses. *Quality Assurance in Education* 2005;13(1):53-65.
- [16] Mathis EF. *The Effects of Co-Creation and Satisfaction on Subjective Well-Being* 2013.
- [17] Mavondo FT, Tsarenko Y, Gabbott M. International and local student satisfaction: resources and capabilities perspective. *Journal of Marketing for Higher Education* 2004;14(1):41-60.

- [18] Rajah E, Marshall R, Nam I. Relationship glue: customers and marketers co-creating a purchase experience. *Advances in Consumer Research* 2008;35:367-373.
- [19] Shaw G, Bailey A, Williams A. Aspects of service-dominant logic and its implications for tourism management: Examples from the hotel industry. *Tourism Management* 2011;32(2):207-214.

A new efficient algorithm for matrix exponential computation

P. Ruiz^b*, J. Sastre[†], J. Ibáñez^b, and E. Defez[‡]

(^b) I3M, ([†]) ITEAM, ([‡]) IMM, Universitat Politècnica de València

November 28, 2014

1 Introduction

Matrix exponential computation has received remarkable attention in the last decades due to its usefulness in a great variety of engineering problems [1]. This work presents a new competitive Taylor scaling and squaring algorithm for matrix exponential that significantly simplifies the algorithms presented previously by the authors in [3] and [4], preserving efficiency. Throughout this paper, $\mathbb{C}^{n \times n}$ denotes the set of $n \times n$ complex matrices, I denotes the identity matrix for this set, $\rho(A)$ is the spectral radius of matrix A , \mathbb{N} is the set of positive integers, norm $\|\cdot\|$ denotes any subordinate matrix norm, and $\|\cdot\|_1$ is the 1-norm. Symbol $\lceil \cdot \rceil$ denote the smallest following integer.

2 Error analysis and new algorithm

Following [3, 4], if we denote $T_m(A) = \sum_{k=0}^m A^k/k!$ the truncated matrix exponential Taylor series with Taylor remainder $R_m(A)$, for a scaled matrix $2^{-s}A$, $s \in \mathbb{N} \cup \{0\}$, we can write

$$(T_m(2^{-s}A))^{2^s} = e^A (I + g_{m+1}(2^{-s}A))^{2^s} = e^{A+2^s h_{m+1}(2^{-s}A)}, \quad (1)$$

*e-mail: pruíz@dsic.upv.es

$$g_{m+1}(2^{-s}A) = -e^{-2^{-s}A}R_m(2^{-s}A), \quad h_{m+1}(2^{-s}A) = \log(I + g_{m+1}(2^{-s}A)), \quad (2)$$

where \log denotes the principal logarithm, $h_{m+1}(X)$ is defined in the set $\Omega_m = \{X \in \mathbb{C}^{n \times n} : \rho(e^{-X}T_m(X) - I) < 1\}$, and both $g_{m+1}(2^{-s}A)$ and $h_{m+1}(2^{-s}A)$ are holomorphic functions of A in Ω_m and then commute with A . As showed in [3], $h_{m+1}(2^{-s}A)$ and $g_{m+1}(2^{-s}A)$ are related with the backward and forward errors in exact arithmetic from the approximation of e^A by the Taylor series with scaling and squaring, respectively. Chosing s so that

$$\|h_{m+1}(2^{-s}A)\| \leq \max\{1, \|2^{-s}A\|\} u, \quad (3)$$

where $u = 2^{-53}$ is the unit roundoff in IEEE double precision arithmetic, then: if $2^{-s}\|A\| \geq 1$, then $\Delta A \leq \|A\| u$ and using (1) one gets $(T_m(2^{-s}A))^{2^s} = e^{A+\Delta A} \approx e^A$, and if $2^{-s}\|A\| < 1$, using (1)–(3) and the Taylor series one gets $\|R_m(2^{-s}A)\| \approx \|T_m(2^{-s}A)\| u$. As we are evaluating explicitly $T_m(2^{-s}A)$, in IEEE double precision arithmetic, $T_m(2^{-s}A) + R_m(2^{-s}A) \approx T_m(2^{-s}A)$, and there is no need to increase m or the scaling to try to get higher accuracy. Using scalar Taylor series in (2) one gets

$$g_{m+1}(x) = \sum_{k \geq m+1} b_k^{(m)} x^k, \quad h_{m+1}(x) = \sum_{k \geq 1} \frac{(-1)^{k+1} (g_{m+1}(x))^k}{k} = \sum_{k \geq m+1} c_k^{(m)} x^k, \quad (4)$$

where $b_k^{(m)}$ and $c_k^{(m)}$ depend on the order m . Moreover, $b_k^{(m)} = c_k^{(m)}$, $k = m + 1, m + 2, \dots, 2m + 1$ and if $\|h_{m+1}(2^{-s}A)\| \ll 1$ or if $\|g_{m+1}(2^{-s}A)\| \ll 1$, then $h_{m+1}(2^{-s}A) \approx g_{m+1}(2^{-s}A)$, see [4]. Using MATLAB symbolic Math Toolbox, high precision arithmetic, 200 series terms and a zero finder we obtained the maximal values Θ_m of $\Theta = \|2^{-s}A\|$ such that (see Theorem 1 from [3])

$$\|h_{m+1}(2^{-s}A)\| \leq \tilde{h}_{m+1}(\Theta) = \sum_{k \geq m+1} c_k^{(m)} \Theta^k \leq \max\{1, \Theta\} u. \quad (5)$$

The new proposed algorithm is a simplification of that presented in [3, p. 1837-1838]. For all norms appearing in the scaling algorithm we will use the 1-norm, and m_M will be the maximum allowed Taylor order. Note that $T_m(2^s A)$ can be computed optimally in terms of matrix products using vaules for m in the set $m_k = \{1, 2, 4, 6, 9, 12, 16, 20, 25, 30, \dots\}$, $k = 0, 1, \dots$, see [2, p. 72–74]. We will first check if any of the Taylor optimal orders $m_k = 1, 2, 4, \dots, m_M$ satisfy (3) without scaling ($s = 0$), testing if

$$c_{m+1}^{(m)} / c_{m+2}^{(m)} \cdot a_{m+1} + a_{m+2} \leq \max\{1, \|A\|\} \cdot u / c_{m+2}^{(m)} \quad (6)$$

holds, where a_{m+1} and a_{m+2} are the 1–norm estimation of $\|A^{m+1}\|$ and $\|A^{m+2}\|$, respectively, computed using the block 1–norm estimation algorithm of [6]. If no value of $m_k \leq m_M$ satisfies (6) we will calculate the optimal scaling s for order m_M in two phases: first, we will calculate an initial value of the scaling parameter, s_0 , and then we will try to refine it, testing if it can be reduced. In this algorithm we have simplified both phases with respect to the algorithms from [3] and [4], avoiding costly and complex checks that rarely allow to reduce the scaling parameter. To calculate s_0 , algorithm computes α_{min} . In [3, p. 1837], the upper bounds a_k for $\|A^k\|$ needed to apply Theorem 1 from [3] in (5) were obtained as

$$\begin{aligned} \|A^k\| \leq a_k = \min \left\{ \|A\|^{i_1} \|A^2\|^{i_2} \dots \|A^q\|^{i_q} \|A^{m_1+1}\|^{i_{m_1+1}} \|A^{m_2+1}\|^{i_{m_2+1}} \dots \right. \\ \times \|A^{m_M+1}\|^{i_{m_M+1}} : i_1 + 2i_2 + \dots + qi_q + (m_1 + 1)i_{m_1+1} \\ \left. + (m_2 + 1)i_{m_2+1} + \dots + (m_M + 1)i_{m_M+1} = k \right\}. \end{aligned} \tag{7}$$

Then, in [3] α_p values from Theorem 1 were obtained with $l = m_M + 1$ for $p = 2, 3, \dots, q, m_1 + 1, m_2 + 1, \dots, m_M + 1$, stopping the process when $(a_p)^{1/p} \leq \max\{(a_k)^{1/k} : k = m + 1, m + 2, \dots, m + p\}$. The minimum value among all values α_p , α_{min} , was selected to compute the appropriate initial minimum scaling parameter $s_0 \geq 0$ so that $2^{-s_0}\alpha_{min} \leq \Theta_{m_M}$, i.e. if $\alpha_{min} \leq \Theta_{m_M}$ then $s_0 = 0$, and otherwise $s_0 = \lceil \log_2(\alpha_{min}/\Theta_{m_M}) \rceil$. It was shown that if $s = s_0$ then (3) holds. In this work, we have simplified all that process by directly approximating

$$\alpha_{min} \approx \max\{a_{m+1}^{1/(m+1)}, a_{m+2}^{1/(m+2)}\}, \tag{8}$$

since numerical tests showed that using only those two terms made no noticeable difference in the accuracy results. Once obtained s_0 , if $s_0 \geq 1$ we check if (3) holds reducing the scaling $s = s_0 - 1$, and using the bounds for $\|A^k\| \leq a_k$ to test if bound

$$\frac{\|h_{m+1}(2^{-s}A)\|}{|c_{m+2}^{(m)}|} \leq \sum_{k=m+1}^{m+2} \left| \frac{c_k^{(m)}}{c_{m+2}^{(m)}} \right| \frac{a_k}{2^{sk}} \leq \max\{1, \|2^{-s}A\|\} \frac{u}{|c_{m+2}^{(m)}|}, \tag{9}$$

holds, truncating the series. Note that we will stop the series summation if after summing the first term, the sum is greater than $\max\{1, \|2^{-s}A\|\}u/|c_{m+2}^{(m)}|$. Table 2 of [5] presents some values of $c_k^{(m)}/c_{m+2}^{(m)}$, and the values $u/|c_{m+2}^{(m)}|$. In

(9) we have simplified the process of determining the error bound with respect to those in [3] and [4], using only the two first terms of the remainder, instead of the q terms used in algorithms from [3] and [4] because we check empirically that using more terms rarely modifies the final result. Typically, the terms of the Taylor series for matrix exponential are decreasing, so the first terms of the remainder tend to determine the error bound. In this step, we have also removed a complex and costly test that previous versions of the new Taylor algorithm do when expression (9) does not hold with $s = s_0 - 1$, see (15) from [3] and (45) from [4]. We have found empirically that when (9) does not hold, then very rarely those tests are satisfied. Then, similarly to the algorithms proposed in [3] and [4], algorithm tests if (3) holds with s and m_{M-1} ; Taylor order $m = m_{M-1}$ will be used if (3) holds, or $m = m_M$ otherwise. Finally, we compute the exponential approximation of the scaled matrix by using the modified Horner and Paterson–Stockmeyer’s method proposed in [3, p. 1836-1837], and we do s squaring steps to obtain the matrix exponential approximation of the original matrix A . See [5] for a detailed description of the algorithm.

3 Numerical experiments

A Matlab implementation of the new algorithm, **exptaynsv3**, have been compared with the functions **exptayns** and **exptaynsv2** from [3] and [4], respectively. New function is available at:

<http://personales.upv.es/~jorsasma/Software/exptaynsv3.m>.

We have used 3 sets of matrices: 100 random 1024×1024 diagonalizable (set 1), 100 random 1000×1000 multiple eigenvalued (set 2) and 32 1000×1000 from the Matrix Computation Toolbox [8] (set 3). The maximum order used for Taylor approximation in all cases was $m_M = 30$.

Table 1 presents the comparison in terms of matrix products. The new algorithm saved one matrix product in 44 and 38 cases in total with respect **exptayns** and **exptaynsv2**, respectively. With regard to accuracy, relative error figures in [5] shows that the three algorithms achieved very similar results. Moreover, we have compared a Fortran version of **exptaynsv3**, available at

<http://personales.upv.es/~jorsasma/Software/exptaynsv3fortran.zip>, with the function **f01ecc** from NAG Library, one of the main commercial software available for computing matrix exponentials, see [9]. In this case, we

Table 1: Comparison of the cost in terms of total number of matrix product evaluations (P) between `exptaynsv3` (P_3), `exptayns` (P_1) and `exptaynsv2` (P_2).

	$P_3 = P_1$	$P_3 < P_1$	$P_3 > P_1$	$P_3 = P_2$	$P_3 < P_2$	$P_3 > P_2$
Matrix sets 1 and 2	157	43	0	163	37	0
Matrix set 3	31	1	0	28	1	3

have used matrix sets 2 and 3 and execution time instead of matrix products was used to evaluate the cost of both functions. The total time taken by `exptaynsv3` to compute all matrix exponentials was 521 seconds, versus 866 seconds taken by `f01ecc` function. Moreover, `exptaynsv3` was significantly more accurate in the majority of cases. See [5] for more exhaustive results.

References

- [1] C.B. Moler, C.V. Loan. Nineteen dubious ways to compute the exponential of a matrix, twenty-five years later, *SIAM Rev.* 45 (2003) 3–49.
- [2] N.J. Higham, *Functions of Matrices: Theory and Computation*, Society for Industrial and Applied Mathematics, Philadelphia, PA, USA, 2008.
- [3] J. Sastre, J. Ibáñez, E. Defez and P. Ruiz, Accurate matrix exponential computation to solve coupled differential models in engineering, *Math. Comput. Model.*, 54 (2011) 1835–1840.
- [4] J. Sastre, J. Ibáñez, E. Defez and P. Ruiz, Accurate and efficient matrix exponential computation, *Int. J. Comput. Math.*, 91(1), (2014), 97–112
- [5] P. Ruiz, J. Sastre, J. Ibáñez and E. Defez, High performance computing of the matrix exponential, Submitted to *Journal of Computational and Applied Mathematics*.
- [6] J. Higham, F. Tisseur, A block algorithm for matrix 1-norm estimation, with an application to 1-norm pseudospectra, *SIAM J. Matrix Anal. Appl.* 21 (2000) 1185–1201.
- [7] N.J. Higham, The scaling and squaring method for the matrix exponential revisited, *SIAM J. Matrix Anal. Appl.* 26 (4) (2005) 1179–1193.

- [8] N. J. Higham, The Matrix Computation Toolbox,
<http://www.ma.man.ac.uk/~higham/mctoolbox>.
- [9] NAG Library Function Document,
http://www.nag.co.uk/numeric/cl/nagdoc_cl23/html/F01/f01ecc.html

The Role of Statistical Tests on Cluster Interpretation

Beatriz Sevilla-Villanueva^{b‡†*}, Karina Gibert^{†‡‡}
and Miquel Sànchez-Marrè^{b‡‡}

(b) Department of Computer Science,

(†) Department of Statistics and Operation Research,

(‡) Knowledge Engineering and Machine Learning Group (KEMLG),

(‡) Universitat Politècnica de Catalunya-BarcelonaTech, Spain

November 28, 2014

1. Introduction.

Cluster interpretation has an important role in the proper understanding of a set of classes, independently if they have been automatically discovered or they are expert-based. This understanding is crucial for further use of these classes as the basis of a decision-making process.

Most of the works found in literature about post-processing the result of a clustering process correspond to the cluster validation using indexes. These cluster validity indexes evaluate the clusters from the structural point of view [1]. However, structural validation does not ensure the usefulness of the clustering, while meaningfulness is the key to guarantee that classes could support further decisions. Nevertheless, few references on Cluster Interpretation can be found. Some, rank the variables by their significance [3], others describe the centroids of the classes or are more concentrated in visualization [4]. However, the most common method for interpreting is a manual analysis of both expert and analysts. As the number of variables and/or classes increases, this process becomes tedious. Thus, cluster interpretation

*e-mail: bea.sevilla@gmail.com

seems still to be an open issue and the presented research tries to contribute in the automatization of this process.

Assuming that the clusters can be distinguished, an analysis of the conditional distribution of variables against classes can be conducted to identify particularities of the classes. Concretely, the interpretation of *nested partitions* is introduced in this work. Nested classes might appear in many scenarios: clusters of different levels of granularity, different cuts of a hierarchical clustering, using different variables, different criteria, crossing partitions, etc. A partition P' is considered to be nested to other partition P if P can be obtained by grouping the classes of P' (see Figure 1).

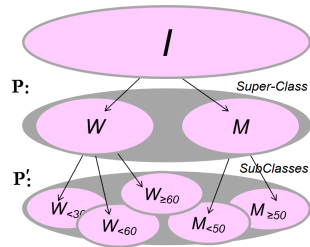


Figure 1. Representation of Nested Partitions

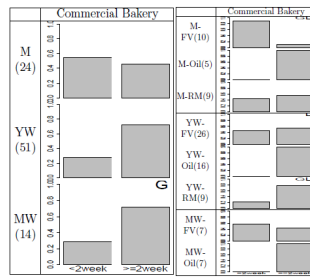


Figure 2. CPG of variable commercial bakery vs partitions P and P'

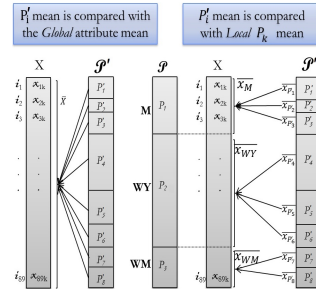


Figure 3. Local Test-Value

2. Interpreting a partition. Given \mathcal{I} a set of individuals and C a class $C \subseteq \mathcal{I}$. The proposed interpretation methodology [7] is:

1. Perform *Test-Value* of all variables against the classes.

X numerical

X qualitative, s a value of X ,

$$\frac{\bar{x}_c - \bar{X}}{\sqrt{(1 - \frac{n_c}{n}) \frac{sd^2}{n_c}}} \sim t_{n_c-1}$$

$$\frac{\frac{n_{sc}}{n_c} - \frac{n_s}{n}}{\sqrt{(1 - \frac{n_c}{n}) \frac{n_s}{n} (1 - \frac{n_s}{n})}} \sim Z$$

being: \bar{X} the mean of X , \bar{x}_c the mean of $X|C$, $n = \text{card}(\mathcal{I})$, $n_c = \text{card}(C)$, sd the standard deviation of X , $n_s = \text{card}(i \in \mathcal{I} : x_i = s)$, $n_{sc} = \text{card}(i \in C : x_i = S)$.

Sometimes the subdivision of a class in several subclasses emerges differences in certain variable X for the subclasses, being X non-significant in the superclass. This kind of specialization might be evident in the CPG (Figure 2, where *commercial bakery* looks non significant in class M but it is in class $M - FV$ a subclass of M) but

non detectable through significances of *Test-Value*. For this reason, the local *Test-Value* is introduced (Figure 3), comparing local subclass means (or proportion) to local superclass mean (or proportion) rather than the global mean (or proportion).

2. View CPG [5] for significant variables.
3. Build a verbose description profiling for each class based on that.

3. The relationship between the interpretations of nested partitions

In this paper, the proposed methodology has been used to interpret two nested partitions P and P' coming from a real dietary intervention trial [2]. Individuals were describe through 34 numerical variables and 31 qualitative variables involving a total of 37 modalities and 216 *Test-Value*.

Comparing both interpretations, the behavior of all variables is analyzed. As a result, the relationship between both interpretations can be described with the following 6 cases:

- 1) New properties arise in subclasses.
- 2) No additional information in subclasses. All subclasses have the same behavior than their corresponding super-classes.
- 3) For some super-class, all subclasses inherits from this super-class. The behavior of some super-class is propagated to all its subclasses but not for all super-classes.
- 4) Some subclasses inherit from super-class. The behavior of a super-class is propagated to some of their subclasses but not to all of them.
- 5) Some subclasses have opposite behavior than their super-class. The behavior of subclasses have been masked in their super-class.
- 6) Properties from super-class disappear in subclasses. None of the subclasses with the same super-class inherits from this super-class.

4. Conclusions. Finally, as a conclusion, CPG and *Test-Value* are tools that help to interpret the resulting classes reducing the effort of this task. For nested classes, the use of the *local Test-Value* allows a higher sensitivity to detect how the behavior of a variable changes in subclasses of the same super-class. The relationship between the interpretations of nested partitions has been analyzed, and 6 different situations identified, depending on how the significance of a variable in a superclass propagates to their subclasses, and representing different degrees of total or partial inheritance of the super-class property to the subclasses. Among them, the last scenario in which a

variable relevant in the superclass disappears from subclasses interpretation represents a contradiction. The significance of the variable for the super-class indicates that the effects in the super-class have higher (or lower, according to the sign of the *Test-Value*) values than the general sample, and this is inconsistent with the idea that none of the corresponding subclasses provide significant test values for that variable. From a total of 65 variables 24 were in this situation. Analyzing in depth those variables it was seen that the reduction of the sample size in the subclasses is decreasing the sensibility *Test-Value*, as usual in classical inference, since variance of statistics is inversely proportional to sample size. Currently, corrections in the test are being investigated to avoid paradoxal interpretation of nested partitions.

References

- [1] Halkidi, M. and Batistakis, Y. and Vazirgiannis M. On clustering validation techniques. *J INTELL INF SYST*, 17(2-3):107–145, 2001.
- [2] Konstantinidou, V. and Covas, M.I et al. In vivo nutrigenomic effects of virgin olive oil polyphenols within the frame of the Mediterranean diet: a randomized controlled trial. *FASEB J*,24(7):2546–57, 2010.
- [3] Cecere, W. and Abreu, D. and et al. A Method for Improving List Building: Cluster Profiling. *Procs. of the Survey Research Methods Section, ASA*, 2010.
- [4] Haughton, D. and Legrand, P. and Woolford, S. Review of Three Latent Class Cluster Analysis Packages: Latent Gold, poLCA, and MCLUST. *AMSATAT*,63(1):81–91, 2009.
- [5] Gibert, K and Sonicki, Z. Classification based on rules and medical research. *Journal of Applied Stochastic Models and Data Analysis, formerly JAMSDA*,15(3): 319–24, 1999.
- [6] Lebart, Ludovic and Piron, Marie and Morineau, Alain. *Statistique exploratoire multidimensionnelle*. 3rd Editionn, Dunob, 2000
- [7] Sevilla-Villanueva, B. and Gibert, K. and Sànchez-Marrè, M. Post-Processing the Class Panel Graphs: Towards Understandable Patterns from Data. *Frontiers in Artificial Intelligence and Applications*, 256:215–224, 2013.

Development of a non-linear quasi-3D model for engine gas-exchange modelling

A.J. Torregrosa,* A. Broatch, F.J. Arnau, and M. Hernández

CMT - Motores Trmicos. Universitat Politcnica de Valncia,

Camino de Vera s/n, 46022-Valencia, Spain.

November 28, 2014

1 Introduction

Internal combustion engine modelling has proven to be an important tool in the design of manifolds and silencers for those engines. Although simple 1D models are generally sufficiently precise in the case of manifold models, they would usually fail to predict the high frequency behaviour of modern compact manifold designs and, of course, of a complex-shaped silencing system. Complete 3D models are able to account for transversal modes and other non-1D phenomena, but at a high computational cost. In this paper, the development and application of a time-domain non-linear quasi-3D model approach is described, whose computational cost is relatively low but still providing an accurate description of the high frequency behaviour of the elements considered [1]. This quasi-3D model is conceived to be used locally in the frame of a 1D model code, and thus the Method of Characteristics is used to impose the boundary conditions required. The model developed makes use of a non-linear second order time and space discretization, based on finite volumes. Also, a Flow Corrected Transport technique developed for 1D finite differences schemes has been adapted to the quasi-3D method in order to achieve convergence and avoid numerical dispersion.

*e-mail: atorreg@mot.upv.es

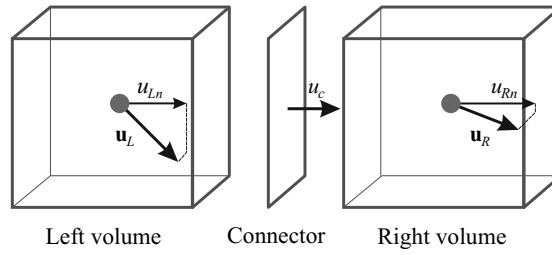


Figure 1: Basic mesh elements and definition of velocity projections.

2 Model description

Two basic elements are considered: Volumes, that contain information about scalar magnitudes such as pressure, density or temperature, and cell volume, and connectors, that contain information on vector quantities (flow velocity or momentum), and on their orientation and equivalent area. A volume may be attached to any number of connectors. As an example, in Fig. 1 two volumes connected by a connector are shown. Now, the discretized continuity and energy equations are written, for the volumes, as

$$\rho^{n+1} = \rho^n + \frac{\Delta t}{V} \sum_{c=1}^{N_c} \rho_c^n u_c^n A_c \quad (1)$$

$$(\rho e_0)^{n+1} = (\rho e_0)^n + \frac{\Delta t}{V} \sum_{c=1}^{N_c} \rho_c^n e_0^n u_c^n A_c + \frac{\Delta t}{V} \sum_{c=1}^{N_c} p_c^n u_c^n A_c \quad (2)$$

Momentum is calculated at the connectors, and only in the direction orthogonal to the connector surface by projecting the flow velocity in the connected volumes onto that direction, as depicted in Figure 1, where the velocity u_c in the connector, and the projections of the volume flow velocity, u_{Ln} and u_{Rn} , are shown. In this way, a one-dimensional momentum equation is solved, which after discretization is:

$$(\rho_c u_c A_c)^{n+1} = (\rho_c u_c A_c)^n + (\Delta t / \Delta L) \left[(\rho u_n^2 + p)_L + (\rho u_n^2 + p)_R \right] A_c \quad (3)$$

Finally, the momentum vector of each volume can be written as:

$$(\rho_c \vec{u} V)_v^{n+1} = \frac{1}{2} \sum_{c=1}^{N_c} (\rho \vec{u}_c A_c \Delta L)_c^{n+1} \quad (4)$$

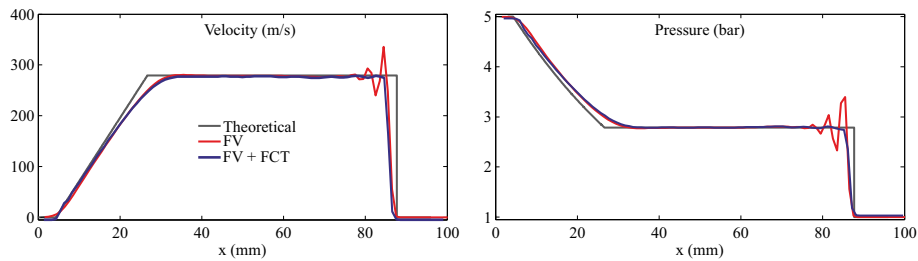


Figure 2: Shock tube results: comparison of theoretical solution and proposed method with and without FCT.

3 Applications

The method was first applied to the simple case of the shock-tube problem [2], in which two gases with different thermo- and fluid-dynamic states are put into contact and the system evolution is computed. The results obtained are shown in Fig. 2, together with the theoretical solution [2]. A noticeable overshooting associated with the propagation of the shock wave can be clearly seen. This is known to appear unless an equivalent friction force [1] or a momentum diffusion term [3] is included in the momentum equation. However, a similar effect is obtained by means of the use of a Flux Corrected Transport (FCT) methodology [4], which has proven to be effective when the flow equations are solved with finite differences schemes. The corresponding results are also shown in Fig. 2, where it can be observed that the overshoots have been successfully removed.

A simple box-shaped muffler with a single impulse boundary condition imposed upstream of the system, with an anechoic termination downstream, was then considered. The mesh used is shown in Fig. 3(a) while comparison of experimental measurements with the transmitted pulse predicted is given in Fig. 3(b), where it can be observed that acceptable results are obtained. However, it appears that the method is dissipative and some of the high frequencies are filtered out.

4 Conclusion

A quasi-3D model which makes use of a non-linear second order time and space discretization based on finite volumes has been developed. A Flow

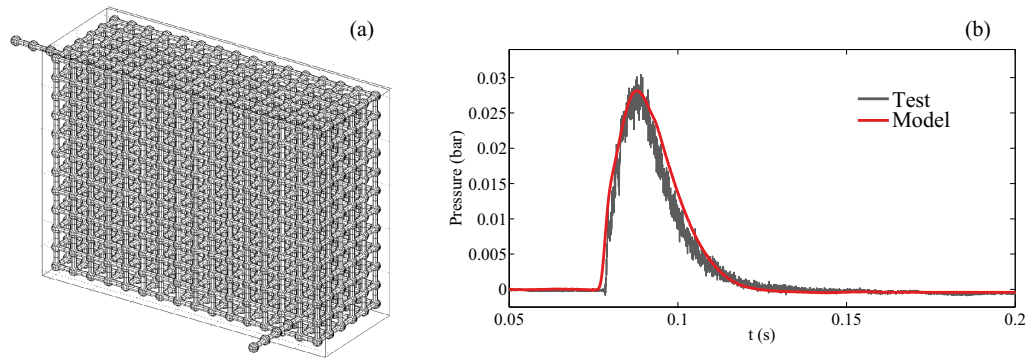


Figure 3: (a) Mesh used. (b) Transmitted pulses: measured and computed.

Corrected Transport technique has been adapted to the quasi-3D method in order to avoid overshoots at discontinuities. The resulting method has been applied to a simple silencer, and comparison with measurements indicates that further work is needed in order to reduce the dissipative character of the method.

References

- [1] T. Morel, R. Keribar, P.N. Blumberg. A new approach to integrating engine performance and component design analysis through simulation. SAE Technical Paper 880131, 1988.
- [2] G.A. Sod. Survey of several finite-difference methods for systems of non-linear hyperbolic conservation laws. *Journal of Computational Physics*, 135: 172–186, 1997.
- [3] G. Montenegro, A. Della Torre, A. Onorati, R. Fairbrother. Nonlinear quasi-3D approach for the modeling of mufflers with perforated elements and sound-absorbing material. *Advances in Acoustics and Vibration*, 2013: 546120, 2013.
- [4] J.P. Boris, D.L. Book. Flux-corrected transport. *Journal of Computational Physics*, 27: 1–31, 1978.

Formal Specification of a Planning Algorithm with Logic of Predicates Extended to Compositions of Learning Paths

Jaime A. Guzmán- Luna PhD.
professor at department of
computer science and the decision
at Universidad Nacional de
Colombia, Medellin Campus.
Medellin, Colombia. E-mail:
jaguzman@unal.edu.co

Francisco Javier Moreno PhD
professor at department of
computer science at Universidad
Nacional de Colombia, Medellin
Campus. Medellin, Colombia. E-
mail: fjmoreno@unal.edu.co

Ingrid-Durley Torres, Engineering
Master and Ph.D. student, at
Universidad Nacional de
Colombia, Medellin Campus.
Medellin, Colombia. e-mail:
idtorresp@unal.edu.co

In general, a planning problem has the following components: a description of the actions in a formal language which constitutes what have been called the Domain Theory [Weld 1999], a description of the initial state of the world and the specification of the desired state. The Domain Theory must allow judgments that represent the relevant aspects such as the conditions of the operations and their effects throughout the world. Generally, the theories of domain follow some type of model of transition of states, that is to say, they introduce a notion of state (or situation), which is an immediate description of the world in a certain point of time. Such a state connects the actions that generate the transitions among the same states. Formally, a planning problem is defined by means of the tuple: (S, S_0, G, A, R) , where S is the group of all the possible states of the world, $S_0 \in S$ denotes the initial state of the world, $G \in S$ denotes the target state of the world that the planning system will try to get, A is the group of actions that the planner could carry out in order to change from one state to another in the world, and the movement relationship $R \in S \times A \times S$ defines the precondition and its effects to implement every action.

Simultaneously, the problem of learning paths composition can be extended as a sequential interconnection, subordinating but not anticipating learning objects (LO), which satisfies a specific objective of knowledge of a user [Garrido et ál 2009a, Garrido et ál, 2009b]. This composition is framed in a virtual environment which is highly dynamic and not controlled by only one participant.

The formal definition of planning can be compared to the problem of composition of learning paths, in which, S_0 and G are the initial state and the objective state specified on the learning requirements of a user, A is a group of available LO and R denotes the switching function of the state of knowledge of the user; if the requirements of each LO are fulfilled. As a result of the previous analogy, this paper has considered to apply, for the process of composition of learning paths, a planning algorithm with extended logics which will take into account the constant perceived information in each planning state in order to add it and make updated decisions considering, in an almost immediate way, any uncertain changes in the virtual environment; incorporating some metrics which allow the evaluation of the accuracy of a LO with regard to several, based on the learning theories [Honey-Alonso, 2000].

The problems in the planning area have motivated the learning domain, where the planner is a mechanism that not must only solves the learning necessity of the user, but also does overlook the correctness of the invocation of the LO s associated to the same paths in its real scenario, must be provided.

In order to provide a composer mechanism which addresses all requirements, it is feasible to consider the application of a specific technique of planning that reaches, in every stage of planning, to consider the information perceived from the environment, aiming to incorporate it and to make updated decisions. In this way, the process of planning (composition) is able to answer to any uncertain event, in an almost immediate way, without waiting for the production of a complete plan. This type of planning is widely used in real time domains where the identified problems in the environment are solved online. In this case, they introduce a notion of state (or situation), which is an instantaneous description of the world at a given point in time. Such state relates actions that generate the transitions among the states. Most of the approaches, included the one proposed in this work, define a state S , as a set of atomic instances (facts). Every atomic instance may change or not its value through time. Thus, those that can change value are called *fluents*, and those that cannot change it are called invariants. Based on these components, the expected result of a planner is a behavior, that is, an ordered sequence of actions such that, if carried out upon the described world in the Initial State S_0 , it enables to reach a goal satisfying the given description in the Goal State G , that is the final state. This sequence of actions is known as a plan. When an action supports another this generates a causal link between them, meaning that the preceding action is finished before starting a succeeding action. With these actions, it is possible to establish a plan of the actions which will be transferred to users (students) from an initial state of knowledge of a course to a state in which formulated objectives are achieved by users (students) themselves. Expressed analogically, with a virtual learning environment, users (students) express their learning requirement depending on one or various concepts (or concept), these concepts are part of a course's contents, and they lead to one or more associated activities. This requirement must be achieved from a state of a student's initial knowledge of that domain (which is even considered null, for the specific case in which an individual knows nothing of the course content); also, including at the same time considerations regarding learning preference and style. Thus, the learning path for this case constitutes a (plan) sequence of learning activities associated to knowledge domain, and customized for a student that the student must follow to fulfill that student's objectives. In this case, the building of a planning problem is done by means of an interpretation that can be conducted computationally on both types of defined relations which may be interpreted by a planning mechanism as *AND* relations and *OR* relations; they refer to *RequiresBy* and *IsBasedFor* respectively. Thus, all the concepts defined as *AND*, must be totally completed before seeing the next, while at least one of the *OR* relations must have been completed to see what is next.

In a virtual learning environment, once an LO has been chosen as part of a sequence which reaches an objective, events may occur as for instance that there has been a change in the metadata of an LO which is part of the current learning route, or a new LO may have appeared in the environment, or that an old LO may have been eliminated, or that the link to an LO's own resource is broken. These events inevitably affect a current composition plan, enabling the possibility of invalidating totally or partially the route currently constructed as a solution to a student's learning need. Then, the idea is to review each step of planning, and see if there has been any change in the environment which may affect the composition plan (learning route) in each step of the planning, and if it happens, an immediate warning must go off allowing one to evaluate if the actions that have already been considered have been affected. In case the answer is yes, the plan is discarded and a new dominion is constructed; on the other hand, the type of event is reviewed and acts depending on an event. An important aspect to highlight is to remember that in this case LOs are available in a repository and that their existence,

elimination or updating is measured depending on the metadata recorded in it since the model adopted does not include the complete download of an LO's own content, because what is done is to record the link of the resource itself. Thus, the idea is to try to manage events from their origin in the repository, so that they may be communicated to the planning mechanism almost instantaneously. External changes in the state of the world potentially affect the planning processes in their actions, statements, facts and objects in the description of the domain's partially-generated plans. To monitor these events, adding an event listener that distinguishes the various types of events is necessary (see Figure 1). In each step of the i plan before invoking a chosen action in an S_i state, the system must listen to the events to validate if there has been one that has altered the state of the world. S_i means there are no events on the event line; then, a is applied to a S_i state followed by the $i+1$ step, assuring that the fragment of actions from S_0 to S_i are correct. Nevertheless, the system must replan in the following types of events: i) lost operator case (LO is eliminated) or ii) a LO metadata is updated.

This mode of on-line operation may be seen in the diagram in Figure 1, in which time is established by the petitions of action the execution model requests [Sapena and Onaidía, 2004]. Then, the functional schema of this reactive planning model is based on the idea of decomposing the original planning problem (PP) into independent sub-problems. Hence, the planning algorithm calculates concurrently a P_i plan separately for each one of objectives of problem " $g_i \in G$ ". The planning algorithm consists of four steps (see Figure1): The first step, which is the preprocessing, consists mainly in an instantiation of the operators and the propositionated predicates in the specification of the domain along with the instantiation of the specification of the planning problem. This step is divided in three tasks: (i) verification of domain and PDDL problem through a parser; (ii) analysis of possibilities for achieving goals, in which all possible actions which lead to a satisfaction state are generated, (iii) data structure to store all the previous information. The second step of the algorithm corresponds to the Relaxed Planning Graph, which is related to generation of the necessary heuristic for the construction of the plans. The RPGs, provides necessary heuristic information for the construction of plans. In our agent, we have modified traditional RPG, because we should have in mind the partial knowledge of Web.

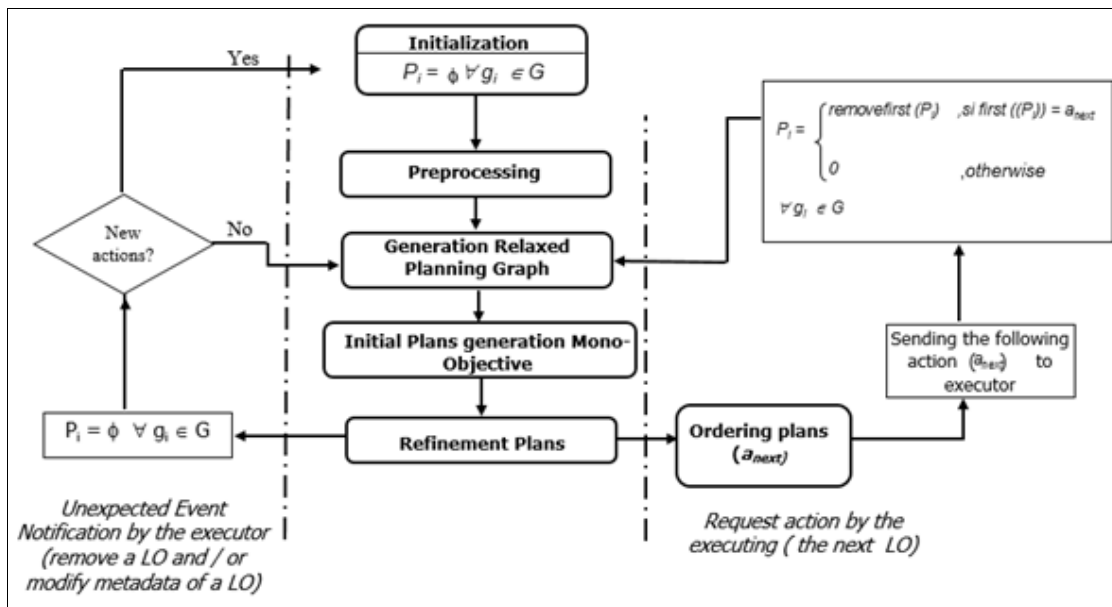


Figure 1. Planning Algorithm

In our agent's RPG, due to the tri-valued logics it uses, literal levels will be called propositional levels because these will have logic propositions (not literal ones). The first level L_0 , will have all logic propositions which are satisfied in S_0 . Actions levels A_t have all actions, which positive and negative pre-conditions are found in level L_t . The following level L_{t+1} , extends L_t with positive and negative effects of actions A_t . A propositional level may have two propositions which represent the same literal, one in a positive way and the other one in a negative way. In this way, in t steps of time, we can obtain that a L_t will then have P_i and $\neg P_i$ propositions. Since during the service composition process, several alternative solution plans appear, it is necessary to consider a metric or optimization function of the problem in order to select the best possible alternative. With this purpose, our RPG, associate each level of graph to the metric's cost the planner tries to optimize. The main difference with traditional RPG is that graph levels do not represent the number f actions applied but relative costs to the metrics of the problem (m). The RPG expands according to cost all possible actions until accomplishing the objectives, see Figure2.

```

1 // Initializing cost
2 cost(p)= { 0 , if satisfy(p, S0) = V' ∀ pi ∈ PL
           ∞ , otherwise
3 //First propositional level
4 t=0; Lt= { p ∈ PL / cost (p) = 0 }
5 New_Prop = φ
6 //RPG expands to all objectives
7 while ∃ g ∈ G / g ≠ Lt do
8 // Levels actions
9 At = { a ∈ A / Lprec (a) ∈ Lt ∧ ExecutionFailed (a) ≠ true } ∪ { α ∈ A / Lprec (α) ∈ Lt
10 cost_reach (a) = ∑p ∈ Lprec(a) cost (p) ∀ a ∈ At
11 // Cost of the effects of At actions
12 for all pi ∈ Leff (a), a ∈ At do
13 new_cost = min (cost_reach (ai) + cost (ai), ∀ ai ∈ At / pi ∈ Leff (ai)
14 cost (pi) = min (cost (pi), new_cost)
15 endfor
16 // New proposals reached
17 New_Prop = New_Prop ∪ Leff (a) - Lt, ∀ a ∈ At
18 if New_Prop = φ, then fail endif
19 //Next propositional level
20 next_t = min (cost (p) ), ∀ p ∈ New_Prop
21 Lnext_t = Lt ∪ { p ∈ New_Prop / cost (p) = next_t }
22 New_Prop = New_Prop - Lnext_t
23 t = next_t
24 endwhile
    
```

Figure 2. RPG with Costs

The calculation of each P_i plan is done incrementally, when a possibly incomplete initial P_i plan is constructed (or a skeleton), constantly monitored by an event monitor, being refined as the planner has available time. Finally, existing conflicts between said plans are studied to decide which action from which plan will be the first to be executed (a_{next}). The planning model sends a_{next} to the execution model when it requests it, and then updates its beliefs of the world assuming that the action sent will have a successful execution. In case an action fails, the execution model notifies the planning model so that it may once again

calculate the plans on the previous state to the a_{next} sent. All of the above process repeats continuously until the user decides to stop the planner's execution, or until when the planning component has reached all objectives; to do so, it returns a special action: *NOP* (no operation).

```

1. RPG expansion until the goal
2.   while  $\exists g \in G / \text{cost}(g) = \infty$  do
3.     //Calculation of the action list sensorization
4.      $L_{sens} = \{ \alpha \in A_t / \exists l_i \in \text{Leff}(\alpha) \wedge (\text{cost}(l_i) = \infty \wedge \text{cost}(\neg l_i) = \infty) \}$ 
5.     if  $L_{sens} = \phi$ , then fail endif
6.     //Determination of Action sensing lower cost
7.      $\alpha = \text{argmin}(\text{cost\_reach}(\alpha_i) + \text{cost}(\alpha_i)), \forall \alpha_i \in L_{sens}$ 
8.     // Calculation of new effects produced  $\alpha$ 
9.      $\text{New\_Eff} = \{l_i\} \cup \{\neg l_i\}, \forall l_i \in \text{Leff}(\alpha) / \text{cost}(l_i) = \infty \wedge \text{cost}(\neg l_i) = \infty$ 
10.    //Inserting  $\alpha$  effects RPG
11.     $t = \text{cost\_reach}(\alpha) + \text{cost}(\alpha)$ 
12.     $\text{cost}(p) = t, \forall p \in \text{New\_Eff}$ 
13.     $L_k = L_k \cup \text{New\_Eff}, k \geq t$ 
14.    // Re-expansion of the RPG (lines 5-24 of Figure 2)
15.    call Expansión-RPG
16.  endwhile

```

Figure 3. RPG algorithm with RPG sensing actions effects

NOP is an action without preconditions or effects which allows the planner to wait some time without performing any task. During this latter time, if a user introduces new objectives, the planner will calculate new plans again. This last objective modification characteristic also applies to any point in time in which the planning process is conducted.

REFERENCES

- [Honey-Alonso 2002] HoneyAlonso. 2002. Honey alonso learning style theoretical basis in spanish. Available at <http://www.estilosdeaprendizaje.es/menuprinc2.htm>.
- [Garrido et ál, 2009a] A. Garrido, E. Onaindía y O. Sapena. Planificación inteligente de rutas de aprendizaje personalizadas. XV JENUI. Barcelona, 8-10 de julio 2009. ISBN: 978-84-692-2758-9. <http://jenui2009.fib.upc.edu/> consultada Agosto 2010.
- [Garrido et ál, 2009b] A. Garrido, E. Onaindía, Ll. Morales, L. Castillo, S. Fernández y D. Borrajo. Modeling E-Learning Activities in Automated Planning. In Proceedings of International Competition on Knowledge Engineering for Planning and Scheduling, ICAPS'09, Thessaloniki (Greece), September. 2009.
- [Sapena and Onaidía, 2004] O. Sapena, E. Onaindia. Domain Independent Anytime Planning for Dynamic Environments, "Frontiers in Artificial Intelligence", volume 113, pp 433-440, 2004.
- [Weld 1999] D.S. Weld. Recent advances in AI planning. AI Magazine, 20(2): pp. 93-123, 1999

Multiple seasonal Holt–Winters models applied to Spanish short–term electricity demand forecasting: an alternative to the Red Eléctrica de España model

J.Carlos García–Díaz^b and O. Trull

^(b) Department of Statistics, Applied Operational Research and Quality,
Universitat Politècnica de València

November 28, 2014

1 Introduction

Short-term electricity demand forecasting is an essential instrument in power system planning, operations and control. The control and scheduling of the demand for electricity in power supply systems using time series forecasting is a powerful methodology used in power distribution systems worldwide. Red Eléctrica de España, S.A. (REE) is the operator of the Spanish electricity system. Its mission is to ensure the continuity and security of the electricity supply. The goal of this paper is to improve the forecasting of very short-term electricity demand (time-horizon of less than 24 hours) using multiple seasonal Holt-Winters models without exogenous variables, such as temperature, calendar effects or day type, for the national electricity market of Spain. We implemented 30 different models and evaluated them using software developed in MATLAB® for this purpose. The performance of the methodology is validated via out-of-sample comparisons using real data from the operator of the Spanish electricity system. A comparison study between the REE models and the multiple seasonal Holt-Winters models is conducted.

Table 1: Implemented models: The first letter defines the trend method(N: None, A:Additive, d:Damped additive,M:Multiplicative,D:Damped multiplicative); the second the seasonal method(N: None, A:AdditiveM:Multiplicative) and the last letter stands for AR(1) adjustment (L:not adjusted, C:adjusted).

Trend \ Seasonality	None	Additive	Multiplicative	None	Additive	Multiplicative
	Normal			AR(1)Adjusted		
None	NNL	NAL	NML	NNC	NAC	NMC
Additive	ANL	AAL	AML	ANC	AAC	AMC
Damped Additive	dNL	dAL	dML	dNC	dAC	dMC
Multiplicative	MNL	MAL	MML	MNC	MAC	MMC
Damped Multiplicative	DNL	DAL	DML	DNC	DAC	DMC

2 implemented models

Double and triple seasonal Holt Winters models (HWT) were introduced by Taylor [1, 2] as an evolution of Holt-Winters methods[3]. Here, we propose a generalisation to n-seasonality of the HWT models, where the time series is divided into recursive equations: level smoothing; trend smoothing; and as many seasonality smoothing equations as seasonal patterns are taken into account. A final forecast equation uses the previous information to provide a k-step-ahead forecast. We denote this model as nHWT, and we summary all available models in Table 1.

3 Spanish short-term electricity demand forecasting

The data set used in this paper covers 1 July 2007 to 9 April 2014. It is provided by REE. REE also provides the forecasts for the next hours. The data set comprises all the transactions done in mainland Spain, not including the Canary Islands or the Balearic Islands. This kind of series is highly dominated by three seasonal patterns: the daily cycles (intra-day), with a period length of $s_1 = 24$, the weekly cycles (intra-week), with length $s_2 = 168$, and the yearly cycles (intra-year), with $s_3 = 8766$.

In order to find the best predictive model, the work carried out is divided into two stages: first, a search for the in-sample forecasting model, and in a second step, a validation of out-of-sample forecasting is carried out.

The optimisation problem was solved using a methodology specifically developed and implemented in the software program running on the MATLAB®

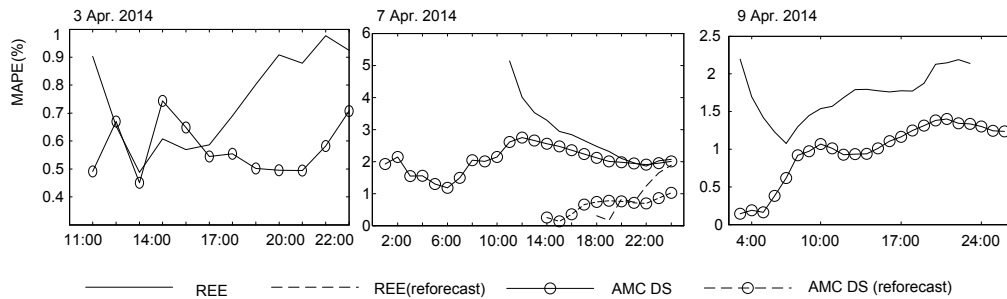


Figure 1: Forecasting accuracy evolution of the chosen model compared to the REE, measured using MAPE along the forecast horizon.

environment. In this Section, an extensive set of computational results and comparative studies are presented to study the performance of the proposed nHWT models for short-term demand forecasting implemented in the software package. The results are compared numerically with those obtained by the REE model in the same periods. Three alternatives, using double and triple seasonal methods for all models, were analysed by computing forecasts using the implemented models. As a result, the AMC DS model is selected. The validation process was carried out by comparing real time forecasts proposed by REE and forecasts obtained with the selected model. The validation took place during the weeks from 3 April 2014 to 9 April 2014, the last dates available at the time the study was carried out. In order to provide forecasts for these dates, models were optimised using the full data set until the forecasting period, and 24-hour forecasts were provided. Figure 1 depicts the evolution of the MAPE obtained during the validation process by the chosen model and REE. The left graph shows the first case, in which 12-hour forecast horizon results are compared, as REE only forecasted until 22:50 hours. The accuracy obtained with our model is around 0.6%, whereas the REE model reaches 0.9%. On the graph on the right, the 9 April 2014 results are analysed. The AMC DS has an average MAPE of around 1%, outperforming the REE, which reaches 1.5%. In order to check the horizon in which our model could provide accurate forecasts, a forecast was made 24 hours ahead, from 01:00 to 24:00 hours on 7 April 2014, with AMC DS. The model outperforms the forecasts provided by REE at 10:30, which asymptotically reaches the performance obtained by the AMC DS. A re-forecast made at 13:00 with AMC DS enhances the results, whereas the re-estimation by

REE at 17:00 hours enhances its performance, but decreases drastically after only a few hours, reaching the MAPE obtained by the original estimation with AMC DS.

4 Conclusions

This paper presents an alternative methodology for forecasting the Spanish short-term electricity demand, using models that parsimoniously provide forecasts comparable to the REE model. A generalisation to n-multiple seasonal models of the HWT models is proposed, and new initialization criteria are developed for multiple seasonal components. The methodology was implemented in a software application using the MATLAB® environment to predict hourly electricity demand in Spain by selecting from 30 multiple Holt-Winters models with improved optimisation of smoothing parameter methods. An analysis using the Spanish data is conducted in two stages. The purpose of the first stage is to select the best model for the forecasts. In a second stage, a validation analysis is conducted by making real time forecasts and comparing them to REE. The REE model has more than 100 parameters that are estimated hourly, and it has a performance of around 2% in terms of MAPE, whereas the methodology presented here shows results similar to those obtained by the REE, obtaining MAPE between 0.6% and 2% in the time period considered, but a maximum of 5 parameters are optimized in the proposed models, significantly reducing the computational effort.

References

- [1] Taylor, J.W. Short-term electricity demand forecasting using double seasonal exponential smoothing. *Journal of Operational Research Society*, 54:799–805, 2003.
- [2] Taylor, J.W. Triple seasonal methods for short-term electricity demand forecasting. *European Journal of Operational Research*, 204:139–152, 2010
- [3] Winters, P.R. Forecasting sales by exponentially weighted moving averages. *Management Science* 6:324–342, 1960

Analysis of mobile Apps lifecycle. Epidemiological modelling approach by random networks

J. Alegre-Sanahuja^{b*}, J.-C. Cortés^b,
F.J. Santonja[†] and R.-J. Villanueva^b,

(^b) Instituto Universitario de Matemática Multidisciplinar,
Universitat Politècnica de València, Spain,

([†]) Departamento de Estadística e Investigación Operativa, Universitat de València, Spain.

November 28, 2014

1 Introduction and motivation

The mobile apps market is a really big market growing every year: Worldwide mobile phone sales to end users totalled 1.8 billion units in 2013, an increase of 3.5% from 2012 [1], and there are millions of apps available to millions of users at the app markets [2]. These application market places are native to the major mobile operating systems, being the most important markets Google Play, for Android OS, and App Store, for iOS. In 2014, global market share was 85% for Android, 11% for iOS, 3% for Windows Phone and the remaining 1% for all other platforms [3]. In June 2014, the number of available apps and downloaded apps at the official most important markets are listed in Table 1, [4, 5].

Furthermore, there are third-party platforms that are non-official market places used as alternatives for operating system native distribution platforms [2]. For Android platform, there are multiple non-official markets, some

*e-mail: juaalsa@doctor.upv.es

App Store	Available Apps	Downloads to date
Google Play	1.200.000	50 bi
App Store (iOS)	1.200.000 +	75 bi +

Table 1: Available apps and downloads. Principal markets. Source [4, 5].

of them preinstalled by other original equipment manufacturers (OEMs) in millions of devices [6]. In these big markets, it would be seem that the key values for the app developers are the number of downloads of their apps and how the app is ranked in the markets, but not less important are the number of active users over the time, the virality of the app and the retention of the users. In this work, we propose an epidemiological model in order to estimate the evolution of the apps over a theoretical network. The paper also includes the analysis of the potential spread of the apps, the user behavior and the user retention, i.e. the lifecycle of the apps. With this model we will be able to understand this lifecycle, in such a way that it permits to classify the apps to know what spread can we expect for an app; the number of active users over the time; the retention of the users, etc. In this way, we will be able to provide crucial information for apps's companies such as when is the best moment to launch an actualization of the app in order to control the user retention.

2 Model Building and parameters

2.1 Model building

Our model will be build by a random network, so we have to define the network attributes that will establish the behavior of the models's agents. These attributes are:

- Type of network.
- Number of nodes.
- Number of edges.
- Number of initial infected nodes.

- Infection rate.
- Recovery rate.

In the extant literature, there are several approaches to modeling the spread of apps [7, 8, 9] and it is well documented the dynamics of viral marketing [10]. These works claim that:

- People who spend more time in face-to-face interaction are more likely to share common apps.
- Apps do spread via social interaction.
- Face-to-face interaction has a strong correlation with app diffusion.
- Social networks play an important role in consumers decisions to download and use mobile apps.

therefore, we will model our network as an epidemiological random network. Specifically, it will be a SIR-type network: the users (nodes) will be infected when an app is downloaded; the users will be susceptible or not *infected* when they have not download the app yet and the users will become recovered (and immune) when the app has been removed.

The number of nodes (or users) will be a random population and the number of edges will be the friendship *face-to-face relations* between users.

The number of initial infected nodes will be random, the infection rate will be defined based on the face-to-face relation (connections or friends) between nodes and the recovery rate will be based on the user retention.

2.2 Model parameters

For our model, we have to define the parameters that will be used for the initialization and simulations of the dynamic network.

The parameters that we have to determine are:

- Simulation time.
- User retention rate.
- Infection rate.

The simulation time will be 100 days, because, as showed in [11], the Android OS app half life is 3 months.

For the user retention rate, we know, from [12], the retention rates of apps by users are 30, 60 and 90 days. We can express these rates as the probability that a user retains the app more than 30, 60 or 90 days, i.e., $\mathbb{P}[X \geq 30]$, $\mathbb{P}[X \geq 60]$ and $\mathbb{P}[X \geq 90]$, respectively. We will model this retention by means of an exponential distribution

$$f(x) = \mathbb{P}[X \leq x] = 1 - e^{-\lambda x}, \quad \lambda > 0, \quad (1)$$

being x the time the user has the app downloaded in his/her device and λ the parameter needed to estimate the user retention days given in the function (1). Given the values in [12], we obtain λ values that will be between 0.008273 (for high retention rates) and 0.03539 (for low retention rates).

We assume that the infection rate parameter will be a function of k/t_s , being k the number of edges (or friends) per node, and being t_s the simulation time

$$\beta = \delta \frac{k}{t_s}, \quad (2)$$

where $0 < \delta < 1$ parameter is the *tuning* parameter needed to estimate the user infection rate β .

Finally, in order to initialize the network we have to determine:

- The population or number of nodes.
- The number of initial infected nodes.
- The face-to-face relations or edges between nodes.

Now, we will fix our random population in 1000 nodes, the number of initial infected nodes will be randomly chosen between 1 and 50 infected users and the user retention rate and infection rate will be a value for λ between 0.008273 and 0.03539, and for δ between 0 and 1.

For the number of edges (or friends of the users), we will based upon the results recently obtained by the authors regarding the Spanish population between 15 and 20 years old [13]. According to this latter paper, we will consider a mean of 13.25 friends and standard deviation of 8.27. We focus on this 15–20 aged people because this group is considered as *Mobile Addicts*, i.e., a consumer that launches apps more than 60 times per day, and then, they are the most susceptible to *app infection* by others than another age groups [14].

2.3 Simulations

For modelling simulations, we will have a set of one fixed parameter and three variable parameters. The fixed parameter will be the number of nodes (1000), and the variable parameters will be:

- Number of initial infected nodes: A random integer number generated within the interval $[1, 50]$.
- Infection rate: A random number generated in the interval $[0, 1]$ being δ the parameter included in (2).
- User retention rate: A random number generated in the interval $[0, 1]$ (normalized values of $\lambda > 0$ parameter that appears in (1)).

In order to compute reliable estimations based on 95% confidence intervals (CI 95%), we will use the technique referred to as Latin Hypercube Sampling (LHS) [15] to select sets of the variable parameters to be substituted into the model. Latin Hypercube Sampling (a type of stratified Monte Carlo sampling) is an efficient method for achieving equitable samples of all input parameters simultaneously. With LHS we obtain an equitable sample of 100 000 input parameters simultaneously. We substitute each set of the 100 000 parameters into the model and then we run a simulation. From the 100 000 simulations, we obtain the 95% confidence interval.

As expected, in Figure 1 one observes that each the mean curve (Infected, Susceptible and Recovered) obtained from the 100 000 simulations, follows the curve for a standard app, with a peak of downloads (infected) around the 20-th day and the 30-th day, and a decreasing trend after the 30-th day [11].

In Figure 2, we have plotted both the mean curves and their 95% confidence intervals. These are big enough to capture all the possible behaviors for apps.

Using the division into quadrants showed in Figure 3, we can classify the apps depending on the set of parameters, user retention rate and infection rate, used for the network simulation.

- The $Q1$ quadrant will be apps with great virality and low retention, as for example, an app for a successful marketing campaign.

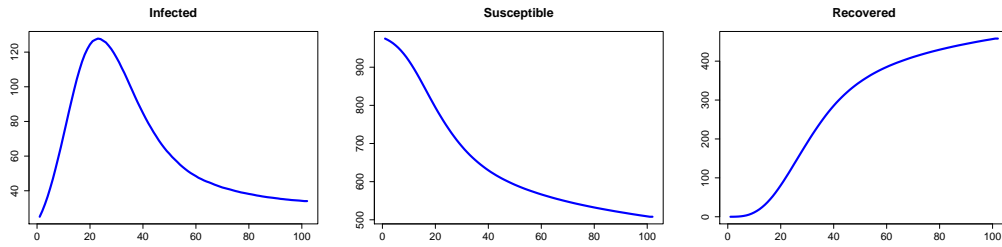


Figure 1: Mean curves for the 100 000 simulations.

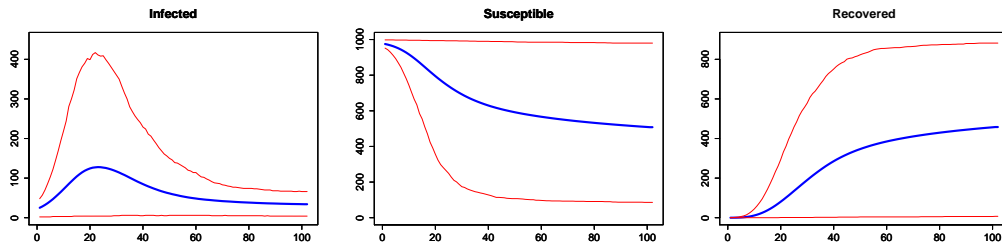


Figure 2: Mean curves (blue) and 95% confidence intervals (red) for the 100 000 simulations.

	User retention rate 0 → 1		
Infection rate 0 ↓ 1	Q1		Q3
		Q5	
	Q7		Q9

Figure 3: Apps classification by quadrants.

- The $Q3$ will show great virality and high retention rate, i.e. very successful apps
- The $Q5$ quadrant will correspond to standard apps, with mean virality and mean retention rates.
- The $Q7$ quadrant will be apps with low virality and low retention, i.e., bad quality apps.
- The $Q9$ quadrant will be apps with low virality and high retention, as for example utilities apps.

For example, the Figure 4 shows some of the curves obtained for the $Q1$ quadrant after 100 000 simulations.

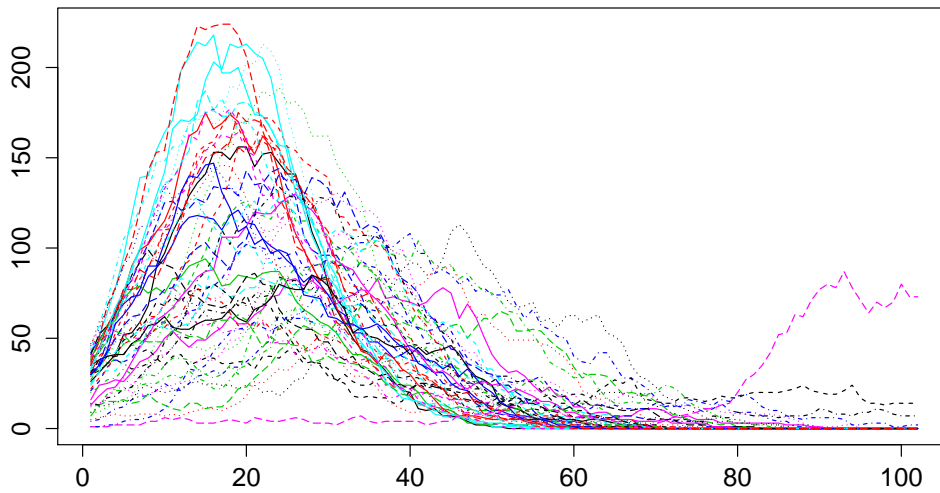


Figure 4: Infected vs Days.

It can be seen the great virality of the app with peaks of more than 200 users around day 20, and the low retention, with a clear decline tendency after the peak of downloads.

With this bank of simulations, we can estimate the evolution of an app knowing the numbers of downloads at the early stages after launching an app. Looking for the curve from our bank that fits better with the behavior (number of downloads at the early stages) of the app that we want to control, we can estimate:

- How quickly is going to grow.
- If it is going to be viral.
- What happens after the number of downloads peaks.
- If the downloads decline quickly or not.
- When we should launch a new version of the app in order to retain the users.

3 Conclusions

We have proposed an epidemiological random network model to analyze the mobile apps lifecycle, based on the assumption of the epidemiological effect for the spread of apps.

The results of the simulations of the model shows the same behavior as known behavior of evolution of standard apps, with peaks of downloads, decline curves and time of life similar to real apps. Therefore, with this model, we can understand the apps lifecycle and classify the apps. Furthermore, the simulations bank resulted from running the model 100 000 times with different sets of realistic parameters, gives us a bank of 100 000 possible behaviors that permits to predict the future behavior of an app looking at its evolution in the early days of its launching and looking for the curve of our bank that best fits evolution. In this way, we can estimate how quickly is going to grow, if it is going to be viral, what happens after the number of downloads peaks, if the downloads decline quickly or not, when we should launch a new version of the app in order to retain the users, etc. This information can be very useful for app developers that want to know the expected evolution of their apps on the market places looking at its evolution in the early days of its launching.

Acknowledgements

This work has been partially supported by the Ministerio de Economía y Competitividad grants MTM2013-41765-P and TRA2012-36932.

References

- [1] <http://www.gartner.com/newsroom/id/2665715>
- [2] http://en.wikipedia.org/wiki/List_of_mobile_software_distribution_platforms
- [3] http://en.wikipedia.org/wiki/Mobile_operating_system
- [4] [http://en.wikipedia.org/wiki/App_Store_\(iOS\)](http://en.wikipedia.org/wiki/App_Store_(iOS))
- [5] http://en.wikipedia.org/wiki/Google_Play
- [6] <http://www.onepf.org/appstores>
- [7] N. Aharony, W. Pan, C. Ip, A. Sandy Pentland: Tracing Mobile Phone App Installations in the *Friends and Family* Study. Pentland MIT Media Laboratory, Cambridge 02139, MA, USA.
- [8] D.G. Taylor, T.A. Voelker, I. Pentina: Mobile application adoption by young adults: A social network perspective.
- [9] W. Pan, N. Aharon, A. Sandy Pentland: Composite Social Network for Predicting Mobile Apps Installation. Pentland MIT Media Laboratory, Cambridge 02139, MA, USA.
- [10] J. Leskovec: The Dynamics of Viral Marketing. Machine Learning Department, Carnegie Mellon University, Pittsburgh, PA. Lada A. Adamic School of Information, University of Michigan, Ann Arbor, MI. Bernardo A. Huberman HP Labs, Palo Alto, CA 94304.
- [11] Benchmarking the Half-Life and Decay of Mobile Apps. Flurry insights. <http://www.flurry.com/bid/108904/Benchmarking-the-Half-Life-and-Decay-of-Mobile-Apps#.VH3dwtKG9e8>

- [12] App Engagement: The Matrix Reloaded. Flurry insights. <http://www.flurry.com/bid/90743/App-Engagement-The-Matrix-Reloaded#.VH2tJNKG9e8>

- [13] E. Navarro-Pertusa, A. Reig-Ferrer, E. Barber Heredia, R.I. Ferrer Cascales (2006): Grupo de iguales e iniciación sexual adolescente: diferencias de género (Groups of pairs and adolescent sexual initiation). *International Journal of Clinical and Health Psychology* 6(1), 79–96.

- [14] The Rise of the Mobile Addict. Flurry insights. <http://www.flurry.com/blog/flurry-insights/rise-mobile-addict#.VH20UNKG9e8>

- [15] A. Hoare, D.G. Regan, D.P. Wilson (2008): Sampling and sensitivity analyses tools (SaSAT) for computational modelling, *Theoretical Biology and Medical Modelling* 5, article 4, 2008.

A compact difference scheme for second order dual-phase-lagging models of heat conduction

M.A. Castro *, F. Rodríguez, J. Cabrera, and J.A.Martín

Dep. Matemática Aplicada, Universidad de Alicante,

Apdo. 99, 03080 Alicante, Spain.

November 28, 2014

1 Introduction

Non-Fourier models of heat conduction have been incorporated in the last years in the modeling of microscale heat conduction in a broad range of engineering and biomedical problems (see, e.g., [1, 2, 3]). The dual-phase-lagging (DPL) model assumes the presence in the Fourier law of time lags in the heat flux and the temperature gradient,[4],

$$\mathbf{q}(\mathbf{r}, t + \tau_q) = -k\nabla T(\mathbf{r}, t + \tau_T), \quad (1)$$

where τ_q and τ_T are, respectively, the phase lags in the heat flux vector, \mathbf{q} , and the temperature gradient, ∇T , t and \mathbf{r} are the time and spatial coordinates, and k is the conductivity. This leads to heat conduction models that include the time lags either in the form of partial differential equations with delay or with terms of different orders, usually up to order two [5, 6, 7, 8]. In this work, second order models are denoted DPL(2,2),

$$\begin{aligned} \frac{\partial}{\partial t}T(\mathbf{r}, t) + \tau_q \frac{\partial^2}{\partial t^2}T(\mathbf{r}, t) + \frac{\tau_q^2}{2} \frac{\partial^3}{\partial t^3}T(\mathbf{r}, t) \\ = \alpha \left(\Delta T(\mathbf{r}, t) + \tau_T \Delta \frac{\partial}{\partial t}T(\mathbf{r}, t) + \frac{\tau_T^2}{2} \Delta \frac{\partial^2}{\partial t^2}T(\mathbf{r}, t) \right). \end{aligned} \quad (2)$$

*e-mail: ma.castro@ua.es

Difference schemes to obtain numerical solutions of different DPL models have already been proposed (see, e.g., [9, 10]). In this work, a compact difference scheme [11] for second order DPL models is developed, showing their properties of consistency, stability, and convergence. Numerical examples illustrate the higher precision of the new method in comparison with a previously proposed lower order scheme [12].

2 Construction and properties of the new difference scheme

Writing

$$A = \frac{1}{\alpha}, \quad B = \frac{\tau_q}{\alpha}, \quad C = \frac{\tau_q^2}{2\alpha}, \quad D = \tau_T, \quad E = \frac{\tau_T^2}{2}, \quad (3)$$

we introduce the two new variables

$$v(x, t) = BT(x, t) + C \frac{\partial}{\partial t} T(x, t), \quad u(x, t) = AT(x, t) + \frac{\partial}{\partial t} v(x, t), \quad (4)$$

so that

$$\frac{\partial}{\partial t} T(x, t) = \frac{1}{C} (v(x, t) - BT(x, t)) \quad (5)$$

and

$$\frac{\partial}{\partial t} v(x, t) = u(x, t) - AT(x, t). \quad (6)$$

Then, it can be shown that Eq. 2 can be equivalently written as

$$\frac{\partial}{\partial t} u(x, t) = a \frac{\partial^2}{\partial x^2} T(x, t) + b \frac{\partial^2}{\partial x^2} v(x, t) + c \frac{\partial^2}{\partial x^2} u(x, t), \quad (7)$$

where

$$a = (C^2 + EB^2 - BDC - ACE)/C^2, \quad b = (DC - BE)/C^2, \quad c = E/C. \quad (8)$$

Using appropriate finite difference approximations, after some algebraic manipulations one can get to the expressions

$$\frac{1}{k} (T_j^{n+1} - T_j^n) = -\frac{B}{2C} (T_j^{n+1} + T_j^n) + \frac{1}{2C} (v_j^{n+1} + v_j^n), \quad (9)$$

$$\frac{1}{k} (v_j^{n+1} - v_j^n) = \frac{1}{2} (u_j^{n+1} + u_j^n) - \frac{A}{2} (T_j^{n+1} + T_j^n), \quad (10)$$

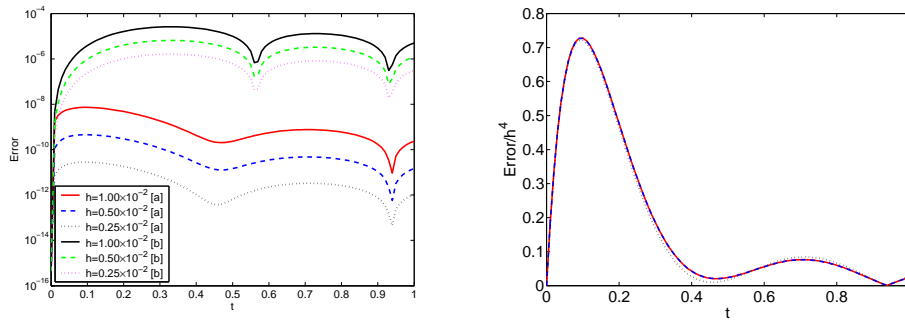


Figure 1: Left: Comparison of the absolute errors for the new scheme developed in this work and the previous method in [12], for three different mesh sizes. New scheme: lower three lines, [a]. Previous method: upper three lines, [b]. Right: Maximum errors of the approximate solutions, in terms of time, in relation with the size of the mesh.

and

$$u_{j-1}^{n+1} + 10u_j^{n+1} + u_{j+1}^{n+1} - (u_{j-1}^n + 10u_j^n + u_{j+1}^n) = 6ak\delta_x^2 (T_j^{n+1} + T_j^n) + 6bk\delta_x^2 (v_j^{n+1} + v_j^n) + 6ck\delta_x^2 (u_j^{n+1} + u_j^n). \quad (11)$$

These expressions constitute the basis to express the scheme in matrix form, and then analyze its properties of stability, consistency and convergence. Assuming sufficient regularity of the solution of the problem, it is not difficult to prove the consistency of the method. To prove its unconditional stability, we used a form of Gronwall inequality and a continuity argument to relate the stability of the new method to that of a classical method for the heat equation. Then, convergency of the method follows from Lax theorem, and the truncation error can be shown to be $O(k^2) + O(h^4)$, where $h = \Delta x$ and $k = \Delta t$ are the spatial and temporal increments, defining the geometry of the mesh for the numerical approximations.

An illustration of the error properties of the new scheme, and its better accuracy as compared with the method in [12], is presented in Figure 1, for a DPL(2,2) model with initial conditions

$$T(x, 0) = \sin(\pi x), \quad \frac{\partial}{\partial t}T(x, 0) = -\pi^2 \sin(\pi x), \quad \frac{\partial^2}{\partial t^2}T(x, 0) = \pi^4 \sin(\pi x), \quad x \in [0, l],$$

and with parameters $l = 1$, $\alpha = 1$, $\tau_q = \frac{1}{16}$, and $\tau_T = \frac{2}{\pi^2} - \frac{1}{16}$.

In Fig. 1, left, the absolute errors of the new method are compared with the corresponding errors of the previous method in [12], showing the higher accuracy of the new scheme. The right subfigure shows the relative errors in relation with the mesh size, in agreement with the order of the method.

Acknowledgements

This work was partially funded by grant GRE12-08 from University of Alicante.

References

- [1] Vadasz J.J., and Govender S. Thermal wave effects on heat transfer enhancement in nanofluids suspensions. *Int. J. Thermal Sci.*, 49:235–242, 2010.
- [2] Xu F., Seffen K.A., and Liu T.J. Non-Fourier analysis of skin biothermomechanics. *Int. J. Heat Mass Transfer*, 51:2237–2259, 2008.
- [3] Zhou J., Chen J.K., and Zhang Y. Dual-phase-lag effects on thermal damage to biological tissues caused by laser irradiations. *Comput. Biol. Med.*, 39:286–293, 2009.
- [4] D.Y. Tzou, Macro- to Microscale Heat Transfer: The Lagging Behavior. Taylor & Francis, Washington, 1996.
- [5] Kulish V.V., and Novozhilov V.B. An integral equation for the dual-lag model of heat transfer. *ASME J. Heat Transfer*, 126:805–808, 2004.
- [6] Xu M. and Wang L. Dual-phase-lagging heat conduction based on Boltzmann transport equation. *Int. J. Heat Mass Transfer*, 48:5616–5624, 2005.
- [7] Tzou D.Y. The generalized lagging response in small-scale and high-rate heating. *Int. J. Heat Mass Transfer*, 38:3231–3240, 1995.
- [8] Tzou D.Y. A unified approach for heat conduction from macro to microscales. *ASME J. Heat Transfer*, 117:8–16, 1995.

- [9] Dai W., and Nassar R. A finite difference scheme for solving the heat transport equation at the microscale. *Numer. Methods Partial Differential Equations*, 15:697–708, 1999.
- [10] Dai W., and Nassar R. A compact finite difference scheme for solving a one-dimensional heat transport equation at the microscale. *J. Comput. Appl. Math.*, 132:431–441, 2001.
- [11] Lele S.K. Compact finite difference schemes with spectral-like resolution. *J. Comput. Phys.*, 103:16–42, 1992.
- [12] Cabrera J., Castro M.A., Rodríguez F., and Martín J.A. Difference schemes for numerical solutions of lagging models of heat conduction. *Math. Comput. Modelling*, 57:1625–1632, 2013.

Simulation of atomization process in diesel sprays

F.J. Salvador^{b*}, D. Jaramillo-Císcar^b, J.-V. Romero[†] and M.-D. Roselló[†]

(^b) CMT-Motores Térmicos, Universitat Politècnica de València,
Camino de Vera s/n, Edificio 6D, 46022 Valencia, Spain,

([†]) Instituto de Matemática Multidisciplinar, Universitat Politècnica de València,
Camino de Vera s/n, Edificio 8G, 2º, 46022 Valencia, Spain

November 28, 2014

1 Introduction

Last decades have been characterized by a continuous increase in computational resources. For the study of diesel spray this increase allows to move forward to use more complex models for breakup, evaporation, coalescence, turbulence, etc.

In terms of turbulence modelling, the classes of models from lower to upper computational cost are: RANS (Reynolds averaged Navier-Stokes) [9, 10], LES (large eddy simulations) [6, 11] and DNS (direct numerical simulations) [3, 5, 4]. While RANS methods [9, 10] have been used along several decades, the use of LES models [6, 11] is more recent and even now the computational requirements for the use of DNS [3, 5, 4] is still very high for study typical current conditions in diesel engines.

However, despite all the computational difficulties some people [5, 4, 2] have tried to approach DNS to diesel sprays. Some basic procedure to use

*Corresponding author, e-mail: fsalvado@mot.upv.es, Telephone: 34-963879659, Fax: 34-963877659

DNS has been to reduce spray velocity and reduce the studies to first millimetres to only consider primary atomization. In the same way we have performed in this study, AMR (adaptive mesh refinement) [4, 2] has been used to reduce the computational cost of simulations.

The aim of this study is to show the potential of a new code [7, 8] to perform simulations of primary atomization in diesel sprays in a DNS approach. For reduce the computational time the following strategy has been used: Low spray velocity and AMR.

The present paper has been split into 5 sections. In Section 2, a brief description of the numerical code will be performed, in Section 3 the computational simulations will be validated against a theoretical model available in the bibliography. After the validation, in Section 4, a study about the influence over the spray of periodic perturbation on the velocity will be described. For finish, at Section 5, main conclusions will be drawn.

2 Numerical Code

For this study the numerical code “Gerris”, developed by Stéphane Popinet [7, 8], has been used. This code solves Navier-Stokes equations with surface tension for incompressible flow (1)–(3)

$$\rho (\partial_t \mathbf{u} + \mathbf{u} \cdot \nabla \mathbf{u}) = -\nabla p + \nabla \cdot (2\mu \mathbf{D}) + \sigma k \delta_s \mathbf{n}, \quad (1)$$

$$\partial_t \rho + \nabla \cdot (\rho \mathbf{u}) = \mathbf{0}, \quad (2)$$

$$\nabla \cdot \mathbf{u} = \mathbf{0}, \quad (3)$$

where $\rho = \rho(\mathbf{x}, t)$ is the fluid density, $\mathbf{u} = (u_x, u_y, u_z)$ is the fluid velocity, p is the pressure field, $\mu = \mu(\mathbf{x}, t)$ is the dynamic viscosity, \mathbf{D} is the deformation tensor, σ is the surface tension coefficient, k and \mathbf{n} are the curvature and the normal vector to the interface, respectively, and δ_s is the Dirac distribution which expresses that the surface tension term is active only in the interface. In our simulations diesel fuel is injected into a gas environment, the density and the viscosity depend of the concentration of diesel (4)–(5),

$$\rho(c) = c\rho_f + (1 - c)\rho_a, \quad (4)$$

$$\mu(c) = c\mu_f + (1 - c)\mu_a. \quad (5)$$

The advection equation for density (2) can be replaced by an advection equation for the concentration (6):

$$\partial_t + \nabla \cdot (\mathbf{c}\mathbf{u}) = \mathbf{0}. \quad (6)$$

A more detailed description of the numerical code can be found in [7, 8] where numerical schemes are explained and the code is validated against linear instability theory.

3 Validation

For the validation the theoretical model from Desantes et al. [1] has been used. The model is based in the momentum flux conservation and considers local density variations and a generic Schmidt number. The following expression, (7), that relates the velocity in the axis with the position is obtained:

$$M_0 = \frac{\pi}{2\alpha} \rho_\alpha \tan\left(\frac{\theta_u}{2}\right) x^2 U_{axis}^2 \sum_{i=0}^{\infty} \frac{2}{2+i \cdot Sc} \left[\left(\frac{U_{axis}}{U_0}\right) \left(\frac{1+Sc}{2}\right) \frac{\rho_f - \rho_a}{\rho_f} \right]^i, \quad (7)$$

where M_0 is the axial momentum flux, Sc is the Schmidt number, ρ_f is the density of the fuel, ρ_a is the density of the air, $U_{axis} = U_{axis}(x)$ is the velocity in the axis, α is the shape factor and θ_u is the velocity spray cone angle.

At Figure 1 the drop in velocity for the theoretical model and for the simulation is showed with good agreement for two Schmidt numbers. The physical characteristics of the fuel are showed at Table 1

D_0	156 μm
ρ_f	843 kg/m^3
ρ_a	17 kg/m^3
μ_f	2.4e-3 $\text{Pa} \cdot \text{s}$
μ_a	2.872e-5 $\text{Pa} \cdot \text{s}$
U_0	100 m/s
σ	2.5e-2 N/m

Table 1: Physical characteristics for validation

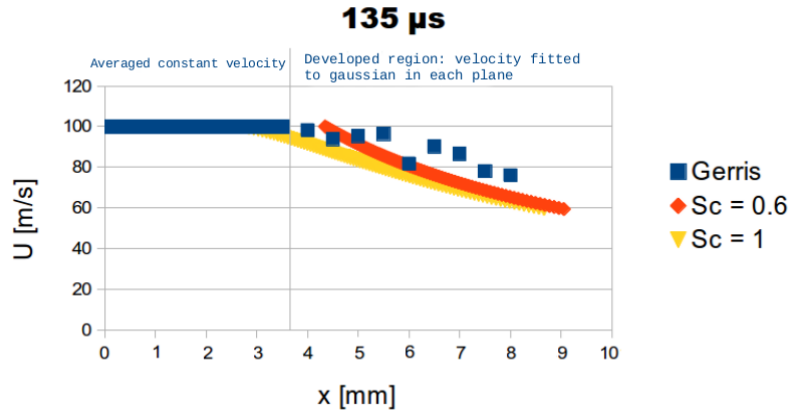


Figure 1: Axial velocity drop

4 Influence of Periodic Velocity Perturbation

After the validation, the objective is to study the influence on the spray morphology of periodic perturbation. In this section, the influence of small sinusoidal perturbation in the inlet velocity (8) has been studied,

$$U = U_0 (1 + 0.05 \sin(2\pi \cdot f \cdot t)). \quad (8)$$

The exterior non-perturbed length, L_{np} , has been chosen in order to study the influence of the perturbations related with the spray morphology. L_{np} is the length measured from the orifice where no perturbation in the spray is measured.

For this study, the physical characteristics of the fuel are showed at Table 2. The frequency has been varied from 0.2 MHz to 2.2 MHz in steps of 0.2 MHz and also a lowest frequency of 0.1 MHz. The spray for the lowest frequency of 0.1 MHz is depicted at Figure 2.

As can be observed at Figure 3, the tendency of L_{np} over frequency has been captured in a good fit. Higher frequency implies lower L_{np} and L_{np} tends asymptotically to zero as the frequency grows.

D_0	100 μm
ρ_f	696 kg/m^3
ρ_a	25 kg/m^3
μ_f	1.2e-3 Pa ·s
μ_a	1.0e-5 Pa ·s
U_0	100 m/s
σ	6.0e-2 N/m

Table 2: Physical characteristics for periodic perturbation study

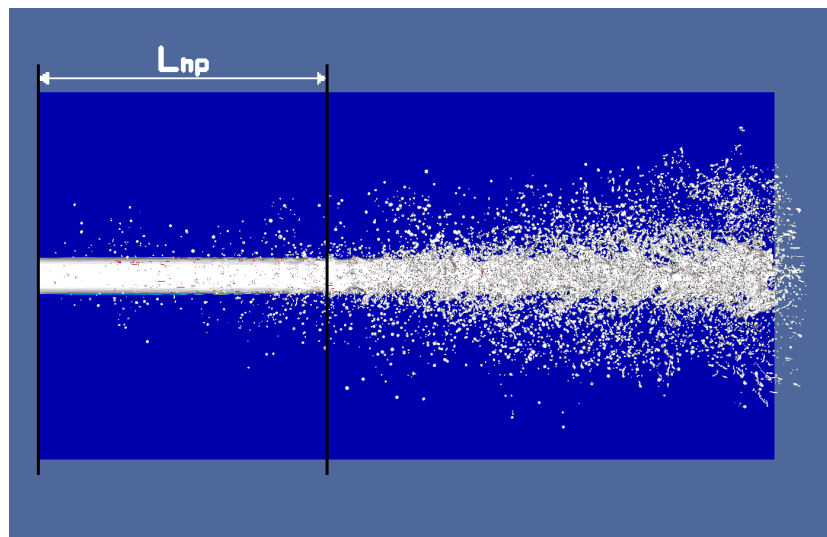


Figure 2: Exterior non-perturbed length

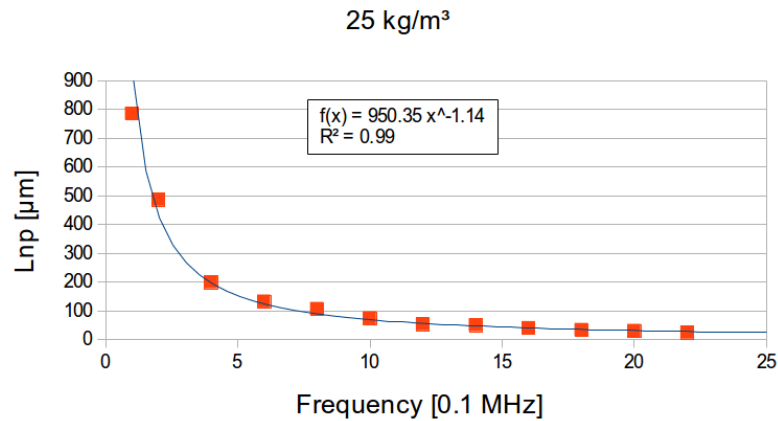


Figure 3: Exterior non-perturbed length over frequency

5 Conclusions

In this study, a new multiphasic code for incompressible flow has been studied for the use on diesel spray. The study has been done with low injection velocity in order to reduce computational cost. A mesh sensitivity study has been performed over the different possible parameters defining the mesh, namely, domain width, refinement levels and fixing the maximum number of cells.

The code has been compared with a theoretical model with good agreement. Periodic perturbations on the spray velocity have been studied. Results obtained for the penetration can be fitted accurately.

Acknowledgements

This work has been partially supported by the Ministerio de Economía y Competitividad grants TRA2012-36932 and MTM2013-41765-P.

The authors would also like to thank the computer resources, technical expertise and assistance provided by the Universidad de Valencia in the use of the supercomputer “Tirant”.

References

- [1] J. M. Desantes, R. Payri, J. M. García, and F. J. Salvador. A contribution to the understanding of isothermal diesel spray dynamics. *Fuel*, 86(7-8):1093–1101, 2007.
- [2] F. Dos Santos and L. Le Moyne. Spray atomization models in engine applications, from correlations to direct numerical simulations. *Oil and Gas Science and Technology*, 66(5):801–822, 2011.
- [3] D. Fuster, A. Bagué, T. Boeck, L. Le Moyne, A. Leboissetier, S. Popinet, P. Ray, R. Scardovelli, and S. Zaleski. Simulation of primary atomization with an octree adaptive mesh refinement and VOF method. *International Journal of Multiphase Flow*, 35(6):550–565, 2009.
- [4] K Mehravaran. Direct simulations of primary atomization in moderate speed diesel fuel injection. *International Journal of Materials, Mechanics and Manufacturing*, 1(2):207–209, 2013.
- [5] T. Ménard, S. Tanguy, and A. Berlemont. Coupling level set/VOF/ghost fluid methods: validation and application to 3D simulation of the primary break-up of a liquid jet. *International Journal of Multiphase Flow*, 33(5):510–524, 2007.
- [6] Y. Pan and K. Suga. Large eddy simulation of turbulent liquid jets into air. 2006. ICLASS Paper ICLASS06-219.
- [7] S. Popinet. Gerris: a tree-based adaptive solver for the incompressible euler equations in complex geometries. *Journal of Computational Physics*, 190(2):572–600, 2003.
- [8] S. Popinet. An accurate adaptive solver for surface-tension-driven interfacial flows. *Journal of Computational Physics*, 228(16):5838–5866, 2009.
- [9] J. Revéillon and L. Vervisch. Spray vaporization in nonpremixed turbulent combustion modeling: a single droplet model. *Combustion and Flame*, 121(1-2):75–90, 2000.
- [10] F. J. Salvador, J. Gimeno, J. M. Pastor, and P. Martí-Aldaraví. Effect of turbulence model and inlet boundary condition on the diesel spray

behavior simulated by an eulerian spray atomization (ESA) model. *International Journal of Multiphase Flow*, 65:108–116, 2014.

- [11] F. J. Salvador, J. Martínez-López, J. V. Romero, and M. D. Roselló. Computational study of the cavitation phenomenon and its interaction with the turbulence developed in diesel injector nozzles by Large Eddy Simulation (LES). *Mathematical and Computer Modelling*, 57(7-8):1656–1662, 2013.

Use of discontinuity factors in high-order finite element methods

A. Vidal-Ferràndiz^b, S. González-Pintor[†], D. Ginestar[‡]*,
G. Verdú^b, C. Demazière[†] and M. Asadzadeh[†]

(^b) Instituto de Seguridad Industrial: Radiofísica y Medioambiental,
Universitat Politècnica de València, Camino de Vera s/n, 46022, València, Spain,

([†]) Department of Applied Physics

Chalmers University of Technology, Maskingränd 2, 412 58 Göteborg, Sweden

([‡]) Instituto de Matemática Multidisciplinar.

Universitat Politècnica de València, Camino de Vera s/n, 46022, València, Spain.

November 28, 2014

1 Introduction

Traditionally, the stationary neutron distribution inside a reactor core is approximated using the energy multigroup neutron diffusion equation [1],

$$-\vec{\nabla} \cdot \left(D_g(\vec{r}) \vec{\nabla} \phi_g(\vec{r}) \right) + \Sigma_{ag}(\vec{r}) \phi_g(\vec{r}) - \sum_{g' \neq g}^G \Sigma_{sg'g}(\vec{r}) \phi_{g'}(\vec{r}) = \frac{1}{k_{\text{eff}}} \chi_g \sum_{g'=1}^G \nu \Sigma_{fg'}(\vec{r}) \phi_{g'}(\vec{r}), \quad (1)$$

where $\phi_g(\vec{r})$ is the neutron flux for the g -th energy group ($g = 1, \dots, G$), $D_g(\vec{r})$ the diffusion coefficient and Σ_{ag} , $\Sigma_{sg'g}$, $\nu \Sigma_{fg'}$, the nuclear cross sections and k_{eff} is the multiplication factor of the reactor.

*e-mail: dginesta@mat.upv.es

To take into account a detailed description of the different cross sections associated with the different materials a reactor core is composed of is a very difficult task with the today's computer capabilities and a piece-wise homogenized version of the reactor core is used for the neutronic computations [2]. The homogenization process is a source of error in the homogenized problem. To circumvent this error flux discontinuity factors are a widely used technique, looking for a solution of the neutron diffusion equation that is discontinuous. Most of the finite element methods proposed for the neutron diffusion equation look for the neutronic flux as a continuous function in the reactor core. Thus, it is difficult to implement in such a methodology forced discontinuities between adjacent subdomains. Here it is proposed to use a high order discontinuous Galerkin finite element method where the jump condition for the neutron flux is imposed in a weak sense using interior penalty terms.

A first step in a homogenization methodology is to choose heterogeneous reactor properties that should be reproduced when the homogenized problem is solved. Usually, these quantities are the node averaged group reaction rates, the surface-averaged group currents and the k -effective of the reactor. In this way, for every energy group g and every nuclear cross section $\Sigma_{\alpha g}$, the equations [3],

$$\int_{V_k} \hat{\Sigma}_{\alpha g}^k \hat{\phi}_g(\vec{r}) d\vec{r} = \int_{V_k} \Sigma_{\alpha g}(\vec{r}) \phi_g(\vec{r}) d\vec{r} , \quad (2)$$

and

$$\int_{S_k} \left(\hat{D}_g^k \vec{\nabla} \hat{\phi}_g(\vec{r}) \right) d\vec{S} = \int_{S_k} \left(D_g(\vec{r}) \vec{\nabla} \phi_g(\vec{r}) \right) d\vec{S} , \quad (3)$$

must be satisfied, where V_k and S_k are the volume of the homogenized region k and its limiting surface, respectively; ϕ_g is the solution of the heterogeneous problem and $\hat{\phi}_g$ is the solution obtained using the homogenized parameters $\hat{\Sigma}_{\alpha g}^k$ and \hat{D}_g^k .

In the generalized equivalence theory [3], flux discontinuity factors are introduced, relaxing the condition of continuity of the neutronic flux in the interior interfaces of the homogenized regions. For a given interface S_j limiting two contiguous homogenized regions, the energy-dependent discontinuity factors are defined as interface constants $f_{g,j}^-$, $f_{g,j}^+$, such that

$$f_{g,j}^- \int_{S_j} \hat{\phi}_g^-(\vec{r}) dS = f_{g,j}^+ \int_{S_j} \hat{\phi}_g^+(\vec{r}) dS , \quad (4)$$

where $\hat{\phi}_g^-(\vec{r})$ and $\hat{\phi}_g^+(\vec{r})$ are the lateral (directional) limits of the homogenized flux in the surface S_j viewed from the two different regions sharing this surface. A possible definition of these discontinuity factors is

$$f_{g,j}^- = \frac{\int_{S_j} \phi_g^- dS}{\int_{S_j} \hat{\phi}_g^- dS}, \quad f_{g,j}^+ = \frac{\int_{S_j} \phi_g^+ dS}{\int_{S_j} \hat{\phi}_g^+ dS}, \quad (5)$$

2 Discontinuous Galerkin method with interior penalty

We present the Discontinuous Galerkin method proposed for the neutron diffusion equation with discontinuity factors, for one-dimensional problems. A similar method can be defined for multi-dimensional problems. To show the method, we start with a source problem associated with the mono-energetic one-dimensional diffusion equation

$$-\frac{\partial}{\partial x} \left(D \frac{\partial}{\partial x} \phi \right) + \Sigma_a \phi = q, \quad (6)$$

for a reactor R discretized in $N + 1$ cells with edges x_0, x_1, \dots, x_{N+1} . Multiplying equation (6) by a test function, v , and integrating over R we obtain

$$-\int_R v \frac{\partial}{\partial x} \left(D \frac{\partial}{\partial x} \phi \right) dx + \int_R v \Sigma_a \phi dx = \int_R v q dx. \quad (7)$$

After integrating by parts, assuming that the neutronic flux and the diffusion coefficients can be discontinuous and making use of lateral limits, introducing the notation

$$\begin{aligned} \{v\}_i &= \frac{1}{2} (v_i^+ + v_i^-), & \left\{ D \frac{\partial}{\partial x} \phi \right\}_i &= \frac{1}{2} \left(D_i^+ \frac{\partial}{\partial x} \phi_i^+ + D_i^- \frac{\partial}{\partial x} \phi_i^- \right) \\ [v]_i &= v_i^- - v_i^+, & \left[D \frac{\partial}{\partial x} \phi \right]_i &= D_i^- \frac{\partial}{\partial x} \phi_i^- - D_i^+ \frac{\partial}{\partial x} \phi_i^+, \end{aligned}$$

and using the continuity condition for the current in the interior vertices, equation (7) is written as

$$\begin{aligned} & \sum_{i=0}^N \int_{x_i}^{x_{i+1}} \frac{\partial v}{\partial x} D \frac{\partial \phi}{\partial x} dx + \sum_{i=0}^N \int_{x_i}^{x_{i+1}} v \Sigma_a \phi dx \\ & - \sum_{i=1}^N \left(\left\{ D \frac{\partial \phi}{\partial x} \right\}_i [v]_i \right) + \sum_{i=1}^N s_i \left([\phi]_{fi} [v]_i \right) \\ & + v_0^+ D_0^+ \frac{\partial \phi_0^+}{\partial x} - v_{N+1}^- D_{N+1}^- \frac{\partial \phi_{N+1}^-}{\partial x} = \sum_{i=0}^N \int_{x_i}^{x_{i+1}} v q dx . \end{aligned} \quad (8)$$

To assess the capabilities of the proposed interior penalty method with assembly discontinuity factors, a code has been implemented in a standard finite element library named Deal.II [5] using Lagrange finite element.

Several one and two-dimensional benchmark problems have been analysed and the results obtained with the finite element method have been compared with the results obtained with a nodal code.

In all the problems analyzed the Discontinuos Galerkin method proposed obtains accurate results when the assembly discontinuity factors are introduced being able to use the advantages of the high order finite element methods as the h-p refinements.

References

- [1] Weston M Stacey, Nuclear reactor physics. New York, John Wiley & Sons, 2007.
- [2] Sanchez R. Assembly homogenization techniques for core calculations. *Progress in Nuclear Energy*, 51(1):14–31, 2009.
- [3] Smith K S. Assembly homogenization techniques for light water reactor analysis. *Progress in Nuclear Energy*, 17(3):303–335, 1986.
- [4] Reed Wm H and Hill T R. Triangular mesh methods for the neutron transport equation. *Los Alamos Report LA-UR-73-479*, 1973.
- [5] Bangerth W, Hartmann R , and Kanschat G. deal.II — a General Purpose Object Oriented Finite Element Library. *ACM Trans. Math. Softw.*, 33(4):24, 2007.

Moving meshes to solve the time-dependent neutron diffusion equation in hexagonal geometry

A. Vidal[†], R. Favez[†], D. Ginestar^{‡,*}, and G. Verd[†]

([†]) Instituto de Seguridad Industrial: Radiofísica y Medioambiental,
Universitat Politècnica de València, Camino de Vera s/n, 46022, València, Spain

([‡]) Instituto Universitario de Matemática Multidisciplinar,
Universitat Politècnica de València, Camino de Vera s/n, 46022, València, Spain,

November 28, 2014

1 Introduction

To simulate the behaviour of a nuclear power reactor it is necessary to be able to integrate the time-dependent neutron diffusion equation inside the reactor core. This model is of the form of

$$[v^{-1}] \frac{\partial \Phi}{\partial t} + \mathcal{L}\Phi = (1 - \beta)\mathcal{M}\Phi + \sum_{k=1}^K \lambda_k \mathcal{C}_k \quad , \quad (1)$$

$$\frac{\partial \mathcal{C}_k}{\partial t} = \beta_k [\nu \Sigma_{f1} - \nu \Sigma_{f2}] \Phi - \lambda_k \mathcal{C}_k \quad , \quad k = 1, \dots, K \quad , \quad (2)$$

*e-mail: dginesta@mat.upv.es

where, K is the number of delayed neutron precursors groups considered and the matrices are defined as

$$\mathcal{L} = \begin{pmatrix} -\vec{\nabla} \cdot (D_1 \vec{\nabla}) + \Sigma_{a1} + \Sigma_{12} & 0 \\ -\Sigma_{12} & -\vec{\nabla} \cdot (D_2 \vec{\nabla}) + \Sigma_{a2} \end{pmatrix}, \quad [v^{-1}] = \begin{pmatrix} \frac{1}{v_1} & 0 \\ 0 & \frac{1}{v_2} \end{pmatrix},$$

$$\mathcal{M} = \begin{pmatrix} \nu \Sigma_{f1} & \nu \Sigma_{f2} \\ 0 & 0 \end{pmatrix}, \quad \Phi = \begin{pmatrix} \phi_1 \\ \phi_2 \end{pmatrix}, \quad \chi = \begin{pmatrix} 1 \\ 0 \end{pmatrix},$$

where ϕ_1 and ϕ_2 are the fast the thermal neutron fluxes, respectively. The diffusion constants and cross-sections, D_g , Σ_{12} , Σ_{ag} , $\nu \Sigma_{fg}$, $g = 1, 2$, appearing in the equations depend on the reactor materials. β_k and λ_k are coefficient are related to the delayed neutron precursor decay.

In this work, for the spatial discretization of the neutron diffusion equation a high order hp-finite element method for reactors has been used [1]. The h - p finite element method used in this work has been implemented using the open source finite elements library Deal.II [2] and the numerical solver SLEPc [3].

Some transient calculations in reactor cores are based on dynamic changes in the reactor configuration due to the movement of control rods, which are usual manoeuvres in the reactor operation. The simulation of these transients presents what is known as the *rod-cusping* problem. This problem is caused by the use of fixed mesh schemes and averaged material properties for the partially rodded node. In this work, a moving mesh strategy is developed to reduce the rod-cusping problem. This method is based on the use of different spatial meshes for the different time steps following the movement of the control rod avoiding the necessity of the use of averaged material properties.

2 Discretization of the problem

Once the spatial discretization was performed using a continuous Galerkin Finite Element Method [1], a discrete version of the time dependent neutron diffusion equation is solved using a implicit methods. Particularly, a first order backward method is used. In this way, equations (1) can be discretized as a system of linear equations of the form

$$T^{n+1} \tilde{\Phi}^{n+1} = R^n \tilde{\Phi}^n + \sum_{k=1}^K \lambda_k e^{-\lambda_k \Delta t} X C_k^n, \quad (3)$$

where the matrices are defined as,

$$T^{n+1} = \frac{1}{\Delta t}[v^{-1}] + L^{n+1} - \hat{a}M^{n+1} ,$$

$$R^n = \frac{1}{\Delta t}[v^{-1}] = \frac{1}{\Delta t} \begin{pmatrix} P v_1^{-1} & 0 \\ 0 & P v_2^{-1} \end{pmatrix} ,$$

and the coefficient \hat{a} is

$$\hat{a} = 1 - \beta + \sum_{k=1}^K \beta_k (1 - e^{\lambda_k \Delta t}) .$$

This system of equations is large and sparse and has to be solved for each time step. The preconditioned GMRES method has been chosen to solve these systems and the preconditioner used has been the incomplete LU preconditioner.

The moving mesh scheme requires the interpolation of the physical solutions of the equations, which are continuous functions, from the old mesh in step n to the next mesh corresponding to step $n + 1$. The mesh interpolation process consists of finding the solution in the new support point values corresponding to the new mesh by polynomial interpolation of the values of the solution in the old mesh. To maintain the accuracy of the solution this interpolation is done using a polynomial interpolation of the same degree as the degree used in the high order finite element method used for the spatial discretization.

In the moving mesh interpolation, only physical quantities, can be interpolated adequately. However, for each time step the obtained quantity the precursors quantity obtained is multiplied by the mass matrix, XC_k . The inversion of the mass matrix is considered by means of a mass lumping technique.

The computation starts with an eigenvalue computation to obtain the stationary configuration of the reactor core, which is used as initial condition. Now, the dynamic calculation starts. First, the neutron precursors concentration is solved in the initial mesh. Then, the control bars and the mesh are moved and the neutronic flux and the precursors distribution are interpolated to the new mesh. Afterwards, the system associated with the numerical scheme is solved obtaining the next flux distribution. This is clearly the most time consuming part of the computation. Finally, the stopping criterion is checked and if it is not fulfilled the dynamic computation is repeated for the next time step.

3 Numerical Results

To test the performance of the method , a small 3D reactor that presents a large rod-cusping problem is studied. The results obtained with the moving mesh scheme proposed in this work are compared with the results obtained with the classical fixed mesh scheme. The reactor is solved with a fixed mesh scheme using 120 axial planes where the rod-cusping problem is very small the results of this computation are taken as a reference. All transient calculations are made using cubic polynomials in the finite element method. As it can be seen the moving mesh scheme produces better results than the fixed mesh scheme when a small number of axial planes are considered for the spatial discretization.

4 Conclusions

To avoid *rod cusping* problem in the simulation of moving control rods, in this work a new method based on a high-order finite element method is proposed. In this method, the spatial mesh is moved together with the control rods in such a way that there is no partially inserted cells. It is demonstrated that the moving mesh has a better performance that the traditional fixed mesh schemes when a small number of axial cells are used. Thus, the moving mesh scheme permits to use a coarser discretization and reduces the computational effort.

References

- [1] A. Vidal-Ferrandiz, R. Fayez, D. Ginestar, and G. Verdú. Solution of the lambda modes problem of a nuclear power reactor using an hb-finite element method. *Annals of Nuclear Energy*, 72(0):338 – 349, 2014.
- [2] W. Bangerth, R. Hartmann, and G. Kanschat. deal.II – a general purpose object oriented finite element library. *ACM Trans. Math. Softw.*, 33(4):24/1–24/27, 2007.
- [3] Vicente Hernandez, Jose E. Roman, and Vicente Vidal. SLEPc: A scalable and flexible toolkit for the solution of eigenvalue problems. *ACM Trans. Math. Software*, 31(3):351–362, 2005.

Second-order implicit methods for estimating the solution of turbulence problems ^{*}

Alicia Cordero [†], Antonio Franques, and Juan R. Torregrosa

Instituto de Matemática Multidisciplinar,
Universitat Politècnica de València,
Camino de Vera, s/n, 46022, Valencia, Spain

November 28, 2014

Abstract

It is known that Burgers' equation is often used to model turbulence problems of different kinds. Under certain conditions, Hopf-Cole transformation can be used to reduce it into the linear heat equation. In this work we present a general procedure that can be used even when Hopf-Cole transformation is not available. It consists on applying the implicit second-order Crank-Nicholson method to Burgers' equation, getting a nonlinear system of equations and using different iterative schemes for solving them.

1 Statement of the problem and design of the procedure

Burgers' equation arises in the theory of shock waves, in turbulence problems and in continuous stochastic processes (see, for example, [1], [2]) and [3]). Many physical phenomena are modeled by this equation,

$$\frac{\partial u}{\partial t} - \frac{1}{Re} \frac{\partial^2 u}{\partial x^2} + u \frac{\partial u}{\partial x} = 0, \quad a < x < b, \quad t > 0, \quad (1)$$

^{*}This research was supported by Ministerio de Ciencia y Tecnología MTM2011-28636-C02-02.

[†]e-mail: acordero@mat.upv.es

with initial condition

$$u(x, 0) = f(x), \quad a < x < b,$$

and boundary conditions

$$u(a, t) = g_1(t), \quad u(b, t) = g_2(t), \quad t \geq 0;$$

where Re is the Reynolds number of the viscous fluid flow problem and $f(x)$, $g_1(t)$ and $g_2(t)$ are given functions. Usually ε instead of $\frac{1}{Re}$ is used, for simplicity. Numerical difficulties have been experienced in getting the solution of Burgers' equation for big values of ε .

In this paper, we apply divided differences directly on the nonlinear equation (1), by means of the implicit second-order methods of Crank-Nicholson, obtaining a nonlinear system of equations to be solved for obtaining the solution in each value of t . These nonlinear systems are solved by using Newton iterative method. This procedure can be applied on any partial differential equation, independently from the kind of initial and boundary conditions; that is an advantage respect other techniques used (see, for example[4]).

Before introducing Crank-Nicholson difference scheme, let us to discretize the independent variables of the problem, (x, t) : we consider $x_{i+1} = x_i + h$ and $t_{j+1} = t_j + k$, where $i = 0, 1, \dots, n - 1$, $j = 0, 1, \dots, m - 1$, $h = \frac{b-a}{n}$ and $k = \frac{t_{max}-t_{min}}{m}$ are respectively the space and time step on the mesh and n and m are respectively the space and time amount of subintervals to be considered. Under this assumptions, let us denote by $u_{i,j}$ the approximated value of the unknown u function on (x_i, t_j) . The mesh generated in this way can be observed in Figure 1.

Crank-Nicholson difference scheme consists of discretizing equation (1) in two consecutive time instants and averaging them, holding a truncation error of order 2 but using only forward and regressive first-order differences.

So, in a first instant t_j we approximate $\frac{\partial u}{\partial t}$ by the forward difference

$$\frac{\partial u(x_i, t_j)}{\partial t} \approx \frac{u_{i,j+1} - u_{i,j}}{k} \tag{2}$$

and in the second instant t_{j+1} we do it by the backward one

$$\frac{\partial u(x_i, t_{j+1})}{\partial t} \approx \frac{u_{i,j+1} - u_{i,j}}{k}. \tag{3}$$

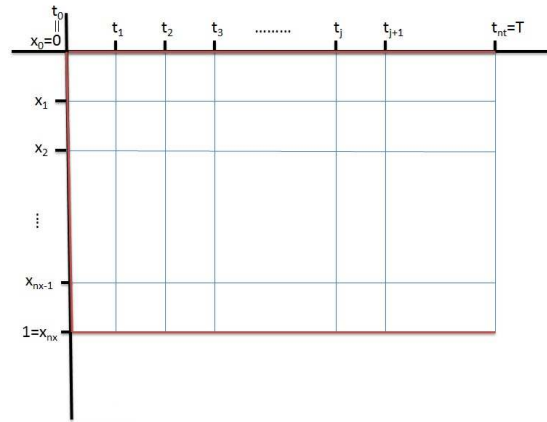


Figure 1: Mesh of independent variables

At both instants we approximate $\frac{\partial u}{\partial x}$ and $\frac{\partial^2 u}{\partial x^2}$ by using the central differences

$$\frac{\partial u(x_i, t_j)}{\partial x} \approx \frac{u_{i+1,j} - u_{i-1,j}}{2h}, \quad \frac{\partial^2 u(x_i, t_j)}{\partial x^2} \approx \frac{u_{i+1,j} - 2u_{i,j} + u_{i-1,j}}{h^2}.$$

By means of this procedure we get, for the first instant,

$$\frac{u_{i,j+1} - u_{i,j}}{k} - \varepsilon \frac{u_{i+1,j} - 2u_{i,j} + u_{i-1,j}}{h^2} + u_{i,j} \frac{u_{i+1,j} - u_{i-1,j}}{2h} = 0 \quad (4)$$

and for the second one,

$$\frac{u_{i,j+1} - u_{i,j}}{k} - \varepsilon \frac{u_{i+1,j+1} - 2u_{i,j+1} + u_{i-1,j+1}}{h^2} + u_{i,j+1} \frac{u_{i+1,j+1} - u_{i-1,j+1}}{2h} = 0. \quad (5)$$

After averaging both expressions, it results

$$\begin{aligned} Bu_{i,j+1}u_{i+1,j+1} &- Bu_{i,j+1}u_{i-1,j+1} - Cu_{i+1,j+1} + 2Cu_{i,j+1} - Cu_{i-1,j+1} + Au_{i,j+1} \\ &= Cu_{i+1,j} + (A - 2C)u_{i,j} + Cu_{i-1,j} + Bu_{i,j}u_{i+1,j} - Bu_{i,j}u_{i-1,j}, \end{aligned}$$

where $A = \frac{1}{k}$, $B = \frac{1}{4h}$, $C = \frac{\varepsilon}{2h^2}$ and the range of indices is $i = 1, 2, \dots, n - 1$ and $j = 0, 1, \dots, m - 1$.

So, we have transformed the original problem on a set of m nonlinear systems of $n - 1$ unknowns and $n - 1$ equations. As we already know the value of $u_{0,j}$ and $u_{n,j}$, $\forall j$ (from the boundary conditions) and $u_{i,0}$, $\forall i$ from the initial condition, each $(j + 1)$ -th column of our mesh is calculated by using the information of the previous one, with index j .

To solve these nonlinear systems we are going to use the classical Newton's method of order two,

$$x^{(k+1)} = x^{(k)} - [F'(x^{(k)})]^{-1}F(x^{(k)}), \quad (6)$$

where $F(x)$ denotes the vectorial real function that describes the nonlinear system and $F'(x)$ is the associated Jacobian matrix.

2 Numerical implementation

We use the R2013a version of Matlab with double precision for obtaining both approximated and exact solutions. The stopping criterion used is

$$\|u^{(k+1)}(x, t_j) - u^{(k)}(x, t_j)\| + \|F(u^{(k+1)}(x, t_j))\| < 10^{-15},$$

in such a way that we are checking, not only the convergence of the process, but also that it converges to a solution of the problem.

We will test our procedure by using the piece-wise conditions proposed by Mittal and Singhal in [4] with the following initial and boundary conditions

$$u(x, 0) = \begin{cases} \sin(\pi x), & 0 < x \leq 1 \\ -\frac{1}{2}\sin(\pi x), & 1 < x \leq 2 \\ 0 & 2 < x \leq 5 \end{cases}$$

and

$$u(0, t) = u(5, t) = 0, t \geq 0.$$

In their manuscript [4], Mittal and Singhal transformed Burgers' equation into a system of nonlinear ordinary differential equations solving it by the Runge-Kutta-Chebyshev second order method. However, we have getsome results very similar to those obtained for Mittal and Singhal on their paper. In Figure 2 we can observe a graph of the approximated solution by our method at different times for $0 \leq x \leq 5$ and for two different values of ε we show the numerical results of this solution for some values of x, t and ε .

References

- [1] R. B. Lowrie. A comparison of implicit time integration methods for nonlinear relaxation and diffusion *Journal of Computational Physics*, 196: 566–590, 2004.

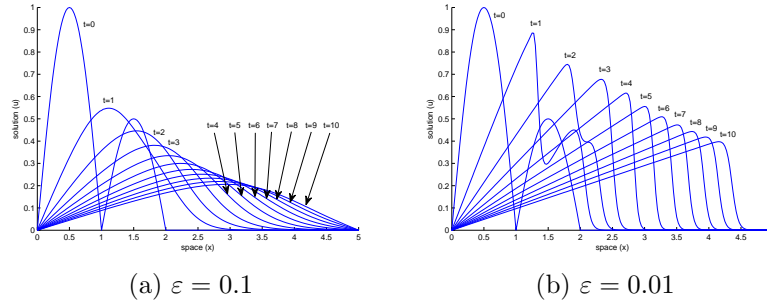


Figure 2: Solution for different times and ε values, both of them with $n = m = 200$ and $t_{max} = 10$

- [2] H. An , Z. Mo, X. Xu and X. Liu. On choosing a nonlinear initial iterate for solving the 2-D 3-T heat conduction equations *Journal of Computational Physics* 228: 3268–3287, 2009.
- [3] D. D. Bruns and J. E. Bailey. Nonlinear feedback control for operating a nonisothermal CSTR near an unstable steady state *Chemical Engineering Science* 32: 257–264, 1977.
- [4] R. C. Mittal and P. Singhal. Numerical solution of Burgers' equation *Communications in Numerical Methods in Engineering* 9: 397-406, 1993.

A computational graph-based algorithm for the management of a car-rental-service

J.A. Conejero^b, C. Jordán[†], and E. Sanabria-Codeçal^{‡*}

(^b) Instituto Universitario de Matemática Pura y Aplicada,

([†]) Instituto Universitario de Matemática Multidisciplinar,

([‡]) Departamento de Matemática Aplicada,

Universitat Politècnica de València.

December 28, 2014

1 Introduction

In the last years, there has been a huge interest in car-shared and bike-sharing rental services, either if they are car-rental companies or car-sharing platforms. In large urban areas, citizens mobility is understood as a mixing of different means of transport where every person may use two or three different means or connections to arrive to his destination as fast as possible. Furthermore, by 2020 we will see the development of mega-city corridors and networked, integrated and branded cities. Rapid expansion of city borders, driven by increase in population and infrastructure development, will force cities to expand outward and engulf the surrounding satellite cities to form megacities [6].

In the particular case of car-rental services, it is a common practice to accept almost all the bookings they received without checking if there are enough cars for attending them. This can lead to fall into the deadhead times required for rearranging vehicles among depots for attending all the

*e-mail: aconejero@upv.es, cjordan@mat.upv.es, esanabri@mat.upv.es

bookings or to hire some cars from another car-rental. This is a more complex management policy than to only admit bookings that can be attended without moving cars from one depot to another one [2]. Further information concerning the whole management of a rent-a-car service can be found in [5].

These problems can be modeled using time-space networks, where nodes stand for cities at different hours, and edges are used for representing either cars used in bookings or cars staying at the parking of a depot. Then, the optimization of the assignment of vehicles for attending the orders can be seen as the solution of a suitable Integer Linear Programming problem of minimization of a cost function tied to the restrictions imposed by the orders.

In this communication we report on a work in progress in order to find a heuristic algorithm for solving the particular case in which there is no limitation in the number of bookings to be admitted and there is neither a limitation respect to the rearrangement of vehicles among the different depots. This last condition can be seen as unrealistic at first sight, but the last great advances in robotics and artificial intelligence have permitted to develop prototypes of autonomous cars. The advances can be followed looking at the DARPA Grand Challenge competition [4]. In fact, motor companies like Audi or BMW have presented their first models very recently [1].

2 Algorithmic approach

We will consider the particular problem tied to the the following assumptions:

1. A number of reservations is given. We consider that the satisfaction of all customer petitions is mandatory. So that, all reservations must be accepted.
2. If there are not enough cars available at a depot, we first try to bring cars from another depot.
3. If, after this rearrangement of vehicles, there are not enough cars available at any depot we subcontract them to other providers.

Given an ordered list of bookings our algorithm tries to attend the first unattended reservation that appears chronologically. This could imply to

move a car of depot, and leave other reservations without a vehicle that could provide those services. Moreover, if a booking cannot be attended with such movements a new vehicle can be used taking it from an external provider.

The scheme of the algorithm is like this:

1. First, we define a time-space network where a node represents a depot at certain time.
2. We assign as weights the initial number of vehicles at every depot and time. We first assign an initial number of cars at every depot. This number is maintained along the time since no booking is accepted yet.
3. In addition we add an external node and we connect it with the rest of the nodes with null weight. This last node represents the aforementioned external provider and the weight of the edges going out of it the number of vehicles to be moved from there for servicing bookings that cannot be attended in any other way.
4. We consider that all the bookings are accepted and we represent this in the network. This can lead to the situation in which a negative number of cars is located at some depots and times.
5. We search for the first unattended booking. Two situation can occur:
 - (a) We look for depots with free cars during the time duration of the booking. If such a depot exists we choose a car from it and we move it to the depot that needs it.
 - (b) If not a car is moved from the external depot to that location at the required time for servicing the unattended booking. The weights of the network are then recalculated.

Details and further information will appear in a forthcoming paper [3].

References

- [1] CNN. *Driverless car tech gets serious at CES* <http://edition.cnn.com/2014/01/09/tech/innovation/self-driving-cars-ces/> April, 7th, 2014.

- [2] Conejero, J.A., Jordán, C., and Sanabria-Codesal, E. An iterative algorithm for the management of an electric car-rental service. *J. Appl. Math.* **2014**, article ID 483734, 11 pages, 2015.
- [3] Conejero, J.A., Jordán, C., and Sanabria-Codesal, E. An algorithm for self-organization of driverless vehicles of a car-rental service. Preprint, 2015.
- [4] DARPA Grand Challenge http://en.wikipedia.org/wiki/2005_DARPA_Grand_Challenge#2005_Grand_Challenge
- [5] Fink, A. and Reiners, T. Modeling and solving the car rental logistics problem. *Transportation Research Part E*, **42**, 272–292, 2006.
- [6] Río+20 - United Nations Conference on Sustainable Development. Report. <http://www.uncsd2012.org>

Damped Newton's method for solving problems associated to the Stewart-Gough platform

Á. A. Magreñán^b*, J. M. Gutiérrez[†] and L. Orcos[‡]

(^b) Universidad Internacional de La Rioja,

26002 Logroño, La Rioja, Spain,

([†]) Universidad de La Rioja,

26002 Logroño, La Rioja, Spain

([‡]) Independent researcher,

Logroño, La Rioja, Spain.

November 28, 2014

1 Introduction

In this study, we are concerned with the problem of approximating a solution x^* of the nonlinear equation

$$F(x) = 0 \tag{1}$$

where F is a differentiable operator defined on a subset Ω of X with values in Y . Using mathematical modelling, many problems in computational sciences and other disciplines can be brought in a form like (1). The solutions of these equations (1) can rarely be found in closed form. Therefore solutions of these equations (1) are approximated by iterative methods.

Now let X and Y be two Banach spaces and let $F : \Omega \subset X \rightarrow Y$ be an operator defined on an open convex subset Ω . Then the derivative of F at

*e-mail: alberto.magrenan@unir.net

x is a linear operator between X and Y . We denote throughout this paper $\Gamma_n = F'(x_n)^{-1}$, $\Gamma_n : Y \rightarrow X$, is linear.

So we can now define damped Newton's method as follows:

$$x_{k+1} = x_k + \lambda \Gamma_n F(x_k) \quad \text{for each } k = 0, 1, 2, \dots, \tag{2}$$

where x_0 is an initial point and $\lambda \in (0, 1)$.

In concrete in this work, we are going to present the study of the semilocal convergence of the damped Newton's method under the α -theory (see [3] when in is applied to an equation related to an Stewart-Gough platform (see [1], [2], [4] or [5]).

2 Convergence result and application

Let be $F : X \rightarrow Y$, where X and Y are two Banach spaces and we consider the damped Newton's method defined in (2) in order to solve the equation (1), where F is an analytic function in the open ball $\Omega = B(x_0, R)$, where x_0 is an initial guess and $R > 0$.

In order to state the result, we consider the following conditions:

- (i) There exists $\Gamma_0 = F'(x_0)^{-1}$.
- (ii) $\|\Gamma_0 F(x_0)\| \leq \beta$.
- (iii) $\frac{1}{k!} \|\Gamma_0 F^{(k)}(x_0)\| \leq \gamma^{k-1}$ para $k \geq 2$.
- (iv) $\alpha = \beta\gamma \leq 3 - 2\sqrt{2} \approx 0.17157$.

where $\gamma, \beta \geq 0$; $x_0 \in \Omega$.

Now we can state the following result (the proof can be seen in [3]).

Theorem 2.1 *Let $F : \Omega \subseteq X \rightarrow X$ be a once continuously differentiable operator defined on a nonempty open convex domain Ω of a Banach space X . Suppose that conditions (i)–(iv) are satisfied. Then, method (2) converges to a solution x^* of the equation $F(x) = 0$. Moreover, the solution x^* is located in $\overline{B(x_0, t^*)}$ and is unique in $B(x_0, t^{**}) \cap \Omega$, where t^* and t^{**} are the roots of the auxiliary function*

$$\phi(t) = \beta - t + \sum_{k \geq 2} \gamma^{k-1} t^k, \tag{3}$$

with $t^* \leq t^{**}$.

As a particular problem we consider the cubic system defined in \mathbb{R}^3 :

$$\begin{cases} 3 + 20y + 2xy = 0 \\ 27 + 140x - 20y + 60z + 2z^2 = 0 \\ 147 + 700x + 280z + 20xyz = 0 \end{cases}$$

Denoting $X = (x, y, z)^T$ and $X_0 = (0, 0, 0)^T$ we can write the system in a easier way using k -tensors notation. In concrete, if $F : \mathbb{R}^3 \rightarrow \mathbb{R}^3$, the system is:

$$F(X) = F(X_0) + F'(X_0)X + \frac{1}{2}F''(X_0)X^2 + \frac{1}{6}F'''(X_0)X^3.$$

Notice that

$$F(X) = \begin{pmatrix} 3 \\ 27 \\ 147 \end{pmatrix} + \begin{pmatrix} 20y \\ 140x - 20y + 60z \\ 147 \end{pmatrix} + \begin{pmatrix} 2xy \\ 2z^2 \\ 0 \end{pmatrix} + \begin{pmatrix} 0 \\ 0 \\ 20xyz \end{pmatrix}.$$

It is easy to see that

$$\Gamma_0 = F'(X_0)^{-1} = \frac{1}{140} \begin{pmatrix} -14 & -14 & 3 \\ 7 & 0 & 0 \\ 35 & 35 & -7 \end{pmatrix}.$$

Moreover,

$$\frac{1}{2}\Gamma_0 F''(X_0)X^2 = \Gamma_0 \begin{pmatrix} 2xy \\ 2z^2 \\ 0 \end{pmatrix} = \begin{pmatrix} -\frac{xy+z^2}{5} \\ \frac{xy}{10} \\ \frac{xy+z^2}{2} \end{pmatrix}$$

and

$$\frac{1}{6}\Gamma_0 F'''(X_0)X^3 = \Gamma_0 \begin{pmatrix} 0 \\ 0 \\ 20xyz \end{pmatrix} = \begin{pmatrix} \frac{3xyz}{7} \\ 0 \\ -xyz \end{pmatrix}.$$

Considering $\|X\| = \max\{|x|, |y|, |z|\}$ and as $F^{(k)}(X) = 0 \forall k \geq 4$, we obtain γ :

$$\begin{aligned} \gamma &= \sup_{k \geq 2} \left(\frac{1}{k!} \|\Gamma_0 F^{(k)}(X_0)\| \right)^{\frac{1}{k-1}} \\ &= \max \left\{ \frac{1}{2} \|\Gamma_0 F''(X_0)\|, \left(\frac{1}{6} \|\Gamma_0 F'''(X_0)\| \right)^{\frac{1}{2}} \right\} = 1. \end{aligned}$$

On the other hand,

$$\beta = \|\Gamma_0 F(X_0)\| = \left\| \left(\frac{3}{20}, \frac{3}{20}, \frac{3}{20} \right) \right\| = \frac{3}{20}.$$

As $\alpha = \beta\gamma = \frac{3}{20} = 0.15 < 3 - 2\sqrt{2} \approx 0.171573$, we can ensure the existence of a solution X^* of the system.

Moreover, $X^* \in \overline{B(X_0, t^*)}$, where t^* is the smallest root of

$$\phi(t) = \beta - t + \frac{\gamma t^2}{1 - \gamma t} = \frac{3}{20} - t + \frac{t^2}{1 - t},$$

that is, $t^* = \frac{1}{5}$. Furthermore, the solution is unique in $B(X_0, t^{**})$, where $t^{**} = \frac{3}{8}$, is the other root of $\phi(t)$. As a consequence, the solution is

$$\{x = -0.137672, y = -0.152094, z = -0.180549\},$$

which is inside the ball $\overline{B(X_0, t^*)}$. Moreover, all the other solutions are outside the ball $B(X_0, t^{**})$.

References

- [1] DASGUPTA, B., MRUTHYUNJAYA, T.S. : The Stewart platform manipulator: a review, *Mechanism and Machine Theory*, 35: 15–40, 2000.
- [2] HERNÁNDEZ, A.: Cinemática de mecanismos. Análisis y diseño, Madrid, Editorial Síntesis, 2007.
- [3] MAGREÑÁN, Á. A.: Estudio de la dinámica del método de Newton amortiguado (PhD Thesis), Logroño, Servicio de Publicaciones, Universidad de La Rioja, 2013. <http://dialnet.unirioja.es/servlet/tesis?codigo=38821>
- [4] MERLET, J.P. : Solving the forward kinematics of a Gough-type parallel manipulator with interval analysis, *Int. J. of Robotics Research*, 23: 221–235, 2004.
- [5] V. PETUYA, J. M. GUTIÉRREZ, A. ALONSO, O. ALTUZARRA AND A. HERNÁNDEZ: A numerical procedure to solve non-linear kinematic problems in spatial mechanisms, *Int. J. for Numer. Methods in Eng.*, 73 (6): 825–843, 2008.

Decision model to optimize the location of logistics and transport facilities in urban environments

A. Fraile[†], J. A. Sicilia^b, E. Larrodé[†], Á. A. Magreñán^b *and L. Orcos[‡]

(b) Universidad Internacional de La Rioja,

26002 Logroño, La Rioja, Spain,

(†) Universidad de Zaragoza,

50018 Zaragoza, Zaragoza, Spain.

(‡) Independent researcher,

Logroño, La Rioja, Spain.

November 28, 2014

1 Introduction

In order to develop the tool, the program used was ArcView which is a software application of ArcGIS. ArcGIS is a GIS software designed by Environmental Systems Research Institute (ESRI) for multi-level work. It is a GIS software to view, create, manipulate and manage geographic information, these correspond to landmarks, addresses, positions in the field, urban and rural areas; regions and any land in certain locations. This information is worked systemically, which represents a substantial contribution to the work-related information with drawings and maps, allowing us to explore, view and analyse the data as parameters, relationships and trends that presents our data, resulting in new layers of difference information, maps and new databases.

*e-mail: alberto.magrenan@unir.net

2 Construction of GIS

For the construction of GIS a serie of maps and their attribute tables that correspond to the common layer information for all scenarios as well as different decision criteria are needed. These planes are represented in ArcGIS by “shapefiles” which is a vector format digital storage where the location of geographic features and attributes associated with them are saved. It can be used as common layer information, although the road map of the study area or the level of urban development plan divided in their cadastral areas. Each of these areas must have the following information: ranking and rating, size, cost of land and geolocation. The different planes will overlap with each other through ArcGIS, so that the optimum locations are being sought according to decision criteria to be determined previously for each case study selected. This methodology allows us to analyse various facilities to be located within an urban environment with different characteristics.

Initially, you must have the layer overview, in case not, you must manually associate the corresponding data in the attribute tables of the most important points of the map. Then we analyse each of the factors taken into account in the selection system, in order to facilitate the resolution on the optimal location of the different facilities, and some decision criteria (C_i):

- C_1 : High ADT (Annual average daily traffic)
- C_2 : Accessibility
- C_3 : Population density
- C_4 : Public transport stops (bus, underground, tram, bike)
- C_5 : Shopping areas
- C_6 : Industrial parks
- C_7 : Land for building development
- C_8 : Existence of bike lane

pertaining to transport and logistics are set. Each of these criteria are associated with weights (W_i) as it can be seen in the next list:

- W_P : Positive weight 0.4

- W_A : Average weight 0.05
- W_N : Negative weight -1

For each case study, the decision criteria will receive a value associated weight. The value between positive, average and negative, applied to each criterion may be modified by the user in order to give priority to other criteria, in accordance with the characteristics that the system must have. The weights of the criteria, such as the creation of exclusion areas are those that receive negative weight, take the value equal to “-1”. There will be cases in which a judgment may receive two weight categories, depending on the area it select, since within the same layer, an area can be favorable and other unfavorable.

3 Formulation

The formulation will be defined from the weights and the decision criteria defined above. When determining the possible locations for the locations of the facilities, and later list them in order of priority, the process will be as follows: The sum of the products of the area factors (C_i) is performed by its associated weights in overlapping areas of preference which will catalog the area with a number:

$$\text{degree of decision} = \sum_i^j (C_i \times W_i) \quad (1)$$

For the final selection of the most suitable siting classification is obtained from optimizing Jenk, a classification system by which the thresholds are identified between classes using a statistical formula [?]. The optimization method called Jenk, is implementing different applications under the option of intervals as natural break points of distribution (natural breaks). This method has the dual purpose of obtaining high internal homogeneity classes, with maximum differences between classes in the number of intervals previously specified. It performs the classification based on the test of goodness of fit (Goodness of Variance Fit - GVF) indicating how well it describes the whole class. This indicator takes different values according to the clusters that provide higher values. This is an iterative process that calculates the mean of each class with the respective variances, and observations moved between classes to obtain the maximum value of GVF [?]:

$$GVF = 1 - \frac{\sum_{j=1}^k \sum_{i=1}^{N_j} (Z_{ij} - \bar{Z}_j)^2}{\sum_{i=1}^N (Z_i - \bar{Z})^2} \quad (2)$$

where z_{ij} is the sum of squared deviations of the mean vector; \bar{z}_j is the sum of squared deviations between classes as stated Baz et al in 2009.

4 Conclusions

This decision model raised allows finding the best location in a facility in a novel way, analysing all the factors affecting transport and logistics in a city-related facilities. The inclusion of GIS technologies allows to plan the correct location to visualize graphically the solutions and more intuitively. The methodology proposed is based on the superposition of layers to enable the prioritization or exclusion of certain areas according to comply or not certain requirements defined in each of these layers. The decision criteria could be extended, if necessary, in any installation to locate or include it and the evaluation of the weights would have to assign the range of weight that would be acquired. The model gets the best solution to the searched location, supporting on Jenks optimization method, as the valuation of the *degree of decision* is the highest of all the studied area, dropping areas for security, inefficiency or other negative factors are not viable for the facility studied. A GIS system that reflects the modelling of the transport system and a set of decision criteria help to determine the size, characteristics and location of the network of hydrogen refuelling stations that minimizes the cost function and maximizes the operatively and functionality one.

References

- [1] Jenks, G.F., Caspall, F.C., Error on choroplethic maps: Definition, measurement, reduction. *Annals of the Association of American Geographers*, 61(2): 217-244, 1971.
- [2] Neutens, T., Delafontaine, M., Scott, D. M., De Maeyer, P., A GIS-based method to identify spatiotemporal gaps in public service delivery. *Applied Geography*, 32(2): 253–264, 2012..

An optimization algorithm for solving the rich vehicle routing problem based on metaheuristics

Juan Antonio Sicilia^b*, Carlos Quemada[†], Beatriz Royo[‡] and David Escuín[‡]

(b) Universidad Internacional de La Rioja, Gran Vía Rey Juan Carlos I 41, 26002, Logroño

(†) Virginia Polytechnic Institute and State University in Blacksurg, Virginia, USA

(‡) University of Zaragoza and Instituto Tecnológico de Aragón, María Luna 3, 50018, Zaragoza

November 28, 2014

1 Introduction

This work presents an optimization algorithm that resolves a Rich Vehicle Routing Problem (RVRP) and arises from a research project carried out for an important Spanish distribution company. The main goal of this project is to manage its resources in urban areas by reducing costs caused by inefficiency and ineffectiveness as much as possible. Therefore, this research consists in reducing the constraints and complexities currently encountered in the urban distribution of goods, using metaheuristic methods in order to obtain a more accurate solution. Given a fleet of vehicles and a set of customers dispersed over a geographic area, the system must be able to attain a feasible solution that leads to a decrease of the total cost of the problem. The purpose is to reach a solution with the minimum number of vehicles minimizing the total distance traveled.

The model of the problem depends on the following requirements: Vehicles have a maximum limit of capacity and are homogeneous (Capacitated Vehicle Routing Problem) [1]; Each customer must be serviced in a set time

*e-mail: juanantonio.sicilia@unir.net

interval (Vehicle Routing Problem with Time Windows) [2]; Certain orders can only be transported by specific vehicles. Therefore, the fleet must be heterogeneous (Site-Dependent Vehicle Routing Problem) [3]; Customers may receive and send goods (Vehicle Routing Problem with Pickups and Deliveries) [4]; The goods that leave the depot must be delivered to customers and the goods that are picked up from customers must be transported to the depot (Vehicle Routing Problem with Backhauls) [5]; Vehicles are not required to return to the depot after visiting the last customer and the route may finish near to the drivers home (Open Vehicle Routing Problem) [6]; Load balance among routes is important since the competitiveness of a transport company depends not only on minimizing costs and distances to obtain higher profit margins, but also depends on its ability to treat employees fairly [7].

2 Mathematical formulation

The RVRP can be described as follows. Let $G = (N, A)$ be a complete graph with $N = \{1\} \cup O \cup \{o + 1\}$ the set of nodes and $O = \{2, \dots, o\}$ the set of orders to be served. The aim is to design a set of routes for a heterogeneous fleet of V vehicles (each has a capacity, a load type and a limited number of orders to be served), servicing a set of O orders. Each arc $(i, j) \in A$ has a cost c_{ij} . The objective function for states that the distance traveled and number of vehicles should be minimized, M being a sufficiently large constant:

$$\min \sum_{k \in V} \sum_{i \in N} \sum_{j \in N} c_{ij} x_{ij}^k - \sum_{k \in V} x_{1h_k}^k M \quad (1)$$

The first term represents the accumulated costs for orders served by vehicles; the second term represents the number of utilized vehicles.

3 Optimization algorithm

The main difficulty of the RVRP problem is that if the number of elements to be combined is relatively large, the combinatorial result grows exponentially turning it into an NP-hard problem. On account of this, it is necessary to apply optimization techniques in order to obtain a high-quality solution in reasonable computational times.

An efficient algorithm is adapted to solve the problem. The RVRP is solved by means of a powerful route construction method that starts with

the determination of a feasible initial solution and the metaheuristics Variable Neighbourhood Descent (VND), General Variable Neighbourhood Search (GVNS) and Tabu Search (TS) based on various elementary neighbourhood operators to obtain an optimum solution.

The route construction method consists of assigning orders to vehicles depending on certain parameters and taking into consideration the limits of load balance between routes. This procedure has been implemented randomly to avoid the obtaining of the same solutions and to diversify the total space of the same.

Once the initial solution has been obtained using the minimum number of routes, the solution is improved through the application of metaheuristics using variable neighbourhood search [8]. The algorithm is described in Figure 1.

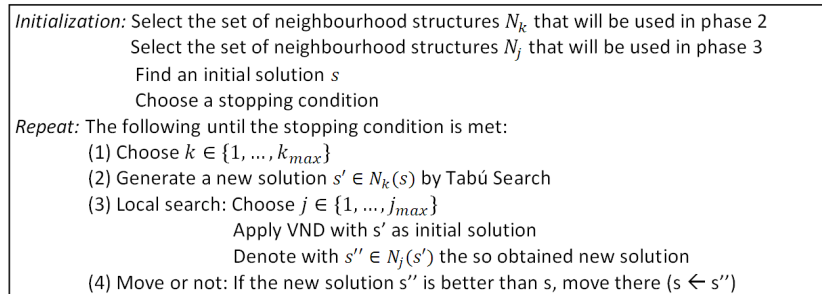


Figure 1: Algorithm

4 Discussion and results

The computational experiments have been extracted from real cases experienced by a large transport company in Spain. This company is in charge of the distribution of goods in urban areas where the distance among different customers is less than 100 kilometers. The results refer to the three methods that compose the algorithm. The first one is the construction method that obtains an initial feasible solution due to the quantity of constraints imposed, the second one is the VND metaheuristic and the last one is the GVNS method with TS.

As the number of available vehicles increases, the distance increases since the algorithm balances the freight to the extent possible. The distance does not rise in respect to the increase in the number of available vehicles and even decreases for most instances with sizes of orders greater than 200 orders especially for metaheuristics methods.

Concerning the result comparison of the three methods, it is important to mention that the VND metaheuristic is performed to minimize the distance of the obtained solution by the construction method while the GVND method with TS prioritizes the reduction in the number of used vehicles although the distance is longer, on condition that the maximum number of orders per vehicle is not exceeded.

5 Conclusions

An optimization algorithm that solves the RVRP problem is presented. This problem takes into consideration constraints and complexities actually encountered in urban freight distribution which are not considered in the classical problem. In order to solve the problem several methods have been modeled taking into consideration their more particular characteristics: time windows, capacity constraints, compatibility between orders and vehicles, maximum number of orders per vehicle, pickup-delivery dependent orders and not returning to the depot.

The motivation for this work arose from the necessity to solve more realistic vehicle routing problems in a research project undertaken for a large Spanish distribution company operating in urban areas. The algorithm is currently integrated into a commercial software tool, which is used by this company daily and whose real data have enabled this algorithm to be tested.

References

- [1] Gendreau M, Laporte G and Potvin J, Metaheuristics for the capacitated VRP, in *The vehicle routing problem*, edited by P. Toth, D. Vigo, SIAM Publishing, Philadelphia, USA: 129–154, 2002.
- [2] El-sherbeny N, Vehicle routing with time windows: An overview of exact, heuristic and metaheuristic methods, *Journal of King Saud University - Science*, 22(3): 123–131, 2010.

- [3] Chao IM, Liou TS, A new tabu search heuristic for the site-dependent vehicle routing problem, in *The next wave in computing, optimization and decision technologies*, edited by B. Golden, S. Raghavan and E. Wasil, Springer, USA: 107–119,2005.
- [4] Goksal F, Karaoglan I and Altiparmak F, A hybrid discrete particle swarm optimization for vehicle routing problem with simultaneous pickup and delivery, *Computers & Industrial Engineering*, 65: 39–53, 2013.
- [5] Zachariadis E and Kiranoudis C, An effective local search approach for the vehicle routing problem with backhauls, *Expert Systems with Applications*, 39(3): 3174–3184, 2012.
- [6] Repoussis P, Tarantilis C, Braysy O and Ioannou G, A hybrid evolution strategy for the open vehicle routing problem, *Computers & Operations Research*, 37(3): 443–455,2010.
- [7] Jozefowicz N, Semet F and Talbi E, An evolutionary algorithm for the vehicle routing problem with route balancing, *European Journal of Operational Research*, 195(3): 761–769,2009.
- [8] Hansen P and Mladenovi N, Variable neighborhood search: principles and applications, *European Journal of Operational Research* 130(3): 449–467,2001.

An innovative mathematical simulation tool of integrated frequency synthesizers in order to estimate the main figures of merit with high accurate

Á. A. Magreñán^b *, A. Cordero[†] †, L. Orcos[‡] ‡, C. Quemada[§] §,
J. A. Sicilia^b ¶ and J. R. Torregrosa[†] ||

(b) Universidad Internacional de La Rioja,
26002 Logroño, La Rioja, Spain,

(†) Universidad Politécnica de Valencia,
46022, València, Spain,

(‡) Independent researcher,
Logroño, La Rioja, Spain.

November 28, 2014

1 Introduction

Nowadays, the wireless LAN market has undergone a significant growth due to the voracious demand for high speed wireless communications. Furthermore, there is a constant desire to reduce power consumption, cost and size of the communication devices to a minimum. This has been possible thanks

*e-mail: alberto.magrenan@unir.net

†e-mail: acordero@mat.upv.es

‡e-mail: laraorcos@gmail.com

§e-mail: cquemada@vt.edu

¶e-mail: juanantonio.sicilia@unir.net

||e-mail: jr Torre@mat.upv.es

to continuing advances in Integrated Circuit (IC) technology, allowing the development of devices capable of operating at carrier frequencies of several GHz achieving data rates competitive with established wired alternatives [1].

In addition to this surge, there is another important factor that has motivated the development of this research project. After a thorough bibliographic review, a noteworthy absence of design methodologies that allow the implementation of integrated Phase Locked Loops (PLL) with accurate figures of merit before the fabrication has been found. The most important PLL figures of merit [2],[3] are the phase noise, the spurious emissions and the lock time. Throughout this bibliographic review, several references that study these three figures of merit and implement frequency synthesizers have been found.

Therefore, the aim of this research work is to develop a design methodology that allows the designer to relate the two kinds of previous bibliographic references and consequently implement an integrated frequency synthesizer with accurate figures of merit at the end of the design flow. This includes from the specification of the initial requirements to the experimental results including the comparison with those initial requirements and with the values collected from the most recent bibliographic references.

2 Development of the Symusin

This tool needs the following inputs:

- The division ratios of the reference (R) and feedback (N) dividers
- The frequency of the reference crystal (Fref)
- The extra attenuation provided by the loop filter to the spurious emissions (ATTEN)
- The Voltage Controlled Oscillator (VCO) gain (Kvco)
- The loop phase margin (PM)
- The 1 Hz normalized phase detector noise floor

- The loop bandwidth (L1Hz)
- The synthesizer output frequency (Fout)
- The Charge Pump (CP) current
- The charge pump leakage current
- The frequency step and the tolerance to calculate the lock time.
- Two empirical constants to estimate the spurious emissions and the phase noise of the feedback divider
- VCO and reference crystal.

And Simusyn gives the following outputs:

- Phase noise at the loop output
- Spurious emissions
- Lock time

3 Validation of the Simusyn

In order to verify the accuracy of Simusyn, the integer frequency synthesizer LMX2330L from National Semiconductor has been employed. Its maximum operation frequency is 2.5 GHz. The variable parameters of this frequency synthesizer are the charge pump current and the division ratios of the reference and feedback dividers. The measurements taken:

- Variation of the charge pump current,
- Variation of the feedback division ratio, which leads to a variation of the output frequency and VCO gain, and

- Variation of the feedback and reference division ratios keeping constant the output frequency but modifying the reference frequency.

The errors of phase noise, spurious emissions and lock time are lower than ± 2.7 dB, ± 1.2 dB and 6% respectively.

4 Conclusions

- An innovative mathematical simulation tool has been developed in order to estimate the phase noise, spurious emissions and lock time with high accuracy.
- This tool has been validated by means of a commercial frequency synthesizer.
- The errors of phase noise, spurious emissions and lock time are lower than ± 2.7 dB, ± 1.2 dB and 6% respectively, which can be considered acceptable for this research work.
- Once this tool has been validated, Simusyn has been applied to the design of a low noise synthesizer for the 5-GHz WLAN IEEE 802.11a standard.
- The high accuracy of the final results strengthens the validity of the mathematical simulation tool Simusyn.

References

- [1] KHAN, N., HOSSAIN, M. AND LAW, K.L.E.: A Low Power Frequency Synthesizer for 60-GHz Wireless Personal Area Networks, *IEEE Trans. Circuits Syst. II, Exp. Briefs*, 58 (10): 622–626, 2011.
- [2] BANERJEE, D.: PLL Performance, Simulation, and Design, 4th Ed. Santa Clara, CA: National Semiconductor, 2006.
- [3] MAXIM, A.: Low-Voltage CMOS Charge-Pump PLL Architecture for Low Jitter Operation, in *Proc. European Solid-State Circuits Conf. (ESSCIRC)*, 423–426, 2002.

A matrix-based optimization algorithm for shape deformation using parametric curves.

L. Hilario^{b,*}; A. Falcó^b, N. Montés[†] and M.C.Mora[‡]

(b) Departamento de Ciencias Físicas, Matemáticas y de la Computación, Universidad Cardenal Herrera CEU,
C/ San Bartolomé, 55 46115 Alfara del Patriarca (Valencia) Spain,

(†) Departamento de Ingeniería de la Edificación y Producción Industrial, Universidad Cardenal Herrera CEU,
C/ San Bartolomé, 55 46115 Alfara del Patriarca (Valencia) Spain,

(‡) Departamento de Ingeniería Mecánica y Construcción, Universitat Jaume I,
Avd. Vicent Sos Banyat s/n 12071 Castellón, Spain

December 22, 2014

1 Abstract

In this paper we propose a tensor based description of the Bézier Shape Deformation (BSD) algorithm, denoted T-BSD. The BSD algorithm is a well-known technique, based on the deformation of a Bézier curve through a field of vectors, [10, 11, 12, 13, 14]. A critical point in the use of real-time applications is the cost in computational time. Recently, the use of tensors in numerical methods has been increasing because they drastically reduce computational costs[1, 2, 3, 4, 5, 6, 7, 8, 9]. Our formulation based in tensors T-BSD provides an efficient reformulation of the BSD algorithm. More precisely, the evolution of the execution time with respect to the number of curves of the BSD algorithm is an exponentially increasing curve. As the numerical experiments shown, the T-BSD algorithm transforms this evolution into a linear one. This fact allows to compute the deformation of a Bézier with a much lower computational cost.

*luciah@uch.ceu.es

2 The use of tensors

One of the most important facts in engineering applications is the cost in computational time. A critical point appearing in this context is related to real-time processes. In consequence, one of the main goals is to develop algorithms that reduce, as much as possible, the execution time of existing real-time algorithms.

Lately, interest in numerical methods that make use of tensors has increased because they drastically reduce computational costs. It is particularly useful for high-dimensional spaces where one must pay attention to the numerical cost (in time and storage).

The main goal of this paper is to introduce tensor calculus in order to improve the procedure described in [12, 13, 14]. The tensor reformulation of the BSD algorithm is called Tensor-Bézier Shape Deformation (T-BSD). As a result, the computational cost is reduced to obtain a suitable real-time performance.

3 Comparing BSD and T-BSD algorithms

The BSD was applied and published in [12, 13, 14]. The BSD algorithm computes the deformation of a continuous Bézier curve through a field of vectors including some constraints. In Figure 1 it is shown an example of a deformation of a Bézier curve.

In [12], it was used to improve the numerical simulation of Liquid Composite Moulding processes. In this case the BSD was used to represent as a continuous curve and update the information of the resin's flow front when the mould is filling.

Later, in [13, 14], the algorithm was applied to mobile robots to obtain a new technique for flexible path planning based on the deformation of a Bézier curve through a field of forces (vectors). The focus of this research was the generation of a smooth collision-free trajectory for an holonomic mobile robot.

With T-BSD the reduction of the computational cost of the BSD algorithm is achieved. Figure 2 shows the evolution in computational time required for the calculation of the deformation of Bézier curves (composed of different number of Bézier curves) with the BSD and T-BSD methods. It is clear that, as the number of curves increases, BSD grows exponentially,

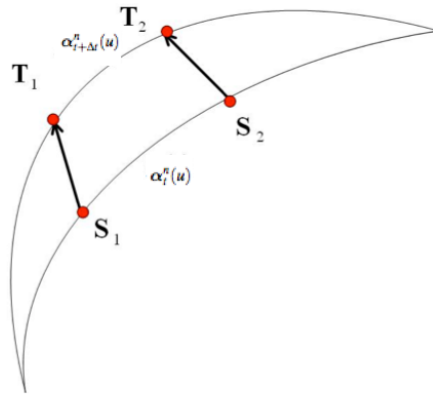


Figure 1: An example of the deformation of a Bézier curve $\alpha_t^n(u)$ through a field of vectors joining the Start Points S_i and the Target Points T_i . The modified Bézier is represented as $\alpha_{t+\Delta t}^n(u)$

whereas T-BSD grows linearly.

Our objective is the use of this algorithm in real-time. In fact, whereas the BSD algorithm can use up to 70 quadratic curves for the computation of the modified Bézier curve in one second (see Figure 2), its reformulated algorithm T-BSD is able to use up to 170 curves within the same period of time, which highly increases the accuracy of the modified Bézier curve when it is compared to the BSD method. The use of tensors reduces the calculation time.

This comparison has been computed using a PC with a 3.06 GHz Intel Core i3 and 4GB RAM.

4 Conclusions

This article presents a use of tensors which reduces the computational cost of the BSD algorithm. The calculation costs depend on the number of curves required to compute a new Bézier curve from a given one. The number of the curves is highly related to the accuracy of the modified Bézier, the more curves are used the better the accuracy of the new Bézier. As a consequence of the use of tensors, the T-BSD algorithm enjoys the same properties but with very low computational time.

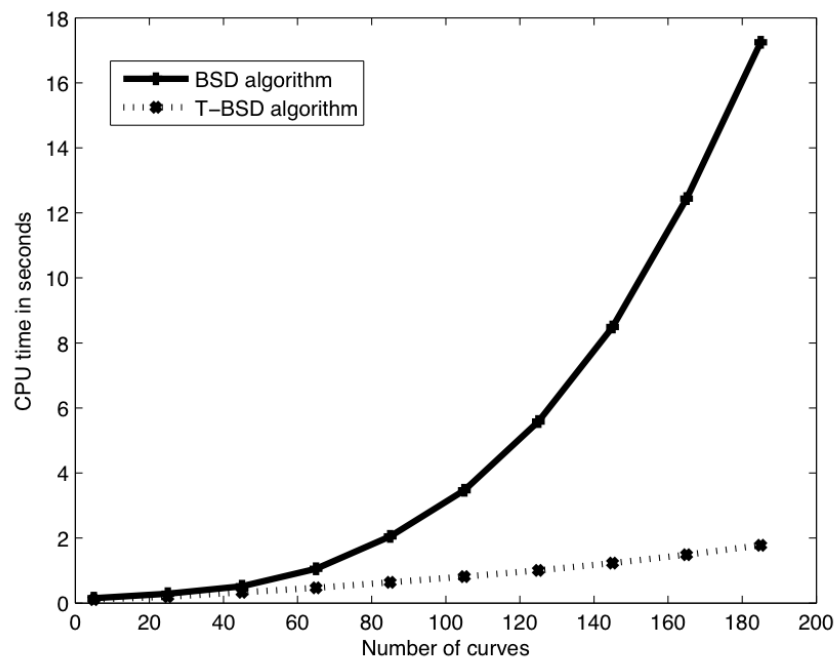


Figure 2: The comparison of the computational cost of BSD and T-BSD methods.

References

- [1] A. Ammar, B. Mokdad, F. Chinesta, and R. Keunings: *A new family of solvers for some classes of multidimensional partial differential equations encountered in kinetic theory modelling of complex fluids*. Journal of Non-Newtonian Fluid Mechanics, 139 **3** (2006) 153–176.
- [2] J. D. Carroll and J. J. Chang: *Analysis of individual differences in multidimensional scaling via an n -way generalization of Eckart-Young decomposition*. Psychometrika, **35** (1970) 283–319.
- [3] A. Doostan and G. Iaccarino: *A least-squares approximation of partial differential equations with high-dimensional random inputs*. J. Comput. Phys., **228** (12) (2009) 4332–4345.
- [4] A. Falcó: *Algorithms and numerical methods for high dimensional financial market models*. Revista de Economía Financiera, **20** (2010) 51-68.
- [5] W. Hackbusch: *Tensor spaces and numerical tensor calculus*. Monograph in preparation.
- [6] T. G. Kolda and B. W. Bader: *Tensor decompositions and applications*. SIAM Rev., **51** (2009) 455–500.
- [7] A. Nouy: *A generalized spectral decomposition technique to solve a class of linear stochastic partial differential equations*. Computer Methods in Applied Mechanics and Engineering, **96** (45-48) (2007) 4521–4537.
- [8] A. Nouy: *Proper generalized decompositions and separated representations for the numerical solution of high dimensional stochastic problems*. Archives of Computational Methods in Engineering, 2010, In press.
- [9] M. A. O. Vasilescu and D. Terzopoulos: *Multilinear analysis of image ensembles: tensorfaces*. ECCV 2002:Proceedings of the 7th European Conference on Computer Vision, Lecture Notes in Comput. Sci. 2350, 447–460. Springer, 2002.
- [10] Xu L., Chen Y.J, Hu N. *Shape modification of Bézier curves by constrained optimization*. Journal of Software(China), Vol.13(6),2002;1069–1074.

- [11] Wu O.B., Xia F.H. *Shape modification of Bézier curves by constrained optimization*. Journal of Zhejiang University-Science, Springer-Verlag GmbH, 2005; 124–127.
- [12] Montés N., Sánchez F., Hilario L., Falcó A. *Flow Numerical Computation through Bézier Shape Deformation for LCM process simulation methods*. International Journal of Material Forming, Vol.1, 2008; 919–922. Lyon (France).
- [13] Hilario L., Montés N., Falcó A., Mora M.C. *Real-Time Trajectory Modification Based on Bézier Shape Deformation*. International Conference on Evolutionary Computation, October 2010. Valencia (Spain)
- [14] Hilario L., Montés N., Mora M.C., Falcó A. *Real-Time Trajectory Deformation for Potential Fields Planning Methods*. IEEE/RSJ International Conference on Intelligent Robots and Systems; 1567–1572, September 2011. San Francisco, CA, USA

Dynamical Study while Searching Equilibrium Solutions in N -body Problem

D. Budzko^b, J.L. Hueso^{†*}, E. Martínez[‡], and C. Teruel[†]

(^b) University of Brest, Belarus,

([†]) Instituto Universitario de Matemática Multidisciplinar,
Universitat Politècnica de València,

([‡]) Instituto Universitario de Matemática Pura y Aplicada,
Universitat Politècnica de València.

November 30, 2014

1 Introduction

The dynamics of different iterative methods for the solution of nonlinear equations has been widely studied (see, for example [1]-[2] and the references therein) by analyzing the properties of the rational functions in the complex plane that arise when applying the method to polynomials of certain degree. Here we deal with an interesting real application of celestial mechanics that produces a 2×2 system of algebraic equations in the real 2-dimensional plane. Our idea is to apply the tools of the theory of complex dynamics to this case.

In the classical N -body problem, the search of relative equilibrium solutions is a very intricate problem itself, because the number of real solutions increases very fast while the number of interacting bodies N grows and at present nobody knows even how to find the number of all equilibrium solutions (or central configurations) for arbitrary N . Only few such results are known for small N ($N = 2, 3, 4$) or for some particular, for example, symmetric cases. The equations that determine relative equilibrium solutions in

* e-mail: jlhueso@mat.upv.es

N -body problem are nonlinear algebraic equations and usually contain some geometric or dynamic parameters.

In this paper we consider the equilibrium solutions in the newtonian planar circular restricted four-body problem [3]-[4], formulated on the basis of Lagrange’s triangular solutions. The corresponding system, which determines equilibrium positions of the body of infinitesimal mass

$$\begin{aligned}
 (\sqrt{3}x - y) \left(1 - \frac{1}{(x^2 + y^2)^{3/2}}\right) + \mu_1 \left(\sqrt{3}(x - 1) + y\right) \left(1 - \frac{1}{((x - 1)^2 + y^2)^{3/2}}\right) &= 0 \\
 2y \left(1 - \frac{1}{(x^2 + y^2)^{3/2}}\right) + \mu_2 \left(\sqrt{3}(x - 1) + y\right) \left(1 - \frac{1}{((x - 1/2)^2 + (y - \sqrt{3}/2)^2)^{3/2}}\right) &= 0,
 \end{aligned}
 \tag{1}$$

has from 8 to 10 solutions, depending on two mass parameters μ_1 and μ_2 . Parameters μ_1 and μ_2 are mass ratios and are chosen in such way to be varied from zero to one.

In order to determine the equilibrium points, we apply Newton’s method, [5], to this system, starting from a given initial approximation. Newton’s iterations generally converge to a solution, but it is not easy to predict to which one, depending on the starting point. The attraction basin of a root is formed by the starting points whose Newton’s iterations converge to this root. We find that the attraction basins of the roots of this system are very irregular, chaotic and full of noise, especially if parameters μ_1 and μ_2 are close to zero (the most interesting case for applications). This means that the problem of choosing initial estimations for the iterative method is very sensitive and needs careful consideration, because the next step is the stability analysis of every solution under any values of parameters. We have confronted the numerical solutions with the solutions obtained in the form of power series [6] in order to determine if the series approximations are suitable as starting points for the Newton’s iterations.

2 Attraction basins for Newton’s method

Let us recall some concept on dynamics. If $G : \mathbb{R}^n \rightarrow \mathbb{R}^n$ is Fréchet differentiable, given $x \in \mathbb{R}^n$, the orbit of x is the set $x, G(x), G^2(x), \dots, G^p(x), \dots$. A point $x_f \in \mathbb{R}^n$ is a fixed point of G if $G(x_f) = x_f$. Let x_f be a fixed point of G . The attraction basin of x_f is the set of points whose orbits tend to that fixed point.

Here we consider the iterative function G obtained by applying Newton's method to system (1) for given values of the parameters μ_1 and μ_2 . The analytic expression of G has been obtained by using symbolic computation in Matlab2011b.

In [3] the authors analyze the number of solutions of the system for different values of parameters μ_1 and μ_2 finding a bifurcation curve that divides the rectangle $(\mu_1, \mu_2) \in [0, 1] \times [0, 1]$ in two zones. For parameter values below the curve, the system presents 8 solutions, 10 above the curve in the upper part and 9 along it. It is interesting seeing how the basins change with the number of solutions and what happens near the bifurcation curve.

Fixing the value of $\mu_1 = 0.9$ and giving different values to μ_2 , we examine different cases for the solutions. The bifurcation curve appears about $\mu_2 = 0.44$. For lower values of μ_2 there are 8 solutions and for higher values 10.

For small values of the parameters, the basins are very intricate. The bigger are the parameters, the simpler are the basins, but they always have a fractal appearance.

3 Power series solutions

This section is devoted to the construction of solution in the form of a power series. If we are interested mostly in case $\mu_1 > \mu_2$ then it is expedient to expand the power series in terms of small parameter μ_2 . In this way the expansions will be more accurate. But if it is required to consider the case $\mu_1 < \mu_2$ then the precision will be better if the power series expansion will be carried out in terms of small parameter μ_1 .

4 Initial estimations

The objective of this section is to assess the suitability of the series approximations of the solutions as starting points for the Newton's iterations to converge to the desired solution.

We consider a discrete mesh of pairs (μ_1, μ_2) in the rectangle $[0, 1] \times [0, 1]$. For each point in the mesh, we compute the Newton iterations starting from a partial sum of the series considered in the former section and see if they converge and to which solution. The pairs (μ_1, μ_2) for which s_j^i belongs to the attraction basin of S_k constitute the S_k -suitability region of the j -th partial

sum of the series i .

5 Conclusions

We have analyzed the attraction basins of the equilibrium solutions of the restricted four-body problem. Due to the complexity of the attraction basins, it is difficult to guarantee that a starting point will converge to the desired solution. By using series expansions one can obtain approximations for the solutions that can be used as starting point for Newton's iterations. We have presented a graphical analysis of the behavior of different series approximations obtaining the suitability regions for different orders and equilibrium points. In particular, we have seen that the partial sums of series do not provide better estimations for Newton's method than its zero term.

References

- [1] J.L. Varona, Graphic and numerical comparison between iterative methods, *Math. Intelligencer*, 24:37–46, 2002.
- [2] S. Amat, S. Busquier, Á.A. Magreñán, Reducing Chaos and Bifurcations in Newton-Type Methods, *Abstract and Applied Analysis*, dx.doi.org/10.1155/2013/726701
- [3] D.A. Budzko, A.N. Prokopenya, SymbolicNumerical Methods for Searching Equilibrium States in a Restricted Four-Body Problem, *Programming and Computer Software*, 39(2):74–80, 2013.
- [4] F. Diacu, The solution of the n-body problem, *Mathematical Intelligencer*, 18(3):66–70, 1996.
- [5] J.F. Traub, Iterative methods for the solution of equations, Chelsea Publishing Company, New York, 1982.
- [6] D.A. Budzko, A.N. Prokopenya, Symbolic-numerical analysis of equilibrium solutions in a restricted four-body problem, *Programming and Computer Software*, 36(2):68–74, 2010.

On the inverse eigenvalue problem of Hermitian reflexive matrix

Silvia Gigola¹, Leila Lebtahi², Néstor Thome³

(¹) Dpto. de Matemática, Facultad de Ingeniería,

Universidad de Buenos Aires, Buenos Aires, Argentina

(²) Universidad Internacional de La Rioja, Logroño

(³) Instituto Universitario de Matemática Multidisciplinar,

Universitat Politècnica de València

emails: silgig@yahoo.com.ar, leila.lebtahi@unir.net, njthome@mat.upv.es

November 28, 2014

1 Introduction

The inverse eigenvalue problem for Hermitian anti-reflexive with respect to a generalized reflection was solved by Peng in 2005, (that is, $A = -JAJ$, where J is involutory and hermitian). On the other hand, the optimization problem related to reflexive matrices with respect to a pair of generalized reflections was studied by Chen. The inverse eigenvalue problem for Hermitian reflexive (anti-reflexive) matrices with respect to a Hermitian tripotent matrix was investigated by the authors. Another similar structured matrices, such as Toeplitz, have been studied in the literature. The inverse eigenvalue problem has been applied in a wide range of areas such as control theory, mechanic engineering, quantic physics and electromagnetism, etc. and some numerical methods were developed to solve them. In this paper, we consider the problem of Hermitian matrices reflexive with respect to a normal $\{k+1\}$ -potent matrix J . This problem extends all these mentioned cases related to reflexivity.

In this paper we consider a normal $\{k + 1\}$ -potent complex matrix $J \in \mathbb{C}^{n \times n}$ (that is, $JJ^* = J^*J$ and $J^{k+1} = J$ for some $k \in \mathbb{N}$).

Definición 1. A Hermitian matrix $A \in \mathbb{C}^{n \times n}$ is called reflexive with respect to the matrix J if $A = JAJ$. The set of all these matrices is denoted by $\mathcal{HJ}^{n \times n}$.

Clearly, the eigenvalues of such matrices are real.

Let $X \in \mathbb{C}^{n \times m}$ and a diagonal matrix $D \in \mathbb{R}^{m \times m}$ two given matrices. The inverse eigenvalue problem can be stated as follows:

- (I) Find all the matrices $A \in \mathcal{HJ}^{n \times n}$ such that $AX = XD$ [3].

Assume that the solution set S of problem (I) is nonempty. In this paper we solve the following problem:

- (II) For a given matrix $\ddot{A} \in \mathbb{C}^{n \times n}$, we want to find $\hat{A} \in S$ such that

$$\min_{A \in S} \|A - \ddot{A}\|_F = \|\hat{A} - \ddot{A}\|_F,$$

where the Frobenious norm is considered.

2 Main results

In [3], the authors found the next Theorem. The structure of the matrix J is

$$J = U \text{diag}(\omega_1 I_{r_1}, \dots, \omega_t I_{r_t}, O_{r_{t+1}}) U^* \tag{1}$$

where $r_1 + \dots + r_t = \text{rango}(J)$ and $r_1 + \dots + r_t + r_{t+1} = n$. Partitioning the matrix $A \in \mathcal{HJ}^{n \times n}$ as

$$U^*AU = \begin{bmatrix} A_{1,1} & \dots & A_{1,t} & A_{1,t+1} \\ \vdots & \ddots & \vdots & \vdots \\ A_{t,1} & \dots & A_{t,t} & A_{t,t+1} \\ A_{t+1,1} & \dots & A_{t+1,t} & A_{t+1,t+1} \end{bmatrix} \tag{2}$$

and considering that the eigenvalues are ordered as follows (when 1 and -1 appear) $1, -1, \omega_3, \bar{\omega}_3, \dots, \omega_{p-1}, \bar{\omega}_{p-1}, 0$, the matrix A can be written as

$$A = U \text{diag}(A_{1,1}, A_{2,2}, \tilde{A}_{3,4}, \dots, \tilde{A}_{p-1,p}, O) U^* \tag{3}$$

where

$$\tilde{A}_{s,s+1} = \begin{bmatrix} O & A_{s,s+1} \\ A_{s+1,s} & O \end{bmatrix} \quad \text{for } s \in \{3, 5, \dots, p-1\}. \quad (4)$$

We use the following notations: $W^{(r)}(X) = I - XX^\dagger$ and $W^{(l)}(X) = I - X^\dagger X$.

Teorema 1. *Let $X \in \mathbb{C}^{n \times m}$, $D \in \mathbb{R}^{m \times m}$ a diagonal matrix and J partitioned as in (1). Consider the partition*

$$X = U \left[X_1^T \quad X_2^T \quad \tilde{X}_3^T \quad \tilde{X}_5^T \quad \dots \quad \tilde{X}_{p-1}^T \quad X_{p+1}^T \right]^T \quad (5)$$

with $\tilde{X}_s^T = \begin{bmatrix} X_s^T & X_{s+1}^T \end{bmatrix}$, $s \in \{3, 5, \dots, p-1\}$. Then there exists a matrix $A \in \mathcal{H}J^{n \times n}$ such that $AX = XD$ if and only if

$$X_iDX_i^\dagger - (X_i^\dagger)^*DX_i^* = (Y_iW^{(r)}(X_i))^* - Y_iW^{(r)}(X_i) \quad \text{for } i = 1, 2; \quad (6)$$

and

$$X_sDW^{(l)}(X_{s+1}) = O, \quad W^{(r)}(X_s^*)DX_{s+1}^* = O, \quad X_s^*X_sD = DX_{s+1}^*X_{s+1} \quad (7)$$

for $s \in \{3, 5, \dots, p-1\}$ and also $X_{p+1}D = O$. In this case, the general solution is given by

$$A = U \text{diag} \left(A_{1,1}, A_{2,2}, \tilde{A}_{3,4}, \dots, \tilde{A}_{p-1,p}, O \right) U^* \quad (8)$$

where

$$A_{i,i} = X_iDX_i^\dagger + Y_iW^{(r)}(X_i), \quad i = 1, 2, \quad (9)$$

$$A_{s,s+1} = (X_s^*)^\dagger DX_{s+1}^* + W^{(l)}(X_s^*)X_sDX_{s+1}^\dagger + W^{(l)}(X_s^*)Y_sW^{(r)}(X_{s+1}) \quad (10)$$

$A_{s+1,s}^* = A_{s,s+1}$, for $s \in \{3, 5, \dots, p-1\}$ and $Y_1, Y_2, Y_s, s = 3, 5, \dots, p-1$, are arbitrary.

If $S \neq \emptyset$, it can be seen that S is a convex closed set. So, Problem (II) has a unique solution ([2], p. 22). In order to solve this problem we need the following result.

Lema 1. *Let $M_1 \in \mathbb{C}^{m \times r}$, $M_2 \in \mathbb{C}^{n \times t}$, $R_1 \in \mathbb{C}^{r \times n}$ and $R_2 \in \mathbb{C}^{r \times n}$. Then the solutions of the optimization problem*

$$\min_{Y \in \mathbb{C}^{r \times n}} \|W^{(l)}(M_1)YW^{(r)}(M_2) - R_1\|_F^2 + \min_{Y \in \mathbb{C}^{r \times n}} \|W^{(l)}(M_1)YW^{(r)}(M_2) - R_2\|_F^2 \quad (11)$$

are the matrices $\hat{Y} \in \mathbb{C}^{r \times n}$ given by

$$\hat{Y} = \frac{1}{2} (R_1 + R_2) + GM_2M_2^\dagger + M_1^\dagger M_1G - M_1^\dagger M_1GM_2M_2^\dagger$$

for arbitrary matrices $G \in \mathbb{C}^{r \times n}$.

The explicit general solution of Problem (II) has now the following form.

Teorema 2. Let $\ddot{A} \in \mathbb{C}^{n \times n}$ such that

$$U^* \ddot{A} U = \begin{bmatrix} \ddot{A}_{1,1} & \dots & \ddot{A}_{1,p} & \ddot{A}_{1,p+1} \\ \vdots & \ddots & \vdots & \vdots \\ \ddot{A}_{p,1} & \dots & \ddot{A}_{p,p} & \ddot{A}_{p,p+1} \\ \ddot{A}_{p+1,1} & \dots & \ddot{A}_{p+1,p} & \ddot{A}_{p+1,p+1} \end{bmatrix} \quad (12)$$

where $\ddot{A}_{i,j} \in \mathbb{C}^{m_i \times t_j}$, $m_1 + m_2 + \dots + m_{p+1} = t_1 + t_2 + \dots + t_{p+1} = n$ and U as in (1). Under the conditions of Theorem 1, if $S \neq \emptyset$, then Problem (II) has a unique solution given by

$$\hat{A} = U \text{diag}(A_{1,1}, A_{2,2}, \tilde{A}_{3,4}, \dots, \tilde{A}_{p-1,p}, O) U^* \quad (13)$$

where $A_{i,i} = X_iDX_i^\dagger + (\ddot{A}_{ii} - X_iDX_i^\dagger)W^{(r)}(X_i)$ for $i = 1, 2$, $\tilde{A}_{s,s+1}$ is given by (4), $A_{s+1,s}^* = A_{s,s+1}$ and

$$A_{s,s+1} = (X_s^*)^\dagger DX_{s+1}^* + W^{(l)}(X_s^*)X_sDX_{s+1}^\dagger + \frac{1}{2}W^{(l)}(X_s^*)(R_s + R_{s+1})W^{(r)}(X_{s+1})$$

for $s \in \{3, 5, \dots, p - 1\}$ where

$$\begin{cases} R_s &= \ddot{A}_{s,s+1} - (X_s^*)^\dagger DX_{s+1}^* - W^{(l)}(X_s^*)X_sDX_{s+1}^\dagger \\ R_{s+1} &= \ddot{A}_{s+1,s}^* - (X_s^*)^\dagger DX_{s+1}^* - W^{(l)}(X_s^*)X_sDX_{s+1}^\dagger \end{cases} \quad (14)$$

The proof of this result is based on the invariance of the Frobenious norm with respect to the unitary transformations. After that, an application of Lemma 1 leads to the result.

Acknowledgements

This paper was partially supported by Ministerio de Economía y Competitividad of Spain (DGI Grant MTM2010-18228) and by Proyecto de la Universidad de Buenos Aires 20020130100671BA (EXP-UBA: 9.011/2013).

Bibliography

- [1] H. C. Chen, *Generalized reflexive matrices: special properties and applications*, SIAM J. Matrix Anal., 19, 1, (1998), 140-153.
- [2] E. W. Cheney, *Introduction to Approximation Theory*, McGraw-Hill, Nueva York, 1966.
- [3] L. Lebtahi, N. Thome, *El problema del valor propio inverso para cierta clase de matrices*, en las Actas del III Congreso sobre Matemática Aplicada, Computacional e Industrial, Argentina (MACI), 3(2011), 495-498, L.R. Castro, M.C. Maciel, S.M. Castro (Eds.)
- [4] Zhen-Yun Peng, *The inverse eigenvalue problem for Hermitian anti-reflexive matrices and its approximation*, Applied Mathematics and Computation, 162, (2005), 1377-1389.